POLLUTANT FORMATION IN A GASEOUS-FUELLED, DIRECT INJECTION ENGINE

by

GORDON PATRICK McTAGGART-COWAN

B.Eng., University of Victoria 1999
M.A.Sc., University of British Columbia 2001

A THESIS SUBMITTED IN PARTIAL FULFILLMENT OF
THE REQUIREMENTS FOR THE DEGREE OF

DOCTOR OF PHILOSOPHY

in

THE FACULTY OF GRADUATE STUDIES

(Mechanical Engineering)

THE UNIVERSITY OF BRITISH COLUMBIA

October 2006

Your file Votre référence
ISBN: 978-0-494-20046-9
Our file Notre référence
ISBN: 978-0-494-20046-9

Abstract

Heavy-duty natural gas engines offer air pollution and energy diversity benefits. However, current homogeneous-charge lean-burn engines suffer from impaired efficiency and high unburned fuel emissions. Direct injection offers the potential of diesel-like efficiencies, but requires further research. To improve understanding of the combustion process and pollutant formation mechanisms in a pilot-ignited, direct injection of natural gas engine with intake charge dilution, the effects of enhanced gaseous jet kinetic energy, gaseous fuel composition (including ethane, propane, hydrogen, and nitrogen), and filtering the recirculated gases were studied.

An experimental investigation was carried out on a single-cylinder heavy-duty engine. Fuel consumption, in-cylinder performance and gaseous and particulate emissions (total mass, size distributions, and black carbon content) were measured. The results indicated that increasing the jet kinetic energy significantly reduced particulate matter (PM) emissions due to improved fuel-air mixing, especially at high load. The addition of hydrogen to the fuel reduced emissions of carbon monoxide (CO), unburned fuel (HC) and PM. The largest effects were observed at high load conditions. The addition of ethane and propane to the fuel resulted in increases in PM and CO emissions at all operating conditions tested; no effect on the combustion progression was detected. The addition of nitrogen to the fuel significantly reduced emissions of CO, PM, and HC due to enhancement of the late-cycle combustion event from increased in-cylinder turbulence. Removing PM from the recirculated gases revealed that these particles had no significant effect on the combustion event or on PM emissions.

In conclusion, mixing and kinetic enhancement both reduced the gaseous fuel ignition delay. The overall combustion event was, at high load, mixing limited; the combustion rate was unaffected by fuel reactivity but was increased with turbulence enhancement. Emissions formation was found to be a result of multiple influences whose relative importance varied with operating condition. Increased mixing and lower fuel carbon content reduced PM emissions. Reductions in emissions through the addition of hydrogen and nitrogen to the fuel may offer a potential technique to offset increases in emissions due to variations in ethane and propane levels in natural gas.

Table of Contents

List of Tables

List of Figures

Nomenclature

50%IHR	=	Mid-point of integrated heat-release rate
°CA	=	Crank angle degree
% H_2	=	Volume percent hydrogen in fuel
% N_2	=	Volume percent nitrogen in fuel
ANOVA	=	Analysis of variance
ATDC	=	After top-dead-center
BC	=	Black carbon
BD	=	Burn duration
COV	=	Coefficient of variation (standard deviation / mean)
DMA	=	Differential mobility analyzer
D_p	=	Particle diameter
DF	=	Degrees-of-Freedom
EGR	=	Exhaust gas recirculation
EOC	=	End of combustion
EPA	=	United States environmental protection agency
GHG	=	Greenhouse gas
GID	=	Gas ignition delay time
GikWhr	=	Gross indicated kilowatt hour
GIMEP	=	Gross indicated mean effective pressure
GISFC	=	Gross indicated specific fuel consumption
GSOC	=	Gas start-of-combustion
GSOI	=	Gas start-of-injection
H:C	=	Molar hydrogen-to-carbon ratio
HACA	=	Hydrogen abstraction, acetylene addition
HC	=	Hyrdrocarbons (total)
HCCI	=	Homogeneous charge compression ignition
HHV	=	Higher heating value
HPDI™	=	High-pressure direct injection (trademarked by Westport Innovations Inc.)
HRR	=	Heat-release rate
IHR	=	Integrated heat-release rate
LHV	=	Lower heating value
LNG	=	Liquefied natural gas
MW	=	Molecular weight
NDIR	=	Non-dispersive infra-red
NG	=	Natural gas
nmHC	=	Non-methane hydrocarbons
NO_x	=	Oxides of nitrogen (include NO, NO_2)
PAH	=	Polycyclic aromatic hydrocarbons
PID	=	Pilot ignition delay time
PIDING	=	Pilot-ignited, direct-injection natural gas
P_{inj}	=	Gaseous fuel injection pressure
PM	=	Particulate matter

$PM_{2.5}$	=	Particulate matter less than 2.5 μm in diameter
P_{max}	=	Maximum in-cylinder pressure
PSOC	=	Pilot start-of-combustion
PSOI	=	Pilot start-of-injection
RIT	=	Relative injection timing (delay between pilot and gas injections)
RPM	=	Revolutions per minute
SMPS	=	Scanning mobility particle sizer
SOC	=	Start of combustion
$T_{adiabatic}$	=	Adiabatic flame temperature
TDC	=	Top-dead-center
TEOM	=	Tapered element oscillating microbalance
VOC	=	Volatile organic carbon compounds
Y_{intO2}	=	Intake oxygen mass fraction
ϕ	=	Equivalence ratio (on oxygen basis)
ξ	=	New index parameter (HHV/H:C ratio)

Acknowledgements

The work described in this thesis could not have been completed without the support of the exemplary colleagues with whom I was fortunate to work. First, I would like to thank my supervisors, Dr. Kendal Bushe and Dr. Steve Rogak, for their unending support, patience, and advice during my time at UBC. The development of both my technical proficiency and my abilities as an independent researcher are a direct result of their guidance and tutelage. I also want to extend special recognition to Dr. Martin Davy, for his support and direction, both during my research program and in my future career direction. And a special thank-you to Dr. Phillip Hill, whose unwavering encouragement helped me consistently achieve more than I would have thought possible.

Without the research staff at both UBC and Westport Innovations, I would not have had an experimental facility to use for my research. At UBC, the ceaseless efforts of Heather Jones and Bob Parry ensured that the research engine was available and operational for me when I needed it. Support from Westport was always quick and comprehensive; however, I want to especially acknowledge the assistance of Brian Buik, Mark Dunn, Dale Goudie, Guowei Li, Sandeep Munshi, and Patric Ouellette.

I also want to acknowledge all the excellent graduate students with whom I have been honoured to work; but in particular, thanks to Jin Bei, Jian Huang, Wu Ning, Conor Reynolds, and Maggie Wang. They always provided me with an ear to listen, and never failed to encourage me when I encountered a pitfall along the way.

Finally I want to thank my family, and especially my parents, for their ongoing support of my educational pursuits. Lastly, and most importantly, to my wife Helen, for your unconditional love and support over the past two years. I hope that I have been able to provide you with even half of the support that you have always given me. This work is dedicated to you; without you, I would never have been able to complete this project.

Co-Authorship Statement

The work presented in this thesis was conceived, conducted, and disseminated by the doctoral candidate. The co-authors of the manuscripts that comprise part of this thesis made contributions only as is commensurate with a thesis committee or as experts in a specific area as it pertains to the work. The co-authors provided direction and support. The co-authors reviewed each manuscript prior to submission for publication and offered critical evaluations; however, the candidate was responsible for the writing and the final content of these manuscripts.

Chapter 1
Introduction

For over a century, heavy-duty internal combustion engines have been a key component to trade and economic activity throughout the world. These engines, fuelled with liquid diesel and running on cycles approaching the thermodynamic 'diesel' cycle, have facilitated cost-effective transportation of people and goods by road, sea, and rail. They have also powered much of the construction of our modern infrastructure and have provided reliable stationary power generation in remote and emergency situations. The principal attractions of diesel engines are their high efficiency, advantageous torque characteristics, and enviable reliability. However, they emit harmful pollutants and use an increasingly scarce natural resource; as such, there is a pressing need to develop improved combustion systems which simultaneously reduce emissions and improve efficiency while reducing the burden on liquid fossil fuels through the use of alternative fuels.

Traditional diesel engines offer many advantages in heavy-duty applications, but also suffer from relatively high levels of regulated and unregulated emissions. Diesel engines are reliable and robust, provide high torque at low speeds, and are as much as 25% more efficient than equivalent gasoline-fuelled engines [1]. As a result of their high efficiency, greenhouse gas emissions are low compared with other in-use transportation motive power sources. However, emissions of harmful species, including 'criteria' pollutants such as fine particulate matter (PM) and oxides of nitrogen (NO_x), as well as air toxics such as benzene, are significantly higher. In Canada in 2000, diesel engines emitted 43% of all anthropogenic NO_x emissions [2]. Although the contribution of diesel engines to regulated PM mass emissions is relatively small, they pose a significant health concern because of their composition, small size, and high concentrations in urban areas.

1.1 Air Pollution

Air pollution has long been recognized as a public nuisance. In the early 20th century, increasing uncontrolled emissions led to acute air pollution events, culminating in London's 'killer fogs' of the early 1950's [3]. As a direct result of these high-mortality incidences, clean-air act legislation was enacted in many countries. In general, these actions were

successful in preventing acute events. However, epidemiological studies have subsequently shown that increased mortality results from exposures to levels of pollutants far below those first legislated in the clean-air acts [4]. Air pollutants of concern include solid and liquid aerosols, classic gaseous pollutants (such as NO_x, sulphur oxides, carbon monoxide and ozone), and carcinogenic 'air toxics' (approximately 200 separate species which are thought to be toxic). In Ontario a recent report estimated that almost 6000 excess deaths per year could be attributed to air pollution [5].

1.1.1 Particulate Matter

Particulate matter is the term used to refer to solid and liquid aerosol particles suspended in the atmosphere. PM is composed of a wide range of natural and anthropogenic species. It can be emitted directly from a source or it can be formed by reactions between gases in the atmosphere. The sizes of particles vary, with typical definitions based on an aerodynamic or effective diameter. Widely-accepted categories include ultrafine (sub 100 nm) and fine (sub 2.5 μm, $PM_{2.5}$) particles. Coarse mode particles (diameter > 2.5 μm) tend to settle out of the atmosphere in hours or days, while ultrafine particles tend to agglomerate into larger particles (diameters between 0.1 and 1.0 μm) in minutes to hours after emission. These agglomerated particles have the longest residence time, as they do not tend to agglomerate further but also have low settling velocities [6]. Combustion processes, such as in diesel engines, tend to generate smaller particles (<1.0μm) either directly in the flame or by post-exhaust condensation of volatile species. Larger particles (>1.0μm) are typically formed from mechanical processes, including road dust, soil tilling, and natural sources. In Canada in 2000, 90% of PM_{10} (PM < 10μm in diameter) and 60% of $PM_{2.5}$ emissions on a mass basis originated from such mechanical (non-combustion) sources [2].

Numerous epidemiological studies have shown that PM significantly increases premature mortality through cardiovascular or pulmonary endpoints [3,4,7,8,9]; other health effects include impaired lung development [10]. PM's adverse health effects are attributed to deposition on the alveoli and other sensitive lung tissues, causing irritation and immune system reactions [11]. Peak deposition of particles in the alveolar region of the lungs occurs for particles with diameters between 0.01 and 0.1 μm; particles larger than 2.5 μm are unlikely to penetrate into the lungs [12,13]. For an equal mass, smaller particles (with larger surface areas) have a greater inflammatory effect and cause greater epithelial damage

[12,14,15]. Smaller particles are also more likely to pass into the bloodstream, thereby directly affecting the cardiovascular system [16]. There is some evidence that observed discrepancies in mass-based PM health effects studies may be at least partially explained by variations in total particle surface area [17].

The composition of the particles can also have a significant impact on health outcomes. Diesel PM includes a significant quantity of adsorbed volatile organics and other potentially toxic or carcinogenic species [18]. Occupational and animal toxicological studies have shown that exposures to diesel PM can have very significant health impacts [19]. Whether these effects are a result of either the chemical composition of the particles or the high concentrations of ultrafine particles in diesel exhaust is unclear. The California Air Resources Board (CARB) has defined diesel PM as an 'air toxic', and estimates that in 2003 diesel PM was responsible for approximately 75% of the cancer cases attributed to all air toxics [20]*.

1.1.2 Gaseous Pollutants

Of the gaseous air pollutants, the most significant relating to diesel engines is NO_x. The direct health impacts of exposures to moderate levels of NO_x (specifically nitrogen dioxide, NO_2) include eye and respiratory tract irritation [6]. Indirect environmental and health impacts result from NO_x's role as an important precursor for the secondary formation of nitrate aerosols and in the formation of nitric acid, which leads to acid rain [6]. However, the primary environmental impacts of NO_x are generally considered to be the formation of ground level ozone (O_3) and photochemical smog. The formation of ground-level ozone is dependant on reactions between NO_x and volatile organics (VOCs). VOCs are emitted from combustion processes (primarily light-duty vehicles) but also from natural and other industrial (non-combustion) sources. The local geographic and meteorological conditions and the relative concentrations of NO_x and VOCs control the rate and quantity of ozone generation; sometimes the process is NO_x limited and other times it is VOC limited [21,22]. As a result, reductions in NO_x may or may not have a substantial impact on ambient O_3 levels, and in fact reductions in NO_x may somewhat increase ambient O_3 under certain conditions [23]. Despite this, regulatory agencies around the world are aggressively pursuing

* CARB recently added environmental tobacco smoke to the air toxic list; due to its prevalence, it poses a greater cumulative health risk than diesel PM, and hence in more recent analyses the relative contribution of diesel PM is less substantial.

the reduction of NO_x emissions. While other ambient air pollutant emissions are also important - for example carbon monoxide (CO), sulfates, and lead - current diesel engines are relatively insignificant emitters of these species.

Another class of gaseous pollutants is the group of gases, commonly referred to as greenhouse gases (GHG's), which have radiative absorption properties in the infrared range. GHG's affect the global climate by absorbing some of the earth's emitted infrared radiation and re-radiating it back towards earth. Their presence influences the earth's radiative energy balance and thus, as their concentrations increase to unprecedented levels, they are altering the earth's climate [6]. Carbon dioxide (CO_2) and methane (CH_4) are the two most significant GHG's whose ambient atmospheric concentrations have been significantly increased by human influences [6,24]. While the specific long-term effects of changes in GHG levels on the global atmospheric-ocean system are uncertain, comparisons with past climatic records indicate that greater climatic instability and higher global average temperatures correlate with higher GHG levels [6]. While the high efficiency of diesel engines, relative to most other motive power sources, minimizes GHG emissions [1], emission levels are still a concern.

1.2 Diesel Emissions Regulations

Heavy-duty engine emission-control legislation is designed to minimize the adverse health and environmental impacts of air pollutants from these engines. In most jurisdictions, including the United States and Canada (Canadian emissions regulations are typically aligned with those for the US), the reduction of emissions from on-road vehicles and engines is achieved by establishing emission limits for those substances [25,26]. For an engine model to "pass" its emissions test, it must meet the legislated levels for each pollutant over a standardized test-cycle. Engine emissions standards have become progressively more stringent over time. The United States Environmental Protection Agency (EPA) emissions standards for NO_x and PM for heavy-duty vehicles are shown in Figure 1.1 [25]. Dramatic reductions in permitted emission levels have resulted in ever cleaner new vehicles; however, due to the relatively long lifetime of heavy-duty vehicles, many vehicles still on the road are emitting at much higher levels. Of particular note is the order-of-magnitude reduction in PM between the current (2004) and the 2007-10* standards. A sample of current or upcoming

* For 2007 half of a manufacturers new heavy-duty vehicles must meet the 2010 NO_x levels, while the rest may emit at the 2004 standard level. Or all vehicles can operate at half of the 2004 standard level until 2010 [25].

emissions standards for various jurisdictions is shown in Table 1.1 [27]. Care must be taken when comparing emissions regulations between jurisdictions because the test-cycles used are not always equivalent (for example, they have different ratios of transient to steady-state operation). Furthermore, data published by engine researchers or developers are frequently based on non-standard test-cycles.

1.2.1 Exhaust Aftertreatment

To meet the upcoming emissions standards, substantial reductions in emission levels from heavy-duty vehicles will be required. One of the techniques which will be critical to meeting these standards is exhaust gas aftertreatment, where harmful pollutants are removed from the exhaust stream downstream of the engine's exhaust port. In light-duty automotive applications, three-way catalytic converters have been shown to effectively reduce NO_x, CO and hydrocarbon (HC) emissions by more than 95% over a wide range of engine operating conditions [28]. These units depend on a very low concentration of oxygen in the exhaust stream to function properly. If there are significant quantities of oxygen in the exhaust (such as from typical diesel engines), the catalytic converter will function as an oxidative catalyst, oxidizing HC and CO emissions, but not reducing NO_x. Advanced strategies to reduce NO_x emissions are under development for diesel engines, including lean-NO_x traps and urea-based selective catalytic reduction [29]. A problem in applying conventional oxidative catalytic converters to natural gas fuelled engines is that CH_4 is not significantly oxidized at normal exhaust temperatures [30,31]. However, special palladium-based catalysts are under development which are capable of achieving CH_4 oxidation rates on the order of 90% in the temperature range typically found in heavy duty engine exhaust [32,33].

To reduce PM emissions, manufacturers are pursuing techniques that use filters in the exhaust stream to capture the particles. The filters need to be regenerated (heated up so that the collected carbon will be oxidized to CO_2); this is normally achieved by increasing the engine exhaust temperature or by combusting a small amount of fuel in the post-exhaust stream. Continuously regenerating traps, such as those under development by Johnson-Matthey Inc., offer the potential to oxidize the collected PM at a much lower temperature [34]. While effective, these aftertreatment devices impose a restriction on the exhaust stream, increasing the amount of work that the engine must do to expel the burned gases. However, optimizing the combustion and then using aftertreatment to remove the harmful pollutants

could improve overall system efficiency while achieving the emissions standards. Notwithstanding the above possibilities, aftertreatment system complexity and capital cost are significant issues that need to be addressed.

1.3 Natural Gas Fuelling

One alternative for fuelling heavy-duty engines, which offers both air pollution and energy diversity benefits, is the use of natural gas. Natural gas, like diesel, is a fossil-based hydrocarbon. Although estimates of the worldwide reserves of conventionally recoverable natural gas vary widely, there appear to be slightly greater energy reserves in readily extractable natural gas than there are in oil [35]. Distribution of the natural gas is a concern, with liquefied natural gas (LNG) being regarded as one alternative; for example, LNG imports into the USA have more than doubled over the past five years [36]. Other alternatives, such as gas-to-liquid (Fischer-Tropsch) conversion to create synthetic liquid fuels, require costly physical plants which are highly energy-intensive, even compared to LNG installations. Despite these concerns, by providing an alternative energy source, natural gas offers an opportunity for a more flexible and diverse energy system. Furthermore, so long as the growth in demand for liquid fuels continues, there is significant potential for economic incentives for natural gas use in transportation.

The main driving force for the consideration of natural gas as an alternative fuel in transportation has been reduced air pollutant emissions due to its relatively clean combustion. Natural gas burns at a lower temperature than most hydrocarbons, resulting in lower NO_x emissions. It also has the lowest carbon/energy ratio of all stable hydrocarbon fuels, resulting in low CO_2 emissions. In addition, its principal component, CH_4, does not have carbon-carbon molecular bonds; the result is a substantially lower probability of benzene (C_6H_6) ring formation. This reduces the formation of carcinogenic polycyclic aromatic hydrocarbons (PAH) and solid carbon particles (soot), lowering PM mass emissions [37]. A detailed discussion of the advantages and drawbacks of natural-gas fuelled heavy-duty engines is presented in Chapter 2.

One technology that is under development to use natural gas in an otherwise unmodified diesel engine is Westport Innovations Inc.'s high-pressure direct injection (HPDI^{TM}) system. This system involves an injection of natural gas directly into the combustion chamber late in the compression stroke, resulting in a non-premixed combustion

process similar to that of a traditional diesel-fuelled engine. A small quantity of diesel, injected prior to the natural gas, is used to initiate the combustion. The system has been the focus of previous research, which has shown that aggressive in-cylinder emissions control techniques can reduce emissions sufficiently to meet either the PM or NO_x standards, but not both [38]. Exhaust-gas recirculation (EGR) has been shown to be the most effective in-cylinder technique for reducing NO_x. However, substantial increases in CO and reductions in efficiency have been demonstrated at the EGR levels required to meet the 2007-10 NO_x standards [39].

Calibration of such a pilot-ignited, direct-injected natural gas (PIDING) engine over an entire test cycle has shown that diesel engine-like performance and efficiency can be achieved while PM and NO_x emissions are significantly reduced. However, further work is required to reduce emissions to the very low levels required by the 2007/2010 standards [40]. NO_x and/or PM aftertreatment may eventually be required even for this relatively clean combustion system. However, to optimize the engine system while minimizing the requirements for complex exhaust treatment equipment, it is necessary to understand the principal sources of the harmful emissions.

1.4 Objectives and Scope

The overall objective of this work was to improve understanding of the combustion and pollutant formation processes in a PIDING engine. Specific interest was placed on the degradation of the combustion process, indicated by increased cyclical variability and slower energy release rates, with intake charge dilution (EGR). The research project was experimentally-based using a single-cylinder research engine to investigate various aspects of the combustion process under moderate and high EGR conditions. Specific project objectives included to:

1) *Understand the influence of physical (mixing) and kinetic (chemical) influences on combustion rate, and the corresponding influence on emissions. Variations in injection pressure and modification of the chemical composition of the gaseous fuel were used to investigate this effect.*

2) *Investigate the role of ignition delay and combustion stability on pollutant emissions, through the addition of hydrogen to the gaseous fuel.*

3) *Explore the role of heavier hydrocarbons on ignition delay and combustion stability, and the corresponding influence on the pollutant formation process.*

4) *Identify the sensitivity of the combustion process to the overall carbon-hydrogen ratio, and identify whether specific species had a significant influence on combustion or emissions.*

5) *Examine the influence of particles recirculated with EGR on combustion instability and PM emission levels.*

By meeting these objectives, a better understanding of the pollutant formation in this engine system was to be achieved, specifically under high intake charge dilution conditions. From this, it may be possible to identify improved operating modes to optimize the combustion process, with the goal of maximizing efficiency while minimizing emissions.

1.5 Thesis Structure

Three papers have been either published or submitted for publication based on the results presented in Chapters 4, 5 and 8. The work presented in Chapters 6 and 7 are currently in preparation for submission. To avoid redundancy and to improve the readability of this work, the papers have been modified such that common elements, including background information on the combustion system and the experimental facility have been presented as separate chapters (2 and 3).

The thesis content is laid out as follows. The current chapter (Chapter 1) provides a general background and the motivation for the research. Chapter 2 provides a detailed review of the current state of knowledge regarding natural gas fuelled heavy-duty engines and of PIDING fuelling applied to heavy-duty engines. The mechanisms of pollutant formation under non-premixed natural gas combustion are also presented. In Chapter 3, a description of the experimental apparatus and procedures are supplied. Then, Chapter 4 presents the effects of increasing the in-cylinder turbulence through higher injection pressures on the combustion process. In Chapter 5, the effect of enhancing local diffusion and flame stability in a non-premixed gaseous jet through the addition of hydrogen to the fuel is examined. Chapter 6 discusses the effect of various fuel compositions on the overall combustion process, focusing on the effects of heavier hydrocarbons on ignition delay time and particle formation. The effect of diluting the fuel with nitrogen on combustion and pollutant formation is explored in Chapter 7. Chapter 8 discusses the effect of recirculated particulate on the combustion

process, and specifically identifies its role in the formation of new particles. Finally, a summary of the main conclusions from the thesis and suggestions for future work are provided in Chapter 9. The tables and figures for each study are provided at the end of the corresponding chapter; references are numbered sequentially from the beginning of the thesis and are located after Chapter 9. Appendices provide further information on the experimental apparatus, procedures, and more details regarding the experimental results.

1.6 Tables and Figures

Table 1.1: Heavy-Duty Engine Emissions Standards, in g/kWhr

Country	USA [25]	Canada [26]	Europe* [27]		Japan [27]	India [27]	China [27]
Year into effect	2007-2010	2007-2010	2008		2005	2010	2002
Standard			Euro V			Euro III	Euro II
CO	20.8	20.8	4.0	1.5	2.22	2.1	4.0
nmHC	0.19	0.19	0.55	0.46†	0.17	0.66†	1.1†
CH_4			1.1‡				
NO_x	0.27	0.27	2.0	2.0	2.0	5.0	7.0
PM	0.013	0.013	0.03	0.02	0.027	0.1	0.15

* - *all engines are to meet both stationary (left) and transient (right) test cycle limits*

† - *total hydrocarbons (including CH_4 and nmHC)*

‡ - *natural gas fuelled heavy-duty engines only*

Note: Levels are not directly comparable, as they are based on different test cycles

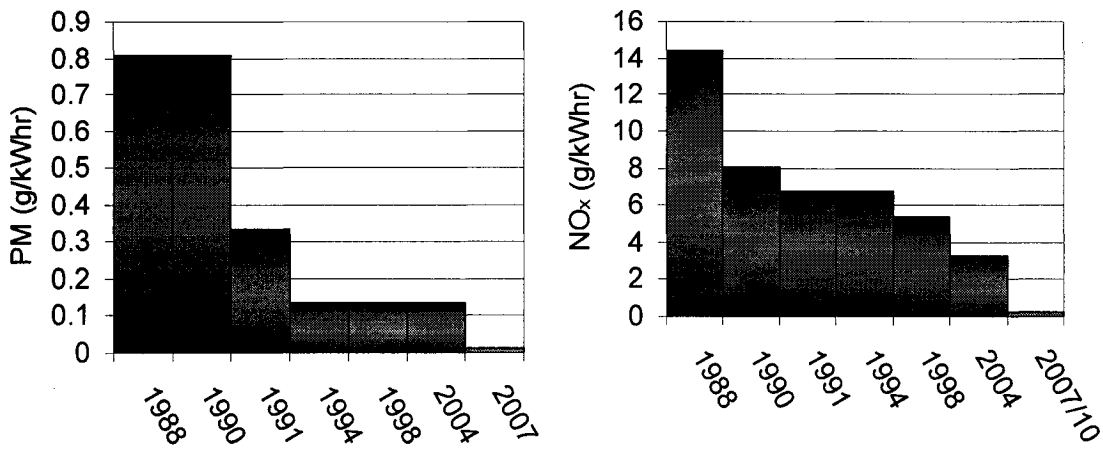

Figure 1.1: US EPA Heavy-Duty Engine Emission Standards, 1988-2010 [25]

Chapter 2
Background Information

Heavy-duty engines fuelled with natural gas provide an opportunity to achieve substantial air pollution benefits compared to conventional fuelling. Furthermore, price differences between natural gas and diesel provide a significant economic incentive for alternative fuelling in some markets. Today, substantial numbers of heavy-duty vehicles, notably in urban transit bus fleets, are fuelled with natural gas. To evaluate the benefits of natural gas fuelling, a number of studies have compared the emissions and performance of natural gas engines to traditional diesel-fuelled engines. Currently, the next generation of more efficient, less polluting natural gas vehicles is under development. One promising technology, which is the focus of this thesis, is pilot-ignited, direct-injected natural gas (PIDING) fuelling. This chapter is intended to provide an overview of the current status of in-service gaseous-fuelled heavy-duty engines, to identify some of the promising technologies for future generations of gaseous fuelled engines, and to review the current state-of-knowledge regarding gaseous combustion under conditions typically found in heavy-duty engines.

2.1 Gaseous Fuelling of HD Engines

A wide range of engine technologies is either in use or under development for gaseous fuelling of heavy-duty engines. One fundamental distinction in these technologies is the method of delivering the fuel to the engine. In externally premixed charge engines (as for most automotive gasoline engines), the fuel is mixed with the air before it is ingested into the cylinder. In direct-injection engines (as in diesel engines), the fuel is injected directly into the combustion chamber just before the combustion is initiated.

A second important distinction is the relative amounts of fuel and oxidizer which are present in the combustion chamber (the stoichiometry). A stoichiometric mixture is when there is just enough oxygen in the combustion chamber to oxidize all the fuel to final products (CO_2 & H_2O). This is the approach typically used in gasoline engines. In the case of lean fuel-air mixtures, there is more oxygen than is needed to burn all the fuel. Virtually all direct-injection engines operate at an overall lean mixture ratio, even at full load.

A key factor in the pursuit of an optimal fuelling technology is the inherent differences in the combustion characteristics of diesel versus natural gas. An important property of natural gas is that it is more resistant to auto-ignition ('engine knock') than most liquid hydrocarbons. This allows premixed natural gas engines to operate at compression ratios as high as 14:1, resulting in higher efficiencies [41]. Conversely, this resistance to auto-ignition results in one of the principal barriers to using natural gas in a compression ignition engine, where the cylinder temperature and pressure are insufficient for the fuel to auto-ignite. Typical ignition delay times for diesel fuel are repeatable and are on the order of 1 ms [42]. Experimental studies have shown that natural gas ignition delay times, under conditions similar to those found in a diesel engine, exceed 5 ms and are highly variable [43]. To overcome this ignition uncertainty in natural gas fuelled engines, a separate reliable ignition source is required.

2.1.1 Premixed technologies

Adding the fuel to the air before it is ingested into the cylinder has a number of benefits, including lower fuel pressures, which reduces parasitic compressor work. The intake and compression strokes also allow time for the fuel to mix with the air, resulting in a nearly homogeneous mixture. However, the need to avoid premature autoignition of the fuel (which can damage the engine) limits the maximum compression ratio to less than that of a diesel engine [41], reducing the engine's theoretical maximum efficiency. A further barrier is the need for a higher-energy spark system to provide reliable ignition of lean natural gas mixtures at high compression ratios [44]. These high-energy ignition systems require a higher voltage input and have increased maintenance requirements.

Lean-Burn with Spark Ignition

The most common natural gas fuelled heavy-duty engines use lean premixed mixtures with a spark ignition system. With lean operation, the throttle (typically used to maintain stoichiometric mixture fractions) is used less, reducing the work required to ingest the fresh charge. However, as the mixture becomes leaner, the rate at which the flame propagates through the combustion chamber is reduced, lengthening the total duration of the combustion event. For very lean mixtures, the flame propagation rate is so slow that the combustion will be terminated by the expansion of the combustion gases in the power stroke before all the fuel-air mixture is consumed. While techniques such as artificially creating a rich mixture in

the vicinity of the spark plug improve the strength of the flame kernel and thereby reduce the overall combustion duration, they do not significantly affect the flame propagation rate [45,46].

Manufacturers currently (spring 2006) offering heavy-duty spark-ignition lean-burn natural gas fuelled engines include John Deere, MAN, and Cummins-Westport. Detroit Diesel's Series 50G and 60G natural gas engines (200-300 kW) appear to be no longer in production. John Deere's 8.1L 6081 series (187-209 kW) is certified at the California Air Resources Board optional low NO_x level, with emissions of 1.6 g/kWhr combined NO_x and non-methane hydrocarbons (nmHC) using an oxidation catalyst for CO and nmHC control [47]. MAN produces a 12L, 180-228 kW engine rated to EURO III standards [48]. Cummins-Westport offers a series of natural gas engines, with the B-gas (5.9L displacement, 145-172 kW), C-gas (8.3L, 186-205 kW), and L-gas (8.9L, 239 kW) engines all using oxidation catalysts. The Cummins-Westport engines are also certified at the optional low-NO_x levels, with NO_x+nmHC emissions of 2.4 g/kWhr (B&C-gas) and 1.88g/kWhr (L-gas) and PM emissions certification at US EPA 2010 levels of 0.013 g/kWhr [49].

A number of studies have compared emissions and performance of in-use natural gas fuelled engines with equivalent conventional medium and heavy-duty diesel-fuelled engines. A summary of some of these studies involving both urban transit buses and trucks is shown in Table 2.1. In most of the studies, multiple 'identical' vehicles were tested to reduce the influence of vehicle-to-vehicle variability. The studies used a range of vehicle test cycles, with some of the studies carrying out tests on two or more cycles (for these studies, the range of results is indicated in the table).

A consistent reduction in PM and NO_x emissions was observed with the natural gas fuelled engines. However, a significant loss in efficiency with natural gas fuelling was observed, although in most cases the net CO_2 emissions were somewhat reduced due to the lower carbon content of the natural gas. The loss in efficiency was primarily attributed to lower compression ratios (reduced from their diesel-engine levels to avoid engine knock) and high unburned fuel emissions at light load conditions. Emissions of nmHC varied substantially between the tests; Chandler *et al.* [50] showed a significant nmHC reduction with natural gas fuelling, while the rest of the studies indicated increases that ranged from a few percent to over an order of magnitude. Those studies with the largest increases in nmHC

(such as Ayala *et al.* [51]) typically used older model natural-gas engines without oxidative aftertreatment.

The effectiveness of oxidation catalysts used with lean-burn natural gas engines was shown by Frailey *et al.* [52], where one of three otherwise identical test vehicles was not equipped with an oxidation catalyst. CO, PM, and nmHC emissions were factors of 20, 8, and 4 higher, respectively, for the vehicle without the catalytic converter. McCormick *et al.* [53] report that conventional oxidation catalysts were found to effectively reduce emissions levels of all non-methane hydrocarbon emissions. Aldehyde emissions were measured, and were found to have mass ratios between 7% and 30% of the nmHC emissions, with lower ratios for more modern engines equipped with oxidation catalysts. Compared to the reference diesels, the nmHC emissions from the natural gas engines were found to have higher masses but were, generally, less toxic and had a lower smog-forming potential [53].

Kado *et al.* [54] found that PAH emissions (semi-volatile and particle-associated) were generally lower for natural gas engines than for diesels. Seagrave *et al.* [55] indicated that the mutagenicity of PM from newer-model natural gas engines equipped with oxidation catalysts was in general substantially lower than from equivalent diesel engines and was similar to low-emission gasoline engines. Holmen and Ayala [56] reported that using a natural gas engine with an oxidation catalyst resulted in particle number concentrations 10-100 times less than from diesel engines.

Only Chandler *et al.* [50] and Kamel *et al.* [57] reported total HC (including methane) values, at levels of 10.9-13.4 g/km and 3.7-6.2 g/km, respectively. Both studies indicated that greater than 95% of the HC's were methane. Although methane emissions are currently unregulated in North America, they are of concern due to methane's role as a greenhouse gas (21 times as absorptive of infra-red radiation as CO_2) [6]. By combining the CH_4 and CO_2 emissions, the net infrared absorption potential of the exhaust was increased by 3-7% (Kamel *et al.*) and by 25-40% (Chandler *et al.*). These studies suggest that older-model natural gas engines generate a net greenhouse gas increase when compared to diesel engines, especially in transport truck applications. A large contribution to this is that the efficiency of the natural gas engines is 20-30% lower than the equivalent diesel, due to throttled operation at idle and light load. The effect is substantially less significant for more modern natural gas engines with better low-load combustion control. A recent study released by the National Renewable

Energy Lab (NREL) reports that, in a comparison between modern natural gas (2001 Cummins-Westport and 2004 John Deere) and diesel (2003 Detroit Diesel Corporation) powered buses, net infrared absorption potential is 20-25% lower for the natural gas fuelled vehicles [58]. The main reason for the difference was that, on the urban transit bus test cycle used in the NREL study, the natural gas engines were only approximately 4% less efficient than the diesels. A further example of the effect of vehicle useage on efficiency is evident when comparing the Chandler *et al.* [50] and McCormick *et al.* [53] studies. McCormick *et al.* report natural-gas fuelled vehicle efficiencies approaching those of diesel engines over certain bus test cycles, while Chandler *et al.* report efficiency more than 30% worse on an urban heavy truck test cycle using very similar natural-gas fuelled engines.

Stoichiometric with Spark Ignition

The primary benefit of using premixed stoichiometric combustion is that an automotive style three-way catalytic converter can be used, allowing substantial reductions in CO, NO_x, and HC emissions. The major disadvantage of such an approach from a commercial perspective is the need for an intake throttle to carefully control the mass of air inducted into the engine at all load conditions, resulting in a significant reduction in efficiency. MAN produces a stoichiometric version of its 12L engine that meets European enhanced environmentally friendly vehicle (EEV) regulations [48]. Of the studies outlined in Table 2.1 only Chiu *et al.* [59] studied the effects of stoichiometric operation with a three-way catalyst. NO_x (0.2 g/kWhr), CO and nmHC were below 2010 levels although PM (0.02 g/kWhr) was above the standard. Efficiency penalties of 10-25% were observed compared to the lean-burn engines. Nellen and Boulouchos [60] demonstrated the use of EGR in place of a throttle on a small (300kW) stationary engine. Low emissions with diesel-like efficiencies were achieved at steady state; however, the aptitude of this method to cope with transient operation was not investigated and unburned methane emissions were not reported.

Lean Burn with Pilot Ignition

Another ignition option that has been suggested for homogenous charge engines is the use of a diesel pilot injection. The pilot fuel will auto-ignite after injection, leading to near-simultaneous ignition of the natural gas charge at multiple points centrally located in the combustion chamber. This results in a more rapid combustion of the premixed charge, leading to lower unburned hydrocarbon emissions and improved efficiency at part load [61].

Manufacturers including Wartsila [62], Fairbanks-Morse [63] and MAN [64] have developed homogenous charge pilot ignition systems for larger stationary and marine applications (>1MW). For heavy-duty on road automotive applications, Park *et al.* [61] have reported full-load efficiencies higher than an equivalent diesel engine, at the expense of increased NO_x emissions. Singh *et al.* [65] and Zuo and Yang [66] showed that even with pilot injection, lean air-fuel mixtures at light load resulted in increased HC emissions and reduced efficiency due to reduced flame propagation rates. Shenghua *et al.* [67] suggested that pure diesel operation (no natural gas) was required at low loads to avoid over-lean charge mixtures. All the studies indicated reductions in NO_x and PM could be achieved, at the expense of efficiency and CO and HC emissions [67,68].

An application of lean premixed natural gas with diesel pilot ignition in a commercial setting is the Dual-Fuel™ system, under development by Clean Air Power Inc. This system has been applied to a Caterpillar C-12 engine, whose performance emissions were evaluated over the European Stationary Cycle 13 mode steady-state test cycle. NO_x emissions of 0.72 g/kWhr and PM levels of 0.0054 g/kWhr were achieved in conjunction with a particulate filter [69]. Brake-specific energy consumption roughly equivalent to 249 g of diesel per kWhr (based on a diesel heating value of 43.2 MJ/kg [28]), was reported, approximately 7% greater than the baseline diesel [69]. To improve low-load performance, skip-firing (where natural gas was supplied to only four of the six cylinders) and a compressor bypass system on the turbocharger were used. Despite these efforts, high hydrocarbon emissions were still observed at part-load conditions, due to slow flame propagation in the premixed lean mixture.

Lean Burn with Compression Ignition

A different ignition concept is that of homogenous charge compression ignition (HCCI) where the premixed charge auto-ignites in the high temperatures and pressures found at the end of the compression stroke. Combustion stability and control have proven to be substantial barriers, while the need to avoid excessive in-cylinder pressures limit its use to low and moderate load conditions [70]. Various methods have been suggested to overcome the variable auto-ignition characteristics of natural gas, including blending with a second fuel (for example, naptha) before the fuel is ingested [71] and the careful control of recirculated

exhaust gases [72]. Significant issues of reliability and control under transient operating conditions remain to be resolved.

2.1.2 Direct Injection Technologies

Natural gas may also be directly injected into the combustion chamber late in the compression stroke, similar to the fuel injection in diesel engines. This results in a primarily non-premixed combustion of a turbulent gaseous jet. Due to the poor auto-ignition qualities of natural gas, a separate ignition source is required to achieve reliable and repeatable combustion initiation.

Direct Injection with Spark Ignition

Using a spark plug as the ignition source has been suggested for direct-injected natural gas. For successful ignition, there needs to be the right proportion of fuel and air in the vicinity of the spark plug at the time of the spark discharge. Preliminary research carried out in quiescent combustion chambers has shown that the spark can repeatably ignite a non-premixed natural gas jet [73]. For real combustion chambers, where charge motion is significant, reliable ignition at different engine operating conditions is challenging to achieve. Changes in charge motion with operating condition and engine age affect the mixing status of the jet in the vicinity of the spark plug, resulting in degradation of the combustion event. Similar difficulties have been encountered in gasoline fuelled, light-duty direct-injection spark ignition engines, where careful optimization of the combustion system and spark timing control has been required to maintain stable operation [74]. Further drawbacks of this system include the fact that the flame is initiated close to the combustion chamber wall, and hence has to propagate from a single remote point through the rest of the combustible mixture. Failure to achieve ignition also results in misfire and high emissions of unburned fuel.

Direct Injection with Hot Surface Ignition

Using a hot surface igniter in a direct-injection engine overcomes some of the difficulties encountered with timing the spark discharge. A continuous transfer of heat is supplied to the charge in the vicinity of the injected fuel. Aesoy & Valland [75] demonstrated that efficiencies higher than those of an equivalent diesel engine could be achieved with direct injection of natural gas and a hot surface igniter. Surface temperatures of 1200-1400 K

were required, and careful control of the injection process was necessary to achieve stable combustion. Caterpillar [76] demonstrated the application of hot surface ignition of direct-injected natural gas for a heavy-duty engine. Reductions in engine-out NO_x were achieved, at the expense of efficiency. Difficulties in ensuring repeatable ignition over a range of operating conditions were also reported [77].

Isuzu and Westport Innovations Inc. [78] have developed a direct-injection of natural gas hot-surface ignition system for a 4.5 L (100 kW) medium-duty diesel engine. Reductions in emissions were reported compared to the standard diesel engine, with no effect on efficiency. This system included an oxidation catalyst (modified to oxidize CH_4) and a separate selective catalytic reduction system for NO_x control. Low emissions of NO_x, nmHC, and CO_2 were observed; CO_2 emissions of 631 g/kWhr were particularly noticeable, given that conventional lean burn natural gas engines emit on the order of 800 g/kWhr CO_2 [78]. While hot surface ignition is promising, the longevity and reliability of the hot-surface materials, which are held at high temperatures for extended periods, are not yet known.

Direction Injection with Pilot Ignition

Using a diesel pilot spray as the ignition source for a non-premixed natural gas jet has also been proposed. Initial development of systems which directly inject both diesel and natural gas fuels have been carried out by Wartsila Engines, for 6-12 MW marine and stationary engines, and by Westport Innovations Inc., for heavy-duty transportation and smaller stationary power generation applications. A single concentric-needle injector is used to inject both fuels. The natural gas fuel is typically injected shortly before the diesel pilot injection (Wartsila) or after it (Westport). This system results in improved efficiency and higher power densities, as well as less sensitivity to natural gas composition, compared to other natural gas technologies [46].

Westport Innovations Inc.'s High Pressure Direct Injection (HPDI^{TM}) system has demonstrated low NO_x emissions levels while retaining diesel engine efficiency through the use of recirculated exhaust gases and careful operating condition optimization. NO_x emissions levels of 0.8 g/kWhr and PM of 0.04 g/kWhr were achieved in transient tests using an oxidation catalyst [40]. Due to poor transient response of the recirculated exhaust gas system, NO_x levels were higher than had been found from an ESC-13 mode steady-state cycle test (0.48 g/kWhr). Further modifications of the injection control processes during

transient conditions may permit improved control over emissions levels. The reliability of the combustion system has been demonstrated in a series of long-duration commercial tests [79,80]. In March 2006, the engine was certified by the California Air Resources Board to meet the 2007-2009 heavy-duty engine phase in requirements for NO_x+nmHC, at 1.6 g/kWhr; PM emissions, at 0.027 g/bkWhr still exceed the 2007 requirements [81].

Premixed and Direct Injection with Compression Ignition

Based on Westport's HPDI^{TM} combustion system, research has also been pursued on a combined system that includes a premixed lean natural gas charge [82]. A carefully controlled injection of diesel pilot early in the compression stroke results in HCCI-like combustion of the premixed fuel-air charge (where the fuel is a mixture of natural gas and evaporated diesel). To increase the engine's power without excessive cylinder pressures, an injection of natural gas shortly after the peak of the premixed combustion event results in non-premixed combustion of this gaseous jet. This later combustion does not significantly increase the peak pressure, but it does significantly increase the net power output. In a stationary power generation system (1.6 – 2 MW), NO_x levels of 0.67 g/kWhr were achieved at diesel-like efficiencies and power densities. Emissions were generally low, with CO_2 levels of 480-520 g/kWhr, CH_4 of 3.75-4.15 g/kWhr, nmHC of 0.54 g/kWhr, and CO of 1.5-2.7 g/kWhr; PM emissions were not reported [82]. Similar developmental results were demonstrated on a 19L 6-cylinder engine.

2.2 Non-Premixed Gaseous Combustion

The various technologies which are either in use or under development for fuelling heavy-duty engines with natural gas all involve significant tradeoffs. Premixed-charge engines face reduced efficiency and high unburned fuel emissions at part load. Late-cycle direct-injection technologies, while more efficient, are harder to ignite. A fixed ignition source (spark or hot-surface) is faced with the challenge of reliably igniting the injected fuel at the desired time. A pilot injection provides better control over the timing and location of the ignition event. This system is, arguably, the most promising of the developmental natural-gas technologies. Unfortunately, the combustion system is based on the non-premixed combustion of a turbulent high-pressure gaseous jet, which has not been as extensively studied as other more typical combustion systems. As such, understanding of the combustion

process, and in particular of the pollutant formation mechanisms, is not as well developed as that of either liquid diesel fuelled systems or of premixed combustion systems.

2.2.1 Combustion Structure

The general structure of combustion in a PIDING system can be divided conceptually into three separate (although overlapping) regimes. The first regime involves the pre-combustion phase, where natural gas is injected into the (relatively) cold oxidizer. The natural gas jet behaves generally as described by Turner [83], with a travelling vortex ball preceding a quasi-steady state jet. Both Hill and Ouellette [84] and Rubas *et al.* [77] have applied this general model to natural gas injection into a diesel engine. These studies have indicated that air entrainment is restricted to the quasi-steady jet with little entrainment into the leading ball. A more recent study by Cossali *et al.* suggested that treating the leading portion as a toroidal structure rather than a ball was more appropriate [85]. Further, significant entrainment of air into the head of the jet was identified during the early stages of the injection process. These processes are not limited to natural gas; similar results have also been identified for transient hydrogen jets [86].

The momentum of the injected fluid provides the principal impetus for the jet propagation. Momentum transfer to the head from the jet increases the size of the head, and the corresponding diameter of the jet, as it extends into the combustion chamber. Prior to ignition, oxidizer will be mixing into the jet, with a general distribution from nearly pure fuel at the core of the jet to a steadily weaker mixture at the jet perimeter. Turbulent mixing will result in spatial and temporal non-uniformity in the mixture fraction around the jet. The total mass in the jet ($\dot{m}(x)$), including both fuel and entrained oxidizer, at a given downstream distance x is given by [84]:

$$\dot{m}(x) = \dot{m}_0 K_s \frac{x}{d}, \tag{2.1}$$

where $\dot{m}_0$ is the mass rate of injected fuel, K_s is a constant (0.32) and d is the diameter of the nozzle.

The location of the external ignition source strongly influences the ignition of the natural gas jet. Typically, the ignition will occur along the sides of the quasi-steady jet rather than in the region of the vortex head [87,88,89]. The flame then propagates from the ignition source through the combustible mixture on the outer periphery of the gas jet. Once the

premixed mixture has been consumed, the flame stabilizes into a non-premixed turbulent gaseous jet flame, which may be considered to be the second quasi-steady stage of the combustion event. Fuel diffuses towards the flame front from the core of the jet while oxidizer diffuses towards the core from the surroundings. The reaction zone will be a surface (fluctuating with turbulent perturbations) around the jet, where the fuel-air mixture is at a near-stoichiometric ratio. Due to the high relative velocity between the gas and the oxidizer at the nozzle exit, and the correspondingly high local strain rates, the flame is lifted from the nozzle. A short distance downstream, the 'lifted' jet burns, in the form of a triple flame. A rich premixed phase (oxidizing air entrained in the lifted section of the jet) burns towards the core of the jet, while a lean premixed flame burns towards the oxidizer. This combustion event 'anchors' the non-premixed flame [90]. Only a small amount of oxidizer mixes into the fuel jet before the triple-flame. As a result the rich combustion zone is limited in extent. Therefore, after ignition the jet contains virtually pure fuel, with only small quantities of oxidizer or combustion by-products.

The third combustion phase occurs at the end of injection. As the injector needle closes, the rate at which fuel is added, and its corresponding momentum transfer, to the jet diminishes rapidly. Effectively, the separated jet now acts as a 'puff' jet [84]. Mixing of the tail end of the jet with oxidizer results in combustion spreading around the fuel cloud, which continues to mix and burn as its momentum carries it away from the nozzle. The combustion process will end when either there is insufficient fuel to sustain the reactions, insufficient oxidizer (which should not occur for diesel-type engines) or when the bulk expansion of the combustion gases (due to the motion of the piston in the power stroke) lowers the temperature of the reactants sufficiently that the reactions are no longer self-sustaining.

The relative importance of these three phases depends on the relative durations of the ignition delay and the injection processes. If ignition does not occur until near the end of the injection, the combustion will never develop into the quasi-steady jet, and will instead only burn as a partially premixed cloud. Therefore, processes which either increase the ignition delay or reduce the injection duration tend to reduce the importance of the quasi-steady mixing-controlled component of the combustion event.

2.2.2 Oxides of Nitrogen

The mechanisms by which NO_x are formed in internal-combustion engines are well understood [28,37]. The bulk of the NO_x is formed as nitrogen oxide (NO) in the combustion chamber, some of which will react to NO_2 during the exhaust process. Some NO_2 may also be formed directly in the combustion chamber. The primary mechanism for NO formation is the thermal (Zeldovich) mechanism [37]. This mechanism is highly dependent on temperature due to the high activation energy of its rate-limiting step. The thermal mechanism is also slow, such that not only high temperatures, but a long (on engine time-scales) residence time at those temperatures is required to reach equilibrium. Due to the turbulent mixing between burned gases and cool unburned charge which typically occurs in diesel engines, the thermal mechanism does not normally reach equilibrium conditions. However, it is still the dominant formation mechanism under most conditions.

Other NO formation mechanisms include the prompt and nitrous oxide routes [37]. The prompt mechanism results in the immediate formation of NO within the flame zone, unlike the thermal mechanism which, due to its low initial rate, does not contribute significantly to flame-front NO. This prompt mechanism involves the reaction of the CH radical with an N_2 molecule to form a series of intermediate species which may eventually form NO. The controlling factor of this reaction is the CH radical, which is highly reactive and is typically found only within the flame region. The nitrous oxide (N_2O) route involves the reaction of N_2 with an oxygen radical and a third body to form N_2O ($N_2 + O + M \rightarrow N_2O + M$). The N_2O will then react with another oxygen atom to form two NO molecules. This reaction is limited by the oxygen radical concentration. Typically, it is only significant between 1000 and 2000 K, where there is a non-negligible quantity of O but where the thermal mechanism rate is very slow.

A fourth source of NO that is discussed in the literature [37] is the fuel-bound NO route. This mechanism is most significant for fuels where significant quantities of atomic nitrogen are chemically bound in the fuel, such as coal or ammonia. Although natural gas may contain significant quantities of nitrogen, it is typically as molecular nitrogen (N_2) and hence participates in the NO forming reactions similarly to the N_2 in the oxidizer.

Not all the NO produced in the combustion will be emitted, as some will decompose later in the process. One proposed mechanism for this is a reaction with the HCCO radical,

which reacts with NO to form HCN and CO_2 [91]. As the HCCO radical is present in significant quantities within the flame zone, in a non-premixed flame, where some of the burned gases (which contain NO) may pass through the reaction zone again, some of that NO will be removed. Another route proposed for NO decomposition in diesel engines is the reverse of the thermal and prompt mechanisms [92,93]. Independent of which mechanism is dominant, these results indicate that a small but significant quantity of the NO contained in the oxidizer when using recirculated exhaust gases will be decomposed in the combustion reaction. How much of the species formed in the decomposition then recombine to form NO is unclear.

2.2.3 Carbon Monoxide

Carbon monoxide is one of the main intermediate species in the oxidation of hydrocarbon fuels to CO_2. In both stoichiometric and rich (overall) combustion conditions, CO results from a lack of oxygen in the reaction chamber. However, in a system which is overall lean, there should always be sufficient oxygen present to oxidize the CO. From such systems, CO is emitted when the fuel-air mixing is insufficient to provide enough oxygen to the reaction zone to oxidize the CO to CO_2. The oxidation of CO can be stopped if the temperature in the reaction zone falls too far. As a result, events which quench the combustion will tend to result in increases in CO emissions. Typically, CO is not a significant concern for direct-injection engines in stable operation [28]. However, in engines operating under more extreme operating conditions (such as in excess of 50% EGR), high CO emissions do start to become a concern [128].

2.2.4 Hydrocarbons

The bulk of the HC emitted from natural gas engines is in the form of unburned methane [50,57]. One potential source of hydrocarbons is unburned fuel retained in the injector sac and nozzle holes, which will gradually enter the combustion chamber as the pressure drops during the expansion stroke. Another potential source is overleaning of the methane which was injected early in the cycle [28]. Some of this may have mixed beyond the lean limit of combustion before ignition occurs. Depending on the amount of excess air and the charge motion, some of this ultra-lean premixed mixture will participate in the combustion event from the oxidizer side. However, some may also be dispersed to the walls or crevices of the combustion chamber, and hence avoid being consumed. Bulk quenching at

the end of the combustion event is also a potential source of unreacted fuel. This occurs in the case of retarded combustion, where the pressure and temperature in the combustion chamber fall as a result of the motion of the piston in the expansion stroke. As the combustion chamber cools, the energy released during the combustion event will be insufficient to maintain the reactions, resulting in unreacted fuel and partial combustion by-products being emitted. This process can be minimized by enhanced late-combustion burn-up, potentially through higher turbulence intensities. Local extinction events caused by excessively high turbulent strain rates may also result in higher hydrocarbon emissions. In the case of local extinction events, 'holes' are created in the flame front through which unreacted fuel and partially reacted species (including CO and PM) may enter the oxidizer [37]. Some of these species will be reacted later in the combustion event; however, some may escape and be emitted. Flame extinction due to high heat losses as the flame approaches a wall (or a cold piston) is also a potential source of unburned hydrocarbons, as is penetration of the fuel jet into the relatively narrow and cold 'squish' region. Studies have suggested that, in the case of liquid fuels, these are significant sources of unburned hydrocarbon emissions due to impaired evaporation of the fuel [94]: while this effect could be expected to be less significant for a gaseous fuel, it is still potentially important. The relative importance of these different hydrocarbon emission sources remains to be clarified.

While methane is the dominant HC emission from a HD natural-gas fuelled engine, emissions of other species are also of potential concern. Aldehydes, and specifically formaldehyde (CH_2O), are a significant health concern. They are also key intermediates in the methane oxidation pathway [37]. Other higher-order hydrocarbons may also be formed, as a significant proportion of CH_4 will pass through ethane (C_2H_6) during the oxidation process. This can lead to the formation of C_2H_2 (acetylene) which is a precursor for the formation of polycyclic aromatic hydrocarbons (PAH's) as well as for carbonaceous particles.

2.2.5 Particulate Matter

Particulate Matter emitted from direct-injection compression ignition engines is composed of a wide range of species, including volatile organics, solid carbon, metallic oxides or ash, and sulphates [18]. The relative fractions of these species vary as a function of, among other parameters, engine age and technology, fuel formulation, and engine operating

condition. The volatile organics are typically derived from unburned liquid fuel and lubricating oil, which has evaporated in the high-temperature combustion chamber and then recondenses during the expansion stroke or in the exhaust stream. These species are typically oxygenated or nitrated PAHs. Ash is formed from metallic compounds, primarily either additives or wear particles in the lubricating oil. Sulphates are formed from the sulphur in the diesel fuel, a small fraction of which is oxidized to SO_3, some of which then reacts with water vapour to form H_2SO_4. This sulphuric acid then reacts in the exhaust and dilution processes to form sulphate particles [95]. It has been estimated that on the order of 4% of the sulphur in the fuel is converted to H_2SO_4 [96]. Because of the low sulphur content of natural gas (on the order of 1 ppm [97]), sulphate formation from the fuel is not a significant concern for a direct-injection natural gas combustion process [98]. Other sources, such as diesel pilot fuel and lubricating oil, will be the primary contributors to sulphate emissions. However, it should be noted that sulphur contribution from the lubricating oil for a heavy-duty engine has been estimated at approximately the equivalent of 20-50 ppm sulphur in the fuel [99]. This level was estimated to be below the level required to allow sulphate nucleation in the exhaust stream.

Solid carbon (soot) is historically the greatest contributor to high-load PM emissions [18]; it is also the most widely studied component of PM. The formation mechanisms for soot in diesel engines are thought to be sufficiently well understood to allow the development of semi-empirical predictive models [100,101]. Understanding of the soot formation processes in high pressure, turbulent, non-premixed methane/air flames is not as well developed. However, the processes have many similarities; as a result, a short description of the current state of knowledge of the soot formation process in diesel engines is relevant.

Soot Formation in Diesel Engines

Diesel soot formation is a result of high-temperature fuel rich oxidation processes. As the liquid spray is injected, it entrains high-temperature air. As the diesel droplets evaporate, the hydrocarbon vapours mix with the surrounding air to form a fuel-rich mixture. This fuel-rich mixture will then undergo an exothermic reaction where the available oxygen is consumed [102]. However, as there is insufficient oxygen for the reactions to proceed to completion, long chain hydrocarbons such as PAHs and polyynes are present in this high-temperature environment. Through the widely accepted HACA (hydrogen abstraction

acetylene addition) mechanism, hydrogen atoms react with the aromatic species, removing a hydrogen atom from the aromatic. This is followed by the addition of an acetylene molecule to the aromatic in place of the removed hydrogen atom [100]. Repeated steps of this process result in the growth of the aromatic PAH molecule. Particle inception occurs as PAH molecules collide and bind at the same time as they continue to grow via the HACA mechanism. The exact point at which the agglomerated PAH molecules form an actual particle is a subject of some debate [6].

Another mechanism which has been proposed for pyrolitic (oxygen-deficient) formation of soot is the polyyne model (polyynes are hydrocarbon species of the form $C_{2n}H_2$, where n is any positive integer greater than 1) [103]. This model suggests that polyynes grow relatively quickly through the addition of C_2H radicals, releasing a hydrogen radical from the polyyne structure in the process. Particulate inception occurs at some stage during the ongoing growth of the polyyne molecule by polymerization of supersaturated polyyne vapours.

While these models differ in detail, in general they agree that formation of soot particles occurs in fuel-rich environments where reactive hydrocarbon species, including acetylene and other radicals, are in abundance. Once the particles pass into a more oxidative environment, oxidation by O_2 and the OH radical occurs [100]. Oxidation of particles emitted from diesel engines has been shown to be substantially different from that of pure graphite particles, possibly due to the presence of metallic ash and other non-hydrocarbon species in the diesel particles [104,105].

PM Formation in Methane Combustion

The principal difference between diesel and methane soot formation is that for methane, recombination reactions are required to form C_2 and higher hydrocarbons. For soot formation from methane, the initial stage involves reacting CH_4 to CH_3 through H, O, or OH radical reactions [37]. Methyl (CH_3) radical concentration has been identified as a key factor in promoting the formation of aromatic rings [106]. If two CH_3 molecules react, then either an ethyl (C_2H_5) or a C_2H_6 molecule may be formed. Hydrogen abstraction from this molecule leads to C_2H_2 [37]. While most of the C_2H_2 will be oxidized by an oxygen radical to form CO and CH_2, some of the C_2H_2 may react to form benzene (C_6H_6), the base ring structure for the formation of PAH's. The relative amount of CH_4 that is converted into C_2 containing

molecules varies with temperature, pressure, and mixture stoichiometry, but can be as high as 80% [37].

Although soot formation in methane flames under diesel-engine conditions has not been extensively investigated, a number of studies have looked at soot formation from methane at a more fundamental level. McCain and Roberts [107] and Thomson *et al.* [108] have studied the role of system pressure on a laminar methane diffusion flame. Both studies showed soot varying with pressure raised to an exponent between one and two (P^y, with $1<y<2$), for pressures from atmospheric to 2 MPa. At pressures between 2 and 4 MPa, the pressure sensitivity of the soot formation process was significantly reduced (exponential factor y approximately 0.1) [108], suggesting that at higher pressures, variations in pressure will have less impact on soot formation. For a turbulent non-premixed methane flame, Brooks and Moss demonstrated that increasing the pressure from 0.1 to 0.3 MPa increased soot volume fraction by almost an order of magnitude [109]. The effect of turbulence was investigated by Bohm *et al.* [110], who found that increasing turbulent strain reduced the formation of soot due to reductions in the formation of PAH precursors (C_2H_2, C_3H_3) as well as enhancing soot oxidation. The applicability of these results to turbulent non-premixed combustion in an engine environment is unclear; however it is apparent that the fluid dynamics of the reacting system will have a strong influence on particulate formation.

The effect of fuel-oxidizer ratio was studied using rich premixed mixtures by Skjoth-Rasmussen *et al.* [111], who found that at low pressures a soot inception limit was approached at a oxygen-to-carbon ratio of ~0.5 (that is, when there were more than ~2 oxygen atoms per carbon atom, soot formation would not occur). They also identified that soot and soot precursor (C_6H_6, C_2H_2) formation were maximized at temperatures around 1500K. At low temperatures, the collected particulate was primarily agglomerated PAH's, while at higher temperatures the PM was carbonaceous soot. The effects of mixture stoichiometry and temperature were also studied by Gruenberger *et al.*, using an atmospheric pressure non-premixed burner apparatus [112]. They found that both incomplete combustion and thermal decomposition could be significant contributors to carbonaceous soot emissions from natural gas combustion. Thermal decomposition was found to lead to solid carbon formation in highly fuel-rich regions, but much of this carbon was oxidized in the flame front. Solid carbon was also formed in the reaction zone due to incomplete oxidation

processes. Both processes were found to be enhanced at higher temperature, although the oxidation of soot formed from thermal decomposition was also hastened. The thermal decomposition was found to have a temperature limit (dependent on stoichiometry) below which soot production did not occur. Although these results are not directly applicable to high-pressure non-premixed diffusion flames, they do indicate that there is a range of combustion temperatures and mixture stoichiometries above and below which soot formation is limited.

Oxidation of PAHs and incipient soot particles was also studied for methane based flames. At low pressures, Smooke *et al.* [113] identified that OH oxidation was the principal mechanism, due to OH concentrations more than 10 times greater than the equilibrium concentration. Skjoth-Rasmussen also found that adding H_2O to the fuel increased oxidation by increasing the concentration of OH radicals [111]. Zhu and Gore [114] identified that at high pressures (4 MPa), the OH oxidation rate was reduced to such an extent that it was similar to the O_2 oxidation rate. In a non-premixed combustion event, OH radicals are typically found mainly within the reaction zone, but O_2 molecules are abundant in the unburned gases. As a result, the increasing importance of the O_2 mechanism at high pressures may have a significant influence on soot oxidation in a natural gas fuelled engine.

The primary particles whose formation (and oxidation) are discussed above are typically formed on the fuel-rich side of a non-premixed flame. These primary particles are typically spherical and of similar diameter, on the order of 5-50 nm [18]. When the particle concentrations are sufficiently high, a significant number of collisions will occur which will result in agglomeration and the formation of particle chains. As the particles (both primary particles and agglomerate chains) pass through the flame front, they will be exposed to high-temperature oxidative environments. Oxidation will reduce both the number and size of the particles by surface reactions, as discussed previously. If the oxygen concentration, temperature, and residence time are high enough, all the particles will be fully oxidized; however, in most diffusion combustion events, there is not sufficient time at high temperature for this to occur. Those particles that survive the oxidation process will pass out of the reaction zone, where they will continue to interact with other particles and form larger agglomerate chains. After the combustion, the full range of aerosol population dynamics results in significant particulate growth and agglomeration, resulting in engine-out PM which

is greatly different, in shape and in composition, from the PM initially formed in the combustion process.

2.2.6 PM Population Dynamics

PM changes significantly in the post-combustion expansion and exhaust process. Volatile hydrocarbons and sulphates will continue to condense onto the existing particles as the exhaust cools, increasing the PM size and coating the soot with a layer of material with significantly different properties from the particle's core. Existing particles will continue to agglomerate, resulting in a reduction in total particle number but an increase in size. New particles may be created by nucleation of sulphur or volatile organic species, if the concentrations of these species are sufficiently high and there is not sufficient surface area for condensation to bring the concentration into equilibrium. These processes will continue through the expansion and exhaust strokes and during passage through the exhaust system [115].

To simulate the dilution process that would typically be undergone by actual exhaust, as well as to provide a more consistent and repeatable measure of particulate matter, samples are normally diluted before being measured. This dilution process significantly influences the particles being measured, by reducing the gas stream temperature (enhancing condensation of volatiles) and simultaneously diluting the exhaust by a factor of 10-20 (reducing partial pressure of volatile species). The effects of the dilution process on sampled particulate matter have been studied extensively [95,99,116,117]; variations in dilution air temperature, relative humidity, and residence time have been identified as the key sources of sampling variability. By holding these parameters constant, inconsistency in the measured particulate attributable to the sampling process can be minimized.

2.2.7 PM Formation in Pilot-Ignited Natural Gas

Natural gas is not pure methane; depending on source, it may contain significant quantities of ethane (C_2H_6) and propane (C_3H_8), as well as trace amounts of higher hydrocarbons [118]. Given that these species have higher sooting tendencies than does methane, they may contribute disproportionately to the formation of soot in the non-premixed combustion of natural gas. Although they contain carbon-carbon bonds, it has been suggested that their primary role in the soot formation process is through enhanced decomposition to methyl (CH_3) radicals [119]. Reaction pathway analysis has also indicated

that the oxidation of both ethane and propane pass through acetylene, generating a larger pool of soot precursor species [37,120,121]. Thus, in PIDING combustion, the natural gas flame may be a significant particulate source. Other sources similar to those in conventional diesel engines include the diesel pilot and the lubricating oil. All three sources can be expected to contribute to the overall PM emissions.

2.3 Pilot Ignited, Direct Injected Natural Gas

A significant amount of research has been carried out on the PIDING combustion process. Ongoing development of PIDING fuelling systems has improved performance and combustion stability while reducing emissions. The initial research focused on optimizing the injection process; more recent studies have investigated the effects of charge dilution and the role of the diesel pilot on pollutant formation. These studies have been carried out at both the research and the commercial development levels. One of the key technologies which has been identified to allow the direct injection of natural gas system to minimize emissions is charge dilution through the use of exhaust gas recirculation.

2.3.1 Exhaust Gas Recirculation

The use of recirculated exhaust gases (EGR) has been shown to substantially reduce NO_x emissions from a pilot-ignited, direct-injection of natural gas engine [39,122]. Similar results have been reported for heavy-duty diesel fuelled engines [123,124]; however, these studies have indicated that PM emissions are substantially increased with high levels of EGR, especially at higher load conditions. However, the natural-gas system's inherently lower PM emissions allow higher levels of EGR over the entire operating range while maintaining acceptable PM exhaust concentrations.

In direct-injection compression-ignition engines, EGR works by reducing the intake charge oxygen concentration. This increased dilution results in the presence of more inert species which must be heated by the chemical energy released in the combustion, reducing the overall temperature in the flame zone. This reduces the formation of NO, as its dominant mechanism is highly temperature-dependant, as discussed in Section 2.2.2. Results from testing at high intake dilution levels with natural gas fuelling suggest that the exponential dependence of NO formation on combustion temperature is consistent to the lowest temperatures at which combustion stability can be maintained [39]. The exponential

dependence of NO_x and linear relationship of combustion temperature with intake dilution are shown in Figure 2.1 [122]. An overall activation energy for NO_x formation in this combustion system was estimated [39,122] based on the peak in-cylinder temperature and was found to be within 5-10% of previous tests on diesel engines [125]. This suggests that, as would be expected, the mechanisms for NO_x reduction with EGR are independent of the fuel being consumed in the direct-injection engine.

EGR, and the corresponding reduction in combustion temperature, also increase combustion instability. A fundamental lower combustion temperature limit, below which the combustion instability was excessive and the combustion event was unsustainable, was proposed for diesel engines [126]. This hypothesis has been contradicted in more recent work, where very high EGR levels were used to achieve combustion temperatures below those where either soot or NO_x formation was significant [127]. However, substantial increases in combustion instability, leading to higher emissions of unburned fuel and degraded fuel efficiency, were observed [128]. With lower oxygen concentrations in the oxidizer, local strain extinction of the flame is more likely to occur at a given temperature [129]. Thus, both the lower oxygen content and lower combustion temperatures due to EGR increase the probability of local strain extinction, substantially increasing combustion instability and emissions of hydrocarbons and CO.

Bulk quenching, which occurs late in the combustion process as the cylinder temperature and pressure fall during the expansion stroke, is also a significant concern with higher levels of EGR. The longer combustion durations due to charge dilution result in the combustion continuing later in the expansion stroke. Bulk quenching results in premature termination of the late-stage oxidation processes which would normally consume byproducts of incomplete combustion (including hydrocarbons, CO, and soot precursors) [28].

Although natural gas burns under a wider range of fuel-air conditions than diesel, increases in combustion instability with EGR are still observed. These instabilities are particularly notable at later injection timings, where larger increases in CO, HC and PM, and greater reductions in efficiency are observed at lower EGR fractions [38,122,130]. Increases in the delay between the start of injection and the observed start-of-combustion of the natural gas (gas ignition delay) have been roughly correlated with increases in unburned fuel emissions [131]. This suggests that over-leaning of early-injected fuel may be a contributing

factor. Similar indications of the aetiology of the observed increases in PM and CO emissions have not been established.

2.3.2 Injection Process

For a PIDING engine, the natural gas injection parameters have been shown to influence emissions and efficiency substantially. Injection timing, duration, and pressure are among the parameters that have been investigated. The number of injector holes, their angle relative to the firedeck, and the angle between the pilot and main gas nozzles are also significant, although fewer published results are available.

One parameter of particular interest in a dual-fuel direct-injection application is the interlace angle between the diesel sprays and gas jets. Early computational studies suggested that this interlace angle could influence both the timing and location of the ignition of the natural gas jet, with direct influences on the overall heat-release rate and on NO_x emissions [87]. In the Westport dual-fuel injector, the diesel pilot nozzles are located in the tip of the gas needle, which rotates during operation. As a result, the interlace angle between the gas jets and the pilot sprays varies over time. With equal numbers of pilot holes and gas jets, it was found that when the jet and spray were aligned, combustion stability was substantially degraded. Unequal numbers of pilot and gas holes were required to ensure that some of the diesel sprays were unaligned with the gas jets [88]. Unfortunately, this also increases the probability of some sprays and jets being in fact aligned, resulting in variations in the ignition times for the different jets. The effect was attributed to the natural gas jet overtaking the diesel spray before ignition occurred, resulting in a cool, fuel-rich mixture which was more difficult to ignite and from which flame propagation was impaired. The results also suggested that having the ignition source closer to the sides of the gas jet, rather than the tip, improved the combustion stability. Interactions between the gas and diesel injections were also identified when the delay between the diesel and gas injections was reduced. One hypothesized effect was that the cool natural gas reduced the temperature in the combustion chamber prior to ignition of the pilot fuel. This increased both the diesel and gas ignition delay times [132]. While efforts to develop more advanced models continue, modelling of the combustion process under EGR conditions is still unsatisfactory [133].

The relative injection delay time (RIT, the delay time between the diesel pilot and main natural gas injections*) was studied in a series of tests. Initial studies under non-EGR conditions were inconclusive as the effects of the relative delay were confounded with variations in the overall combustion timing [88]. With the combustion timing fixed, relatively small effects of the RIT were observed. At very short RIT's, when the gas and diesel injections were occurring simultaneously, increased combustion instability was observed. Similarly, at long relative delays, the ignition of the natural gas was impaired by dissipation of the hot gases from the pilot flame [134].

With EGR, the RIT was found to have a more substantial influence on the combustion event. PM emissions were shown to be substantially reduced by shortening the delay so that the diesel and natural gas injections overlapped, as shown in Figure 2.2 [130,135]. The combustion intensity was increased and the duration decreased compared to a more conventional RIT (typically on the order of 1 ms). When the gas and pilot injections overlapped, the gas injection was completed before the diesel pilot ignited. The combustion of the natural gas was mainly premixed (although neither homogeneous nor necessarily stoichiometric), resulting in lower particulate formation. The higher intensity combustion resulted in a significant increase in NO_x emissions. Unburned fuel emissions were also substantially increased, the result primarily of increased overleaning of the natural gas prior to ignition. The results were found to be sensitive to engine speed and load and to the phasing of the combustion event [130].

A parameter which has been widely recognized as a technique to control PM and NO_x emissions from late-cycle direct injection engines is varying the absolute injection (and hence combustion) timing [28,136]. Later combustion timings result in lower NO_x emissions due to lower combustion temperature at the expense of generally higher PM and reduced efficiency. Similar effects were observed with and without EGR for direct injection of natural gas engines [88,134]. With EGR, increases in combustion variability at later timings were also detected. Of particular interest is the comparison of the trade-offs between NO_x, PM, and fuel consumption as a function of both EGR and combustion timing, as shown in Figure 2.3 [38]. To achieve equivalent NO_x and PM emissions, either higher EGR fractions (~40%) with early combustion timing or moderate EGR (~20%) with late timings could be used.

* HPDI™ injection timing processes are discussed in more detail in section 3.1.2

Efficiencies were almost 10% higher at the high EGR, advanced timing condition. The fact that higher EGR is preferable raises system complexity issues, as larger EGR fractions require larger cooling systems and have a greater impact on the engine's air exchange system. Significant interactions between RIT, EGR level, and injection timing indicated that all three parameters need to be optimized over the entire engine operating map [130].

The injection pressure of both the diesel and the natural gas may also have a significant impact on the combustion process. Initial studies suggested that higher injection pressures reduced fuel consumption but increased NO_x and unburned hydrocarbon emissions [88]. The NO_x and efficiency effects were due to earlier combustion (the injection timing being held constant), as the ignition delay was shorter at high injection pressures. At a single operating condition, fixing the combustion timing and increasing the injection pressure reduced PM emissions with little impact on combustion efficiency or NO_x emissions [135]. However, the effects appeared to be sensitive to operating conditions, particularly the relative pressure between the injector and the cylinder gases. The testing was unable to determine the fundamental effects of injection pressure [137]. Further study is required to clarify the effects of this parameter.

2.3.3 Diesel Pilot Influence

The role of the diesel pilot flame has been investigated in both premixed and non-premixed combustion systems. For premixed charge conditions, the timing of the pilot injection is used to control the combustion timing. Earlier pilot injections advance the combustion, improving efficiency and reducing PM emissions but increasing NO_x emissions [138]. The use of a diesel pilot (or a pre-injection) has also been studied as a technique to reduce emissions and combustion noise from diesel engines [139,140]. Although experimental results have varied, in general the pilot injection has been found to reduce the main fuel ignition delay time by increasing the temperature in the combustion chamber as well as providing an increase in radical concentration. The shorter ignition delay time of the main fuel leads to higher NO_x emissions due to higher combustion temperatures. Excessively early pilot timing results in overleaning of the pilot while late injection results in interactions with the main fuel and impairs the penetration of the main fuel spray [141].

In a PIDING engine, the combustion timing depends primarily on the timing of the natural gas injection. The natural gas ignition delay, however, is dependant on the timing and

relative location of the diesel pilot flame [87]. This ignition delay time influences the amount of fuel-air mixing that occurs before the jet is ignited. The strength of the pilot flame, along with its location (as discussed in section 2.3.2), will influence both the timing and location of the natural gas ignition.

The diesel pilot has also been shown to have a significant impact on PM emissions. A source apportionment study revealed that the diesel pilot contributes between 5 and 40% of the black-carbon component of the PM, with higher load or EGR conditions resulting in lower diesel pilot contributions [142]. Of specific interest was that increasing the pilot quantity from ~3 to 6% of the total energy substantially increased both the total PM and the relative contribution from the natural gas. This outcome may have been due to a reduction in the non-premixed natural gas combustion phase. A shorter ignition delay time may also have resulted in a significantly richer early combustion phase. Higher concentrations of particulate precursors, formed in the diesel combustion event, may also have contributed to the observed increase in natural-gas sourced PM.

2.4 Summary / Literature Gap

Testing on both diesel and natural-gas fuelled direct-injection engines has indicated that EGR can be used to substantially reduce combustion temperature, leading to lower NO_x emissions. However, increased combustion variability, in conjunction with slower heat release, results in higher emissions of partial combustion by-products as well as reductions in efficiency. A survey of published results suggests that there are a number of competing influences which lead to higher emissions and lower efficiency with EGR in diesel engines, including local extinction and bulk quenching. Similar effects may be occurring for natural gas combustion; however, fundamental differences between the combustion of a gaseous jet and a diesel spray mean that different processes may be dominant. Further research is required to attempt to clarify these effects and to develop a better understanding of the principal pollutant formation mechanisms in direct-injection natural gas combustion systems.

There are certain areas of interest in natural gas direct-injection combustion where significant gaps in the literature exist. The role of injection pressure has been shown, over a limited number of test conditions, to provide substantial emissions benefits; whether this is consistent over a wider range of controlled conditions needs to be determined. As well, the influence of fuel composition has been identified as a potential contributor to emissions;

however little research has been published studying the effects of heavier hydrocarbons, hydrogen, or fuel diluents in non-premixed combustion applications. Finally, the increases in PM emissions with EGR have been well described; however the influences of these recirculated particles on the combustion process, and their corresponding effects on emissions, have not been assessed. The work described in the following chapters will attempt to address these issues, and thereby develop an improved overall understanding of combustion and pollutant formation in a non-premixed gaseous-fuelled engine.

2.5 Tables and Figures

Table 2.1: Selected results from in use natural-gas fuelled HD engine studies

Study	McCormick *et al.*	Chandler *et al.*	Frailey *et al.*	Kamel *et al.*	Ayala *et al.*	Chiu *et al.*	
Publication year	1999	1999	2000	2002	2002	2004	2004
Manufacturer	Cummins	Cummins	Cummins	CWI	DDC	Mack	Mack
Engine model (year)	B5.9G (1997)	L10-300 (1997)	B5.9G (1997)	BGas+ (2001)	50G (2000)	E7G	E7G
NG stoichiometry	Lean	Lean	Lean	Lean	Lean	Stoich	Lean
NG aftertreatment	oxidation	none	oxidation	oxidation	none	3-way cat.	oxidation
Engine Power (kW, NG)		300	145	280		242	242
Displacement (L, NG)	5.9	9.8	5.9	8.3		12	12
Compression Ratio (NG)	10.5		10.5	10		11.5	11.5
efficiency (% of diesel)	85-98%	70%	83%	80%		75-90%	90-95%
CO (% of diesel emissions)	5-10%	265%	16%	10-15%	400%	*4.8* g/kWhr*	
nmHC (% of diesel emissions)	1000-1500%	41%	220%	100-120%	1000-1500%	*0.0* g/kWhr*	
NOx (% of diesel emissions)	65%	21%	40%	55-75%	30-50%	6%	33%
PM (% of diesel emissions)	5%	5%	3%	<10%	15-33%	*0.02* g/kWhr*	
CO_2 (% of diesel emissions)	80-90%	102-113%		93%	80-95%		

*percentages calculated as NG/diesel*100, in comparison with closest equivalent diesel engine used in study,* **except**
** - absolute emissions values (g/kWhr)*

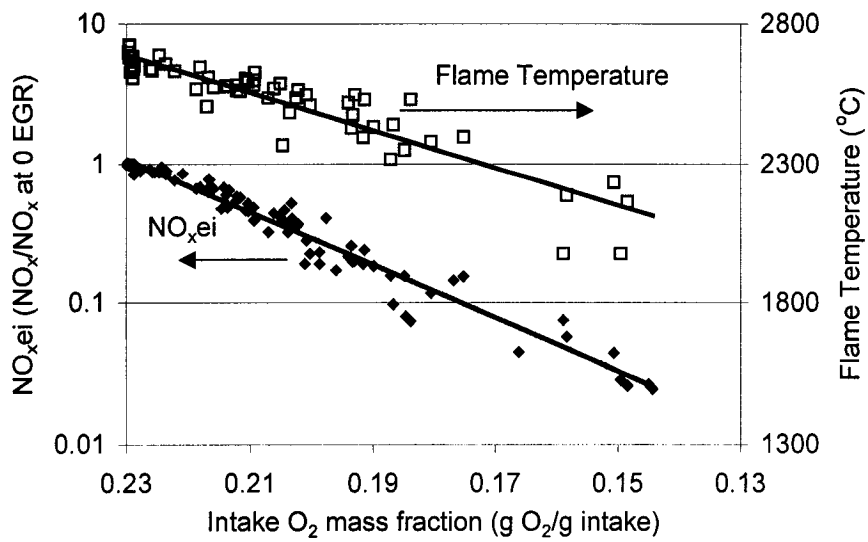

Figure 2.1: Effect of intake oxygen dilution on peak combustion temperature and NO_x emissions over a range of engine test conditions. NO_x emissions are represented as emissions relative to the non-EGR emissions at the same engine test condition.

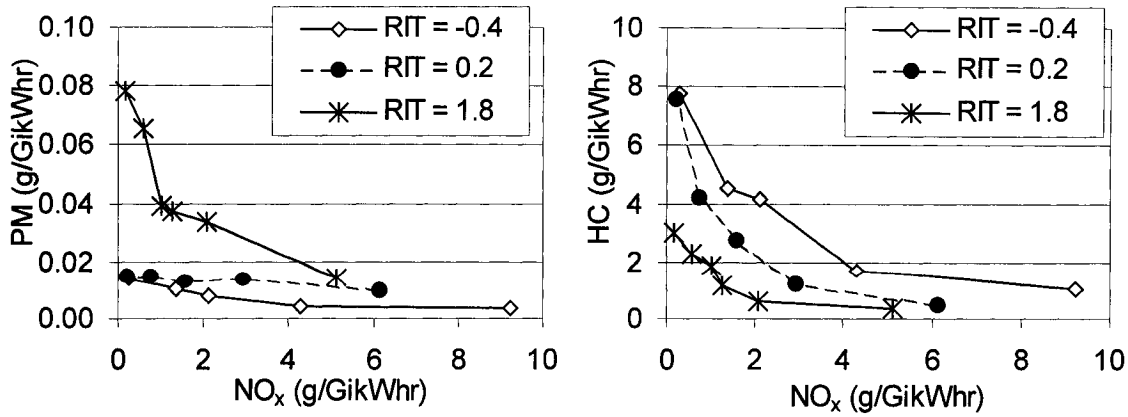

Figure 2.2: Effect of delay between natural gas and diesel injection on PM-NO_x and HC-NO_x trade-offs as EGR level is varied (lower NO_x at lower EGR levels).

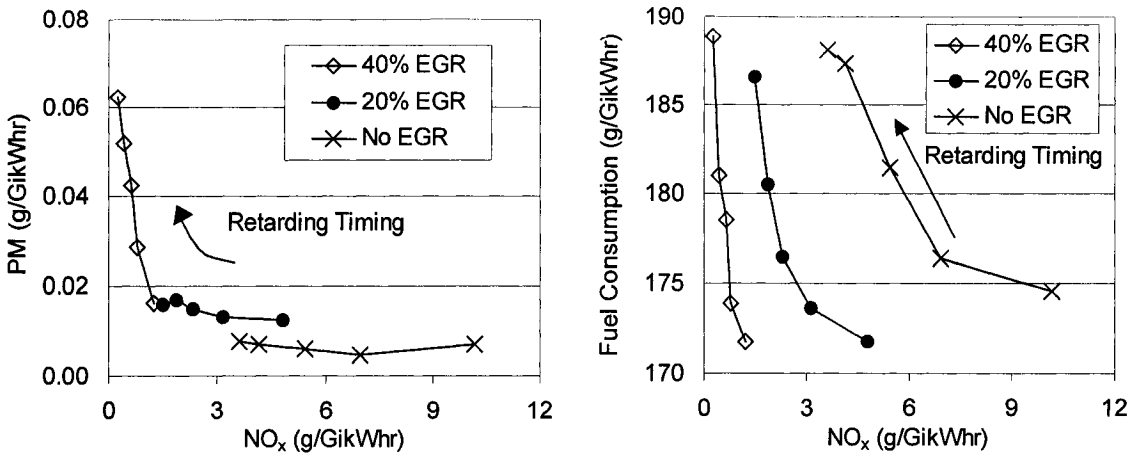

Figure 2.3: Combustion timing and EGR fraction effects on PM-NO_x and fuel consumption-NO_x trade-offs over a range of EGR conditions. Mid-point of combustion timing varied between 2.5° (early) and 17.5° (late) after top-dead-centre.

Chapter 3
Apparatus and Procedures

3.1 Research Engine

The single-cylinder research engine facility was developed to provide the widest achievable range of test conditions on a heavy-duty gaseous-fuelled engine. The core of the facility is a heavy-duty Cummins ISX series engine (serial #4026530). This inline six-cylinder direct injection diesel engine series, typically used in transportation and stationary power generation applications, covers a power range between 300 and 480 kW (400 and 650 hp). The base multi-cylinder engine was modified so that only a single cylinder (number six, nearest the flywheel) fired. The other five cylinders were deactivated by sealing the valves, replacing the injectors with dummies, and drilling holes through the pistons to reduce compressive work. To maintain the engine's balance, the mass removed in drilling through the pistons was replaced by mass added to the wrist pin. To retain the best achievable speed stability under single-cylinder conditions, the largest available flywheel (inertia ~6.8 $kg \cdot m^2$) was provided. Previous work has shown that the single-cylinder engine performance closely resembles that of an equivalent multi-cylinder engine [143].

Details regarding the single-cylinder engine's specifications are shown in Table 3.1. Two compression ratios are shown as two separate combustion chambers were used during different stages of the testing described in this work. The first set of tests (described in Chapter 4) involved the use of the higher compression-ratio piston, which was the standard Cummins ISX piston for the 1998 model year. The later tests were carried out using a newer Cummins piston, developed to meet more recent emissions standards through the use of EGR. The lower compression ratio was required to avoid exceeding the cylinder pressure limits with the higher charge masses associated with EGR. Only the clearance volume was affected; the engine bore, stroke, displacement, etc. were unchanged between the two pistons.

To overcome the single-cylinder engine's high internal friction, an external 30kW (40hp) motor was used. This motor was controlled by a torque-control vector-type drive, with the motor providing torque greater than the friction being absorbed by the engine. A General Dynamics 150 kW (200 hp) eddy-current dynamometer coupled to a Digilog controller was used to absorb extra torque. The dynamometer and vector drive were mounted

in series, with the vector drive providing constant torque (greater than required to drive the engine) and the dynamometer absorbing varying torque levels to maintain the engine speed at the desired setting. This system proved capable of controlling the engines speed to within ±1% of the desired speed.

Engine cooling was provided by a closed-loop recirculating system filled with a 50/50 blend of glycol and distilled water. The engine's internal thermostats were used to maintain the coolant temperature at the outlet from the block at 80±2°C. A liquid-to-liquid heat exchanger was used to reject excess heat from the coolant to the city water mains. The coolant regulated the oil temperature; the oil temperature varied between 90 and 110°C depending on the engine operating condition, but was repeatable on a day-to-day basis (±2°C). Energy rejection from the dynamometer was also provided by a separate mains water-cooling system. A sufficient supply of water was provided to ensure that the discharge temperature of either water system did not exceed 40°C at any operating condition. Intake and exhaust fans were used to provide ventilation and temperature control inside the test cell. The exhaust fan, ducted to the outside, was sized larger than the intake fan to ensure that the air pressure inside the test cell was lower than that in the control area.

3.1.1 Air Exchange System

A highly flexible air exchange system was developed to provide the widest possible range of intake air and EGR conditions. Combustion air was supplied to the engine from an industrial rotary screw-type air compressor (Atlas Copco GA45FF). Water vapour was removed from the compressed air by a refrigerated air dryer (dew point of -40°C) and any oil carried over from the compressor was filtered with a pair of high-efficiency filters. Sampling of the intake air showed that aerosol concentrations were below those of ambient air. Boost pressures from atmospheric to 350 kPa (absolute) pressure were achieved through a two-stage regulation system. The air flow-rate was measured with a custom-built subsonic venturi. A 50 L surge tank installed upstream of the engine reduced the amplitude of acoustic waves in the intake system by approximately 95%. The intake air was then supplied to the stock internal intake manifold. The intake header, port, and valve seat geometry were unmodified from the base engine. Details of the intake air system are shown in Figure 3.1.

The stock engine's external exhaust manifold was replaced by a custom-designed system in order to more closely simulate the multi-cylinder engine. An electronically

controlled butterfly valve was used to exert the back-pressure which would normally have been supplied by a turbocharger. An insulated 50L high-temperature surge tank was used to damp out pulsations in the exhaust stream. Both exhaust emission samples (gaseous and aerosol) were drawn from the exhaust downstream of the surge tank. While this resulted in some ageing of the exhaust (average residence time in the surge tank at 1200 RPM was on the order of 10 s), it was required to avoid sample biasing caused by inhomogeneity in the exhaust stream interacting with acoustic pulsations in the exhaust system between the engine and the exhaust surge tank.

Upstream of the back-pressure valve, a fraction of the exhaust was directed through the EGR loop. This loop was composed of a second remotely controlled butterfly valve (to control pressure-drop and hence EGR flow rate) and a cooler. The cooler controls were set to hold the EGR temperature at 50±10°C throughout the testing. The EGR was mixed into the intake air upstream of the intake surge tank, to ensure complete mixing of the charge. A small sample (1 litre/minute) of the intake flow was drawn from downstream of the intake surge tank to determine the EGR fraction and to measure the intake aerosol loading.

3.1.2 Fuelling System

The fuel supply system provided diesel and natural gas to the engine at pressures up to 31 MPa. A hydraulic pump driven by an 11.2 kW (15 hp) electric motor was used to compress the pilot diesel fuel. The natural gas was compressed by a multi-stage electrically driven compression system which maintained the supply gas pressure between 32.4 and 34 MPa (4700 and 4900 psi). A high-pressure accumulator was used to reduce the compressor cycling time and to minimize the fluctuations in the supply pressure. A manual regulator was used to set the diesel pressure, while a dome-loaded regulator held the natural gas at a pressure ~200 kPa below the diesel pressure, to prevent leakage of the natural gas into the diesel. The fuel was supplied to the engine's internal fuelling rails, which delivered the fuel to the injector. The diesel fuel was also used to control the operation of the injector, and excess flow was returned to the low-pressure reservoir. The pilot fuel for all tests was road-grade low-sulphur (<500 ppm) diesel which met Canadian General Standards Board specification CAN/CGSB-3.520. The main fuel was commercially supplied natural gas (Terasen Inc.); while the composition varied somewhat (analyses are provided in the individual chapters), sulphur was at all times < 7 ppm (by volume).

The injector used in this work was a Westport J36 prototype injector. The injector, very similar to that shown in Figure 3.2, injected the diesel and the gas through separate injection holes. Concentric needles, actuated by separate solenoids, were used to allow independent control of the diesel and natural gas timings. Details of the injector are provided in Table 3.1; more information on the injector design and development are provided in the references [144,145]. The injection process used in this work involved an initial injection of diesel (at approximately 5 mg/injection) followed after a 1 ms delay by the gaseous-fuel injection. The timing process and related command parameters are shown in Figure 3.3. Briefly, the quantity of fuel injected was controlled by the duration of the injection (pulse width) for both the liquid pilot and gaseous main fuels. The start-of-injection of the pilot was controlled relative to top-dead-centre (TDC) of the operating piston while the gaseous injection was fixed relative to the commanded end of injection timing for the pilot.

3.1.3 Instrumentation and Data Acquisition

The research engine facility was fully instrumented, including temperature, pressure and flow sensors as well as in-cylinder condition monitors. A brief description is given below, further details on the instruments used, including ranges, accuracy, and serial numbers, are provided in Appendix 3:

- Airflow was measured using a custom-built subsonic venturi (estimated uncertainty ± 1%) located in the combustion air supply line between the two regulator stages. The differential pressure between the upstream and throat was measured with a differential pressure transducer (Omega PX2300-2DI).
- The mass flow rate of gaseous fuel was measured using a Micromotion corriolis mass flow meter (sensor CMF010P, transmitter RFT9739). As the sensor measured mass flow directly, it was insensitive to the composition of the fuel.
- Diesel pilot flow was measured using a custom-built gravimetric system, where the change in mass of fuel in the diesel reservoir over time was monitored. Regression analyses of the diesel mass data collected over sample durations in excess of 5 minutes were found to provide measurements within 5% of long-duration means.
- Temperatures in the intake manifold, exhaust and EGR system, as well as standard engine and auxiliary system temperatures, were measured using standard accuracy Omega k-type thermocouples.

- Intake and exhaust stream pressures were measured using Setra type 209 diaphragm transducers.
- The intake manifold pressure was measured at high frequency (every half crank angle - ½°CA) with a PCB (model PCB1501) piezo-resistive transducer.
- The in-cylinder pressure was also measured every ½°CA with an AVLQC33C flush-mounted water-cooled transducer. The signal from the sensor was amplified and converted into a measurable voltage by a Kistler model 503 charge amplifier.
- The crank location was measured using a BEIXH25D shaft encoder. This unit output both an index pulse and a square wave to provide ½°CA resolution. The encoder was indexed to the engine's TDC. The pulse offset from true TDC was measured and used as a correction factor in the data acquisition system. The offset used in the work presented here was 1.7° before TDC.

The data was collected through a custom-built data acquisition system. The core of the unit was a National Instruments SCXI1001 bus connected to a PCI-MIO-16E-1 card in a PC computer. The PC computer was running Labview 6.0, in which all the data acquisition routines were written. Two separate routines were used; one collected 45 consecutive cycles (at ½°CA resolution) of the crank angle, intake manifold pressure and in-cylinder pressure, while the other collected all the other data (flows, temperatures, pressures) at a frequency of 1 Hz. The index pulse was imported directly into the timing circuit and was used to trigger the high-frequency data collection. Three separate data acquisition modules were used for low-frequency sampling in the SCXI1001 bus. One was dedicated for thermocouples (with a thermistor to provide the reference junction temperature, SCXI1303/1102), while the other two measured voltages. One of the voltage boards was unfiltered (SCXI1100) and the other was filtered at 200 Hz (SCXI1102). The measurements were conducted through the unfiltered module unless excessive noise was observed on the sensor.

Data collection periods varied for different test conditions, with a minimum duration of 5 minutes for low-frequency data. For most test points, two or more high-frequency data sets were collected (sampled at the start and end of the low-frequency sampling) to ensure that the engine's in-cylinder conditions had not changed appreciably over the sampling duration.

3.2 Emissions Measurements

Emissions measurements were carried out with a fractional raw system for gaseous emissions and a fractional diluted system for particulate. As was mentioned in section 3.1.1, separate samples for the gaseous and particulate emissions analysis were drawn from the exhaust system downstream of the exhaust surge tank. For the gaseous emissions sample, an insulated 1m long ¼" diameter tube was used to connect the exhaust sample point to the emissions handling system. A heated sample line (set to 190°C) was used to transfer the sample to the gaseous emissions bench. For the particulate sampling system, a separate 1m long ¼" diameter tube was used to transfer the sample to the dilution point. The sample handling and dilution process for the particulate sample will be discussed in section 3.2.2. Further details of the sample handling systems are shown in Figures 3.1 and 3.4.

3.2.1 Gaseous Emissions

The gaseous emissions system was a raw exhaust system custom assembled in 1992 by Galvanic Analytical Inc. Sample handling included a pair of heated filters (coarse and fine), a heated pump, and a chiller to remove water vapour (dew point <1°C). Upstream of the chiller, a sample was drawn through the heated flame-ionization detector to measure hydrocarbon concentration (Ratfisch RS232). After the water separator, the remaining dry sample was fed to the specific gas analyzers. Non-dispersive infrared (NDIR) analyzers were used for the exhaust CO_2 (Beckmann 880), CO (Siemens Ultramat 21P) and CH_4 (Siemens Ultramat 22P). A chemiluminescent analyzer (API 200AH) equipped with a Mini-HICON high temperature $NO_2 \rightarrow NO$ converter was used to measure total NO_x. A paramagnetic sensor (Siemens Oxymat 5E) was used to measure oxygen concentration.

A dedicated sampling and analysis system was used to measure the CO_2 concentration in the intake to determine the intake charge dilution level. The sample was drawn from the intake manifold downstream of the intake surge tank, ensuring that the charge was homogeneous. The sampling system included a pressure regulator, to reduce the manifold pressure to ambient, as well as a particle filter and a liquid-water separator. A Permapure nafion-membrane gas-to-gas dehumidifier removed water vapour from the sample line. The manufacturer's stated performance for the unit was ~90% removal for the flow rates used. A condensation test was conducted and no condensate was detected in the stream after

the drier at temperatures as low as 2°C. A California Analytical (Model 100) NDIR analyzer was used to measure the CO_2 concentration in the intake stream.

3.2.2 Particulate Measurement

A separate sampling and measurement system was used for the particulate matter measurements. To coincide with standard vehicle PM sampling procedures [146], as well as to ensure a stable and repeatable PM sample with low enough concentrations to be measured accurately, dilution of the exhaust sample was required. A micro-dilution tunnel was used to dilute a small fraction (1-2 LPM) of the exhaust flow at dilution ratios of approximately 15:1. Due to the wide range of exhaust flow-rates at different engine operating conditions and the fixed flow requirements of the emissions measuring system, it was not possible to ensure isokinetic sampling for all conditions. However, as the aerosol particles of interest were significantly less than 1 μm in diameter, the effect of velocity biasing on the sample was negligible [147]. The PM sampling and dilution system is shown in Figure 3.4.

To reduce the pressure in the PM sample system, an insulated ¼" sample line (~1 m long) connected the exhaust sample point to the dilution system. A bypass regulator was used to control the pressure at this point, with a fraction of the sample being vented through the regulator to atmospheric pressure. The remaining sample passed through a pressure-reducing orifice, after which it was mixed with dry, bottled nitrogen. As the mixing occurred immediately downstream of the orifice plate, a high degree of local turbulence and hence more rapid mixing was achieved. The diluted sample then passed through a 3 m long (3/8" diameter) mixing section. The dilution ratio was controlled with the bypass regulator by varying the pressure upstream of the orifice. By maintaining a constant dilution ratio and flow rate of diluent, the sample's residence time in the sampling system was held constant. The orifice and mixing section were heated to maintain the diluted gas temperature at 55°C. The dilution ratio, on a molar (or standard-volume) basis, was calculated based on the CO_2 concentrations in the exhaust, diluent, and diluted sample streams, by:

$$DR = \frac{[CO_2]_{exh} - [CO_2]_{diluent}}{[CO_2]_{diluted\ sample} - [CO_2]_{diluent}}, \tag{3.1}$$

Where $[CO_2]_{exh}$ was the measured CO_2 concentration in the exhaust stream from the raw emissions sample, $[CO_2]_{diluent}$ was the dry nitrogen CO_2 concentration (measured at less than 10 ppm) and $[CO_2]_{diluted\ sample}$ was the measured CO_2 concentration in the diluted sample. A

California Analytical NDIR analyzer (model 100) measured the diluted sample CO_2 concentration. The CO_2 concentrations, which were measured on a 'dry' basis, were corrected for the presence of water vapour by assuming a concentration of water vapour in the raw exhaust stream based on the hydrogen : carbon ratio of the fuel. Dilution ratios between 14-18:1 (by volume) were used, as at these levels the dilution ratio was found to have little or no influence on the measured PM levels. An analysis of the effects of dilution ratio on PM mass and size distribution measurements is provided in Appendix 1.

The residence time of the sample was approximately 4 seconds in the mixing section, which allowed sufficient time for complete mixing as well as evolution of the aerosol population to steady-state conditions. After the mixing section, samples were drawn off the main stream for the various particulate measurement units. The temperature of the diluted sample in the diluted sample section was held at 50°C. Excess sample was exhausted to atmosphere.

Total PM mass

The total mass of particulate measured at 50°C was composed of solid and liquid particles which had either been emitted from the engine as an aerosol or had condensed during the exhaust or dilution processes. A tapered element oscillating microbalance (TEOM – Rupprecht and Patashnick Model 1105) was used to provide on-line total mass measurements. The TEOM collected all aerosol mass (irrespective of composition) on an oscillating filter, with the frequency of oscillation being a function of the collected mass. Previous work has shown the TEOM to be sensitive to sample humidity and filter face temperature [148,149]. By maintaining high filter face temperatures (50±2°C), a constant dilution ratio, and sufficient stabilization time, the effects of water content on the TEOM were minimized.

To validate the TEOM results, gravimetric filter samples were collected for approximately 1/3 of the test points; the filters were then weighed to determine the mass of particulate collected over the sampling period. EPA standard protocols were followed for the PM sampling, with a pair of 47 mm Pallflex Emfab™ (borosilicate microfibers reinforced with woven glass cloth and bonded with PTFE) filters sampled in series. The filters and housing were pre-heated prior to being installed in the sample system to minimize condensation on the filter face. The filters were pre- and post-weighed following EPA

recommended practices [150] with a Sartorius CP2 microbalance, after being left in a temperature and humidity controlled room (20±2°C, 35±5%RH) for between 24 and 72 hours. The mass collected on the second filter was subtracted from the mass collected on the first filter to remove the effects of vapour absorption on the filter substrate [151]. The mass concentration in the exhaust stream was then calculated from the mass collected on the filter, the sample flow rate, the dilution ratio, and the sample duration.

A strong correlation between the TEOM and the gravimetric filters was achieved, as shown in Figure 3.5. The TEOM results were consistently approximately 15% below the gravimetric filters; this is a similar offset to results reported by other researchers [148,152]. A Chi-squared goodness-of-fit test showed a high degree of correlation for particle concentrations less than 2 mg/hr ($p<0.001$). However, for the few test points where the particle concentrations were greater than 2 mg/hr a substantially different response was observed, with the TEOM reading approximately 40% below the gravimetric filters. While the reasons for this result are unclear, the response of the TEOM was very similar to gravimetric filter measurements over a wide range of test conditions. This demonstrates that for virtually all the test conditions, the TEOM provided a valid representation of the actual PM mass in the exhaust stream. However, as can be seen in Figure 3.5, significantly more scatter in the correlation was observed at the lowest PM loadings. As a result, PM levels measured by the TEOM at the lowest loadings may not be as accurate as those at intermediate PM concentrations.

Ultrafine particle Concentration

To provide some insight into the particulate loadings at very low emission levels, as well as to develop an improved understanding of the particulate structure, number/size distributions were also measured with a TSI Model 3936 Scanning Mobility Particle Sizer (SMPS). The SMPS is composed of two principal units, a short-column differential mobility analyzer (DMA, TSI Model 3085) sized for ultrafine particles (5-155 nm mobility diameter) and a condensation particle counter (CPC, TSI Model 3022A). The fundamental operating principles of the DMA have been described by Knutson and Whitby [153], while Wang and Flagan [154] have developed a comprehensive description of the SMPS. A series of recent review studies have demonstrated the applicability of the SMPS system to PM emissions measurements from both diesel and gasoline-fuelled vehicles [155,156]. Some concern has

been expressed regarding the SMPS's ability to measure particles greater than 1000 nm in mobility diameter; however, the use of an impactor with a 50% cut diameter (diameter at which 50% of particles are removed from the sample stream) substantially less than 1000 nm resolved this issue [157].

The functioning of the SMPS has been described in detail in other work [154]. In brief, the sample first passed through an impactor to remove large particles. This was followed by a Kr^{85} charge neutralizer, where the particles achieved a standard charge distribution (dependant on particle size, as predicted by Fuchs charging theory [158]). The neutralized particles then entered a sample column, through which a laminar flow of clean air was maintained and across which an electric field was generated. The rate at which a particle crossed the streamlines was a function of the charge on the particle, its size and shape (related to atmospheric drag forces), and the strength of the electric field. Only those particles with the right 'mobility' crossed the stream in the proper time to reach the sample port. By varying the strength of the electric field, different particle sizes were sampled through the same port. The monodisperse aerosol being drawn from the sample port was then directed through the CPC. Inside the CPC, the sample passed through a super-saturated alcohol environment that caused all the particles to grow by condensation until they reached an optically-detectable size. By inverting the measured concentrations over time and correcting for multiple charges on the individual particles (based on Fuchs charging theory), the number of particles in 50 size ranges between 5 and 150 nm were determined.

To avoid saturating the CPC, dilution ratios in excess of 100:1 were required. A filtered recirculation system was used to provide secondary dilution at a ratio of 5-14:1, resulting in overall dilution ratios between 200 and 300:1 (total diluted flow : raw exhaust). The effects of secondary dilution on particle size distributions are shown in Appendix 1.

Validation of the results from the SMPS was difficult, as there was no 'gold standard' with which it could be reliably calibrated. The mobility diameter measured by the SMPS was a function of both the size and the shape of the particle, and was not the same as the diameter that a spherical particle of the same mass would occupy. Hence, the mobility size distribution cannot simply be integrated to provide the particle volume or mass. Previous work for diesel ultra-fine particles has identified effective densities in the range of 0.57 to 1.2 g/cm^3 with a strong dependence on particle size, with higher effective densities for smaller diameter

particles [159,160]. The fractal-like structure of the agglomerate has also been shown to have a significant influence on the effective density of the particulate for larger particles; at smaller sizes, the projected area has the primary influence on mobility [161]. An estimate of the effective density for a given size range can be made based on the fractal dimension for particles of a given mobility diameter [162]. Using the results from the previous work, a relationship between effective density and diameter can be developed [159]:

$$\rho_e(\phi) \propto \phi_b^{d_{fm}-3}, \tag{3.2}$$

where $\rho_e(\phi)$ is the effective density at the given diameter, ϕ_b is the mobility diameter, and d_{fm} is the fractal dimension. Fractal dimensions from 1.8 to 3 have been suggested for diesel exhaust particles [159,163,164]. Fractal dimensions approaching 3 imply that the agglomerates are essentially spherical and that the density is constant with size; for the current work, TEM images (Appendix 7) indicate that the larger agglomerates are more chain-like. However, for smaller particles (made up of fewer primary particles, whose diameter is on the order of 20-40 nm), the fractal dimension will approach 3.

For the purpose of comparing the SMPS results to measured PM mass emissions, three different fractal dimensions were assessed: 1.8, which was the lowest value identified in the literature for diesel-like combustion aerosol; 2.5, which provided a reasonable intermediate value; and 3.0, which results in a constant density. The corresponding effective density for the particles, calculated using equation 3.2 and assuming a primary particle density of 1.2 g/cm^3 and a maximum diameter of 40 nm, is shown in Figure 3.6. Using this relationship and the number of particles in a given size range recorded by the SMPS, it was possible to estimate a total mass of particles of a given mobility diameter range:

$$m_{SMPS}(\phi) = \rho_e(\phi) \cdot N(\phi) \cdot \frac{4}{3}\pi\left(\frac{\phi}{2}\right)^3, \tag{3.3}$$

where $N(\phi)$ is the number of particles counted at that mobility diameter. By summing this parameter over the full range of particle sizes measured, an estimate for the total mass of particles smaller than 150 nm in mobility diameter was developed.

Integrating the SMPS measurements and comparing them to the TEOM data provides an indication of the capability of the SMPS to resolve trends similar to those observed by the TEOM. The results of the integration for all the data points for which both TEOM and SMPS data were collected for three different fractal dimensions are shown in Figure 3.7. A strong

correlation between the TEOM and integrated SMPS results was observed, independent of fractal dimension. However, the fractal dimension had a strong influence on the strength of the association between the total integrated mass and the TEOM readings. This was anticipated, given that the two instruments are measuring different properties, with the total mass expected to be greater than the ultrafine particle mass observed by the SMPS. The fact that the constant density case tended to over predict the ultrafine particle mass, while the other two tended to under predict it, suggests that the appropriate fractal dimension lies somewhat below 3, but probably above 2. However, further work is required to determine this value more precisely.

Another notable feature of the SMPS integration results in Figure 3.7 is that there is a zero offset of approximately 2 $mg/m^3_{rawexhaust}$ for the TEOM. This indicates that the TEOM is collecting mass, either from condensed lubricating oil or other sources, which are not in the ultrafine particle range even at the lowest PM levels. Although a total mass can be calculated from the SMPS results, this value is highly uncertain due to the uncertainties in the assumed equivalent density. As a result, in the remainder of this thesis, integration of the SMPS results will be used to provide a mobility volume. This value provides a representation of the total volume (which correlates with mass) of ultrafine particulate observed; however it cannot be used for direct mass-basis comparison. The mobility volume will provide a reasonable indication of the trends in total ultrafine particle concentration, allowing further insight to be gained from these measurements. In general, comparison of the SMPS and TEOM results indicate that, although integration of the SMPS results may not give a mass measurement which can be compared directly with the TEOM results, the mobility volume can be used to investigate PM emissions at levels below the observation threshold of the TEOM.

Black-Carbon Fraction

Another parameter of interest in measuring the particulate emissions from engines is the amount of the PM which is composed of soot (or black carbon) compared to the amount originating from condensed volatiles. In the current work, an Aethaelometer (Magee scientific, AE21) was used to measure the black-carbon content of the PM. First developed in 1984 [165] the Aethalometer is based on the fact that the black carbon (BC) component of PM deposited on a filter reduces the intensity of visible light based on the Beer-Lambert law:

$$I = I_o e^{-b_{abs} x}, \tag{3.4}$$

where I is the intensity of the attenuated light, I_o the intensity of the incident light, b_{abs} the absorption coefficient and x the distance that the light has passed through the sample [166]. In the Aethalometer, the particles are deposited on a prefired pure quartz filter (Pallflex Q250F). A light is then shone at these collected particles, and the percent attenuation (normally given by $\ln[I/I_o]$) can be measured. By measuring the attenuation of the light intensity, the quantity of BC deposited on the filter can be determined [167].

The Aethalomter used in the work reported here was equipped with two light sources, one at 880 nm (in the visible range) and the other at 370 nm (in the near-ultraviolet range). The two wavelengths are typically used to identify black carbon (visible light) and the volatile concentration (ultraviolet). Unfortunately, as the absorption of light in the ultraviolet regime by volatile organics depends strongly on the specific nature of the volatile species collected, a quantitative measure of the volatile concentration cannot be determined. As a result, only the black-carbon concentration is reported in the current work.

One characteristic of the Aethalometer is that over a finite sampling time, the light absorption of the deposited particulate will change because of the increased path length and scattering by collected particles. As a result, a series of post-analysis corrections are required to generate meaningful results from this unit [167]. Further information regarding the functioning of the Aethalometer, the application of the required correction factors, and the main uncertainties in the analysis procedure are provided in Appendix 2.

3.3 Experimental Parameters

The conditions under which the single-cylinder engine is operated have been shown to have a substantial impact on the engine's performance and emissions [38,122]. The parameters used to describe the operating condition of the single-cylinder engine included measures of power, overall mixture stoichiometry, combustion timing, and intake dilution. To indicate power, the brake torque (torque at the engine's output) could be used, calculated as:

$$T_{brake} = T_{dyno} - T_{vectordrive}, \tag{3.5}$$

where T_{dyno} was the torque absorbed by the dynamometer and $T_{vectordrive}$ was the torque being supplied by the external motor. The engine's high internal friction led to brake torques which were often negative, and were always substantially lower than for an equivalent multi-

cylinder engine at equivalent operating conditions [168]. As a result, the brake power, calculated from the torque by [28]:

$$P_{brake} = 2\pi N T_{brake}, \tag{3.6}$$

where N is the engine speed (in revolutions per second), was found to be a poor indicator of the engine's load condition. As a result, a more independent measure of load was required.

3.3.1 In-Cylinder Conditions

To provide a more reliable representation of engine performance, the in-cylinder pressure trace may be integrated to provide the net work done on the piston over the engine cycle. The engine's friction is thereby excluded, providing a more repeatable and representative measure of the single-cylinder engine's performance. By integrating the pressure trace over the compression and power strokes only, the engine's power and torque were defined on a gross-indicated basis. The gross indicated work per cycle (W_{GI}) was calculated as suggested by Heywood [28]:

$$W_{GI\ per\ cycle} = \oint_{comp,expansion} pdV, \tag{3.7}$$

where p was the in-cylinder pressure at a given crank angle and V was the instantaneous cylinder volume at the same crank position. By including the intake and exhaust strokes, the net indicated work could also have been calculated. However, the work in these strokes was primarily a function of the conditions in the intake and exhaust manifolds. Increased measurement inaccuracies due to the small difference in pressure over these strokes led to higher uncertainties in the calculations for the pumping work than for the gross-indicated work. As a result, the base unit used in this thesis to define the engine's power was the gross indicated work, which was used to calculate the gross-indicated power (P_{gross}) from:

$$P_{gross} = \frac{W_{GI\ per\ cycle} \cdot N}{2}, \tag{3.8}$$

where the 2 was needed to convert N from revolutions/second to cycles/second for a 4 stroke-cycle engine. Normalizing by the cylinder displacement volume (V_d) and engine speed gave the gross indicated mean effective pressure (GIMEP):

$$GIMEP = \frac{P_{gross} \cdot 2}{N \cdot V_d}, \tag{3.9}$$

which was used as the base representation of engine power as it is independent of speed and cylinder volume, thereby allowing for easier comparison with other heavy-duty engines.

The in-cylinder pressure was also used to estimate the heat-release rate (Q_{net}), as given by:

$$\frac{dQ_{net}}{d\theta} = \frac{\gamma}{\gamma - 1} p \frac{dV}{d\theta} + \frac{1}{\gamma - 1} V \frac{dp}{d\theta}, \tag{3.10}$$

where θ was the crank angle and γ was the specific heat ratio (c_p/c_v – assumed constant). The net heat release rate represented the rate of energy release from the combustion processes less wall heat transfer and crevice flow losses. By integrating the heat-release rate the total heat released during the combustion process (IHR) was estimated with:

$$IHR = \int \left(\frac{dQ_{net}}{d\theta} \right) d\theta, \tag{3.11}$$

By integrating up to a certain crank angle (CA), and normalizing by the total heat release, the fraction of the energy released up to that point was estimated. Typical points of interest in this work included the 5%, 10%, 50% and 90% points (i.e. the crank angle at which the IHR reaches the stated fraction of its total). Of these, the midpoint (50% IHR) was used to define the combustion timing, as it provided the most reliable representation of when the bulk of the combustion occurred, and was independent of ignition delay variability which could have influenced other combustion timing measures.

Evaluation of the heat-release rate was also used to estimate the timing of the ignition process. A sample of the net and integrated heat-release rate of a typical pilot-ignited gaseous fuel combustion event is shown in Figure 3.8. The timing of the diesel ignition (pilot start-of-combustion, PSOC) has been identified as the first significant increase in the heat release rate as indicated in Figure 3.8 [131]. The timing of the gas start-of-combustion (GSOC) was typically less distinct, with a gradual increase in heat release rate being observed over a couple of crank-angle degrees. To define a reproducible 'start-of-combustion' timing for the gaseous fuel, the slope of the IHR between 30 and 70% of the total heat release was calculated. This slope was then extrapolated back to the point where it reached the 5% IHR level to represent the gas start-of-combustion. The SOC timings for each test condition were calculated, but they were also validated visually to ensure that the definitions were reliable. The commanded start-of-injection timings for both the gaseous (GSOI) and pilot (PSOI)

fuels are also shown in Figure 3.8. To calculate the ignition delay times, the difference between the commanded injection and observed combustion timings were used. The timing parameters of greatest interest include the gas ignition delay time (GID), defined as GSOI – GSOC, the pilot ignition delay time (PID), defined as PSOI-PSOC, and the relative combustion delay, PSOC-GSOC.

The in-cylinder pressure data collection process was the same for all the test conditions. Pressure as a function of crank angle data was collected for 45 consecutive cycles. The relative pressures recorded from the piezo-electric in-cylinder sensor were referenced to the intake manifold pressure at bottom-dead-center, just before the start of the compression stroke and approximately 15° before the intake valve closed. Cyclical variability in the pressure trace, including variations in peak cylinder pressure and the GIMEP, were found to be useful measures of combustion variability when reported in the form of the coefficient of variation (COV – standard deviation / mean). In most cases, the cylinder pressure was averaged before the heat-release rates were calculated.

3.3.2 Fuel/Oxidizer Ratio

The indicated power provided a reasonable representation of the power being developed in the combustion event. However, it did not provide any insight into the overall mixture stoichiometry. For a direct-injection engine, the relative proportions of fuel and oxidizer are typically represented by the equivalence ratio (ϕ), which is defined in Heywood [28] as:

$$\phi = \frac{\left(m_{fuel} / m_{air} \right)_{actual}}{\left(m_{fuel} / m_{air} \right)_{stoich}}. \tag{3.12}$$

However, when using EGR, the exhaust contains oxygen that is not included in this definition. As such, an oxygen equivalence ratio, where m_{oxygen} replaces m_{air} in the preceding equation, was found to provide a better representation of the overall fuel : oxidizer ratio in the combustion chamber.

Normally, the dilution of the intake charge by recirculated exhaust is represented by the EGR mass fraction:

$$\%EGR = \frac{m_{EGR}}{m_{EGR} + m_{freshair}}, \tag{3.13}$$

where m_{EGR} is the mass of recirculated exhaust (per cycle, or as a mass flow rate) and $m_{freshair}$ is the amount of fresh air in the ingested charge. For an engine running overall lean (as for almost all late-cycle direct-injection engines) this is not a good representation of the charge dilution, as the recirculated exhaust contains a varying quantity of oxygen. Thus, the dilution effect for a given EGR fraction varies with the engine's equivalence ratio. A better measure of the dilution of the charge was found [131] to be the intake oxygen mass fraction, Y_{intO2} (volume or mole fraction would be equally effective):

$$Y_{intO2} = \frac{m_{O2}}{m_{EGR} + m_{freshair}} = \frac{m_{EGR} \cdot Y_{O2exh} + m_{freshair} \cdot Y_{O2\,freshair}}{m_{EGR} + m_{freshair}}, \tag{3.14}$$

where Y_{O2exh} represented the mass fraction of oxygen in the exhaust, which varied with load condition, and $Y_{O2freshair}$ represented the mass fraction of oxygen in the fresh air (constant at 0.2295).

3.3.3 Data Presentation Parameters

By defining the engine speed, indicated power, ϕ (oxygen-based), Y_{intO2}, and timing (50%IHR) the operating condition of the single-cylinder engine was fully constrained. Examples of the use of these parameters to provide a complete definition of the engine operating condition have been provided elsewhere [131]. Other parameters unique to the pilot-ignited direct-injection of natural gas system used in this work included the diesel pilot fraction and the gross indicates specific fuel consumption (GISFC). The diesel pilot fraction is defined as:

$$\%pilot = \frac{m_{pilot} \cdot Q_{LHV,diesel}}{m_{pilot} \cdot Q_{LHV,diesel} + m_{NG} \cdot Q_{LHV,NG}}, \tag{3.15}$$

where Q_{LHV} represented the lower heating value of the fuel on a mass basis. The GISFC provides a measure of the fuel conversion efficiency, and is calculated on a diesel energy-equivalent basis from:

$$GISFC = \frac{m_{pilot} + m_{NG} \cdot \dfrac{Q_{LHV,NG}}{Q_{LHV,diesel}}}{P_{gross}}, \tag{3.16}$$

where P_{gross} was the gross-indicated power. Most of the emissions data were also normalised by this latter parameter, resulting in emissions units of mass per gross-indicated power. A summary of the control and output parameters is given in Table 3.2.

3.4 Repeatability and uncertainty analysis

Establishing the degree of certainty in the experimental results is mandatory for assessing whether observed variations in output are actually significant. The uncertainty of the measured outcomes based on the uncertainties in the measuring instruments can be determined using a traditional calculated uncertainty analysis [147]. This procedure has been executed for most of the presented data and the results are shown in Table 3.3 (details of the uncertainty analysis procedure are given in Appendix 4). The percentage errors were found not to vary substantially with operating condition, as the published instrument accuracies were typically given in percentage values. The values in this table are actually only a representative uncertainty, as they represent simply the potential error from the various instrument readings based on the manufacturer's published values. This excludes potential contributions to overall non-repeatability of the results due either to small variations in engine operating condition or to random effects.

A repeatability analysis at a single non-EGR operating condition was carried out, the results of which are included in Table 3.3 [168]. However, this form of analysis neglects the fact that the repeatability of the operating conditions, and even the variability of the engine, differs substantially between different operating conditions. To conduct similar repeatability tests at all the engine operating conditions would be prohibitively time consuming.

The development of statistical techniques has allowed the pooling of experimental errors from multiple operating conditions. From this pooled error, it is possible to determine whether differences between readings are statistically significant [169]. In this work, experimental design/statistical analysis techniques have been applied as often as possible to evaluate the significance of differences within the data. In most cases, sufficient repeated data was available to provide an estimate of the uncertainty through the use of 95% confidence intervals or other statistical measures. In those cases, the uncertainty ranges in the data are represented by these confidence intervals. Otherwise, uncertainty ranges are based on the calculated measurement uncertainty shown in Table 3.3. For all the results, the sources of the uncertainty estimates are identified.

3.5 General Methodology

The specific test conditions used varied for the different sections of this work. In Chapter 4 (the effects of injection pressure), a wide range of engine operating conditions was used in order to investigate the effects of injection pressure over the entire engine map. This also serves as a demonstration of the effects of the various engine operating conditions on performance and emissions. For the hydrogen/methane blend work (Chapter 5), a selected low-speed, low-charge mass (but moderate equivalence ratio) mode was selected. This was chosen to minimize the required gaseous fuel mass flow rates. A limited set of tests was also conducted at a more representative mid-speed, high-load condition. For the fuel composition work (Chapters 6 and 7) a condition very similar to the mid-speed, high-load point from Chapter 5 was selected to provide a reasonable indication of engine conditions near the peak-torque operating condition. Finally, the filtered EGR testing (Chapter 8) was carried out at a mid-load condition, where the PM loading in the exhaust stream was high enough to provide reasonable resolution of the influences of removing the PM. This condition also reduced the mass flow-rate of EGR, resulting in less mass deposition on the filter and hence longer test-times before the filter needed to be changed. For all the test conditions various combustion timings were used to provide a range of combustion conditions by which to evaluate the influences of the various effects under investigation.

For almost all the test sets, data points were replicated and statistical analyses were carried out. The nature of the analyses used varied somewhat, depending on the test set. More replications were used for the filtered PM work, to provide the best possible precision for the test. Fewer replications were used for the injection pressure work, due to the large number of test conditions; however, through the use of ANOVA, it was possible to analyze both the main effects and interactions between operating conditions and injection pressure. While the unavoidable non-randomness of the sampling procedure for the fuel composition work precluded the use of statistical techniques for data analysis, sufficient replication of the data points provided a reasonable estimate of the uncertainty in the experimental results. Further details regarding the test points and statistical analysis techniques used, as well as the motivation for selecting these conditions, are provided in the individual results chapters.

3.6 Tables and Figures

Table 3.1: Single cylinder engine specifications

Engine	Single cylinder 4-stroke
Fuelling	Direct injection, diesel pilot, natural gas main fuel
Displacement	2.5 L
Compression Ratio	17:1; 19:1
Bore/Stroke/Connecting Rod Length	137/169/261 mm
Lubricating Oil	Esso 3XD Extra 15W-40; sulphates <1% by weight
Injector	Westport Innovations Inc. dual-fuel concentric needle prototype
Injection control	Separate diesel and CNG solenoids
Injector holes	7 pilot, 9 gas
Injection angle	18° below firedeck

Table 3.2: Single cylinder engine control and output parameters.

Control Parameter	**Units**	**Key Measurements**
Pilot fraction	%	Diesel mass; Time; Gaseous fuel flow
GIMEP	bar	In-cylinder pressure; Crank angle; Engine parameters
50%IHR	°CA	In-cylinder pressure; Crank angle; Engine parameters
Y_{intO2}		Air flow; Exhaust CO_2; Intake CO_2
ϕ_{O2}		Air flow; Exhaust CO_2; Intake CO_2; Exhaust O_2; Gaseous fuel flow
Output Parameter	**Units**	**Key Measurements**
GISFC	$g_{(diesel\ equivalent)}$/ GikWhr	Gaseous fuel flow; Gross indicated power
Emissions	g/GikWhr	Emissions measurement; Gross indicated power; Air flow rate
Ignition Delay	°CA	In-cylinder pressure; Crank angle
COV GIMEP	%	GIMEP

Table 3.3: Calculated uncertainty and repeatability analysis for key parameters

Parameter	Units	Calculated Uncertainty	Repeatability Uncertainty [168]	Principal Sources of Uncertainty
GIMEP	bar	2%	5%	In-cylinder pressure; Crank angle
Y_{intO2}		5%	N/A	Air flow; Exhaust CO_2; Intake CO_2
ϕ_{O2}		5%	N/A	Air flow; Exhaust CO2; Intake CO2
GISFC	g/GikWhr	2%	2%	Gross power; Gaseous fuel flow
CO	g/GikWhr	5%	10%	CO analyser; Air flow
CO_2	kg/GikWhr	5%	N/A	CO_2 analyser; Air flow
NO_x	g/GikWhr	4%	5%	NO_x analyser; Air flow
HC	g/GikWhr	4%	10%	HC analyser; Air flow
PM	mg/GikWhr	8%	N/A	TEOM; Air flow

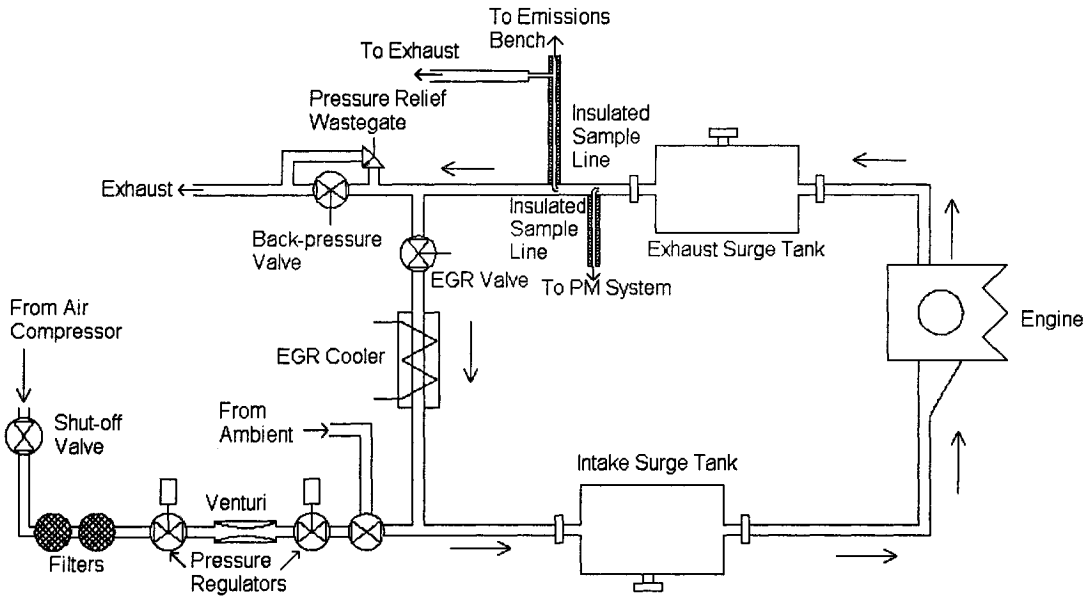

Figure 3.1: Air Exchange System Layout

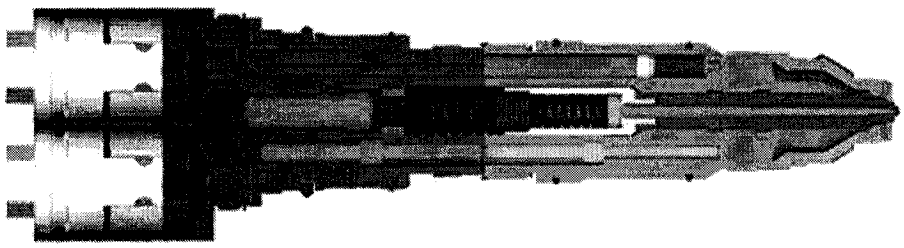

Figure 3.2: Westport HPDI^{TM} Injector Schematic

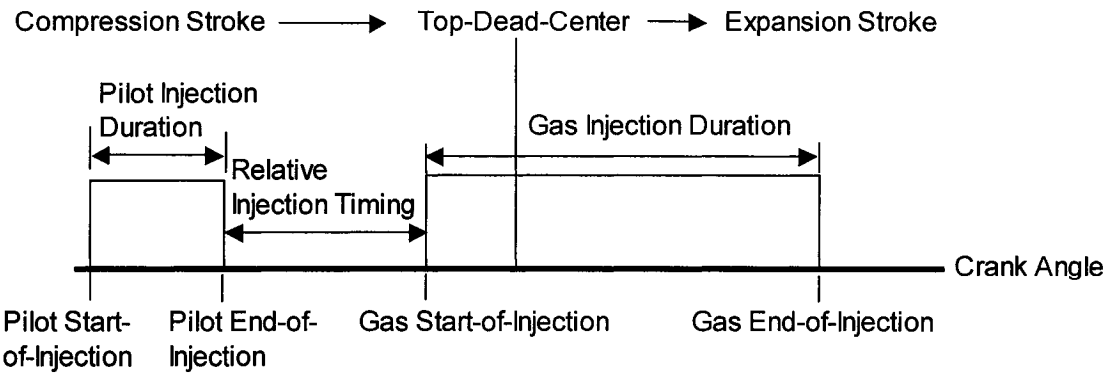

Figure 3.3: Westport HPDI^{TM} injector commanded injection timings.

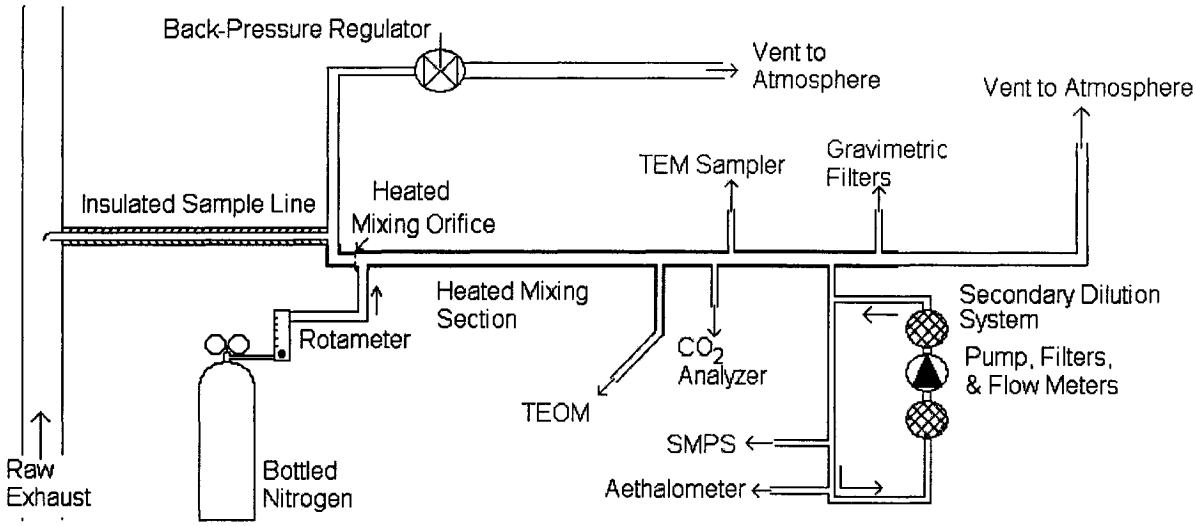

Figure 3.4: PM sampling and dilution system schematic.

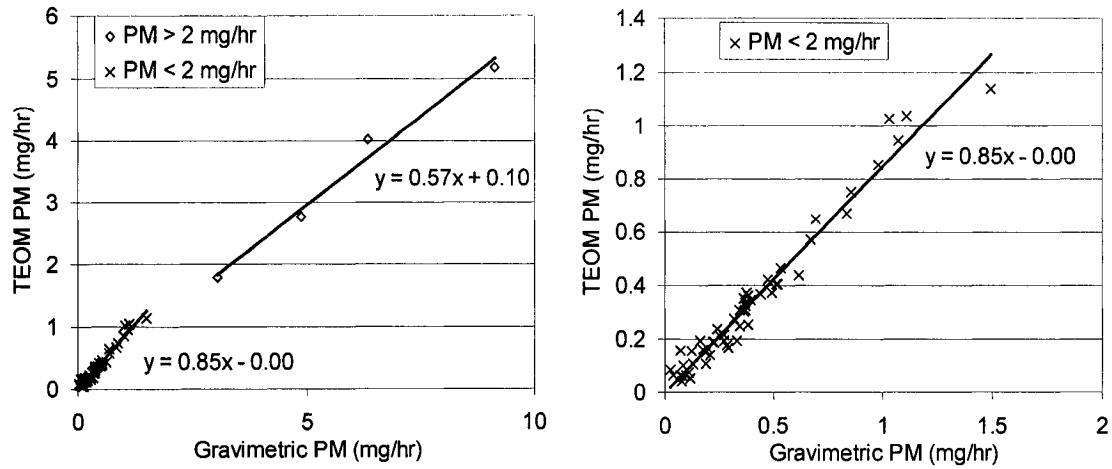

Figure 3.5: Correlation between TEOM and gravimetric filter results. The plot on the left includes PM > 2 mg/hr (measured by the gravimetric filters), while the plot on the right is only PM < 2 mg/hr.

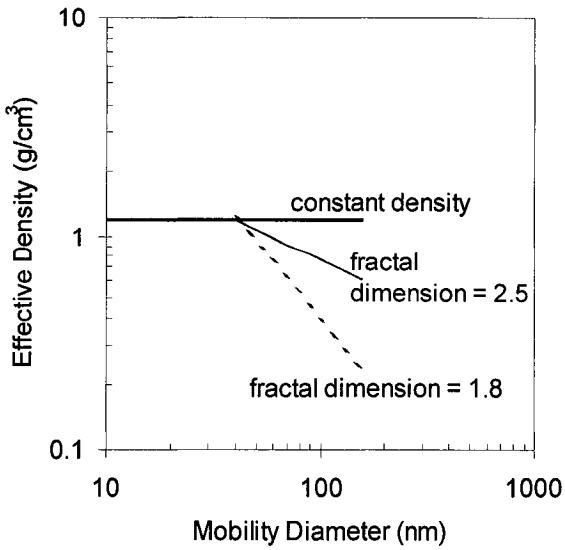

Figure 3.6: Assumed effective density of SMPS particles as a function of mobility diameter, for three different fractal dimensions (d_{fm} = 3 for constant density). Assumed size of primary particles is 40 nm. Based on work from Virtanen *et al.* [159].

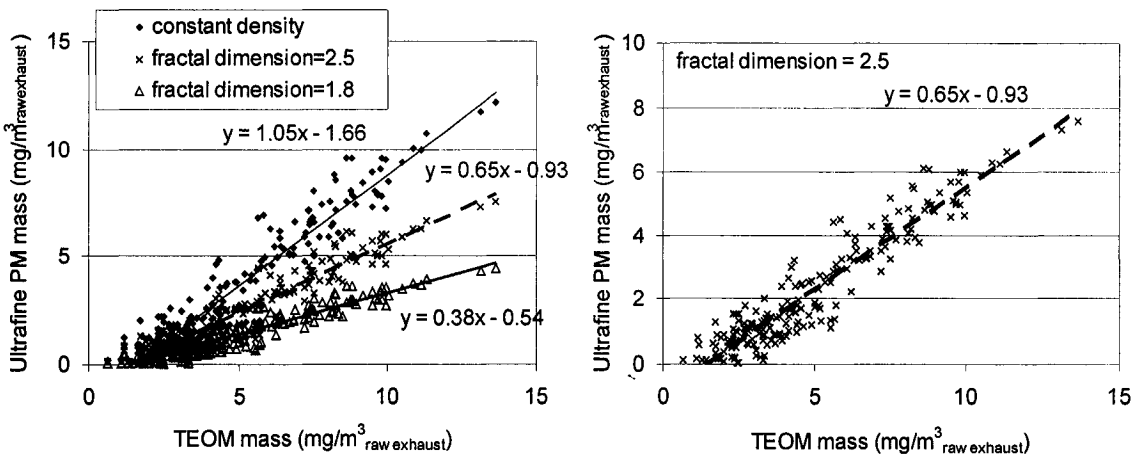

Figure 3.7: Mass concentration comparison between TEOM measurements and calculated ultrafine particle mass based on SMPS measurements. Left: Ultrafine particle mass calculated based on effective particle density calculated from three fractal dimensions (3, 2.5, 1.8). Right: Ultrafine particle mass for fractal dimension of 2.5 only.

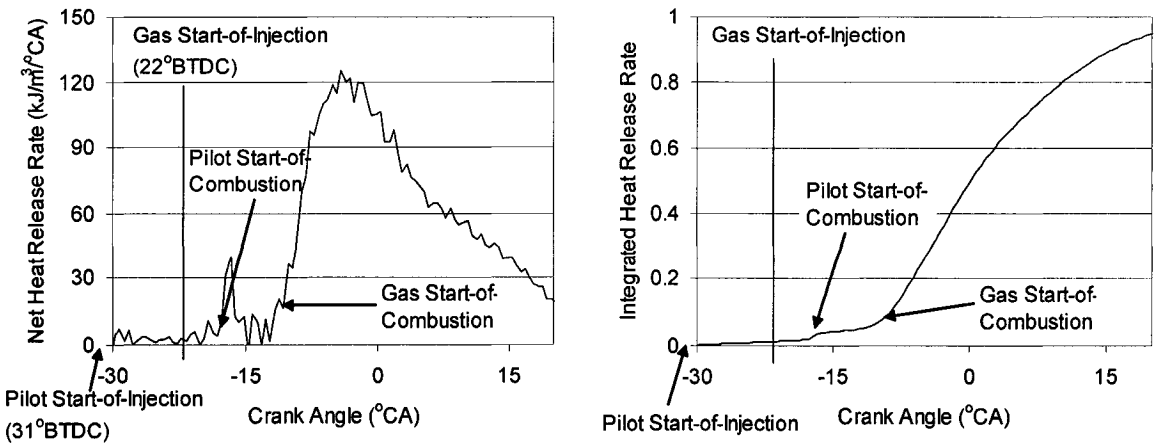

Figure 3.8: Typical net and integrated heat-release rate plots, showing the commanded start-of-injection and observed start-of-combustion timings for the pilot and gaseous fuels.

Chapter 4
Injection Pressure*

4.1 Introduction

The combustion process in a PIDING engine depends on both the reaction kinetics and on the fluid mechanics of the injection and mixing processes. The fluid mechanics of the gaseous jet prior to the start of combustion are highly dependent on the properties and structure of the injected fuel. The characteristics of the medium into which the fuel is being injected, including composition (presence of recirculated exhaust gases), density (temperature, pressure), and motion are also critical. These factors can have a substantial influence on the initiation of the combustion event, its propagation, and its eventual termination. Key parameters include the differential pressure across the injector nozzle, the kinetic energy of the jet, the quantity of air entrained into the jet, the distance that the jet penetrates into the combustion chamber, and the turbulent strain rate in the air where the fuel and oxidizer are mixing. This chapter aims to elucidate the effects of injection pressure on performance and emissions over a wide range of in-cylinder conditions. From these results, further insight into the combustion and pollutant formation processes in the PIDING engine may be derived.

4.2 Injection Pressure Influences

Increasing the injection pressure in diesel engines generates significant reductions in PM emissions. These reductions are attributed primarily to improved atomization and enhanced air entrainment, resulting in a leaner mixture in the core of the spray, and hence lower carbonaceous particle (soot) formation [170,171,172]. Conversely, in-cylinder studies suggest that soot formation may actually increase, due to the more rapid evaporation of the fuel; however, the improved mixing also increases soot oxidation rates, resulting in a net reduction in the engine-out soot [173,174].

---

* A modified version of this chapter was presented at the ASME Internal Combustion Engine Division Fall Technical Conference, 2005. The paper is also in press for publication in the ASME Journal of Engineering for Gas Turbines and Power. McTaggart-Cowan, G.P., H.L. Jones, S.N. Rogak, W.K. Bushe, P.G. Hill and S.R. Munshi. The Effects of High-Pressure Injection on a Compression-Ignition, Direct Injection of Natural Gas Engine. ASME Technical Paper ICEF2005-1213. 2005. All tables and figures reprinted with permission from ASME, © ASME 2005,2006.

One drawback to the use of higher injection pressures in diesel engines is higher NO_x emissions. Increases as great as factors of two or three are reported in the literature, although this magnitude varies substantially with engine type and operating condition [171,174]. In-cylinder gas sampling indicates that the concentration of the HCN radical is substantially increased; this radical is an important precursor in the prompt-NO mechanism [175]. However, in general the increase in NO_x is primarily attributed to higher combustion temperatures induced by the more rapid mixing and evaporation of the fuel spray, leading to a larger initial pre-mixed combustion event. On the other hand, some researchers suggest that at high EGR fractions, NO_x is relatively insensitive to injection pressure [176].

One confounding effect in most of the reported studies is that the injection timing was fixed: because of higher injection rates and shorter ignition delays, the combustion event occurs earlier in the cycle. That these reductions in ignition delay are not as significant with EGR may explain why the injection pressure has less influence on NO_x under high EGR conditions. In general, more advanced combustion substantially increases NO_x emissions [136], a result of higher in-cylinder temperatures which lead directly to more NO formation via the Zeldovich thermal NO mechanism (see section 2.2.2). To avoid this influence, in investigating the effect of injection pressure it is important to fix the combustion, rather than injection, timing.

As mentioned above, higher injection pressures tend to reduce the ignition delay time of diesel fuel. The ignition delay of a non-premixed combustion event can be separated into a physical delay (the time required for the spray droplets to mix with the air, evaporate, and reach a combustible mixture) and a chemical delay (the time required for the break-up of long-chain hydrocarbons and the formation of radicals in the pre-combustion reactions) [171,176]. For a liquid fuel, increasing the injection pressure tends to reduce the physical delay through improved atomization and mixing. However, it does not significantly affect the chemical delay, which is more dependent on the in-cylinder conditions, including temperature, pressure and oxygen concentration [42,174]. Experimental results suggest that, for an auto-igniting natural gas jet, higher injection pressures tend to reduce ignition delay times primarily due to a reduction in the physical delay [89]. In a PIDING engine, the gaseous jet is not auto-igniting, but rather is ignited by the burning diesel; as a result, the

relative locations of the gaseous jet and pilot spray in the combustion chamber have a strong influence on the delay between the injection and the ignition of the gaseous fuel.

The reduced ignition delay time has an effect on the rest of the combustion process, as do the increased injection rate and the more rapid mixing induced by higher shear stresses between the jet and surrounding charge. In general, higher injection pressures tend to increase the intensity of the premixed combustion event. This is somewhat counter-intuitive, given that the ignition delay time has been reduced; however, the unaffected chemical delay combined with the higher injection rate and enhanced mixing result in more fuel having mixed to a combustible level before ignition occurs [171].

The effects of injection pressure depend strongly on the engine operating condition. In particular, increased engine speeds result in enhanced squish-related charge motion and mixing, thereby reducing the absolute physical ignition delay (in ms). Increases in the cylinder pressure and temperature also act to reduce the chemical delay [171,174]. Higher load conditions will typically lead to longer combustion durations, which result in more PM formation for both diesel and PIDING engines [38,170]. With the same injector, higher injection pressures will typically reduce the overall injection duration.

Particulate size distributions are also substantially influenced by injection pressure. For heavy-duty diesel engines, early timings combined with high injection pressures reduce total particle mass but increase the number of nucleation mode particles [172]. Under certain conditions, some researchers suggest that there is a very strong shift from primarily accumulation-mode (particle mobility diameter, D_p, > 50 nm) to mainly nucleation-mode (D_p < 50 nm) particles [172]. This effect is most pronounced at light load; at higher load conditions, increases in nucleation mode particles are not observed while fewer accumulation mode particles are emitted [172]. Higher engine speeds, which correspond to higher turbulence and potentially more enhanced particulate agglomeration, also reduce the magnitude of this shift towards smaller particles [177]. These effects have been attributed to increased concentrations of volatiles species at high injection pressures. Furthermore, the particulate surface area on to which these volatiles condense is reduced substantially (surface area scales with the square of particle diameter). As a result, higher volatile concentrations are present in the exhaust stream; under these conditions the volatiles may be self-nucleating,

generating the substantial nucleation-mode particle concentrations observed experimentally [178].

For a PIDING engine, increasing injection pressure will most likely reduce the physical component of the pilot ignition delay (where auto-ignition occurs). Due to fundamental differences between a high-pressure evaporating liquid spray and an underexpanded gaseous jet, the influence of injection pressure in the gaseous combustion event may differ substantially from the effects observed in diesel engines. Rubas *et al.* [77] and Hill and Ouellette [84] have studied the fundamental effects of injection pressure on gaseous jets under engine-like conditions. In both studies, the gas jet is considered as a two-part system, with a traveling vortex ball being supplied mass and momentum from a quasi-steady jet, as discussed in section 2.2.1. Increasing the injection pressure increases the momentum transfer and the gas density relative to the cylinder charge. This increases the jet penetration distance; however, the increase is only proportional to the ¼ power of the change in density (i.e. doubling the density of the jet will only increase the penetration by 20%) [84]. Because kinetic energy increases with the square of velocity, increasing the injection velocity with a higher pressure differential between the fuel jet and the combustion chamber leads to a higher total kinetic energy transfer to the charge. This results in increased in-cylinder turbulence even after the end of the injection process.

Varying the injection pressure, in conjunction with other combustion modifications, has been used as one of a number of techniques to optimize the performance of PIDING engines over a full test cycle [40,137]. These previous studies made no attempt to systematically identify the influence of injection pressure independent of other parameters. Preliminary studies suggest that, at one operating condition, increased injection pressures reduce PM with little effect on NO_x emissions or other engine performance measures [131,135]. The focus of the current work is to further investigate the effects of increased injection pressure over the full range of engine operating conditions.

4.3 Experimental Methodology

The effects of injection pressure on a PIDING engine were investigated using the single-cylinder research engine described in Chapter 3. The combustion chamber used in this work was from the baseline 1998 model ISX engine, with a 19:1 compression ratio. The fuelling system was configured to provide rail pressures of up to 31 MPa for both the diesel

and the natural gas. For the particulate emissions measurements, TEOM and gravimetric filter measurements of the total mass as well as particulate size distributions were recorded.

4.3.1 Experimental Conditions

One of the principal objectives of this study was to evaluate the influences of injection pressure over a wide range of engine operating conditions. As a result, testing was conducted over the full range of engine operating conditions accessible to the single-cylinder research engine. The operating conditions, based on the parameters defined in section 3.3, are identified in Table 4.1. Other relevant parameters that were held constant were combustion timing (50% IHR at 10°ATDC), the separation time between pilot and gas injections (1.0 ms), and the pilot injection mass (5 mg/injection). The constant pilot flow resulted in a pilot fraction that varied (on an energy basis) from 11% at low load to 3% at high load.

To investigate the effects of injection pressure over the entire engine operating map, a completely randomized experimental design was developed. The design was based on a replicated factorial analysis (with two independent samples per test condition); this resulted in eight test points per speed/load operating condition and a total test matrix of 48 independent test points. A further set of tests was carried out at the peak-torque condition (point #5 in Table 4.1). For these tests, the injection pressure was varied over a wider range (four values, from 18 to 30 MPa); this was intended to provide information on the linearity of the injection pressure influences. For this second set of tests, two charge dilution conditions (non-EGR, $Y_{intO2} = 0.23$; and moderate EGR, $Y_{intO2} = 0.19$) were compared. For the EGR case, the combustion timing was also retarded (50%IHR delayed from 10° to 17.5°ATDC) to evaluate the effect of injection pressure on enhancing the late-stage combustion process.

An analysis of variance (ANOVA) was used to evaluate the statistical significance of the measured results. To avoid high-order interactions between engine speed and load, two separate ANOVAs were conducted; one for the three conditions where load was constant (3, 5 and 6) and one where speed was constant (1, 2 and 3). These two analyses independently identified the effect of speed (with injection pressure and EGR level) and load (also with injection pressure and EGR level). The general representative model is given by:

$$Y_{ijkl} = \mu + OC_i + Y\text{int}O2_j + Pinj_k + OC \cdot Y\text{int}O2_{ij} + OC \cdot Pinj_{ik} + Pinj \cdot Y\text{int}O2_{jk} + OC \cdot Pinj \cdot Y\text{int}O2_{ijk} + \varepsilon_{(ijk)l} \quad (4.1)$$

In this equation, *OC* represents the effect of operating condition – either load or speed (whichever was varying). Y_{ijkl} is the measured response (emissions, fuel consumption, etc.), μ represents a general effect for the whole experiment, *OC*, *YintO2*, and *Pinj* the main effects (combinations represent the interaction terms), and $\varepsilon_{(ikj)l}$ represents the error 'nested' within the condition (that is, the variation between the repeated values at each test condition). In carrying out the analysis, an α-level of 0.05 (1 in 20 chance of identifying a significant effect when one was not present) was used. Further details on the model development and analysis procedure can be found in statistical design text-books (e.g., Hicks and Turner [169]).

4.4 Results

The influences of the various engine operating condition parameters on PIDING engine performance and emissions interact in a statistically significant and highly non-linear fashion [130]. Therefore, any analysis that includes multiple operating condition parameters will routinely exhibit third-order and higher interactions, making interpretation of the results difficult. In this work, the primary interest in the effects of operating condition is how they relate to the effects of injection pressure. As a result, it is more informative to analyze the effects of injection pressure as a function of speed and load independently.

4.4.1 Effect of Load

Investigating the interactions between injection pressure and load involved three operating conditions at constant speed (800 RPM; Table 4.1, conditions 1, 2, 3). Equation 4.1 provides the statistical model used for this analysis. The ANOVA results are shown in Table 4.2. Significant associations (*P*-value < 0.05) are shown in the shaded cells. Degrees of freedom (DF) represent the number of unconstrained data points used in calculating the influence of the parameter.

The ANOVA results indicate that for most emissions, load interacts significantly with both the injection pressure and the intake oxygen mass fraction. (Recall that an interaction term indicates that the response of the dependent variable to one independent variable varies for different levels of a second independent variable; i.e., if dependent variable C responds differently to a change in parameter A at different levels of parameter B, then there is an interaction effect between A and B on C.) As the results include significant second-order interaction terms, the lower order terms (main effects) may not be accurately represented by

the ANOVA [169]. In these cases, it is necessary to evaluate the results graphically to identify whether consistent trends are present.

The results indicate that at fixed speed, the GISFC is independent of injection pressure or intake dilution (EGR); only load has a significant effect. The effects of load and intake dilution on combustion duration interact, due to the longer injection durations at higher loads (more fuel to inject at a given injection pressure), while intake dilution tends to reduce the combustion rate. The fact that injection pressure is a significant factor suggests that it directly affects the combustion duration; however, this result is not statistically reliable given the higher-order interaction between load and intake dilution.

The analysis of CO and NO_x emissions also displays significant second-order interactions between injection pressure and load and intake dilution and load. The fact that no significant interaction between injection pressure and intake dilution is present indicates that the response to injection pressure is consistent with and without intake dilution. Interestingly, while the HC emissions (>95% unburned CH_4) show an interaction between load and intake dilution, there are no interactions with injection pressure. This indicates that the effect of injection pressure is independent of both load and intake dilution. The fact that injection pressure does not statistically influence HC emissions (at either interaction or main-effect level) suggests that injection pressure does not have a consistent influence on unburned fuel. Not surprisingly, given their complicated formation mechanisms, the particulate matter mass emissions show a third-order interaction between load, injection pressure, and intake oxygen mass fraction. Further interpretation of the PM results must be conducted through graphical means.

4.4.2 Effect of Speed

Investigating the effect of injection pressure over a range of engine speeds (RPM), involved three test points with constant engine load & equivalence ratio (conditions 3, 5, and 6 from Table 4.1). The results of this ANOVA are shown in Table 4.3, with an α-level of 0.05. As with the load results (Table 4.2), higher-order interactions are present for most of the measured parameters. As in the load effect analysis (section 4.4.1), the GISFC is independent of injection pressure; it depends only on speed and intake dilution independently.

Engine speed, intake dilution, and injection pressure all interact for the CO and HC emissions. As a result, evaluation of the lower-order interactions and main effects must be deferred to a later section. NO_x emissions vary with speed and intake dilution, but are independent of injection pressure. Unlike the load-effects analysis, PM emissions depend only on the main effects of speed, intake dilution, and injection pressure; no significant interactions occur. While the fact that these factors are significant is not surprising, it is interesting that no higher-order interactions are significant. This indicates that the effects of injection pressure on PM are consistent, at high load, over the full range of speeds and intake dilution conditions.

In general, the ANOVA results indicate that operating condition has a strong effect on the measured results, while the injection pressure tends to interact with speed and load but not as commonly with intake dilution (EGR level). These second-order interactions limit the statistical evaluation of the significance of the main effects; graphical interpretation is required to provide further insight into the influences of injection pressure.

4.4.3 Effects of Operating Condition

As shown in the preceding statistical analyses, the emissions and performance of the PIDING engine depend strongly on operating condition. Most of the dependent variables show substantial interactions between operating condition, intake dilution, and injection pressure. To provide further insight, the results are presented graphically in Figures 4.1-4.5, with each dependent parameter plotted individually. Each plot includes all six operating conditions (speed/load), while the individual bars on the plots represent the low and high injection pressure cases, with and without intake dilution (EGR). The values shown are averages of the two values collected for each test point. Error bars represent the calculated uncertainty (Table 3.3). The results are also presented in tabular form in Table 4.4. This table also includes the pressure ratio between the injection pressure and the peak cylinder pressure (P_{inj}/P_{max}) for each condition. This pressure differential indicates that for the low-load cases, the pressure ratio is as much as five times greater than the cylinder pressure; however, at the high-speed, high-load, low injection pressure condition, the pressure in the fuel rail is only 30% higher than the peak cylinder pressure. Furthermore, as the pressure drop through the injector is estimated at 15-25% of the rail pressure, the actual differential pressure across the

nozzle outlet may be quite small. As will be discussed further, this has a substantial influence on the effects of injection pressure at different operating conditions.

Injection pressure has an insignificant effect on GISFC, as shown in Figure 4.1; this agrees with the ANOVA results in Tables 4.2 and 4.3. Of the other parameters, load has the largest influence, with optimum efficiency (lowest GISFC) at the mid-load cases. Higher speeds (at equivalent load) also tend to improve efficiency. The fact that GISFC reaches a minimum at part load for a given speed agrees with basic compression-ignition understanding, due to the trade-off between quasi-constant friction losses and increasing heat transfer [28]. The high HC emissions seen at the low load case also tend to reduce efficiency.

No statistically consistent influence of injection pressure on NO_x emissions is observed (Figure 4.2, Tables 4.1 and 4.2); the emissions are, however, sensitive to operating condition. Intake dilution reduces NO_x emissions due to the reduction in combustion temperature, as has been demonstrated in previous work [122,130,135]. Also consistent with previous results, higher speeds reduce power-specific NO_x emissions [130]. This may be attributed to the higher turbulent intensities at higher speeds, which reduce the time the burned gases are at high temperatures before they mix with cool charge. This results in less time for the relatively slow thermal NO mechanism (section 2.2.2) to approach equilibrium, thereby reducing NO formation. Higher injection pressures tend to increase NO_x without EGR (except at 1600 RPM), as suggested previously [135]; however, the magnitude of the effect varies substantially with operating condition.

The fact that NO_x emissions depend primarily on the peak combustion temperature has been demonstrated previously [122]. The peak temperature relates to the intensity of the initial combustion event, and is directly related to the rate of pressure rise in the combustion event. Higher injection pressures increase the maximum rate of pressure rise at all conditions except the high-speed (1600 RPM) case. This suggests that at 1600 RPM the ignition and early-combustion phases are kinetically (rather than mixing) limited; as a result, a higher injection pressure does not significantly increase the combustion rate, resulting in no significant change in the combustion temperature for the early combustion stages. This effect may explain the reduction in NO_x emissions with increased injection pressures without EGR at 1600 RPM, a finding contrary to the results at the other non-EGR conditions.

With EGR, the NO_x results show no consistent dependence on injection pressure. Only at mid-load (0.45ϕ, at both 800 and 1200 RPM) are NO_x emissions significantly increased at higher injection pressures. The particularly large increase at 800 RPM is due to test condition repeatability, where both low-injection pressure cases had, by chance, intake oxygen mass fractions of approximately 0.185, compared to 0.191 for the high injection pressure cases. The extreme sensitivity of NO_x to intake dilution has previously been demonstrated [131]. This was the only condition where the difference in intake oxygen concentration is greater than 0.003; as a result, this effect should not influence the accuracy of the results at any of the other conditions. It does, however, mean that the results at this condition (mid-load, low-speed with intake dilution) are somewhat less certain than would be desirable; it also demonstrates the importance of ensuring operating condition consistency.

The statistical results indicate that the CO emissions depend on injection pressure, intake dilution, and operating condition; however, the statistical significance of these parameters individually cannot be evaluated due to high-order interaction terms. A plot of the CO emissions, Figure 4.3, demonstrates these complex interactions. In general, the CO emissions are greatest at the highest loads. Intake dilution doubles the CO emissions at almost all the operating conditions, which agrees with previous results [122]. At low speed (and mid-speed mid-load) higher injection pressures tend to reduce CO emissions. However, at high load at intermediate speed, the CO emissions are relatively unchanged by higher injection pressure, while at high speed the CO emissions are significantly increased. This non-linear behaviour of CO with injection pressure may be due to the competing influences of enhanced mixing and increased turbulent shear stresses as the injection pressure increases, as will be discussed further in section 4.4.4.

Similar to the CO emissions response, the effects of injection pressure on HC emissions, Figure 4.4, vary with operating condition. At all the conditions, the HC emissions are primarily unburned methane. Hydrocarbon emissions are, on a power-specific basis, highest at low-load. This may be at least partially a result of unburned fuel from fixed-volume sources such as the nozzle sac; the amount of fuel which is retained during the combustion event, and is then released late in the combustion cycle, will be essentially constant on a per-cycle basis, leading to higher power-specific emissions at low power levels. Another factor, which may be contributing to the high HC emissions at low load, is over-

leaning of the injected fuel prior to ignition of the gas jet by the pilot. One possible influence of higher injection pressures is more over-leaning of the fuel, resulting in higher HC emissions. Increases in HC emissions, potentially attributable to this effect, occur at many operating conditions, including most of the higher speed and EGR test conditions. However, at a number of conditions increasing the injection pressure reduces HC emissions; this may be due to changes in gaseous fuel ignition delay time, which will be discussed in section 4.4.5, as shorter ignition delay times will tend to result in less fuel having overmixed before ignition occurs. Other factors, including increased turbulent strain leading to more local extinction events may also be contributing to the HC emissions. The variability in the HC emissions with operating condition demonstrates the complex interactions between these various potential mechanisms. At all the operating conditions the effects of injection pressure on HC emissions are secondary to the influences of operating condition and intake dilution.

Injection pressure has a strong and relatively consistent influence on PM emissions, as shown in Figure 4.5. The PM emissions are also affected by intake dilution and operating condition, as demonstrated in Table 4.2. At low- and mid-load at low speed, PM emissions are relatively insensitive to intake dilution or injection pressure, although there is an apparent slight reduction in PM with injection pressure at low load. At high load, the PM emissions at the low injection pressure case are substantially higher; increasing the injection pressure results in reductions in PM emissions by a factor of almost three both with and without intake dilution. Similar influences are seen at 1200 and 1600 RPM. In general, at low-load PM emissions are relatively low, and increases in intake dilution do not substantially increase them. This is consistent with previous results that have shown that most of the PM emissions at low load conditions are volatiles [142], probably formed from evaporated (but uncombusted) lubricating oil and liquid fuel which condense in the exhaust stream. While increasing the pressure of the diesel pilot will likely influence the volatile concentrations attributable to the pilot spray, much of the pilot contribution to the volatiles may be originating from diesel fuel leaking from the injector sac volume late in the expansion stroke, after the combustion has terminated. These species would be emitted unreacted, as the cylinder temperature would be too low to fully oxidize them; this process would not be substantially influenced by injection pressure. At higher load conditions, and especially with

higher intake dilution, the natural gas contribution to the PM emissions is substantially greater than the volatile fraction [142].

The observation that injection pressure significantly reduces solid carbon PM (soot) formation is consistent with results from diesel engine research [170-176]. In diesel engines, the most commonly proposed mechanism is increased air entrainment into the fuel spray, which leans out the soot-inducing fuel-rich reactions occurring in the core of the spray as it evaporates, as proposed in the phenomenological model of Flynn, Dec *et al.* [102,179]. While a diesel spray combustion model does not completely describe the combustion of pilot-ignited natural gas jets, higher gas velocities are expected to increase air entrainment just downstream of the injector. Based on shock-tube experiments it is known that the natural gas flame is lifted from the nozzle, and parameters that increase air entrainment (i.e. reduction in nozzle hole size) decrease soot formation [89]. The pilot combustion has a strong influence on the gas combustion, but at high load, most of the soot is derived from the natural gas [142]. Thus, soot emissions from the natural gas engine may be being reduced by mechanisms similar to those found in a conventional diesel engine. An alternative explanation of soot emission reduction is that with higher injection pressures, less fuel is burned late in the cycle, where the falling temperatures will lead to slower soot oxidation. In-cylinder heat release rates suggest that this may not be the case (see below); this is an area of ongoing research involving in-cylinder turbulence enhancement through combustion chamber optimization.

4.4.4 Injection Pressure Effect Details

In the preceding section, a range of operating conditions was investigated at only two injection pressures (21 and 30 MPa). As such, any non-linear effects of injection pressure would not be identified. A more detailed study was carried out at the near-peak-torque operating condition (test condition #5 in Table 4.1). A wider range of injection pressures (18-30 MPa) were tested, with and without intake dilution. For the diluted case, both the standard combustion timing (combustion mid-point at 10°CA after top-dead-center) and a late-timing case (combustion mid-point at 17.5°CA) were studied.

In conducting the tests, variations in the operating condition were minimized by restricting the randomization of the tests. Due to this restriction, the results were not analyzed statistically. The operating condition was set (including intake oxygen mass fraction), then

the injection pressure was varied (in random order) over the testing range. While this procedure allows greater precision in studying the individual effects of injection pressure, the accuracy of comparisons between the operating conditions is reduced.

In general, the trends in emissions and performance for the three conditions, shown in Figure 4.6, are comparable to those in the earlier tests. For all three cases, a generally linear reduction in PM emissions with increased injection pressure is observed; in all cases, the reduction between the lowest and highest pressures is approximately 50%. The effects on NO_x and HC are relatively small, with NO_x being slightly increased and HC slightly reduced with increased injection pressure. There are no consistent trends in GISFC. The CO emissions, however, show a substantially non-linear response to injection pressure. At all three conditions, a maximum is reached between 22 and 26 MPa injection pressure. The strong influence of operating condition on CO emissions (Figure 4.3) may be explained by this response, as at different operating conditions the location of the peak CO emissions levels varies substantially. At 1600 RPM, the peak may be shifted towards higher injection pressures, resulting in the observed increase between 21 and 30 MPa. This is most likely due to changes in in-cylinder turbulence intensity, as well as the increased overall combustion duration (in ^{o}CA) for the higher speed condition.

Comparisons between operating conditions suggest that dilution tends to somewhat increase CO, HC, and PM emissions, while substantially reducing NO_x and slightly reducing GISFC. Delaying the combustion for the diluted condition results in a further increase in CO and HC emissions, as well as an increase in GISFC; however, NO_x and PM emissions are substantially reduced. At the lowest injection pressure, the late timing results in significantly higher PM, due possibly to the low pressure-ratio between the cylinder and the injected fuel. At this operating condition, it would appear that the general trends in emissions and performance due to changes in the injection pressure are relatively independent of intake dilution and combustion timing. However, the specific levels of the emissions vary substantially.

4.4.5 In-Cylinder Performance

The in-cylinder pressure measurement provides an indication of the influences of injection pressure and operating condition on the combustion event. The gaseous fuel ignition delay, shown in Figure 4.7, is in general reduced with higher injection pressures,

most likely due to enhanced mixing of the injected fuel with the charge air. This suggests that the mixing is limiting the gaseous fuel ignition process over a wide range of operating conditions. The fact that the effects of injection pressure on ignition delay are relatively small (on the order of 5-15%); suggests that other mechanisms (for example chemical kinetics) are also posing a limitation on the ignition process. Variations in the mechanical injector operation, due to changes in fuel rail and cylinder pressure, could also be affecting the observed results. However, increasing the rail pressure from 24 to 28 MPa has been shown to shorten the mechanical injector delay by less than 0.13°CA, indicating that the mechanical effects are relatively insignificant [180].

The combustion duration, Figure 4.8, (measured as the crank angle range between the 5% and 90% integrated net heat release points) is reduced with injection pressure. The fact that the rate at which the fuel is introduced into the combustion chamber has a significant impact on the combustion duration indicates that the overall duration of the combustion process is at least partially controlled by the mixing rate. As such, any method which increases the injection rate will tend to reduce the combustion duration. For most cases, intake dilution reduces the combustion duration, primarily due to the longer ignition delay (Figure 4.7), which results in more of the fuel being at a combustible mixture prior to ignition. As the combustion duration is measured from start-of-combustion (approximately) to end of combustion, a later start of combustion leads to a shorter combustion duration, even if the overall process (start-of-injection to end-of-combustion) is longer. While intake dilution has been shown to increase combustion duration, this occurs only at dilution levels greater than those tested in this work [39].

Further information about the combustion event can be discerned from the in-cylinder pressure trace and its derivative, the heat-release rate. These parameters are shown for the low-load, low-speed condition (point #1, Table 4.1) in Figure 4.9. The peak HRR is higher without dilution (left plot), while the injection pressure has only a very minor influence on the combustion rate or combustion intensity. The most significant difference is that the peak heat release rate is increased with the higher injection pressures in both cases. This is a result of the more rapid injection process, which is approximately 25% faster for the higher injection pressure case. This leads to more fuel being available to burn in the initial combustion event, resulting in a shorter combustion duration and a higher peak HRR.

However, the fact that the combustion duration is significantly influenced by the higher injection pressure indicates that, even at this low-load, short injection duration condition, the rate of mixing between the fuel and oxidizer is still controlling the overall combustion rate.

The pressure trace and heat-release rate for the mid-speed, high-load case is shown in Figure 4.10 (Appendix 6 shows the remaining pressure traces and HRR's). Increasing the injection pressure substantially increases the combustion rate, with and without intake dilution. The main-fuel combustion starts significantly (~2°CA) earlier for the lower injection pressure, but the late-phase combustion process (after 15°CA) is essentially the same. At this condition, and at the other higher-load operating conditions, the combustion duration is substantially reduced by the higher injection rate of fuel into the combustion chamber and the correspondingly more rapid mixing process.

4.4.6 Effect on particle size distributions

The preceding sections included total mass measurements of particulate matter emissions. However, the accuracy of these measurements for low particle concentrations is uncertain (see section 3.2.2). Furthermore, smaller particles (especially those in the ultrafine range with a diameter <100 nm), pose significant health and environmental concerns but are poorly represented by total mass measurements [178]. As a result, an analysis of the size distribution of the emitted particles is pertinent. The size distributions presented here cover the range of aerodynamic diameters between 5 and 150 nm. On the distribution plots, the low and high injection pressures are plotted together, with the undiluted and diluted distributions shown in adjacent plots. The distributions have been adjusted for dilution ratio, such that they represent the number concentration per unit volume of raw exhaust.

The particle size distributions at the low-speed, low-load condition are shown in Figure 4.11. Both with and without intake dilution, the injection pressure has very little influence on the number distribution. In both cases, there is a discernable 'nucleation-mode' peak, although with intake dilution, a significant 'accumulation mode' peak is also present. For diesel engines, the nucleation mode particles are thought to be primarily condensed liquid droplets, comprised of sulphuric acid, water, and volatile hydrocarbons that have nucleated in the exhaust stream [99]. Diesel-engine researchers report that the mode of the nucleation peak occurs at particle diameters of approximately 10 nm [181], which is similar

to the mode of the peak shown in Figure 4.11. This provides further evidence that the bulk of the particulate emissions at this condition are attributable to the emissions of volatile species.

At the same speed but high load (point #3 in Table 4.1) the particle size distribution (Figure 4.12) has been significantly altered from the low-load case. The particle distribution is now uni-modal with no indication of a separate nucleation-mode peak. This indicates that engine-out particles are making a greater contribution to the total emissions, as these particles will tend to be larger due to a longer residence time as well as higher concentrations in the pre-dilution exhaust system resulting in greater particulate agglomeration. At the same time, any volatiles in the exhaust will tend to condense onto these particles rather than forming new nucleation mode particles. Higher injection pressures reduce both the number and the mode of the ultrafine particle distribution, both with and without EGR. The number concentration of ultrafine particles (less than ~ 25 nm in mobility diameter) is as much as an order of magnitude lower at higher injection pressures. The fact that the particles are both smaller and fewer in numbers suggest that the higher injection pressure is leaving less time for particulate inception to occur. This would be consistent with higher fuel-air mixing rates, resulting in a shorter residence time for the particle precursors to form particles in the high-temperature fuel-rich region of the combustion zone.

Size distributions for the high-speed, high-load case (point #6 in Table 4.1) are shown in Figure 4.13. As at the previous condition, intake dilution tends to shift the particle distribution towards more and larger particles. However, at this speed the effect of injection pressure is significantly reduced, which coincides with the smaller (relative) influence on total particle mass shown in Figure 4.5. The reduced effect of injection pressure on the size distributions at higher speeds agrees with results from diesel-fuelled engine research [177]. This provides further evidence that the injection pressure is having less of an effect on improving the turbulent mixing process at higher speeds. For this operating condition, it is apparent that many of the particles are greater than 150 nm in diameter, and as a result are not measurable with the particle sizing instrumentation.

4.5 Discussion

The results show that the injection pressure can significantly influence emissions, without impacting combustion efficiency. The effect varies with engine speed and load due to changes in the in-cylinder conditions. At low speed, the in-cylinder turbulence will be at

its lowest levels. As such, higher injection pressures will tend to enhance the turbulence, aiding the rapid completion of the combustion event. While this appears to be significant at high load (where the reduction in PM is very substantial), it has little effect at lower loads. The most likely reason for this is that the 21 MPa injection pressure is already substantially higher than the in-cylinder pressure, providing sufficient turbulence for the combustion to complete rapidly. Hence, turbulent mixing is not the limiting factor for the combustion event at low-load conditions, with and without EGR, at constant oxygen equivalence ratio. From the particulate size distributions, it appears that at low-load conditions nucleation of volatile hydrocarbons and sulphates is a significant contributor to the PM loading. The fact that injection pressure does not influence the size distribution suggests that it also has little influence on volatile emissions.

At higher loads, the effect of injection pressure is more significant, as the in-cylinder pressure is higher. The relative change with injection pressure of the differential pressure between the combustion chamber and the fuel is also substantially greater. The higher injection pressure tends to increase the density gradient between the gaseous jet and the combustion chamber while also increasing the kinetic energy of the jet. This has a substantial influence on the combustion process, primarily through enhanced turbulence in the combustion chamber. The higher gas-jet velocity is also more likely to entrain air, which will tend to reduce the equivalence ratio in the core of the jet. As soot precursor formation is most likely occurring in the core region, the lower equivalence ratio at higher injection pressures generates fewer soot precursors, resulting in less soot formation. Soot oxidation in the late stages of combustion may also be enhanced by the higher turbulent intensity, resulting in the observed reduction in PM emissions. More rapid mixing also reduces the amount of time for formation of particle precursors in the high temperature fuel-rich region of the combustion zone. As the high equivalence ratio cases typically have a higher soot fraction (volatiles are less significant), the reduction in soot emissions leads directly to substantially lower PM mass emissions and number densities. This effect is even more significant with intake dilution, where the in-cylinder pressure is higher and the combustion duration is longer. Increased injection rates with higher injection pressures also make a significant contribution to this effect. Offsetting these influences at the higher speeds are the increases in the in-cylinder turbulence due to the more rapid piston motion and the longer

injection duration (relative to the piston motion; the absolute time for injection is essentially unchanged).

4.6 Conclusions

1. At high loads, higher injection pressures substantially reduce both mass and number of PM emissions. At low load, post-exhaust nucleation mode particles dominate the PM loading; the mass and number of these particles are independent of injection pressure. The effects of injection pressure on PM become less significant as in-cylinder turbulence increases with engine speed.
2. The combustion process at all operating conditions is restricted by the rate at which the fuel and oxidizer are mixing. Increasing the injection pressure increases both the mass flux of fuel into the combustion chamber and the in-cylinder turbulence, resulting in enhanced mixing, reducing the combustion duration and increasing the peak combustion intensities.
3. The injection pressure has a significant impact on emissions but little influence on fuel consumption. The nature of the influence depends strongly on operating condition parameters including engine speed, load/equivalence ratio, and intake oxygen mass fraction. Significant high-order interactions between operating condition parameters indicate that most of the emissions are a result of multiple competing influences, the relative importance of which varies substantially with operating condition.
4. The effects of injection pressure on CO are highly non-linear, displaying a maximum at intermediate injection pressures. The response is also sensitive to operating condition; this is possibly due to changes in the relative contributions of cylinder and gaseous-jet induced turbulence to the combustion process. The effects of injection pressure on HC emissions are inconsistent and insignificant compared to the effects of operating condition and intake dilution.
5. At higher in-cylinder pressures (high load), the differential pressure between the injected fuel and the cylinder is lower; hence increasing the injection pressure has a greater influence on the combustion process. With high differential pressures, the flow through the nozzle is choked, resulting in less sensitivity to in-cylinder conditions.
6. Without EGR, NO_x emissions are slightly increased with higher injection pressures due to more rapid and more intense combustion. With EGR, the effects of injection

pressure on NO_x are not significant; differences due to variability in the intake dilution level dominate the observed variations in the NO_x emissions.

7. Relatively small variations in the operating condition setting have a significant influence on the emissions results, even when the test points are replicated. As a result to ensure that the experimental precision is adequate, it may sometimes be necessary to sacrifice absolute accuracy by restricting test point randomization.

4.7 Tables and Figures

Table 4.1: Engine test conditions

ID	Speed (RPM)	GIMEP (bar)	ϕ	Y_{intO2}	P_{inj} (MPa)	Pilot %
1	800	3	0.25	0.23, 0.19	21,30	11
2	800	8.5	0.45	0.23, 0.19	21,30	6
3	800	13.5	0.6	0.23, 0.19	21,30	3
4	1200	8.5	0.45	0.23, 0.19	21,30	6
5	1200	13.5	0.6	0.23, 0.19	21,30	3
6	1600	13.5	0.6	0.23, 0.19	21,30	3

Table 4.2: ANOVA results as a function of load at 800 RPM

		P-value					
Term	DF	GISFC	CO	NO_x	HC	PM	Comb. Dur.
Load	2	0	0	0.01	0	0	0
$YintO_2$	1	0.16	0	0	0	0	0.05
P_{inj}	1	0.86	0	0	0.06	0	0
Load * $YintO_2$	2	0.06	0	0	0	0	0
Load * P_{inj}	2	0.17	0	0.03	0.13	0	0.14
$YintO_2$ * P_{inj}	1	0.24	0.09	0.07	0.3	0.06	0.06
Load * $YintO_2$ * P_{inj}	2	0.35	0.33	0.75	0.93	0.02	0.49
Experimental Error	23						

Table 4.3: ANOVA results as a function of speed at 13.5 bar GIMEP

		P-value					
Term	DF	GISFC	CO	NO_x	HC	PM	Comb. Dur.
Speed	2	0	0	0	0	0.03	0
$YintO_2$	1	0.04	0	0	0	0	0.00
P_{inj}	1	0.77	0.004	0.85	0.38	0.04	0
Speed * $YintO_2$	2	0.14	0.027	0	0	0.23	0.97
Speed * P_{inj}	2	0.17	0	0.25	0.01	0.08	0.00
$YintO_2$ * P_{inj}	1	0.07	0.169	0.84	0.4	0.49	0.20
Speed * $YintO_2$ * P_{inj}	2	0.69	0.019	0.34	0	0.25	0.07
Experimental Error	23						

Table 4.4: Summary of results from operating condition tests

Operating Condition		800RPM 2.5 bar		800 RPM 8.5 bar		800 RPM 13.5 bar		1200 RPM 8.5 bar		1200 RPM 13.5 bar		1600 RPM 13.5 bar	
Parameter	Pinj / Y_{intO2}	21	30	21	30	21	30	21	30	21	30	21	30
GISFC	0.23	210	210	188	189	203	196	183	184	193	192	189	189
(g/GikWhr)	0.19	215	224	189	187	199	199	181	184	191	191	180	184
NO_x	0.23	7.2	8	6.2	7.9	5.8	6.1	4.4	4.8	4.3	4.4	4.3	3.6
(g/GikWhr)	0.19	1.1	1.1	0.94	1.9	1.2	1.3	0.83	1	0.96	0.93	0.62	0.6
CO	0.23	3.9	3.1	0.96	0.97	11.6	3.1	2.7	1.6	10.3	9.3	6	8.5
(g/GikWhr)	0.19	6.7	6.2	4.2	2.6	19.6	8.8	5.3	4.1	17.6	17.7	7.8	15.5
HC	0.23	3.4	2.5	0.43	0.55	0.3	0.4	0.46	0.55	0.28	0.32	0.38	0.4
(g/GikWhr)	0.19	8.3	6.9	2.34	1.82	0.82	0.67	1.58	2.01	1.2	0.98	1.14	1.5
PM*100	0.23	2	1.7	1.1	1.1	3.4	0.84	1.1	1	5.4	2	4.6	3.8
(g/GikWhr)	0.19	2.5	2.1	1	1	10.8	3.5	2.5	1.2	19.2	9.3	12.9	9.3
Comb. Dur.	0.23	5	4.7	15.5	11	24.5	19.8	24.3	22.3	31	27.3	38	31.8
(°CA)	0.19	8	7	11.5	10	22.3	18	22	18	28.5	25.3	38.5	27.3
Pinj/Pmax	0.23	3.3	4.8	2.1	2.7	1.5	2.2	2.1	3	1.5	2.2	1.5	2.1
	0.19	2.8	3.9	1.8	2.4	1.4	1.9	1.9	2.7	1.4	2	1.3	1.9

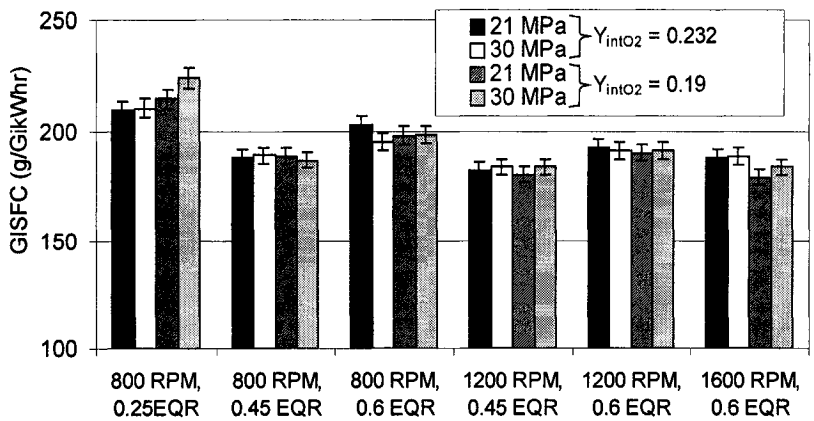

Figure 4.1: Effect of injection pressure and operating condition on GISFC

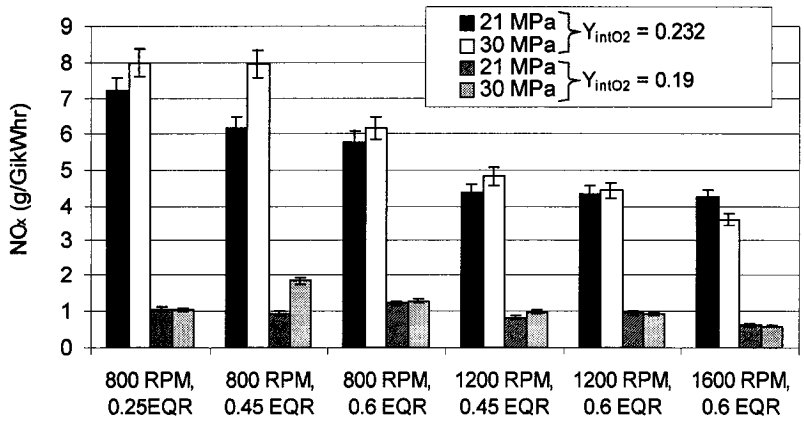

Figure 4.2: Effect of injection pressure and operating condition on NO_x emissions

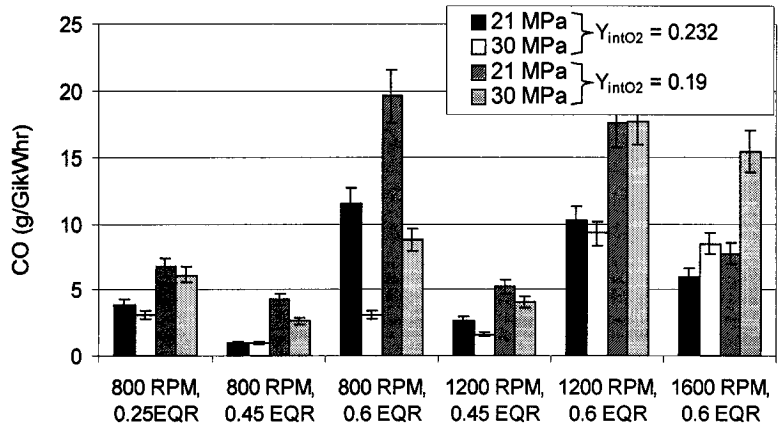

Figure 4.3: Effect of injection pressure and operating condition on CO emissions

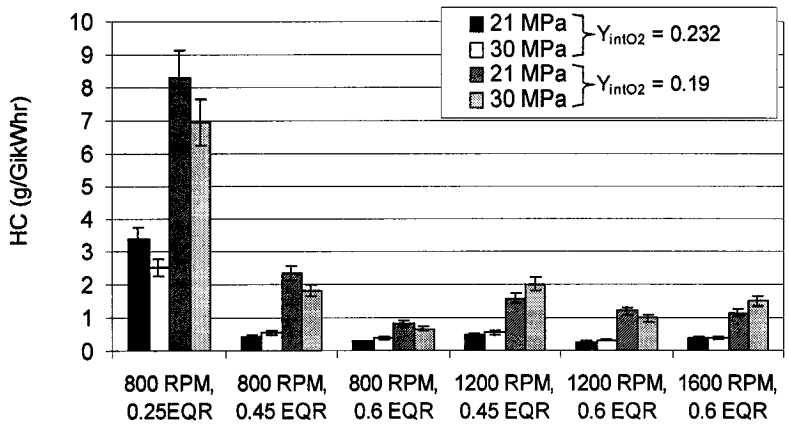

Figure 4.4: Effect of injection pressure and operating condition on HC emissions

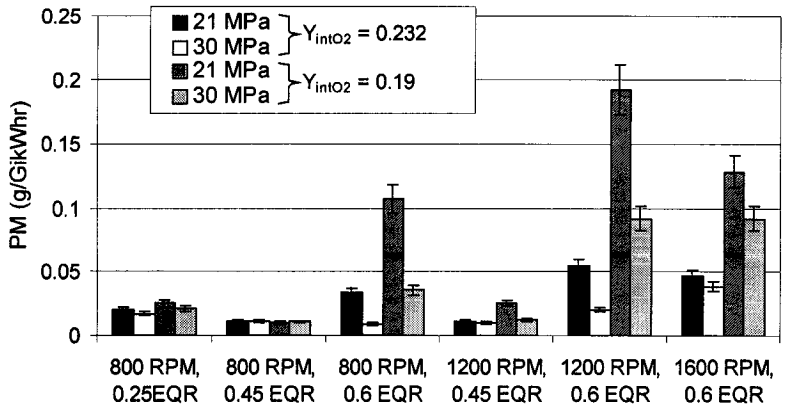

Figure 4.5: Effect of injection pressure and operating condition on PM emissions

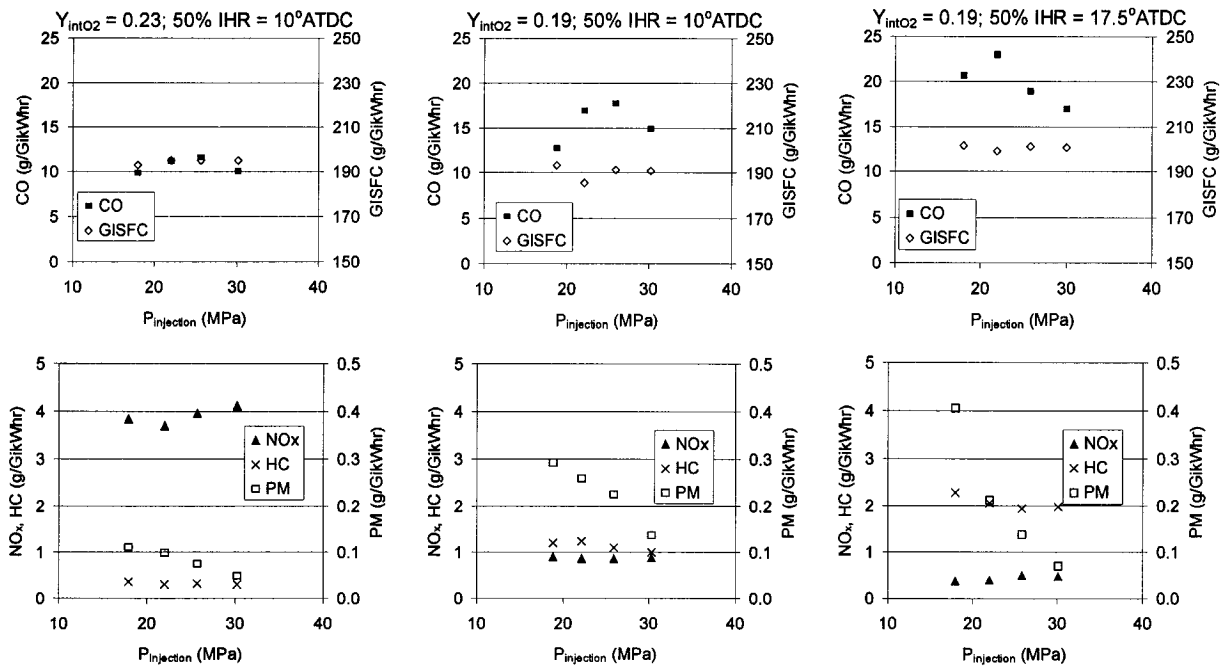

Figure 4.6: Emissions and GISFC variations with injection pressure, at near peak-torque. Operating conditions (L-R): Y_{intO2} = 0.23, 50%IHR = 10°ATDC; Y_{intO2} = 0.19, 50% IHR = 10°ATDC; Y_{intO2} = 0.19, 50%IHR = 17.5°ATDC. For all: 1200 RPM, ϕ = 0.6, 13.5 bar GIMEP.

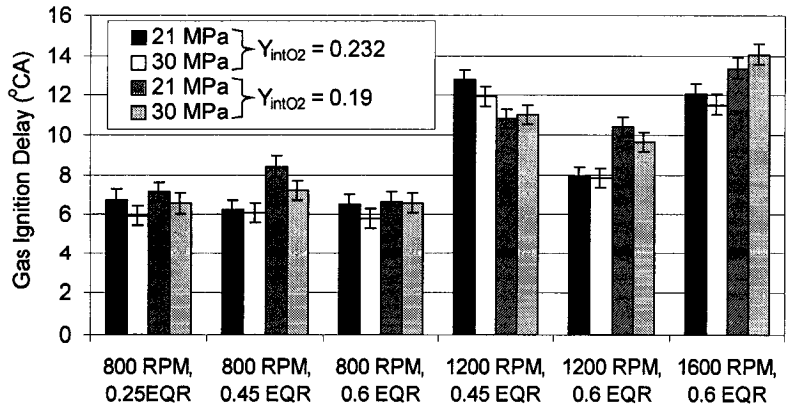

Figure 4.7: Effect of injection pressure and operating condition on gas ignition delay (GID)

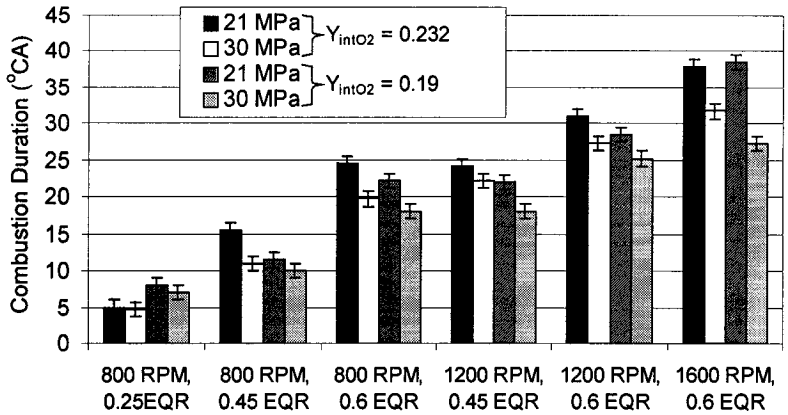

Figure 4.8: Effect of injection pressure and operating condition on combustion duration

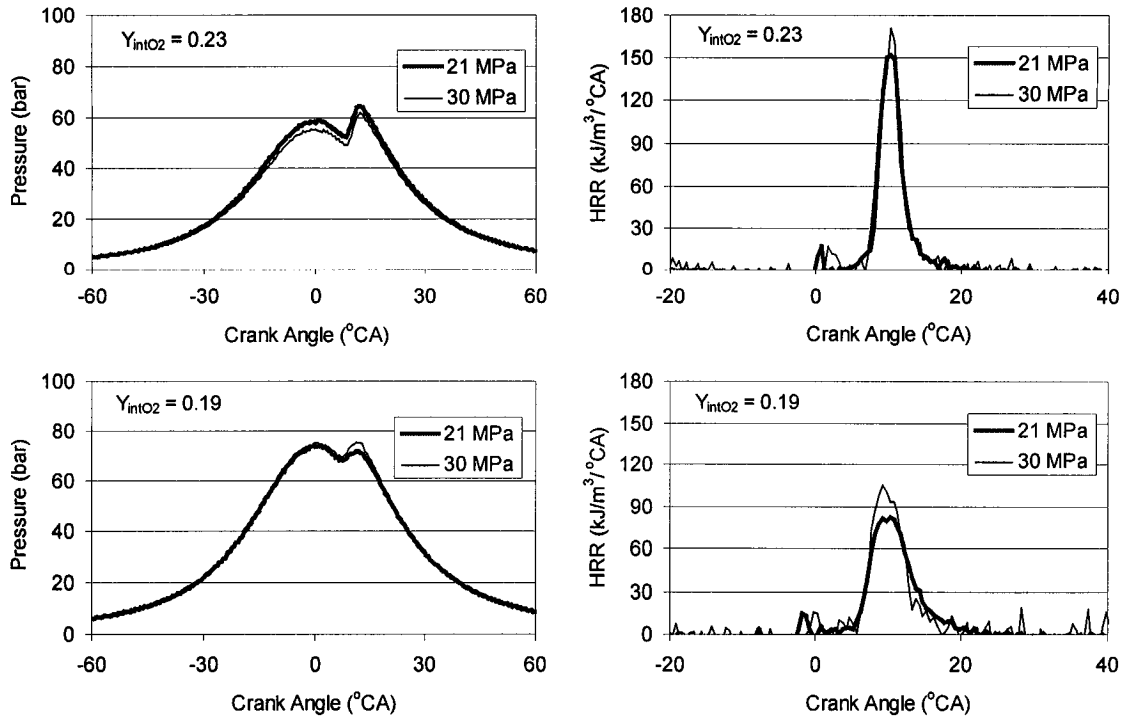

Figure 4.9: In-cylinder pressure and net heat-release rate, at 800 RPM, 3 bar GIMEP, ϕ = 0.25.

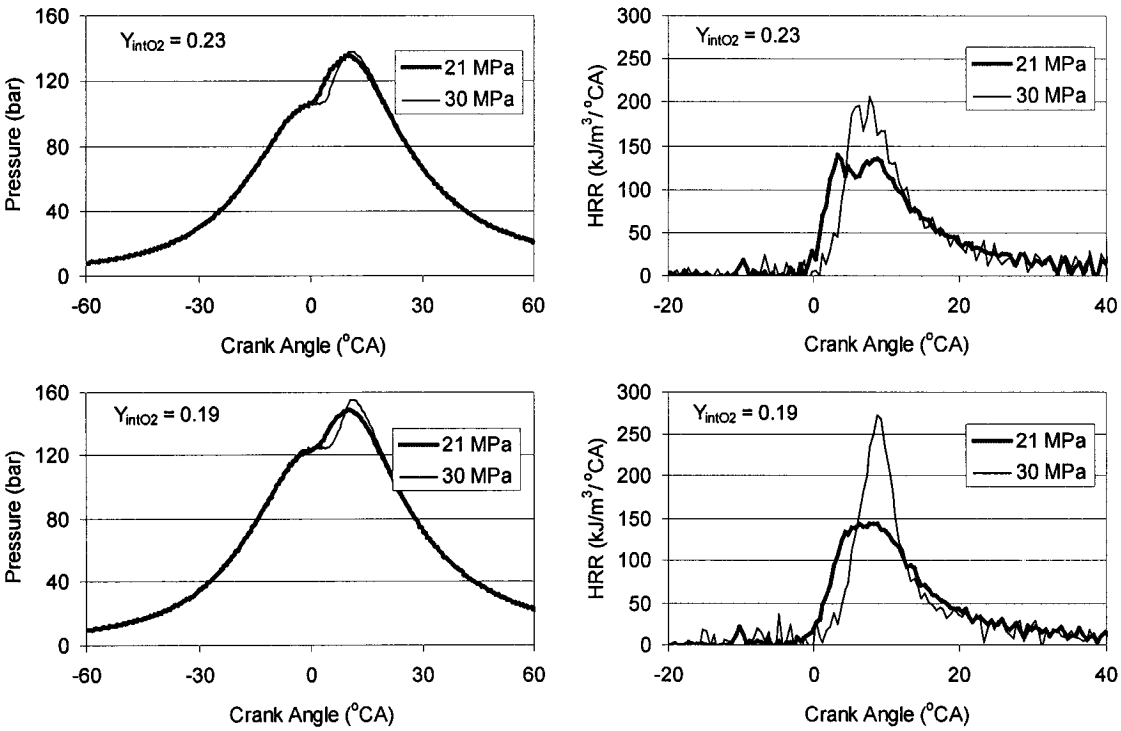

Figure 4.10: In-cylinder pressure and net heat-release rate, at 1200 RPM, 13.5 bar GIMEP, ϕ = 0.6.

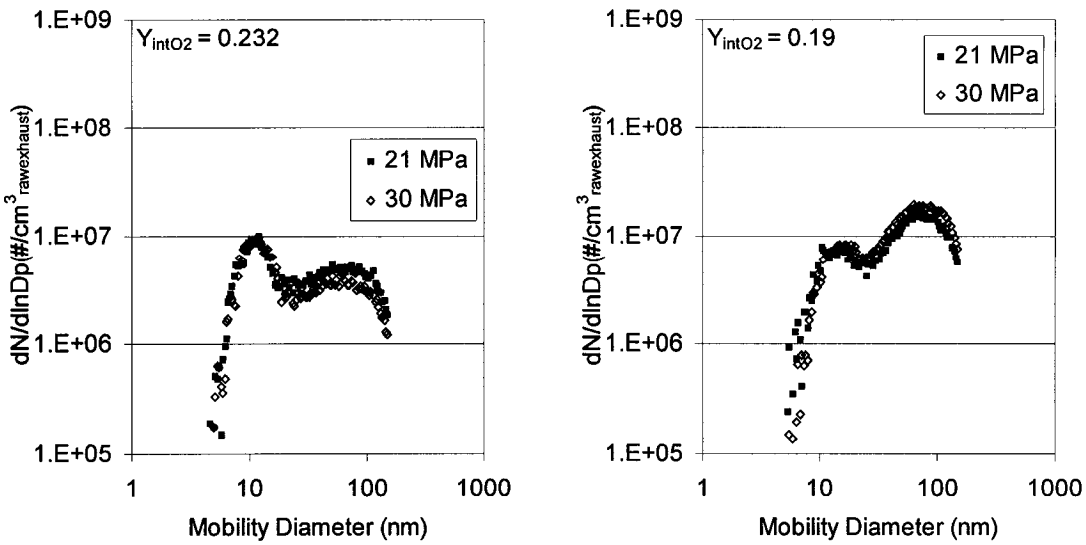

Figure 4.11: Particle size distributions at low-load, low-speed (800 RPM, 3.5 bar GIMEP)

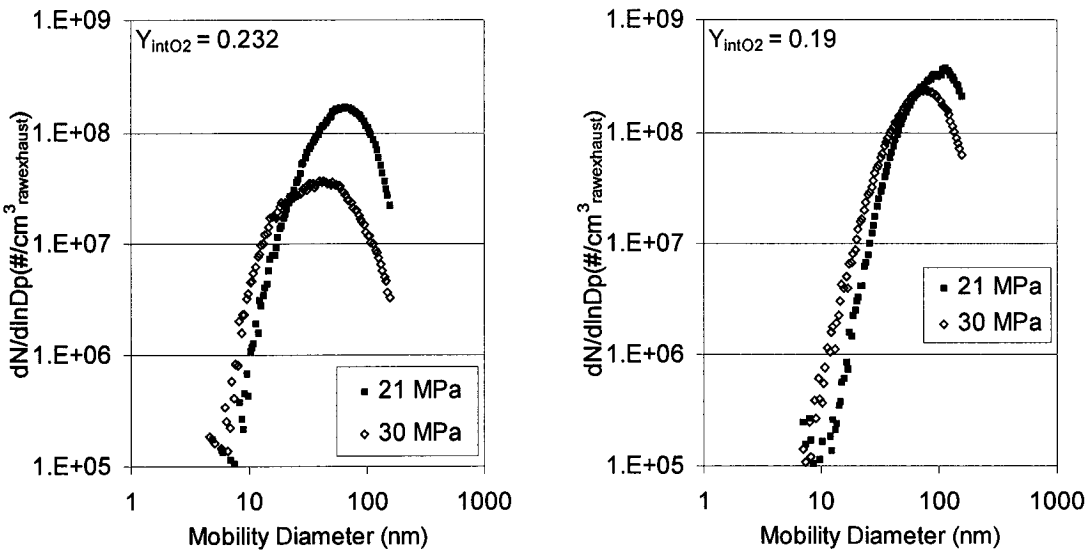

Figure 4.12: Particle size distributions at high-load, low-speed (800 RPM, 13.5 bar GIMEP)

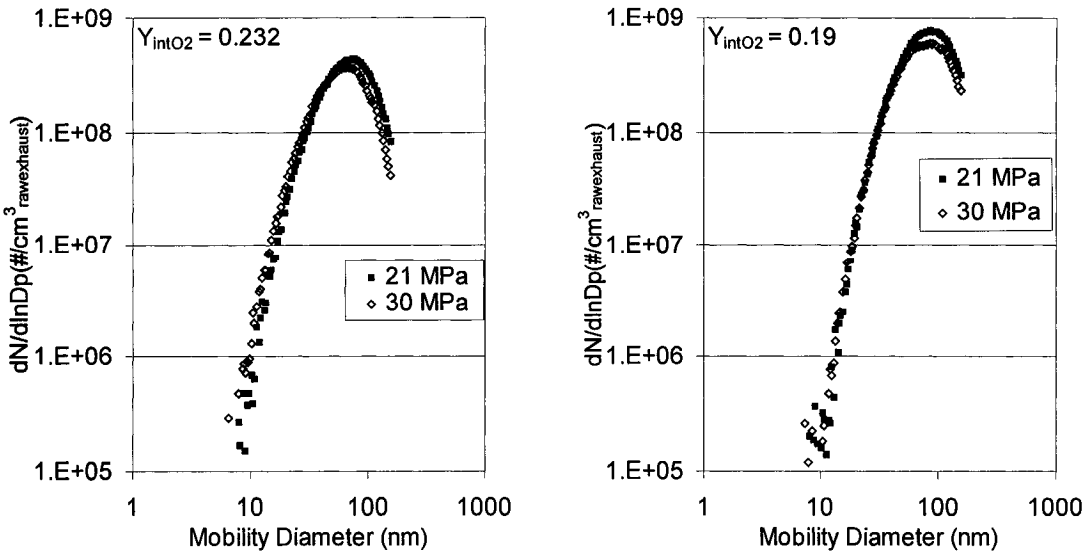

Figure 4.13: Particle size distributions at high-load, high-speed (1600 RPM, 13.5 bar GIMEP)

Chapter 5
Direct-Injected Hydrogen-Methane Mixtures*

5.1 Introduction

The use of gaseous fuels in internal combustion engines has long been seen as a possible method for reducing emissions while maintaining engine performance and efficiency. Most research has focused on the use of natural gas, due to its wide availability and relatively low cost (compared to other gaseous fuels); in fact, an estimated 5 million natural gas fuelled vehicles are currently in service world-wide [182]. More recently, hydrogen has received both popular and scientific attention as a potential long-term replacement for liquid hydrocarbon fuels in transportation applications.

Both natural gas and hydrogen have benefits and drawbacks as mobile vehicle fuels. In an internal combustion engine, natural gas provides excellent anti-knock properties, but suffers from low flame propagation rates and high auto-ignition temperatures. Hydrogen's low ignition energy results in a stronger tendency to knock compared to natural gas, limiting the compression ratio (and hence maximum theoretical efficiency) for homogeneous-charge hydrogen engines. When added to the air upstream of the intake port, hydrogen's low volumetric energy density also reduces the energy content of a given volume of inducted charge [183]. However, hydrogen does have a higher flame speed than natural gas, and it is easier to ignite. This suggests that a combination of these two fuels could be a superior vehicle fuel than either individually. While hydrogen production and onboard storage are issues that have yet to be overcome, a relatively small amount of hydrogen, potentially derived from renewable sources and blended with compressed natural gas, could provide substantial benefits with little modification to an engine system developed for natural gas fuelling.

A significant amount of research has been conducted investigating hydrogen/methane blend combustion in spark-ignition engines; however, few studies were identified which investigate the non-premixed combustion of hydrogen/methane blends. The purpose of this

* Part of the work presented in this chapter was previously presented at the SAE World Congress in Detroit, MI, April 2 2006. McTaggart-Cowan, G.P., H.L. Jones, S.N. Rogak, W.K. Bushe, P.G. Hill and S.R. Munshi. Direct-Injected Hydrogen-Methane Mixtures in a Heavy-Duty Compression Ignition Engine. SAE Technical paper 2006-01-0653. 2006. Extracts reprinted with permission from SAE.

work is to understand the influences of hydrogen addition to the fuel in a PIDING engine. This study aims to identify the benefits and drawbacks of hydrogen/methane blend fuelling. Furthermore, in the previous chapter, higher injection pressures reduced the overall combustion rate through enhanced mixing; the current chapter investigates whether enhancing the reaction kinetics (through hydrogen addition) has a similar influence.

5.1.1 Hydrogen/Methane Blend Combustion

The concept of using hydrogen as an additive to improve the combustion rate in spark-ignition engines was first suggested for conventional gasoline fuelling [184,185]. Several more recent studies have investigated the effects of blending natural gas and hydrogen for use in homogenous charge, spark-ignition engines [186—192]. These results have shown varying positive and negative results. The most important influence of hydrogen addition is under lean premixed conditions, where the lean limit is substantially extended [186,187,190]. This has been attributed to an enhanced combustion rate and shorter ignition delay [186,193]. For a given air-fuel ratio (including both stoichiometric and lean operation), NO_x emissions are higher with hydrogen addition, due to the higher flame temperature, while CO and HC emissions are reduced [187,190]. These effects become more significant as the lean limit is approached. However, because of hydrogen's ability to extend the lean limit, lower NO_x emissions are achieved by running at leaner air-fuel ratios with hydrogen addition [188,190]. Flame stability in the presence of EGR is also improved at all air-fuel ratios [189,191]. The effects of hydrogen addition on efficiency appear to depend on operating condition, with some studies indicating improved efficiency [186,187,194], and others reporting reduced efficiency [191,192].

The fraction of hydrogen in the fuel (typically reported on a per-volume basis) varies between the different studies. Values of 15-20% generally achieve substantial improvements without impairing knock resistance [188,189,194]. Above 30%, substantial reductions in the charge energy density, coupled with a higher potential for knock, pose substantial handicaps while generating little further benefits in emissions or stability [191,192]. The lower energy density of the gaseous charge can be overcome through turbocharging: however, this further increases the chance of knock at high hydrogen concentrations [188,190].

More fundamental premixed studies indicate that the preferential diffusion of hydrogen in a turbulent combustion event results in a higher flame propagation rate, even

when the laminar flame speed is constant [195]. The flame's greater resistance to stretch results in fewer local extinction events, reducing CO and HC emissions [196]. The presence of H_2 in the lean premixed flame increases the concentration of H, OH, and O radicals [196]. Increased OH concentrations may contribute to the more rapid oxidation of the methane; using 20% hydrogen may increase peak OH radical concentrations by as much as 20% [191,197].

5.1.2 Non-Premixed Hydrogen/Methane Flames

Non-premixed combustion of hydrogen/methane blends has not been as extensively studied as the premixed case. In a low-pressure, low-temperature co-flow burner experiment, non-premixed flame stability is enhanced by the higher flame speeds and improved mixing associated with hydrogen addition to either the fuel or the oxidizer [198]. Differences in fuel-stream density with hydrogen addition are secondary [198,199]. The higher diffusivity of the hydrogen also increases flame thickness under partially-premixed conditions [200]. In industrial gas turbines and boilers, hydrogen addition enhances prompt NO formation (due to high H and OH radical concentrations) while flame stability is improved [201].

The auto-ignition of direct-injected hydrogen, on a time-scale similar to diesel, requires a combustion chamber temperature in excess of 1100K [202]. Interestingly, reducing the charge oxygen concentration (by, for example, EGR) has little effect on ignition delay or combustion rate. Shock-tube studies of the auto-ignition of methane-hydrogen mixtures show that while hydrogen somewhat reduces the ignition delay, it is insufficient to achieve ignition under diesel-engine conditions within the time scales needed for compression-ignition engine operation [203]. In non-premixed counterflow methane/heated air jet experiments, the concentration of hydrogen in the methane influences the ignition mechanism. At concentrations below 30% by volume, the presence of H radicals enhances the methane ignition, while above this value hydrogen ignition dominates the process, with delays independent of the relative H_2/CH_4 concentration [204].

In internal combustion engines, the use of hydrogen mixed in the oxidizer improves the combustion rate of a spark-ignited direct-injected natural gas jet. Emissions of CO and HC are reduced, but the higher flame temperature results in increased NO_x emissions [205]. Similar results are reported for hydrogen addition to diesel-fuelled engines, where substantial reductions in particulate matter (PM) emissions are also observed [206]. These studies

indicate substantial potential benefits of direct-injection, non-premixed fuelling with hydrogen/natural-gas fuel blends.

5.2 Experimental Methodology

The experimental work presented in this section was carried out on the single-cylinder heavy-duty research engine (SCRE) whose general configuration was discussed in sections 3.1 and 3.2. For this work, the 17:1 compression ratio piston was installed in the engine. An alternate fuel supply system was also developed, which fed gas from storage bottles directly into the high-pressure compressor, thus providing fuels of varying composition to the engine at high pressures. As the gaseous fuel mass-flow sensor worked on the coriolis force principle, it was insensitive to the composition of the fuel. Finally, to maximize the accuracy of the fuel blends, as well as to alleviate safety concerns, the hydrogen/methane blend fuel was supplied in industrial style compressed gas cylinders. As a result of the high costs of fuelling the engine in this manner, the quantity of fuel available was limited; this restricted the number and scope of the tests conducted.

5.2.1 Experimental Conditions

The operating parameters used for controlling the SCRE are discussed in Section 3.3. For the current work, two separate test conditions were used to evaluate the influence of hydrogen/methane blend fuelling over a range of engine operating modes. The first condition was selected to minimize the fuel flow rate (hence increasing the amount of testing that could be carried out using the limited quantity of fuel available). The second set of tests was carried out at a test condition more representative of actual engine operation.

For the first round of tests, the experimental condition was selected to minimize fuel consumption while still generating relatively high emissions levels, so that the effectiveness of hydrogen at enhancing poor natural gas combustion could be determined. The condition selected (Table 5.1) used a high EGR fraction, at low speed and low load but moderate oxygen-equivalence ratio (ϕ). To establish influences over a range of combustion conditions while minimizing the required changes to the operating mode, a range of combustion timings was used. By varying combustion timing, highly stable conditions (early timings) and very unstable conditions (late timings) could be tested at the same baseline condition (EGR fraction, load, speed). By fixing the operating condition, then varying the timing, it was

possible to minimize variations due to non-repeatability of the operating condition setpoint. Replication of timing sets was used to establish repeatability. Most of the testing was carried out at 16MPa, to ensure that the commanded injection opening durations were repeatable (in excess of 0.9 ms).

The second test mode used in this work was more representative of a mid-speed, high-load (~75% of rated power) condition at a relatively high EGR rate. Due to the high gaseous fuel flow rate (in excess of 5 kg/hr) and limits on the available quantity of fuel, only one set of combustion timings (0-15°ATDC for the 50% IHR) for each fuel blend could be conducted. This test condition was similar to that used in Chapters 6 and 7, and to test condition 5 from Chapter 4 (Table 4.1).

5.2.2 Fuel Blends

The fuel used in these tests included natural gas (from the building supply), pure methane, and 10, 15, 23, and 35% hydrogen (by volume) in methane. While it would have been interesting to investigate higher H_2 concentrations, the upper limit was selected out of concern regarding the safety of the fuel supply system. Of the gas blends, the methane was supplied at a certified grade 2.0 (>99% purity [207]), while the 10%, 23%, and 35% H_2 (balance methane) were supplied at certified standard accuracy (analyzed accuracy ± 2%, impurities <0.1%). The 15% H_2 bottles contained some heavier hydrocarbons, as they were partially blended with natural gas as well as pure methane. Gas chromatograph analyses of the natural gas, pure methane, and 15% H_2 blends were performed by Westport Innovations Inc. For the remaining bottles the industrial supplier, Praxair Inc., performed the composition analysis. The analytical results for the gas blends are provided in Table 5.2. Heating values, molecular weights, and H/C ratio are based on the reported compositions. The natural gas, and the 10% and 23% hydrogen in methane blends, were tested in the first set of tests (mode 1). The second set of tests (mode 2) used natural gas, methane, and 15% and 35% hydrogen in methane.

5.2.3 Replications and Randomization

For the first set of tests, fuel flow rates were sufficiently low that the test points were replicated. Three separate tests were conducted for the natural gas while the 23% hydrogen in methane tests were replicated twice. At the 10% case, only a single data set was collected. The tests were conducted in a paired manner, with each test point being tested on a hydrogen

blend and then on natural gas. The 10% and 23% tests were carried out on different days. All timings were tested at one operating mode before the operating condition was changed. Due to this restriction on randomization, the results cannot be analyzed in a statistically valid manner. For the 23% hydrogen and natural gas fuel blends, the uncertainties presented in the experimental results are based on the 95% confidence intervals. As only a single data set was collected for the 10% hydrogen case, the average of the percentage errors for the natural gas and 23% hydrogen cases were used to represent the uncertainty.

For the second round of tests, the high fuel flow rates limited the testing to only one set of timings for each fuel blend. As a result, the uncertainties presented are those derived from the replicated natural gas tests carried out in Chapter 6 at a similar operating condition. While not statistically valid, this procedure provides an indication of the uncertainty in the measured results including both experimental variability and instrumentation errors; as such, it is superior to the estimated uncertainty calculated in Section 3.4.

5.3 Results

There were significant differences between the fuel blends and the operating condition used in the two sets of tests. The presentation of the results is divided into first and second-round results, relating to these two separate test sets. The general emissions results are presented first, followed by the detailed particulate-matter analysis and the effects on the combustion process as indicated by the in-cylinder conditions. Finally, the influence of hydrogen addition on net greenhouse gas emissions is presented.

5.3.1 Emissions

At the low-load operating condition, the effect of hydrogen addition is most significant on the CO and HC emissions at 23% H_2, as shown in Figure 5.1. The 10% H_2 level has a relatively minor influence on emissions, with no detectable effect on NO_x or PM. The CO and HC emissions appear to be slightly reduced, although the magnitudes of the differences are quite small (on the order of 5-10%, less than the experimental uncertainty).

The use of 23% H_2 in the methane fuel has a much more substantial impact on the emissions than does 10% H_2. Further, these effects are largest at later combustion timings; for the earliest timings, adding hydrogen to the fuel has little effect on emissions. Specifically, CO and HC emissions are reduced, while the NO_x emissions are slightly

increased. The only observed significant influence is at the latest timings, where PM is substantially reduced with 23%H_2. The presence of hydrogen in the combustion zone may affect pollutant emissions due to an increase in the concentration of the OH radical. This highly reactive molecule provides more rapid oxidation of unburned fuel and partial-combustion species such as CO and HC. Hydrogen also effectively reduces local flame extinctions induced by high turbulent strain-rates, events that may generate substantial pollutant emissions. These influences are more substantial at later combustion timings, where the combustion temperature is lower and instability is greater, leading to higher emissions of partial combustion by-products. The fact that NO_x emissions are slightly increased at the 23% H_2 case is most likely due to the small increase in flame temperature. An increase in the prompt-NO mechanism may also result from the higher OH concentrations [202]. Irrespective of the source, the increase in NO_x emissions is relatively small.

High-Load Emissions

The effects of hydrogen addition to the fuel are more significant at high-load operating conditions, as investigated in the second round of testing. The pure methane results are presented to provide a comparison between the natural gas used as a reference in the first round of testing and the pure methane used as the balance gas in the majority of the hydrogen/natural gas blend fuels. The emissions results (CO, HC, PM, and NO_x) are presented in Figure 5.2. The results indicate that using pure methane in place of natural gas does not substantially influence the NO_x or HC (unburned fuel) emissions, but has a more substantial effect on PM and CO. As would generally be expected, the methane fuel has lower PM emissions than does the natural gas, due primarily to the smaller quantities of ethane and propane in the fuel (Table 5.2). Pure methane does, however, increase the CO emissions, although the cause of this effect is not clear. A more comprehensive investigation of the effects of these additives on emissions and performance at a very similar operating condition is provided in Chapter 6. In general, the differences between methane and natural gas are relatively small, suggesting that the composition of the balance gas should not have a significant effect on the influences of hydrogen addition.

Both the 15 and 35% H_2 cases (Figure 5.2) show a significant reduction in CO compared to natural gas. This may be due either to a kinetic effect (increasing OH radical concentration) or a physical/thermal effect (higher combustion temperature, better mixing).

As well, some reduction in CO would be expected due to the reduction in the carbon content of the fuel (Table 5.2). The fact that the addition of hydrogen results in higher NO_x emissions at the 35% H_2 case may also be due to either thermal effects or kinetic effects. Kinetically, increases in OH radical concentration tend to enhance the thermal NO mechanism [37]. The 80K increase in the adiabatic flame temperature due to the hydrogen addition (Table 5.2) also increases the rate of the thermal NO formation mechanism. The higher flame temperature explains the increase observed at 35% H_2 (and at 23%). The relatively small difference in temperature at the lower concentration results in changes in the NO formation rate that cannot be differentiated from background variability.

Hydrogen addition to the fuel substantially reduces HC and PM emissions. The presence of higher concentrations of H and OH radicals are the most likely cause for reduced HC emissions, as they tend to accelerate the oxidation of methane. Similarly, the higher concentration of these radicals substantially increases the oxidation rate of solid carbon particles and PM precursors. Under these conditions, either reductions in PM formation or increases in oxidation dominate the PM emission rate. There is no evidence of a reduction in hydrogen abstraction resulting in increases in PM formation through the HACA mechanism (Section 2.2.5). However, this effect may be occurring but being offset by increases in oxidative mechanisms.

5.3.2 Particulate Matter

Further insight into the effects of hydrogen addition to the fuel is provided by the particle size distributions collected by the mobility particle sizer and the black-carbon concentration measured by the Aethaelometer. For the low-load case (first round of tests), the black carbon content is reduced for both the 10% and the 23% H_2 cases, as shown in Figure 5.3. The black-carbon fraction of the total measured PM is also reduced with 23% H_2. In both cases, the earliest timing cases, where the PM levels are in general lowest, show no significant differences. The particle size distributions (Figure 5.4) show similar results, with significant reductions in particle sizes numbers at the later timings with the 23% H_2 fuel but no significant changes at early timings or with 10% H_2. These results are consistent with the mass measurements discussed in section 5.3.1, and suggest that the hydrogen addition is having a greater effect at reducing PM at those conditions where the PM loading is highest. They also suggest that the reduction in PM mass is mainly attributable to a reduction in

black-carbon mass, whereas the volatile contribution to the total PM is relatively unchanged. This indicates that the volatile PM was originating primarily from either the liquid fuel or the lubricating oil, as was discussed in Chapter 4.

More details on the PM emissions under high load are shown in Figures 5.5 and 5.6. The black carbon content of the PM (Figure 5.5, both absolute emission level and the relative fraction of the total PM as measured by the TEOM) is not significantly different between the natural gas and methane cases. The 15% H_2, however, significantly reduces the black carbon level, while for the 35% H_2 case emissions levels approach the detection limits of the Aethalometer. This corresponds to a reduction in the black-carbon fraction of the PM from as much as 45% to 5% for the same operating condition. This indicates that the PM measured by the TEOM is primarily volatiles which are either condensing in the exhaust stream or on the face of the TEOM filter. Further evidence of the presence of significant volatile concentrations in the exhaust is demonstrated by the particle size distributions, Figure 5.6. These measurements indicate that at 35% H_2, there is a significant 'nucleation mode' of particles; these particles are typically attributed to post-dilution nucleation of volatile species [99]. This 'nucleation mode' is not present for conditions where PM levels are higher, most likely due to the presence of sufficient solid PM (black carbon) surface area for volatile condensation to occur. In general, volatile condensation onto existing particles is thermodynamically favoured over direct nucleation of new particles [6]; however, at the 35% H_2 case, the lack of existing surface area leads to significant volatile nucleation rates.

5.3.3 Combustion Analysis

The sensitivity of the pollutant emissions to the addition of hydrogen to the fuel indicates that the hydrogen is significantly influencing the combustion event. Further insight into the combustion process can be gained from the in-cylinder pressure trace and its derivative, the net heat-release rate, as discussed in section 3.3.1. For the low-load condition, the burn duration (10-90% of integrated heat release), fuel consumption (GISFC), peak heat-release rate, and coefficient of variation (COV) of the GIMEP are shown in Figure 5.7. The GISFC (calculated based on an energy-equivalent mass of diesel) shows no significant influence of either timing or fuel composition. On the other hand, the burn duration is substantially reduced for the hydrogen-fuelling cases at late timing, especially with 23% H_2; however, the burn duration for the earlier timings is unaffected. This suggests that different

mechanisms may be restricting the combustion rate at early and late timings, with a chemical kinetic limit at late timings, compared to a mixing-limited condition for early timings. The peak heat-release rate (corresponding roughly to the maximum rate of chemical energy being released from the fuel) averages approximately 20% higher at 23% H_2 fuelling than for the natural gas. The difference at the 10% H_2 case is much less significant, although there is a slight increase in peak HRR at most timings. The use of hydrogen/methane blend fuel also substantially reduces the combustion variability (COV of the GIMEP). For the 10% H_2 fuel, the variability is significantly reduced only at the latest combustion timings. The 23% H_2 reduces variability at all timings, although the effect is most substantial at the latest timing. This reduction in combustion variability, most likely due to increased flame stability with the addition of hydrogen, contributes directly to the observed reductions in CO and HC emissions.

Switching from natural gas to hydrogen/methane blended fuel has no significant effect on the pilot ignition delay, as shown in Figure 5.8. Similarly, the gas ignition delay at 10% H_2 fuelling is no different from natural gas; however for the 23% H_2 case, the gas ignition delay is reduced by, on average, 20%. Both pilot and gaseous fuel delays are defined as the time between the commanded start of injection and the observed start of combustion. As such, they include any physical delay within the injector, as well as both mixing and chemical delay times for the injected fuel. The commanded start-of-injection is a recorded value while the start-of-combustion timing is determined by examination of the heat-release rate. Further details on the timing definition process are provided in section 3.3.1.

The shorter gas ignition delay time with H_2 addition is consistent with previous premixed and non-premixed auto-ignition of methane tests, which show that hydrogen addition substantially reduces ignition delay times [203,204]. While the process in this situation relates to a non-premixed jet being ignited by a pilot flame, and hence is not directly comparable to either of the cited works, it is not surprising that the addition of H_2 reduces the ignition delay. However, the previous work suggests that even at 10% H_2, a noticeable reduction in ignition delay occurs; the current results indicate that a more substantial quantity of hydrogen is required before it has a significant effect.

The shorter gas ignition delay has a number of effects on the combustion process, including reducing the time available for mixing prior to ignition. In general, the lower

density of the blended fuel reduces the turbulent mixing rate and the penetration distance of the gaseous jet. It is unlikely that the higher molecular diffusivity of the hydrogen offsets this effect, as the mixing process is turbulence dominated. The shorter ignition delay leads to less methane having over-mixed during the ignition delay period, contributing to the reduced HC emissions. The addition of hydrogen also results in wider flammability limits of the mixture during the initial combustion-initiation phase, leading to more fuel being available to burn during the immediate post-ignition partially premixed burn; this increases the peak heat-release rate.

The influence of hydrogen addition on the observed pressure trace and the heat-release rate is relatively small, as shown in Figure 5.9 for the 5 and 15°ATDC cases. The 10% H_2 case shows no significant difference from natural gas, while the 23% H_2 case has a more significant effect; the shorter ignition delay is one of the main contributing factors. The 23% H_2 fuelling also substantially increases the peak heat-release rate, as suggested in Figure 5.8. This effect is relatively consistent, although the increase in HRR is more substantial at 15°ATDC than at the earlier timings. These results indicate that the greatest influence of hydrogen addition is on the early stages of the combustion event, with a shorter ignition delay and a more intense early combustion phase.

High-Load Combustion Performance

The effect of hydrogen addition to the fuel on combustion performance at the high-load condition differs significantly from the influences observed at the low-load case. The effects on the peak heat-release rate, combustion duration, and two measures of combustion variability (COV of the peak pressure and of the GIMEP) are shown in Figure 5.10. The heat release-rate plots at combustion timings of 5 and 15°ATDC are shown in Figure 5.11. Contrary to the low-load case, the maximum heat-release rate is substantially reduced by the addition of hydrogen to the fuel. The net heat-release rates shown in Figure 5.11 indicate that the methane and low-hydrogen cases both have a significant impact on the combustion process at earlier timings, but that at the latest timings only the highest hydrogen concentration significantly influences the combustion event. This suggests that the combustion event at the early timings may be sensitive to changes in chemical kinetics, but that at the later timings the main factor affecting the combustion rate is the mixing process.

At this operating condition, both 15% and 35% H_2 addition significantly reduce the gas ignition delay (Figure 5.12), while the methane and natural gas delays are indistinguishable. The shorter gas ignition delay for the hydrogen/methane cases result in less gas having pre-mixed to a combustible mixture when the gas ignites, resulting in less energy release in the early premixed burn phase of the combustion event and hence lower peak heat-release rates. The fact that the wider flammability range of the hydrogen/methane fuel does not offset this reduction in the ignition delay time, as it did in the low-load case, suggests that there is an injection-rate limit to the initial combustion at high load, while the limiting factor at low loads is kinetic-limited. As the overall burn duration (Figure 5.10) is not influenced by hydrogen addition to the fuel, it is evident that the total combustion duration is primarily dependent on the rate of injection and mixing of the fuel, and that kinetic effects related to the easier flammability of the hydrogen are not significantly influencing the overall burn duration. The observation that the early-stage combustion stability (measured by the COV of the peak cylinder pressure) is substantially improved suggests that hydrogen is not only reducing the ignition delay but also that it is providing a more repeatable ignition event. That the overall combustion stability (indicated by COV GIMEP, Figure 5.10) is not significantly influenced provides further evidence that the primary role of the hydrogen addition on the overall combustion event is to enhance the ignition process.

5.3.4 Greenhouse Gas Emissions

The preceding emissions and performance results demonstrate that hydrogen addition to natural gas fuel can substantially reduce emissions of harmful combustion by-products while maintaining combustion efficiency. A further advantage of hydrogen is that it contains no carbon, resulting in reduced engine-out CO_2 emissions. The effects of hydrogen on the CO_2 emissions for the two sets of tests carried out are shown in Figures 5.13 and 5.14. That the addition of hydrogen to the fuel also reduces the unburned fuel (primarily methane) emissions provides a further GHG benefit, as methane is a key contributor to global IR absorption. Combining methane and CO_2 emissions provides a net infrared-absorption value which can be expressed as an equivalent mass of CO_2. At the low-load case, the relative contribution of the unburned fuel is substantial. The 23% H_2 reduces CO_2 emissions by ~8%; at early timings, the reduction in net GHG emissions is equivalent to this reduction in CO_2, due to the low level of unburned fuel emissions (see Figure 5.1). However, at the late timings

where the unburned fuel emissions are significantly greater, the net GHG emissions are reduced by almost 25%. At the high-load case, the majority of the GHG emissions are attributed to CO_2, with the 35% hydrogen blend reducing CO_2 emissions by ~12% (equivalent to the fraction of carbon replaced, on an energy basis, in the fuel); including the reduction in unburned fuel, the net GHG emissions are reduced by ~15%. Although the use of H_2 can substantially reduce the GHG emissions (in excess of the simple reduction in CO_2 due to carbon replacement), this reduction applies only for engine-out emissions; the net GHG impact depends on how the H_2 is generated, a topic which is beyond the scope of this thesis.

5.4 Discussion

The results demonstrate that the addition of varying quantities of hydrogen to natural gas has a significant impact on the overall combustion event. These results can be used as guidance in developing an optimum procedure for blending natural gas and hydrogen to achieve substantial reductions in harmful pollutant emissions while maintaining or improving system efficiency.

5.4.1 Combustion Implications

The implications of the hydrogen addition on the combustion process are discussed in detail in earlier sections. In general, the results indicate that the ignition process is dependant at least in part on chemical kinetics, with hydrogen addition substantially reducing ignition delay. It also improves combustion stability, especially early in the combustion cycle and at those conditions with normally greater instabilities. The improved stability most likely contributes to the observed reduction in combustion by-products.

The effect of hydrogen addition to the gaseous fuel on the particulate matter emissions provides significant insight into the relative importance of different PM sources and formation processes. Higher hydrogen concentrations (23% and 35%) reduce the emission of solid carbon by a substantially greater fraction than would be expected simply due to the reduction in fuel carbon content (~8% and ~11% on an energy basis, respectively). It is not possible to identify whether the initial solid carbon formation process is being impaired or if the later-stage oxidation is being enhanced. The simultaneous appearance of a significant concentration of nucleation-mode particles indicates that volatile nucleation may

be significant in the absence of sufficient particulate surface area upon which condensation may occur. The significantly greater influence of 35% H_2, compared to 23%, indicates that there is benefit to going to higher hydrogen concentrations; however, given that the black-carbon content is negligible at 35% H_2, it is unlikely that concentrations greater than this value will further reduce PM levels. This suggests that there is a lower limit on the PM mass emissions, which may be attributed to volatile contributions from the lubricating oil or the diesel pilot fuel.

The addition of hydrogen to the fuel at two different operating conditions has generally similar effects on emissions, although the effects on the net heat-release rate are significantly different. This indicates that the overall combustion progression, as described by the net heat-release rate, is not the primary factor influencing most of the pollutant formation processes. The fact that the influence of hydrogen addition on the combustion process varies with operating condition is similar to the observed variations with operating condition discussed in Chapter 4. Specifically, at low-load conditions, the addition of hydrogen substantially increases the heat release rate, most likely due to enhanced chemical kinetics. Conversely, at the higher load case (where the differential pressure between the fuel rail and the combustion chamber is lower) the addition of hydrogen reduces the intensity of the combustion event. This is most likely due to the slower injection rate and reduced mixing caused by the lower density of the injected fuel. Furthermore, it suggests that at higher loads, the overall combustion rate is mixing-limited, while at lighter loads there is a significant kinetic limit to the combustion rate. However, the fact that the emissions are uniformly reduced, especially at the higher load case, suggests that enhancement of the kinetics and reduction of combustion variability have very significant impacts on the emissions of combustion by-products.

5.4.2 Emissions and Applications

The application of hydrogen-blended natural gas to a direct-injection engine suggests a number of intriguing possibilities. Hydrogen-blended natural gas offers the potential to achieve substantial net GHG reductions. Assuming an equal energy requirement, an equivalent amount of hydrogen could be used to fuel either a single pure hydrogen powered vehicle or 15 vehicles using 20% (by volume; ~7% on an energy basis) hydrogen in natural gas. While the reduction in CO_2 emissions would be equivalent, the reduction in CH_4

emissions from the 15 vehicles would be substantially greater than the reduction that could be achieved by removing a single vehicle; this could result in as much as a 50% greater reduction in net GHG emissions for an equivalent amount of hydrogen. Although hydrogen-fuelled vehicles (either internal-combustion or fuel-cell powered) may offer some potential improvements in efficiency, benefits in well-to-wheel efficiency will most likely not be of the same magnitude as the net reduction in GHG emissions indicated here.

The addition of varying levels of hydrogen to natural gas over a range of operating conditions substantially reduces emissions and improves combustion performance. This provides a number of potential opportunities for application to a heavy-duty mobile power plant. Through the addition of hydrogen, the engine's operating condition range can be extended before excessive levels of harmful pollutants and combustion instability are reached. This could be combined with higher levels of EGR and more advanced timings to achieve lower NO_x levels and higher combustion efficiency while maintaining low PM, CO, and HC emissions. Further work is obviously required to evaluate the true potential for this concept over an entire engine duty cycle.

The benefits discussed above are somewhat offset by the need to provide significant amounts of hydrogen. Furthermore, practical on-board storage would most likely be limited to compressed gases, and a greater work input would be required to compress the blend to the injection pressure, due to the lower density of the gaseous mixture (discussed in section 7.5.1). An alternative for applying the blended H_2 and natural gas combustion system that could overcome some of these drawbacks would be to provide varying control over the hydrogen content of the fuel. This could be achieved by providing separate gaseous reservoirs (which increases system complexity), and then varying the rate of blending. As such, larger quantities of H_2 could be provided to the engine at times when combustion instability is higher and emissions of PM, HC, and CO greater, for example during start-up or transient conditions. Whether the potential offered by such a system could compensate for the increased cost and complexity requires further study.

Compared to pure hydrogen fuelling, hydrogen blended with natural gas has a number of practical advantages. One is that on-board fuelling systems (either port- or direct-injection) can operate with little or no modification on the blended fuel; modifications, in terms of materials, design, and safety requirements, for pure hydrogen will substantially

enhance the near-term cost and complexity of these vehicles. Furthermore, natural gas supply and distribution networks currently exist, while fuelling stations could then blend the natural gas with hydrogen (delivered in liquefied form by tanker-truck, for example) at the pump. These results identify some of the potential benefits to using hydrogen-blended natural gas as a near-term transportation fuel alternative; the implications will be discussed further in Chapters 6 and 7.

5.5 Conclusions

1. Both the engine's operating condition and hydrogen concentration have a substantial impact on the influence exerted by hydrogen addition to the natural gas. At low load, the addition of 10% H_2 to methane has little impact on performance or emissions, while higher concentrations (23%) have significant impacts. At high load, both low (15% H_2) and high (35%) concentrations significantly impact both the combustion progression and emissions.
2. In general, particulate matter levels are reduced by H_2 concentrations greater than 10%, with larger reductions at those conditions where the PM levels are highest. Higher hydrogen concentrations also significantly reduce CO and HC emissions. Hydrogen addition at high load generates significantly greater effects on emissions than at low load.
3. At very high (35%) H_2 concentrations, black-carbon (soot) concentrations are negligible, but significant quantities of nucleation-mode particles are formed. These particles are composed primarily of volatiles that self-nucleate due to insufficient surface area being available for condensation. This suggests that there is a baseline PM level composed of volatiles, attributable to lubricating oil, diesel pilot, etc. which are not significantly influenced by the gaseous combustion process.
4. At low loads, the addition of hydrogen to the gaseous fuel improves the combustion stability, increases the peak heat-release rate, and reduces the combustion duration. This indicates that chemical kinetics can enhance the combustion at low loads.
5. At high loads, the peak combustion intensity is reduced because of the lower energy density of the fuel; the overall combustion duration, however, is not affected. The fact that enhanced chemical kinetics do not reduce the combustion duration suggests that

mixing limitations are the primary restriction on the combustion process at higher load conditions.

6. Hydrogen addition to a non-premixed gaseous jet combustion system has no significant effect on fuel conversion efficiency. Net greenhouse gas emissions are reduced, through both the lower carbon content of the fuel and the reduction in unburned methane emissions.
7. Higher H_2 concentrations generate higher NO_x emissions. This is most noticeable at the highest H_2 levels (35%), although a small (non-significant) increase is also detectable at 23% H_2. These increases may be attributed to increases in the combustion temperatures of the hydrogen/methane blended fuels.
8. The addition of hydrogen to the fuel reduces the gaseous fuel ignition delay time, by approximately 15% for 15% H_2, 20% for the 23% H_2, and 30% for the 35% H_2 cases. This indicates that chemical kinetics are playing a substantial role in the ignition process, as the effects of the hydrogen addition on the mixing process would be to reduce the jet density leading to lower penetration and less mixing.
9. The principal difference between the natural gas tested (composition in Table 5.2) and methane fuels at high-load conditions is a reduction in PM and an increase in CO for the pure methane fuel. Ignition delays are slightly longer with pure methane, resulting in higher peak heat-release rates. Early-stage combustion variability is also slightly greater. The effects of ethane and propane in the natural gas are investigated in greater detail in Chapter 6.

5.6 Tables and Figures

Table 5.1: Engine operating mode for hydrogen/methane blend testing.

Parameter	1st Round	2nd Round
Speed (RPM)	800	1200
GIMEP (bars)	6	13.5
ϕ_{O2}	0.5	0.6
EGR (mass %)	40	30
Y_{intO2}	*0.175*	*0.19*
Fuel Pressure (MPa)	16,21	21
50%IHR (°ATDC)	0, 5, 10, 15	0, 5, 10, 15
Pilot (mg/inj)	5	5

Table 5.2: Gas composition as analyzed by gas chromatography

Component	Natural Gas	CH_4	10%H_2*	15%H_2	23%H_2*	35%H_2*
He	0	0	0	0	0	0
O2	0	0	0	0	0	0
H2	0	0	10.0	14.7	23.3	35.1
CO	0	0	0	0	0	0
n-Butane	0.09	0	0	0.06	0	0
i-Butane	0.10	0	0	0.03	0	0
i-Pentane	0.03	0	0	0	0	0
n-Pentane	0.02	0	0	0	0	0
Hexane	0.005	0.001	0	0	0	0
Heptane	0	0	0	0	0	0
Octane	0	0	0	0	0	0
Nitrogen	1.05	0	0	0.34	0	0
Methane	96.12	99.999	90.0	84.0	76.7	64.9
Carbon Dioxide	0.43	0	0	0.05	0	0
Ethane	1.70	0	0	0.75	0	0
Propane	0.45	0	0	0.19	0	0
MW (kg/kmol)	16.76	16.04	14.6	14.14	12.74	11.09
LHV (kJ/kg)	48404	50007	50959	51151	52561	54433
HHV (kJ/kg)	53661	55489	56685	56837	58664	60977
$T_{adiabatic}$ (K)	2485	2470	2490	2500	2520	2550
H:C ratio	3.94	4.00	4.22	4.32	4.61	5.08

* - composition analysis by Praxair (all other species <0.1%)

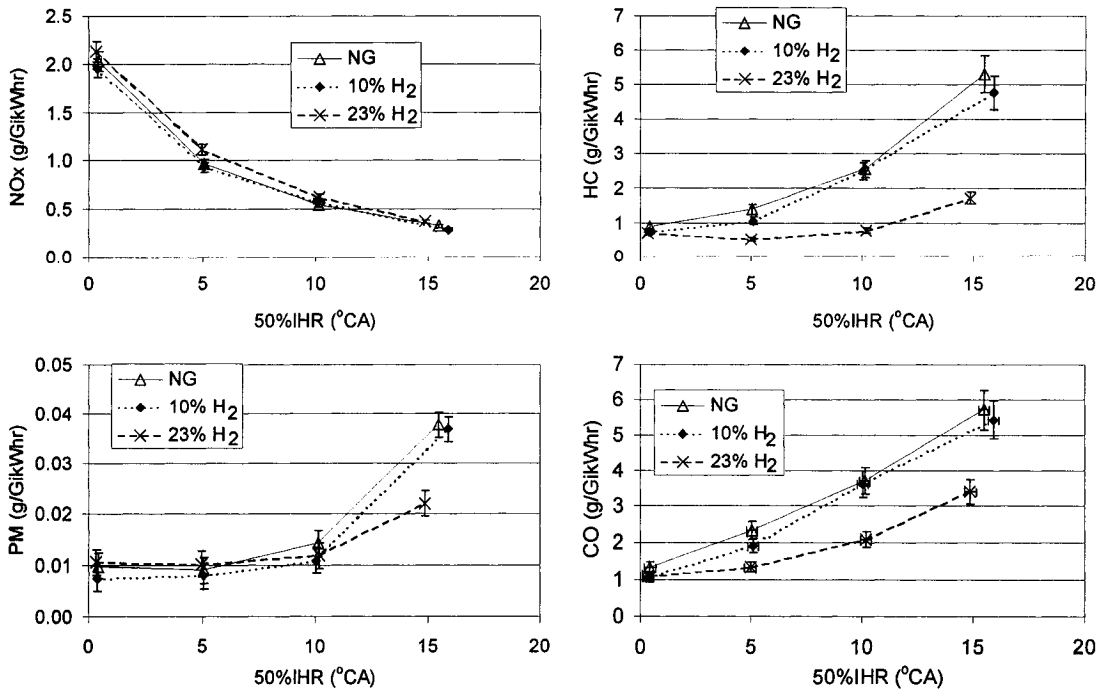

Figure 5.1: Emissions comparison between natural gas fuelling, 10% and 23% H_2. 800 RPM, 6 bar GIMEP, 0.5 ϕ, 0.175 Y_{intO2}, Injection Pressure = 16 MPa. *(reprinted with permission from SAE 2006-01-0653. © SAE International 2006)*

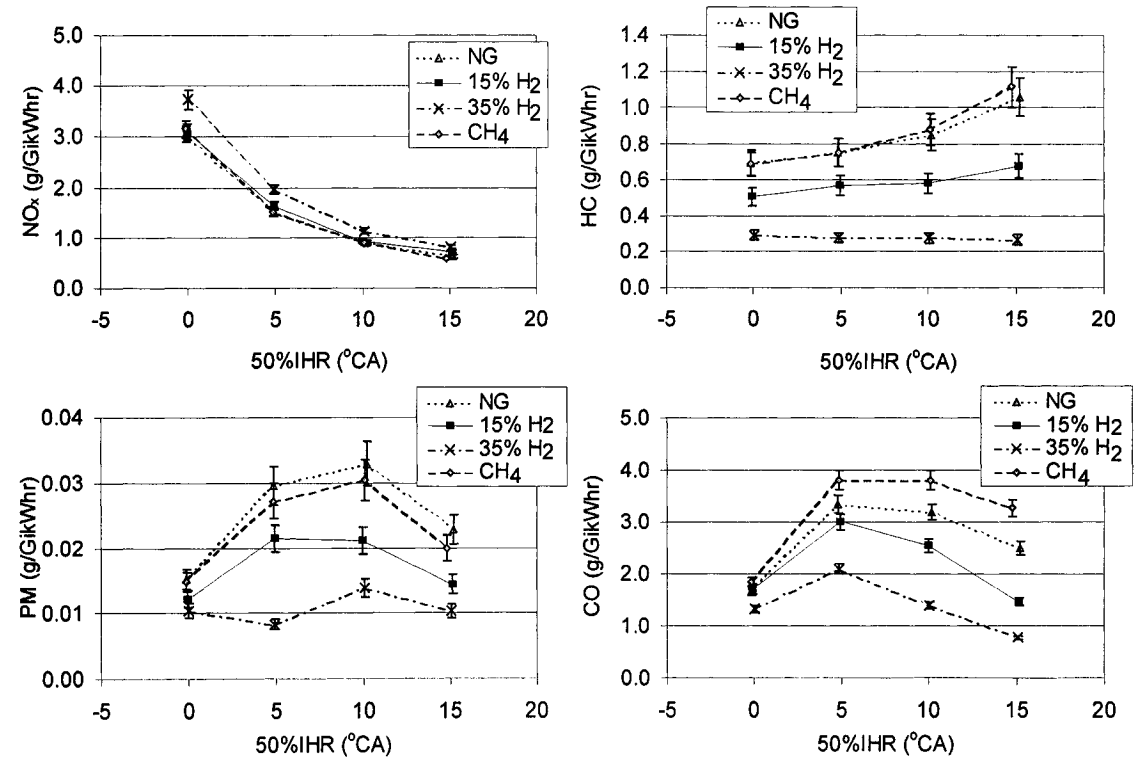

Figure 5.2: Emissions comparison between natural gas, pure methane, 15% and 35% H_2. 1200 RPM, 13.5 bar GIMEP, 0.6 ϕ, 0.19 Y_{intO2}, Injection Pressure = 21 MPa.

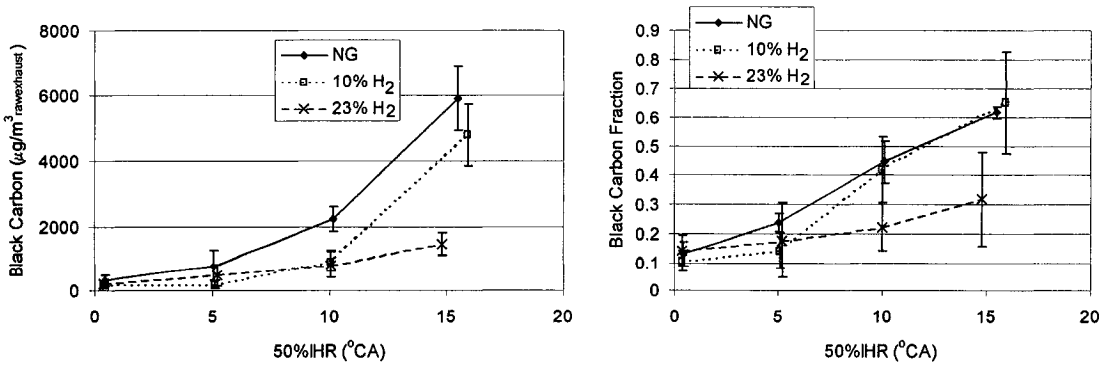

Figure 5.3: Black-carbon PM content comparison between natural gas fuelling, 10% and 23% H_2. 800 RPM, 6 bar GIMEP, 0.5 ϕ, 0.175 Y_{intO2}, Injection Pressure = 16 MPa.

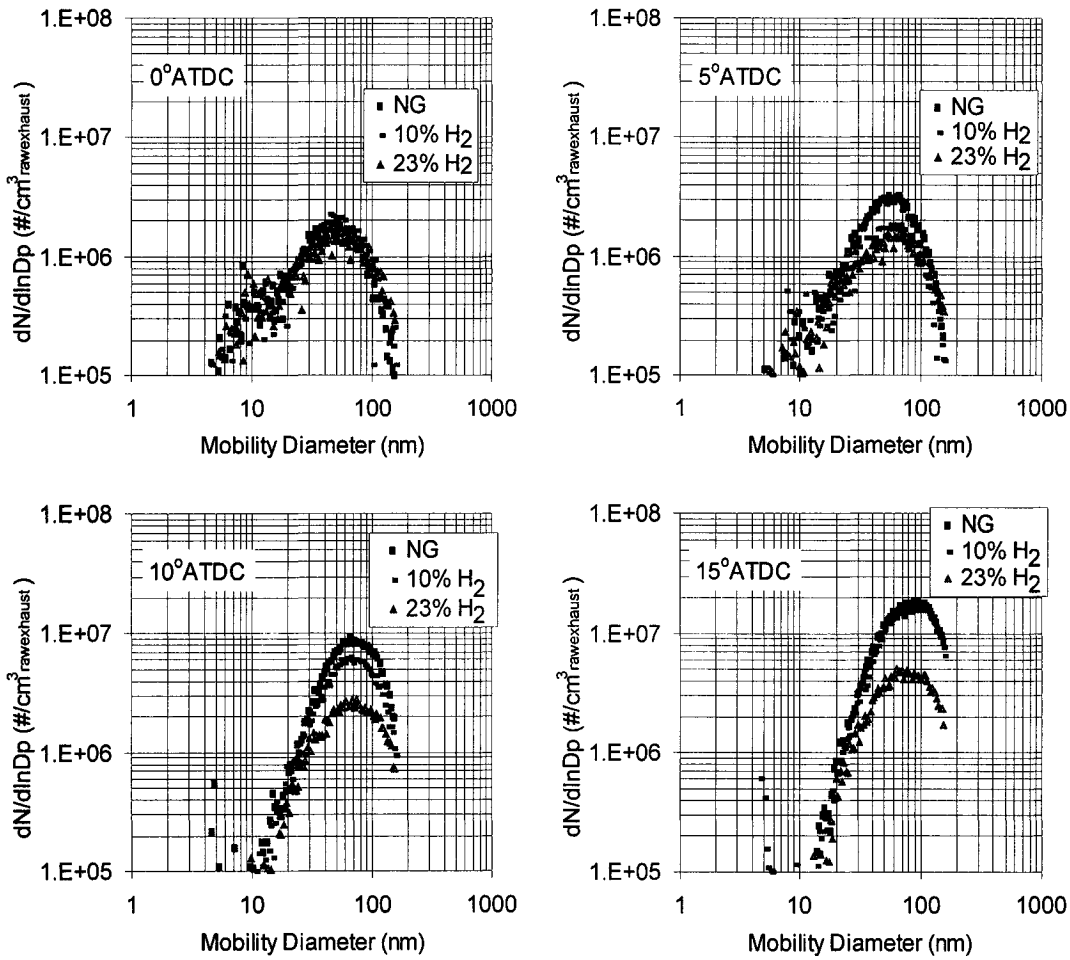

Figure 5.4: Particle size distribution comparison between natural gas fuelling, 10% and 23% H_2. 800 RPM, 6 bar GIMEP, 0.5 ϕ, 0.175 Y_{intO2}, Injection Pressure = 16 MPa.

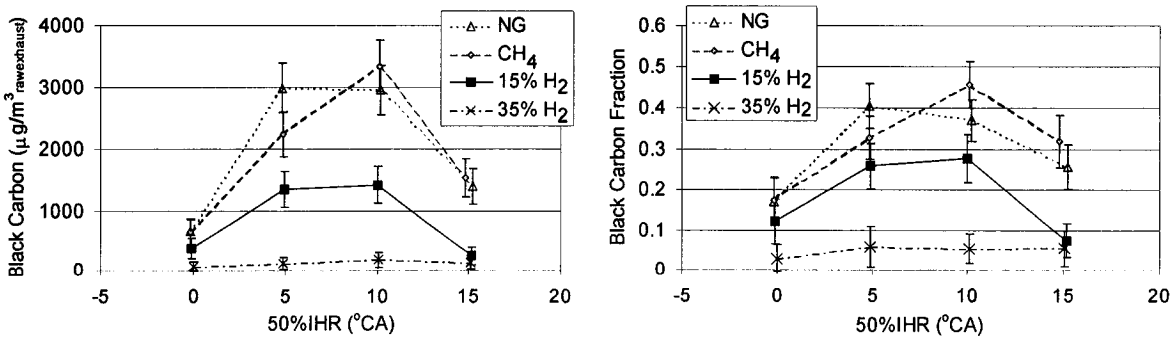

Figure 5.5: Black-carbon PM content comparison between natural gas, pure methane, 15% and 35% H_2. 1200 RPM, 13.5 bar GIMEP, 0.6 ϕ, 0.19 Y_{intO2}, Injection Pressure = 21 MPa.

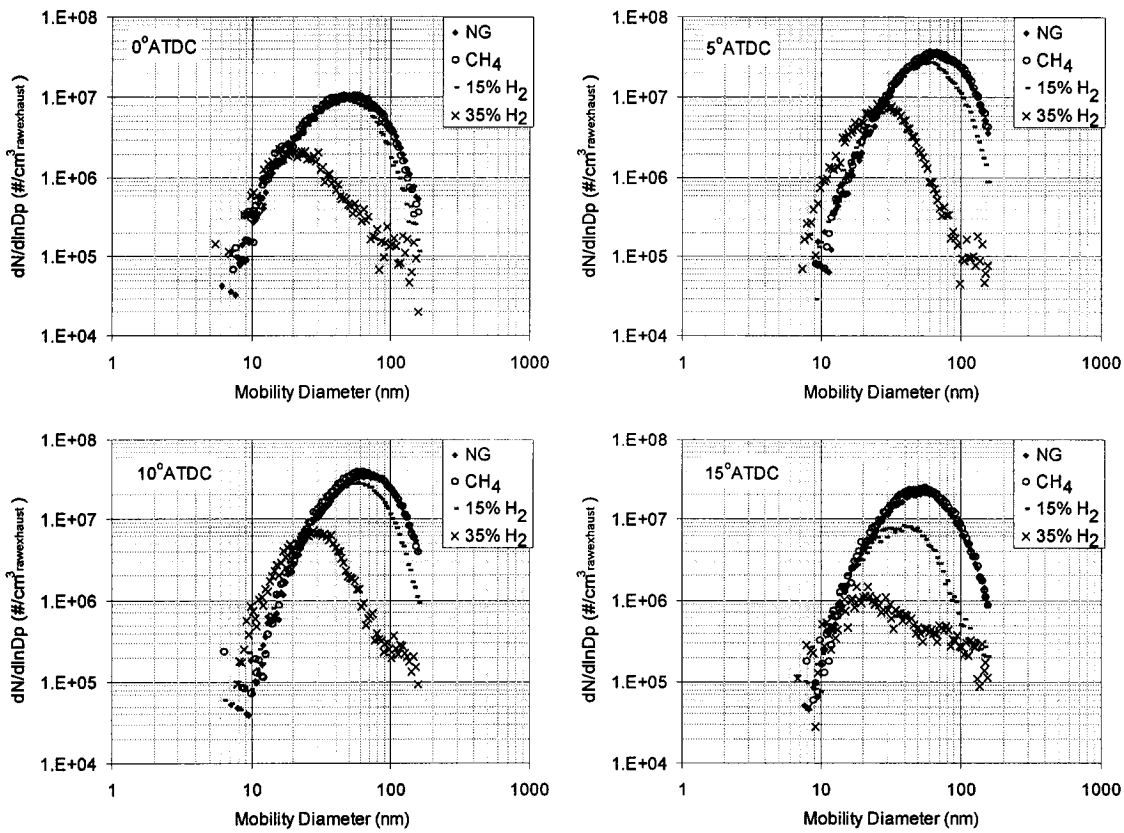

Figure 5.6: Particle size distribution comparison between natural gas, pure methane, 15% and 35% H_2. 1200 RPM, 13.5 bar GIMEP, 0.6 ϕ, 0.19 Y_{intO2}, Injection Pressure = 21 MPa.

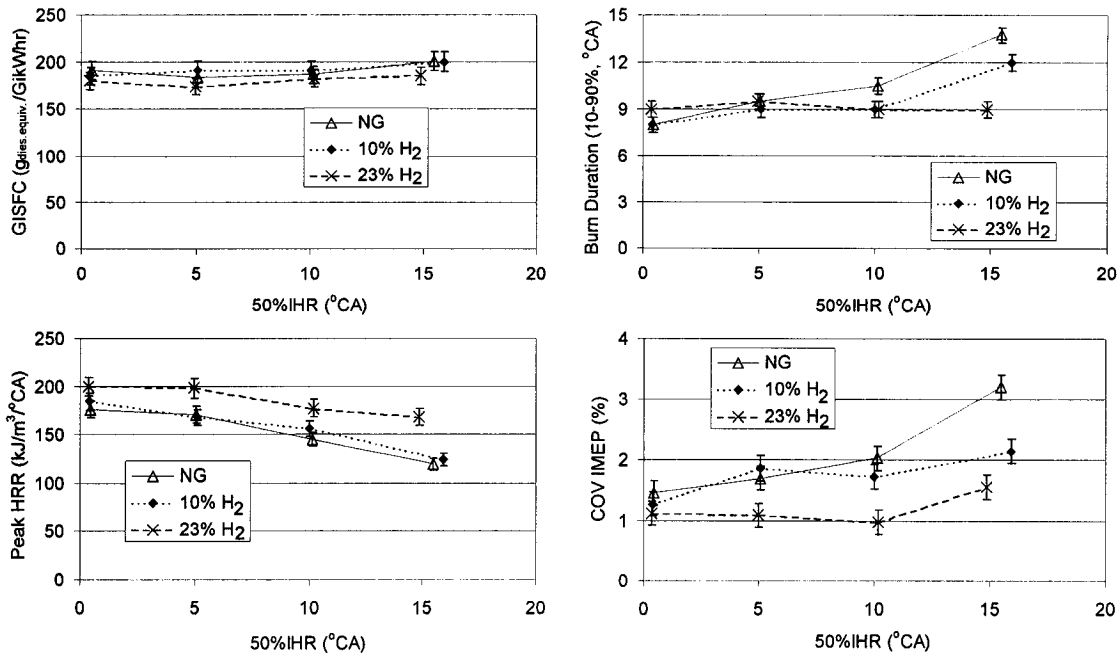

Figure 5.7: Combustion performance comparison for natural gas, 10% and 23% H_2. 800 RPM, 6 bar GIMEP, 0.5 ϕ, 0.175 Y_{intO2}, Injection Pressure = 16 MPa. *(reprinted with permission from SAE 2006-01-0653. © SAE International 2006)*

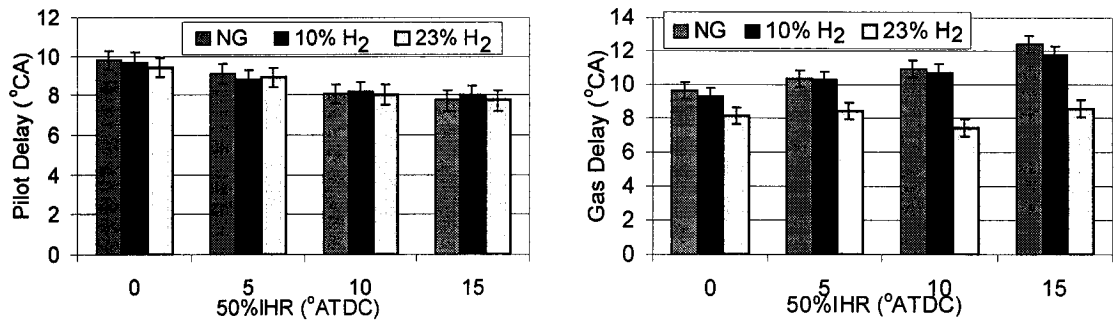

Figure 5.8: Comparison of pilot and gaseous fuel ignition delay times for natural gas, 10% and 23% H_2. 800 RPM, 6 bar GIMEP, 0.5 ϕ, 0.175 Y_{intO2}, Injection Pressure = 16 MPa. *(reprinted with permission from SAE 2006-01-0653. © SAE International 2006)*

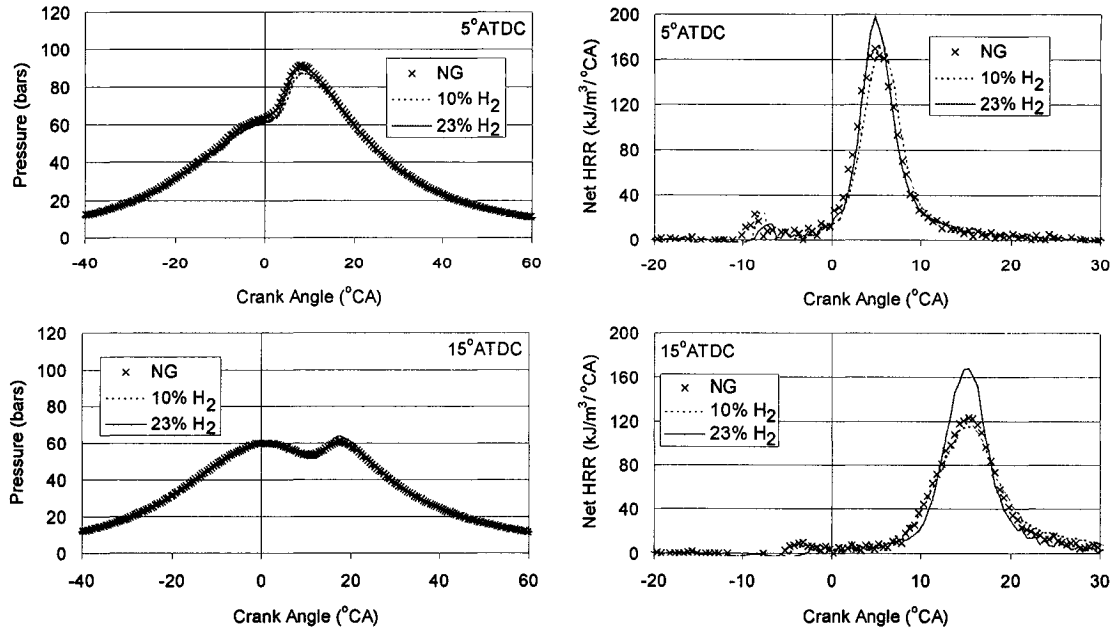

Figure 5.9: Pressure trace and estimated heat release rates, comparisons between natural gas, 10% and 23% H_2. 800 RPM, 6 bar GIMEP, 0.5 ϕ, 0.175 Y_{intO2}, Injection Pressure = 16 MPa. *(reprinted with permission from SAE 2006-01-0653. © SAE International 2006)*

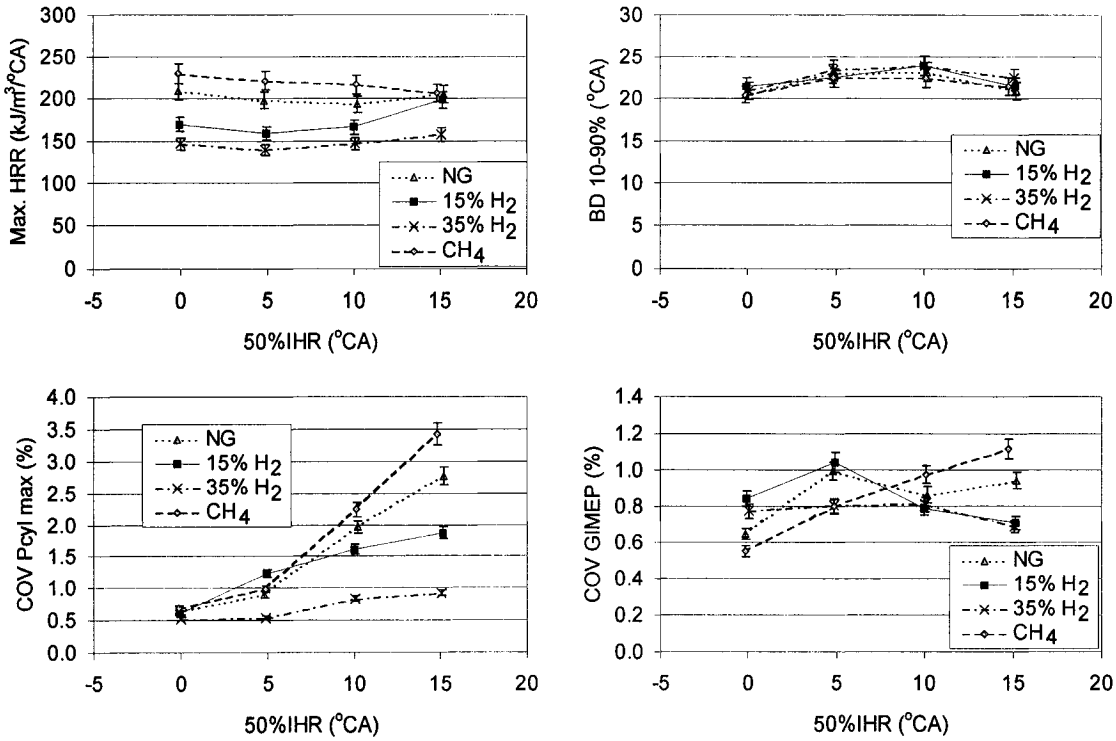

Figure 5.10: Combustion performance comparison for natural gas, methane, 15% and 35% H_2. 1200 RPM, 13.5 bar GIMEP, 0.6 ϕ, 0.19 Y_{intO2}, Injection Pressure = 21 MPa.

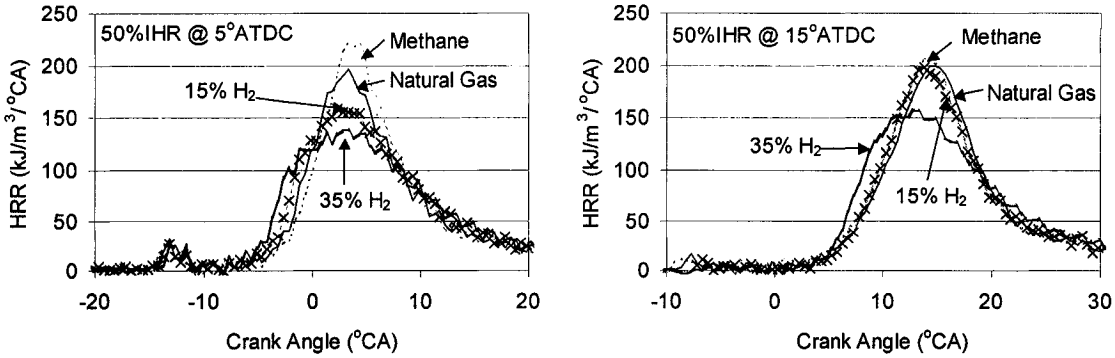

Figure 5.11: Net heat release rates for natural gas, methane, 15% and 35% H_2 at 50%IHR of 5 and 15°ATDC 1200 RPM, 13.5 bar GIMEP, 0.6 ϕ, 0.19 Y_{intO2}, Injection Pressure = 21 MPa.

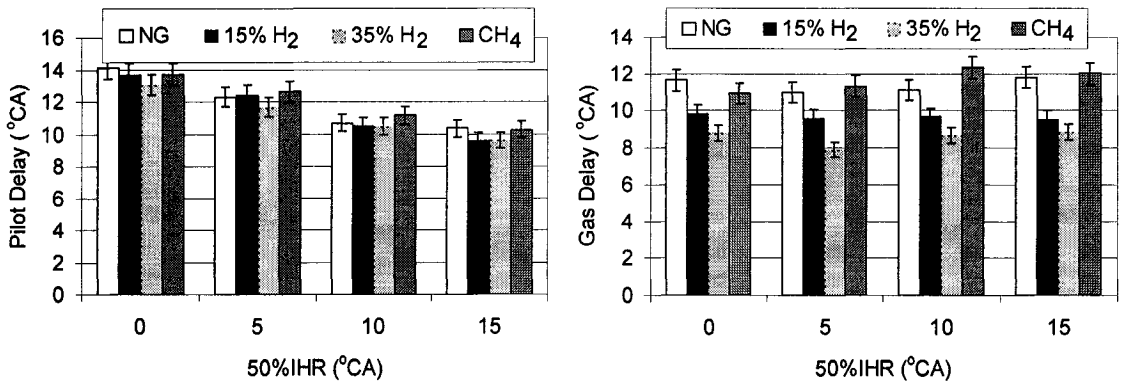

Figure 5.12: Pilot and gaseous fuel ignition delay comparison for natural gas, methane, 15% and 35% H_2. 1200 RPM, 13.5 bar GIMEP, 0.6 ϕ, 0.19 Y_{intO2}, Injection Pressure = 21 MPa.

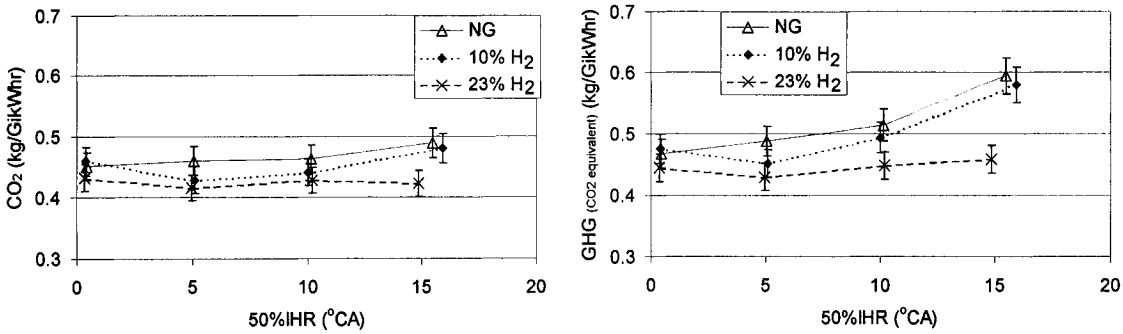

Figure 5.13: CO_2 and net GHG emissions for natural gas, 10% and 23% H_2. 800 RPM, 6 bar GIMEP, 0.5 ϕ, 0.175 Y_{intO2}, Injection Pressure = 16 MPa.

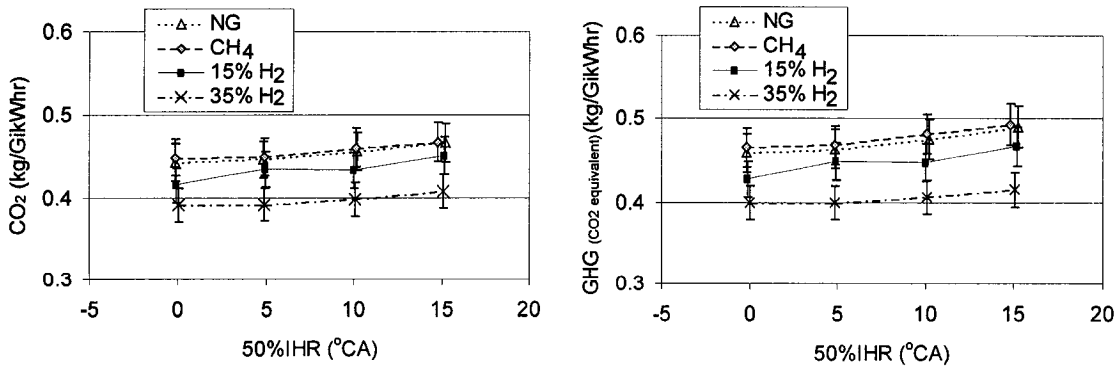

Figure 5.14: CO_2 and net GHG emissions for natural gas, methane, 15% and 35% H_2. 1200 RPM, 13.5 bar GIMEP, 0.6 ϕ, 0.19 Y_{intO2}, Injection Pressure = 21 MPa.

Chapter 6
Fuel Composition

6.1 Introduction

Like many fuels, natural gas is a mixture of various hydrocarbon molecules. Commercial grade natural gas compositions vary from 70-95% methane (CH_4), with the balance composed of heavier hydrocarbons (primarily ethane, C_2H_6, and propane, C_3H_8) as well as diluents such as N_2 and CO_2 (see Appendix 5). This chapter focuses on the role of the heavy hydrocarbons (ethane and propane); the effects of diluting the fuel with nitrogen will be discussed in Chapter 7. By studying the effects of varying the quantity of C_2H_6 and C_3H_8 in the fuel, it should be possible to identify the sensitivity of the combustion system to these species. Specifically, knowing whether the heavy hydrocarbons promote the gaseous ignition process will help to identify whether that process is limited by chemical kinetics or by mixing. Furthermore, by identifying the sensitivity of the particulate matter formation processes to the concentrations of these heavy hydrocarbons, their contribution to PM emissions can be identified.

These objectives are important not just from an academic standpoint but also operationally, given that natural gas compositions vary significantly by season, geographical area, and supplier. As a result, understanding the effects of varying fuel compositions on both engine performance and emissions is vital. As well, as more effort is focused on non-conventional gases (such as coal-bed methane and biologically derived synthetic gases), improved understanding of the sensitivity of the combustion process to variations in fuel composition is required. Understanding these effects will also be critical for engine developers and regulators to ensure that engines (and fuels) can meet current and future emissions standards.

6.2 Previous Work

The effect of fuel composition on the combustion process and on the emissions from natural gas fuelled engines has been addressed in both fundamental and applied studies. As the majority of in-service internal combustion engines are premixed charge spark ignition types (see Chapter 2), these have received the most research attention. However, some

fundamental research has also been carried out on the non-premixed autoignition of natural gas under conditions similar to those found in a heavy-duty diesel engine.

For premixed charge combustion, the greatest influences of ethane and propane on the combustion of natural gas are in the ignition and early combustion phases. The ignitability of the mixture is enhanced, due primarily to pre-combustion increases in the concentration of H, OH, and HO_2 radicals from decomposition of the heavier hydrocarbons [60,208]. The formation of hydrocarbon radicals, including C_2 species such as the ethyl radical (C_2H_5) and acetylene (C_2H_2), is also enhanced, although formation of these hydrocarbons also occurs in reactions involving only pure methane, through recombination of the methyl (CH_3) radical [209]. The importance of the H, O, and HO_2 radicals appears to apply mainly at higher temperatures; at low temperatures, significant formation of the methylperoxy (CH_3O_2H) radical by either ethane or propane decomposition appears to be the primary mechanism for enhanced ignition [210]. At these low temperatures, ethane and propane have very similar ignition promoting effects, as the two fuels have equivalent CH_2O_2H formation rates. At higher temperatures (>1200K) the formation of H radicals from propane and of OH from ethane appear to be the dominant ignition enhancing mechanisms [210]. The fundamental and applied studies available from the literature generally agree that significant enhancement of the ignition process is achieved with ethane or propane addition due to enhanced radical formation.

The improved ignitability of the fuel-air mixture has a direct impact on engine system development. For example, the spark energy required to ignite the mixture is reduced. However, the propensity for auto-ignition of the fuel/air mixture (engine knock) increases. Thus, more advanced spark timings are required to avoid knock in the presence of significant quantities of ethane or propane in spark-ignited engines [60,211]. Conversely, the auto-ignition process is used as the desired ignition source in homogeneous charge compression ignition (HCCI) engines; while ethane and propane addition can improve the ignitability of the fuel-air mixture, varying quantities of these species pose a significant challenge for HCCI engine control [212].

While the effects of ethane and propane addition to natural gas are greatest on the ignition process, flame propagation and pollutant formation are also affected. By promoting radical formation in the combustion process, the heavier hydrocarbons enhance combustion

stability and extend the lean combustion limit [213,214]. The flame's resistance to turbulent stretch (which can lead to local extinction events) is also enhanced, as is the flame propagation rate [215]. The effects of hydrocarbon addition on emissions are not as repeatable between studies as the ignition and combustion results. In some studies, NO_x emissions are slightly increased as a result of higher flame temperatures [216]; however this effect is not consistently observed [217]. No significant effects on CO emissions are reported in most of the studies; however, some researchers report reductions in HC emissions with increased ethane and propane concentrations [218].

As well as variations in reactivity of the fuel-air mixture, changes in the energy density of the fuel also affect the overall engine performance. Even when the composition varies, little influence on performance is observed at constant Wobbe indices (ratio of fuel energy content to specific gravity) [213,219]. Higher Wobbe values tend to result in reduced hydrocarbon emissions and higher engine power levels [220]. The development of closed-loop engine control [219] and fuel quality sensors [221] has allowed spark-ignition engines to operate over a wide range of gaseous fuel compositions with minimal impacts on engine performance. Typically, impacts on emissions for in-use vehicles are minimized through the use of efficient exhaust catalyst systems.

The principal influence of natural gas composition on non-premixed combustion is also on the ignition process. At high temperatures (>1400 K) fuel additives have little effect as this process is mixing limited [222]. At lower temperatures, the addition of either ethane or propane is found to reduce ignition delay times by as much as 0.7 ms. However, there is a limit to the effectiveness of improved kinetics, especially at higher temperatures; beyond a certain point mixing limitations dominate the ignition processes. The shorter ignition delay time has also been identified as a potential source for increased NO_x emissions with ethane addition to the fuel [89]; however, substantially more work is required to understand the effects of the heavier hydrocarbons on the ignition and pollutant formation mechanisms of a natural gas engine using a non-premixed direct-injection combustion system.

6.3 Experimental Information

UBC's single-cylinder research engine was used to investigate the effects of heavier hydrocarbons on a direct-injection of natural gas engine. The facility was in most respects unmodified from that described in Chapter 3. The re-entrant bowl-in-piston geometry, with a

17:1 compression ratio, was used for all the testing. Modifications were also made to the fuel supply system to permit the addition of ethane and propane additives to the standard building-supplied natural gas. To prepare the fuel blends, four large high-pressure natural gas storage tanks (internal volume 115L/tank) were emptied of gas. Measured amounts of the specific additives from compressed gas supply bottles (all industrially-supplied, 99.9% purity grade 2.0 or better) were put into the storage tanks. The tanks were then refilled with commercial natural gas and allowed to sit for at least 2 days prior to use, to ensure that the fuel mixture was homogenous. Composition control during mixing was achieved through the use of partial pressures, while gas chromatograph analysis was carried out on the blended gas (sampled just upstream of the engine part way through the testing) to verify the actual fuel composition. The fuel compositions reported in this work refer exclusively to the gas chromatograph measurements.

Four blends were prepared and compared to standard commercial natural gas. These were low and high C_2H_6 (targets were 5% and 10% by volume) and low and high C_3H_8 (targets 2% and 4% by volume). These concentrations were selected to minimize the chance of condensation of the hydrocarbons after the blend was compressed to full system pressure (up to 30 MPa). Although the gas composition varied, the fuel flow rate measurements were not affected as the flow meter (MicroMotion coriolis force) measured mass flow directly. The compositions of the various blends, as analysed at Westport Innovations Inc., are shown in Table 6.1. In some cases, and in particular for the C_2H_6 case, the actual compositions were significantly different from the target compositions. As the maximum concentrations were still well below the saturation partial pressures, and as the original target concentrations were arbitrarily selected, the final conclusions are not affected by this discrepancy in composition.

6.3.1 Operating Condition

The engine operating condition selected for this testing was at high-load but moderate speed, approximating the peak-torque condition for the ISX series engine. This point was very similar to the second-round engine condition investigated in Chapter 5 (Table 5.1). The constants and variables for this operating condition are outlined in Table 6.2. The only variable was combustion timing, which was controlled (based on the midpoint of the heat release, 50%IHR, as discussed in section 3.3.1) from 0° to 15° after top-dead-center (ATDC). All other parameters, including the oxygen equivalence ratio (ϕ), speed, and intake oxygen

mass fraction (Y_{intO2}) were fixed. This process minimized the variability in the operating condition while maximizing the testing time available with the limited quantity of fuel available. By varying the combustion timing, a range of combustion conditions was achieved without significantly affecting the air-exchange parameters.

6.3.2 Experimental Process

For all the fuel blends, at least three repetitions of each test condition were carried out. Full randomization of the testing was not possible, as only one gas blend could be prepared at a time. The test sequence was as follows: First, a full set of natural gas tests was performed. Then, to minimize the number of times the tanks needed to be emptied, the tests with the high concentration gas blend of each species was conducted, followed by the tests with the low concentration gas mixture. To complete the sequence, the full set of natural gas tests was repeated. Comparing the natural gas results from before and after the test sets showed no significant variation in operating condition setting, emissions or performance. The sequence of the test points was fully randomized within each fuel composition. As a result of the lack of randomization or replications between blocks, statistically valid tests between the fuel compositions were not possible, as the influence of fuel composition could not be differentiated from day-to-day variability. However, the fact that no significant differences in performance or emissions were detected between the initial and final natural gas tests indicates that no systematic errors were present which would have biased the results.

6.4 Results

The role of the heavier hydrocarbons in the overall combustion event is of particular interest because of their varying concentrations in natural gas. Previous results have found that the ignition process, combustion rate, and emissions formation are all affected by fuel composition. These preceding studies relate primarily to premixed combustion; the effects on direct injected natural gas under conditions similar to those of a modern diesel engine have not been previously investigated in detail.

6.4.1 Combustion Effects

One of the principal effects of the presence of ethane and propane in the natural gas is on the ignition process, as shown in Figure 6.1. The pilot ignition delay time (see section 3.3.1 for the ignition timing definitions) is unaffected by the addition of ethane or propane.

This is expected, given that the pilot fuel composition is no different and that pilot ignition occurs before the start of gas injection. The gas ignition delay time, however, is reduced by as much as 10% with either propane or ethane added to the gaseous fuel. The addition of significant quantities of either hydrocarbon significantly increases the ignitability of the natural gas by increasing the concentration of specific radicals [210]. As the diesel pilot ignites the gaseous jet, the gaseous start-of-combustion is not truly an auto-ignition process. However, the presence of more reactive radicals in the gaseous jet will increase the ignitability of the jet. Ignition can thus occur at lower temperatures and over a wider range of fuel-air stoichiometries than with pure methane. In comparison, there is no consistent difference in ignition delay between the pure methane and natural gas cases (see section 5.3.3). However, this is most likely a result of an inability to resolve the effects of the relatively small concentrations of ethane and propane in the natural gas. The fact that both low and high ethane cases show the same reduction in the gaseous ignition delay suggests that the upper limit to the ignition-promoting effects of ethane may be being approached. This conclusion agrees with previous work, which suggests that once the chemical (kinetic-related) component of the ignition delay is minimized, a significant delay remains due to the time required for the fuel and air to mix to a combustible stoichiometry [222]. For both ethane and the high propane cases, the gaseous ignition delay is similar. This suggests that the potential benefits of improving kinetics have been achieved, and that the primary factor affecting the ignition delay at this condition is physical relating to the mixing of the fuel and air.

A significant effect of the shorter gas ignition delay time is a reduction in the premixed component of the combustion event (Figure 6.2). The reduction in peak heat-release rate indicates that the amount of energy released during the early partially premixed burn phase is dependent on the amount of fuel injected and mixed to a combustible mixture prior to ignition. With the shorter ignition delay, less combustible fuel-air mixture is available when ignition occurs and hence the peak energy release is reduced. The overall burn duration is also increased by a corresponding amount (approximately 5%, Figure 6.3), resulting from the earlier ignition combined with constant end-of-combustion timing. (The end-of-combustion timing is designated in Figure 6.3 by the crank angle at which 90% of the fuel energy has been released, 90%IHR.) These relatively small effects, including the

reduction in peak heat-release rate and earlier start-of-combustion timing, are also shown in the pressure trace and net heat release rates shown (for a single combustion timing) in Figure 6.4. The pressure traces at the other timings indicate similar trends; these may be found in Appendix 6. These observations indicate that the principal factors influencing the combustion event are the injection and mixing rates; the influence of improved kinetics is limited to enhancing the ignition process.

The importance of combustion stability on performance and emissions is demonstrated in Chapter 5, with hydrogen significantly enhancing combustion stability. With the hydrocarbon additives, the ignition process is enhanced, but overall combustion stability, represented by the COV of the GIMEP, is not significantly affected (Figure 6.5). At the operating condition tested, the combustion stability is generally very good (<1%COV) for all the fuel conditions. Only one condition, with low propane addition, has a COV consistently higher than the other cases. The reasons for this effect are unclear, but this may have a significant impact on emissions for this fuel blend. The potential for ethane or propane addition to improve stability at conditions with high combustion variability was not investigated.

Previous results [60] have suggested that fuel-conversion efficiency is influenced by the presence of heavier hydrocarbon additives. In this work, the efficiency is represented by the specific fuel consumption (GISFC), shown in Figure 6.6. For all cases, the fuel consumption is calculated on an energy-equivalent mass of diesel basis (see section 3.3.3). The addition of propane slightly reduces the fuel consumption, while the ethane slightly increases it. However, these effects are relatively small, and in general the conversion of chemical energy in the fuel to piston work is independent of fuel composition over the range of compositions and the engine conditions tested. This is not surprising, given the relatively small influence of the additives on the overall combustion progression (indicated by the in-cylinder pressure and heat-release rate, Figure 6.4).

6.4.2 Gaseous Emissions

Adding propane or ethane to the gaseous fuel has a significant influence on some of the measured emissions. These effects are, in most cases, more significant than would have been expected from the relatively small changes in the observed combustion progression. Interestingly, The hydrocarbon additives did not significantly influence the NO_x emissions

(shown in Figure 6.7). This could be expected given that the adiabatic flame temperature is not significantly affected (Table 6.1) and the peak combustion intensity (Figure 6.2) is only slightly reduced.

The HC emissions are, in general, slightly reduced with the addition of ethane or propane to the gaseous fuel (Figure 6.8). In all cases, the hydrocarbon emissions are indistinguishable from the exhaust methane measurements, suggesting that at least 95% of the exhaust HC are unburned methane. The observed reduction in unburned fuel emissions may have been a result of reduced over-leaning due to the shorter gaseous ignition delay provided by the ethane and propane additives. The fact that the low propane case shows no significant improvement in HC emissions may be related to the higher combustion variability observed at this condition (Figure 6.5). For most of the conditions tested, the largest reductions in HC emissions occur at the latest timing, which is the only condition with significant reductions in the combustion variability compared to the natural gas fuel.

Similar to the HC emissions, the effects of fuel composition on the emissions of CO (Figure 6.9) are sensitive to combustion timing and fuel composition. The general trend with timing – reaching a maximum at intermediate timings, with lower emissions at both early and late timings – is contrary to previous results at lower loads, as shown both in Chapter 5 and in some previous work [135], as well as differing from conventional diesel-engine emission formation wisdom [28]. However, some other previous results suggest that, at mid-speed and high-load conditions, CO emissions may be higher at intermediate timings [130,134]. In the previous work, this effect was attributed to interactions between the burning gas jet and the piston, with both earlier and later timings resulting in less interaction, due to changes in charge motion, piston location, and combustion rate.

In general, the addition of ethane or propane to the fuel increases CO emissions. At the latest combustion timing, the CO emissions from the natural gas fuelling case are substantially higher than most of the fuel additive cases; this may be a result of the higher combustion variability encountered at this point (Figure 6.5). The combustion variability also appears to influence the low propane addition case's CO emissions levels, which are significantly higher than the emissions at the high-propane fuelling condition. These results provide further evidence that combustion instability is one factor that can contribute significantly to CO emissions. However, whether the increased variability is a result of

competing mechanisms in the propane oxidation process or simply due to day-to-day performance or measurement variability cannot be conclusively determined. In general, CO emissions are substantially increased through the addition of heavier hydrocarbons to the natural gas. As the combustion stability is not significantly influenced, the results suggest that the influence of the heavy hydrocarbons on CO emissions is through the chemical kinetics either increasing CO formation or reducing its oxidation to CO_2. As the late stages of the combustion event and the overall oxygen concentrations in the combustion chamber are generally unaffected by the fuel composition, it is likely that the addition of the heavy hydrocarbons is enhancing the chemical formation of CO. This agrees with basic understanding of CO formation in methane flames, which tends to be enhanced by the presence of ethane or propane in the fuel [37,217].

6.4.3 Particulate Matter

The PM total mass emissions, Figure 6.10, demonstrate trends generally similar to those of the CO emissions. The addition of ethane or propane tends to substantially increase PM emissions, while higher PM levels are also observed at the intermediate combustion timings. Increases in PM with the hydrocarbon additives are greater than a factor of two at certain conditions, demonstrating the very strong influence of ethane and propane on the PM emissions. The fact that the low propane additive case was indistinguishable from the high propane case may be a result of effects similar to those that induced the higher CO emissions at this condition, as discussed in the preceding section. The PM was most significantly increased with the high ethane concentration, which also has the lowest H:C ratio of any of the fuels (Table 6.2). The increases in emissions are generally consistent for the intermediate and late timings; only at the earliest timings are substantially smaller increases observed. This suggests that at the earliest combustion timings, the greater residence time in the high-temperature post-combustion gases may result in more PM being oxidized. At the intermediate timings, impairment of late-cycle oxidation through interaction between the burning fuel-air mixture and the piston may result in premature quenching of the combustion. Since the unburned fuel emissions are not increased (Figure 6.8) it would appear that it is the very-late stage combustion which is being impaired. A plausible explanation is that the majority of the methane which was going to burn has already been consumed; only partial combustion products (CO, PM) are not being fully oxidized.

Further insight into the PM formation and oxidation processes with the addition of ethane and propane to the natural gas can be identified from the particle size distributions (Figures 6.11 and 6.12). These demonstrate general agreement with the measured mass distributions, with no discernable difference in number concentrations between the low and high propane cases, although both are greater than the natural gas case. For ethane addition, substantial increases are observed between the natural gas, low ethane, and high ethane cases. In general, a shift towards both a greater number of particles and larger diameters is observed, consistent with accepted theories of particulate growth during the dilution process [6]. If a larger number of particles are formed initially, there will be a greater likelihood of these particles combining into agglomerates and thereby forming longer chains. This process will tend to reduce the individual number of particles measured; therefore, the observation of a larger total number of particles, along with a larger mobility diameter, suggests that the number of particles formed in the initial combustion event is substantially increased. This leads to more agglomeration resulting in the observed increase in particle size. These results are confirmed by TEM images (Appendix 7), which do not indicate a difference in primary particle size for different fuel compositions. None of the conditions tested show a significant nucleation-mode peak, indicating that the particle surface areas are consistently large enough to ensure that adsorption of volatiles occurs preferentially to the post-exhaust nucleation of new volatile particles.

The relative fraction of volatile material in the particle mass, measured using an Aethalometer, is shown in Figure 6.13. The black carbon content of the exhaust stream increases substantially at all timings with the addition of either ethane or propane to the fuel. The black carbon fraction (BC mass / PM total mass), shown in Figure 6.14, also increases at the earlier injection timings with the fuel additives. However, at the later timings, this ratio is independent of the fuel composition. This indicates that the mass of both BC and of volatiles in the PM increases with the addition of the heavier hydrocarbons to the methane fuel. The estimated mass rate of volatile emissions (PM total mass less BC mass) is shown in Figure 6.15; the large error bars are a result of the combined uncertainty from the total mass and BC measurements. One possible explanation for the larger volatile concentration is that the gaseous fuel is contributing significantly to volatile emissions. As discussed in section 2.2.5, the formation pathways for carbonaceous PM involve the formation of many polycyclic

hydrocarbons; not all of these species will form PM during the combustion event, and if they are not oxidized, they will be emitted as volatiles which could condense post-exhaust. Another potential explanation is that the increased surface area of post-combustion particulate adsorbed substantially more of the volatile materials, which would otherwise be emitted in the vapour phase.

6.5 Discussion

Ethane or propane addition to the natural gas results in a significant increase in PM. As shown in the previous chapter (Chapter 5) the use of pure methane, compared to commercial natural gas, has only a small effect on PM emissions (Figure 5.2). As suggested by reaction kinetics analyses, a significant fraction of methane may combine (via the methyl radical, CH_3) to form either ethane (C_2H_6) or ethyl (C_2H_5), most of which will pass through acetylene (C_2H_2) as they dissociate [223]. By increasing the ethane concentration, the initial response may be a reduction in the amount of ethyl recombination forming ethane. As a result, small quantities of ethane in the fuel may not significantly increase the formation of acetylene. However, as the ethane quantity increases further, acetylene formation is enhanced as the fuel-side concentration of ethane becomes larger than the amount which would have been formed via ethyl recombination. This may explain both the relatively small differences in PM between pure methane and natural gas and the much larger differences between natural gas and higher ethane and propane additives.

The addition of either propane or ethane to the natural gas fuel results in reductions in the global hydrogen to carbon (H:C) ratio in the fuel (Table 6.1). Whether the global H:C ratio or kinetics relating to the specific hydrocarbon molecule has a greater influence on PM emissions may be deduced from the plots of total PM mass and black carbon mass as a function of H:C ratio, shown in Figures 6.16 and 6.17 for two timings (50% IHR at 5 and 15°ATDC). For both timings, the particulate mass increases dramatically at H:C ratios less than 3.9, but decreases relatively slowly at ratios greater than 4 (pure methane and the hydrogen results from Chapter 5). Similar results are observed for the black carbon mass, providing further indication that the gaseous fuel has a significant impact on carbonaceous particulate formation. The right-hand plot in both figures (6.16 & 6.17) shows the H:C ratio effects on PM and BC for ratios between 3.8 and 4.0 (pure methane, natural gas, ethane and propane addition cases). These indicate that the propane (for an equal H:C ratio) generates

significantly more total and black carbon PM than the ethane; this suggests that the H:C ratio is not the only factor relating to PM formation.

The results indicate that relatively small quantities of heavy hydrocarbons are not substantially influencing PM emissions. However, as concentrations increase above the baseline level, significant increases in PM emissions are observed. One technique that could mitigate these increases would be to change the engine's operating mode (either through the use of more advanced timing or lower EGR levels); however, this would tend to increase NO_x emissions. Another option would be to consider adding a small amount of another additive to the fuel to offset the observed increases in PM and CO. Hydrogen is one obvious alternative, as was shown in Chapter 5. Some natural gas fuels do contain significant quantities of diluents, including nitrogen; if the level of these diluents could be used to offset the effects of propane or ethane addition, a low-cost technique for achieving low emissions over a wide range of fuel compositions could be achieved. Chapter 7 investigates the effect of fuel dilution with nitrogen on emissions and performance, as well as providing further discussion of the effects of fuel composition.

6.6 Conclusions

1. CO and PM emissions are generally increased with the addition of ethane and propane to the fuel. The substantial increases in PM are attributed to the formation of acetylene as a reaction intermediary of the decomposition of ethane and propane [223], leading to increased polycyclic aromatic hydrocarbon formation and higher levels of PM.
2. The global H:C ratio of the gaseous fuel generally predicts the observed trends in both PM and black carbon. However, consistent differences in PM levels between the ethane and propane cases at equivalent H:C ratio suggests that kinetic effects relating to the specific molecules play a significant role in the formation of black carbon and total PM.
3. The addition of either ethane or propane to the natural gas increases the ignitability of the gaseous mixture. However, increasing the ethane from moderate to high levels did not reduce ignition delay any further; this indicates that kinetic limitations have been minimized and that the ignition process has become dependent on the time for the gaseous jet to mix to a combustible stoichiometry.
4. The shorter gaseous-fuel ignition delay results in a smaller amount of fuel having premixed to a combustible level, resulting in a reduced peak heat-release rate. This

results in a longer duration for the gaseous fuel combustion, suggesting that the overall duration of the combustion event is limited by the rate at which the fuel and air mix.

5. The addition of heavier hydrocarbons did not significantly affect NO_x emissions. HC emissions were slightly reduced, possibly due to small improvements in combustion stability resulting from the ethane and propane in the fuel.
6. The effects of ethane and propane in the fuel on PM emissions have significant implications for engine development. Aftertreatment may be required to ensure that ultra-low PM emissions levels are retained over the range of fuel compositions that may be experienced. An alternative would be to provide more careful control over the composition of natural gas fuels supplied to vehicles.

6.7 Tables and Figures

Table 6.1: Fuel composition as measured by gas chromatography

	Natural Gas	Low Ethane	High Ethane	Low Propane	High Propane
n-Butane	0.05	0.05	0.04	0.08	0.08
i-Butane	0.07	0.07	0.06	0.09	0.09
i-Pentane	0.02	0.02	0.02	0.02	0.03
n-Pentane	0.02	0.02	0.01	0.02	0.02
Hexane	0.01	0.01	0.00	0.01	0.01
Heptane	0.00	0.00	0.00	0.00	0.00
Octane	0.00	0.00	0.00	0.00	0.00
Nitrogen	1.47	1.09	1.19	2.02	2.82
Methane	96.6	91.43	89.39	93.5	91.3
Carbon Dioxide	0.44	0.40	0.34	0.41	0.38
Ethane	1.41	6.60	8.62	1.59	1.50
Propane	0.32	0.32	0.28	2.23	3.73
MW (kg/kmol)	16.70	17.37	17.63	17.34	17.85
LHV (kJ/kg)	48080	48279	48220	47540	46883
HHV (kJ/kg)	53313	53462	53372	52658	51891
$T_{adiabatic}$ (K)	2485	2530	2550	2495	2510
H:C ratio	3.94	3.88	3.86	3.91	3.88

Table 6.2 Operating condition constants and variables

Parameter	Value
Speed (RPM)	1200
GIMEP (bars)	13.5
ϕ_{O2}	0.6
EGR (mass %)	30
Y_{intO2}	*0.19*
Fuel Pressure (MPa)	21
50%IHR (°ATDC)	0, 5, 10, 15
Pilot (mg/inj)	5

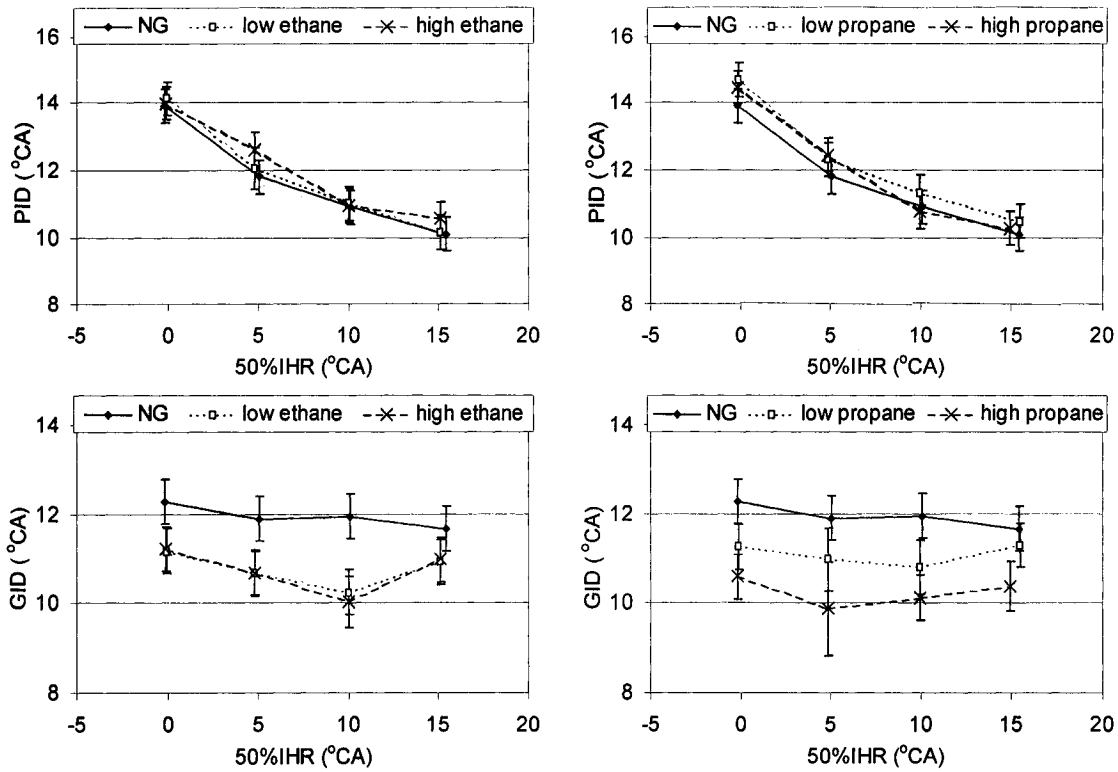

Figure 6.1: Pilot (PID) and gas ignition delay (GID) times (relative to commanded start-of-injection) for ethane (left) and propane addition (right) additives, compared to natural gas fuelling.

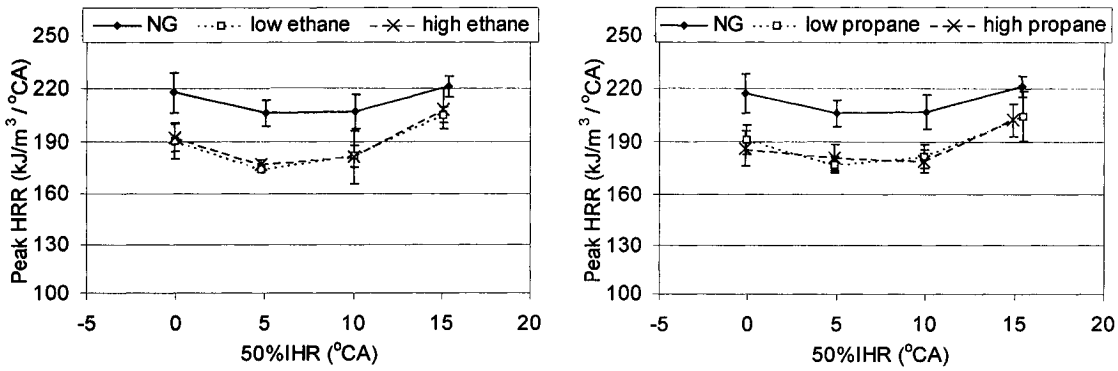

Figure 6.2: Peak heat-release rate for ethane (left) and propane (right) additives, compared to natural gas fuelling.

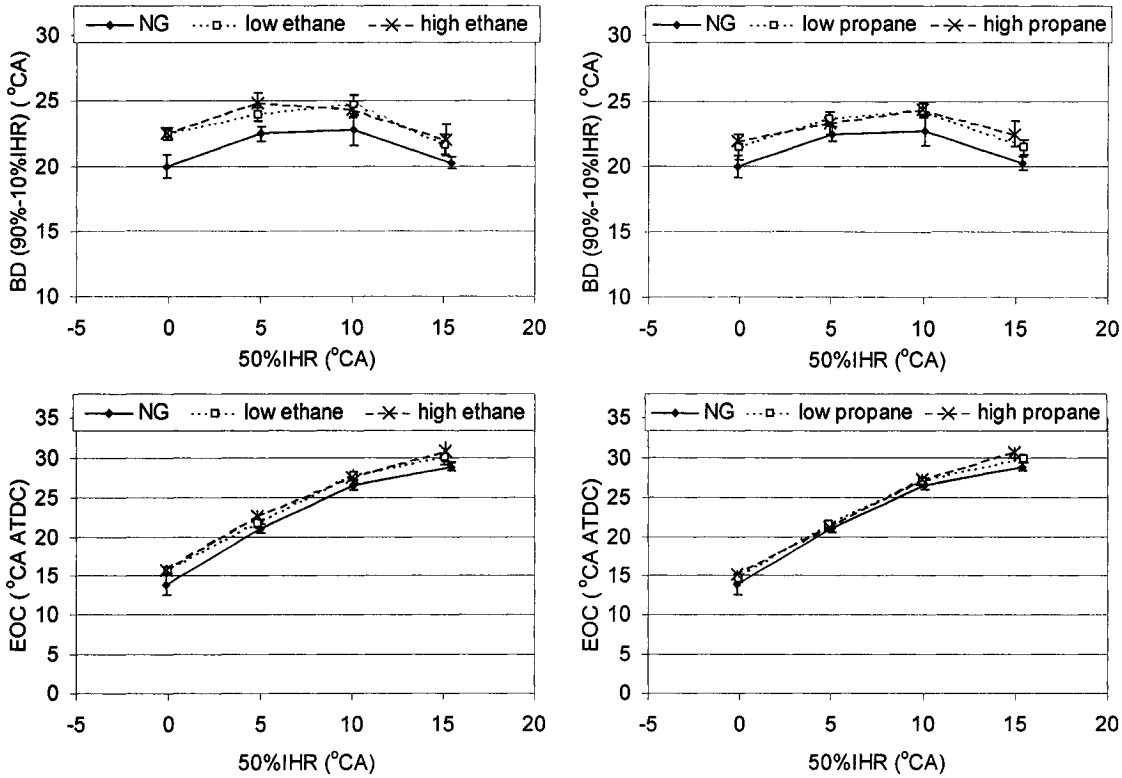

Figure 6.3: Burn duration and end-of-combustion (EOC) timing (90%IHR) for ethane (left) and propane (right) additives, compared to natural gas fuelling.

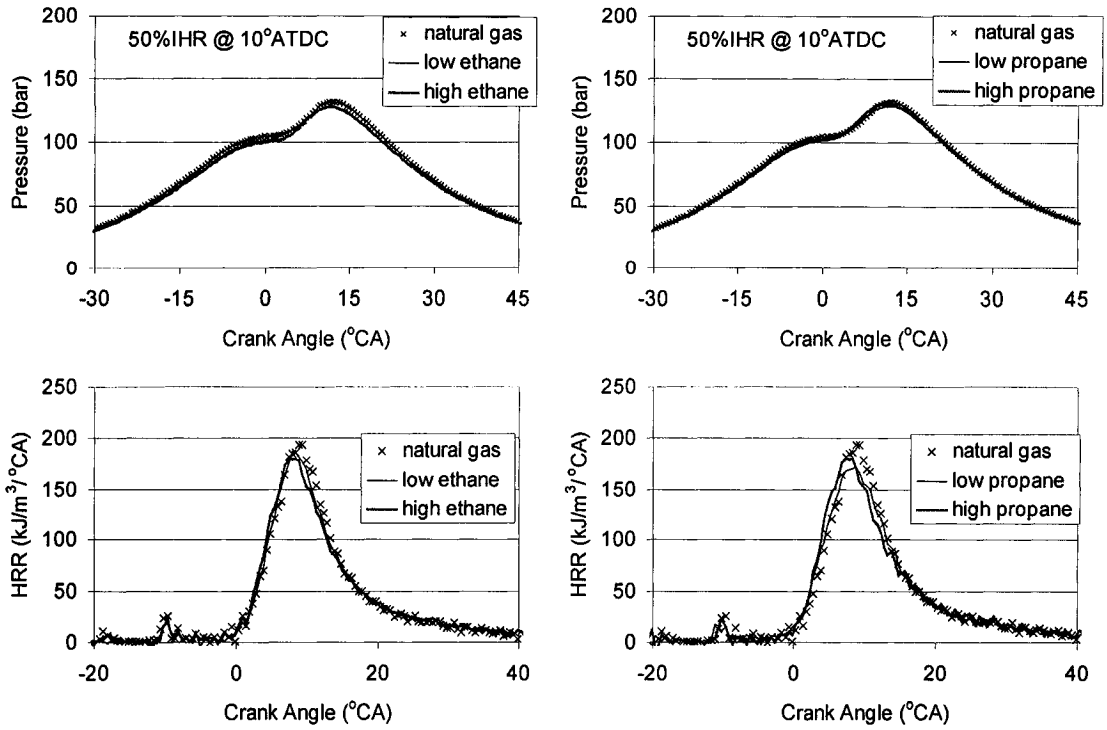

Figure 6.4: In-cylinder pressure trace and net heat-release rate for the mid-timing condition (50%IHR at 10°ATDC) for ethane (left) and propane (right) additives, compared to natural gas fuelling.

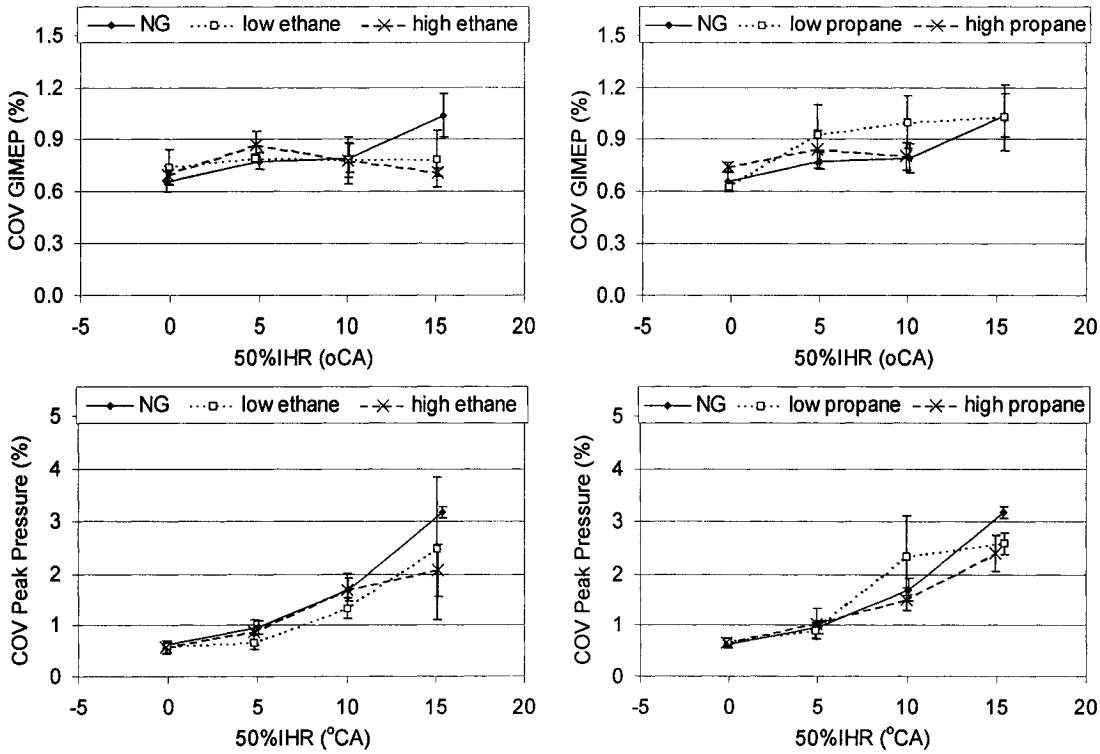

Figure 6.5: Combustion stability (COV of GIMEP and COV of peak cylinder pressure) for ethane (left) and propane (right) additives, compared to natural gas fuelling.

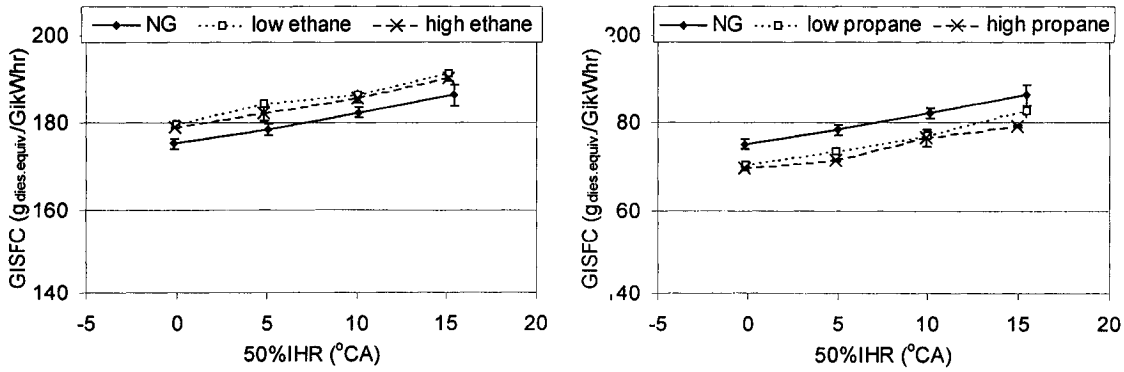

Figure 6.6: GISFC with ethane (left) and propane (right) additives, compared to natural gas fuelling.

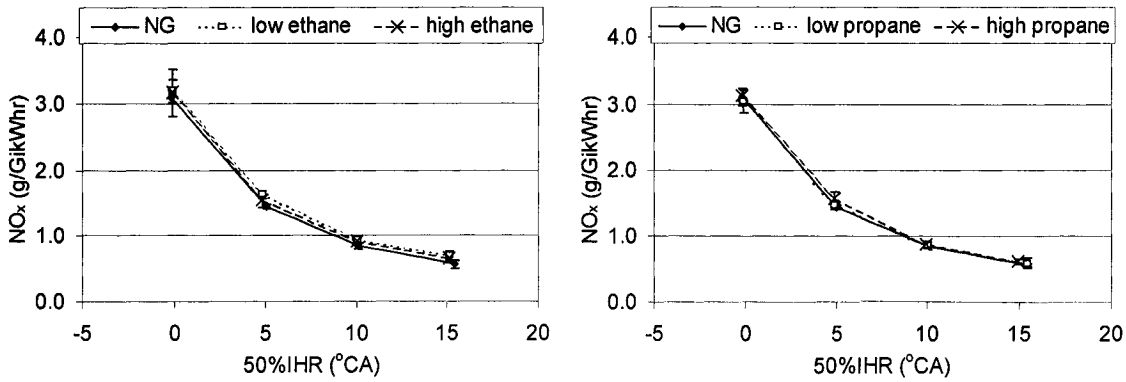

Figure 6.7: NO_x emissions as a function of timing, for ethane (left) and propane (right) additives, compared to natural gas fuelling.

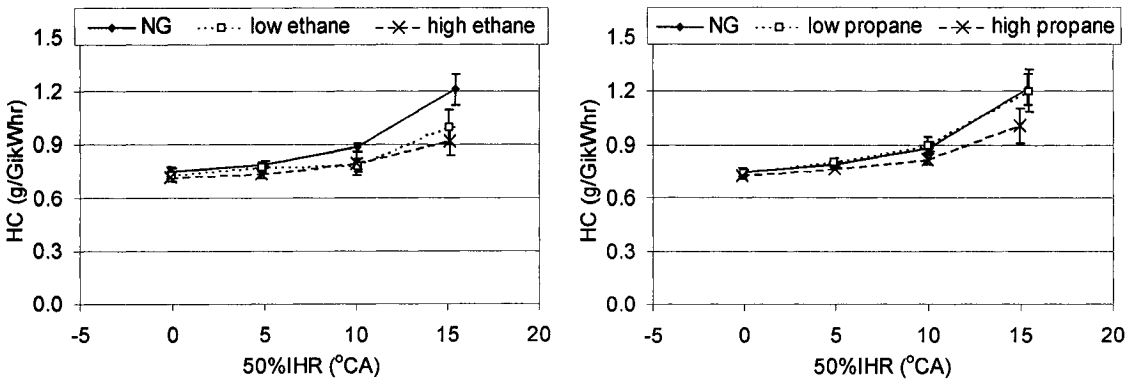

Figure 6.8: Hydrocarbon emissions as a function of timing, for ethane (left) and propane (right) additives, compared to natural gas fuelling.

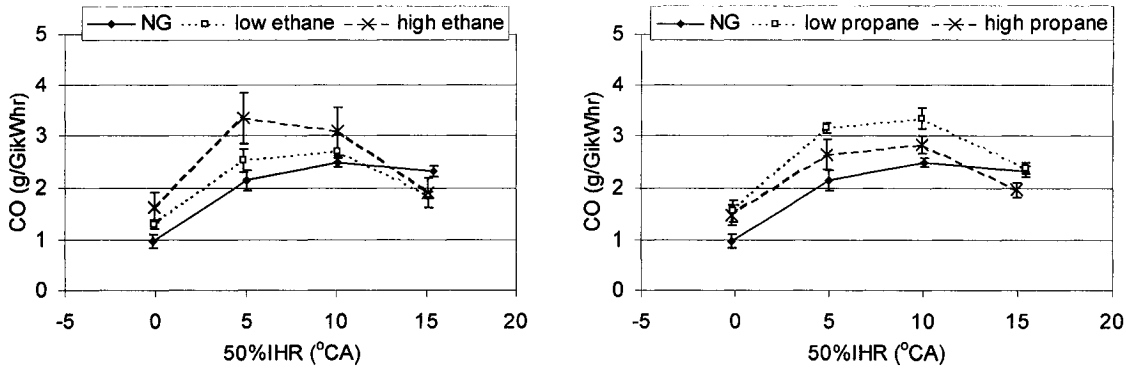

Figure 6.9: CO emissions as a function of timing, for ethane (left) and propane (right) additives, compared to natural gas fuelling.

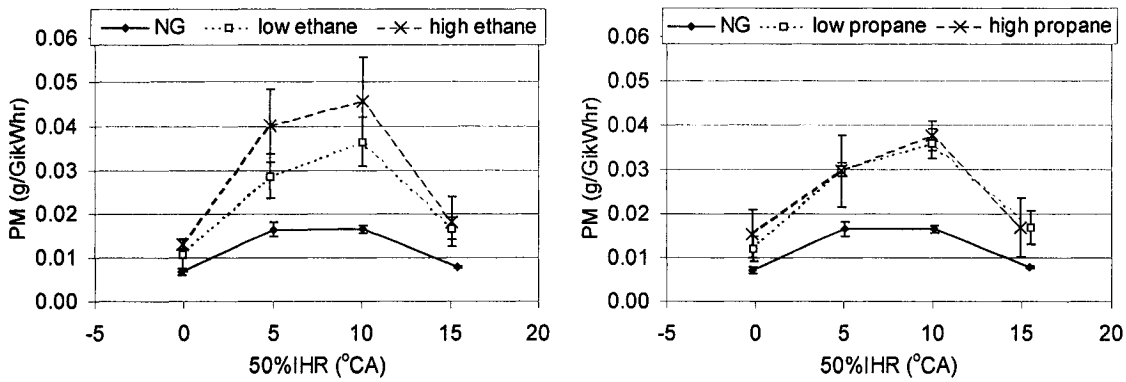

Figure 6.10: PM emissions as a function of timing, for ethane (left) and propane (right) additives, compared to natural gas fuelling.

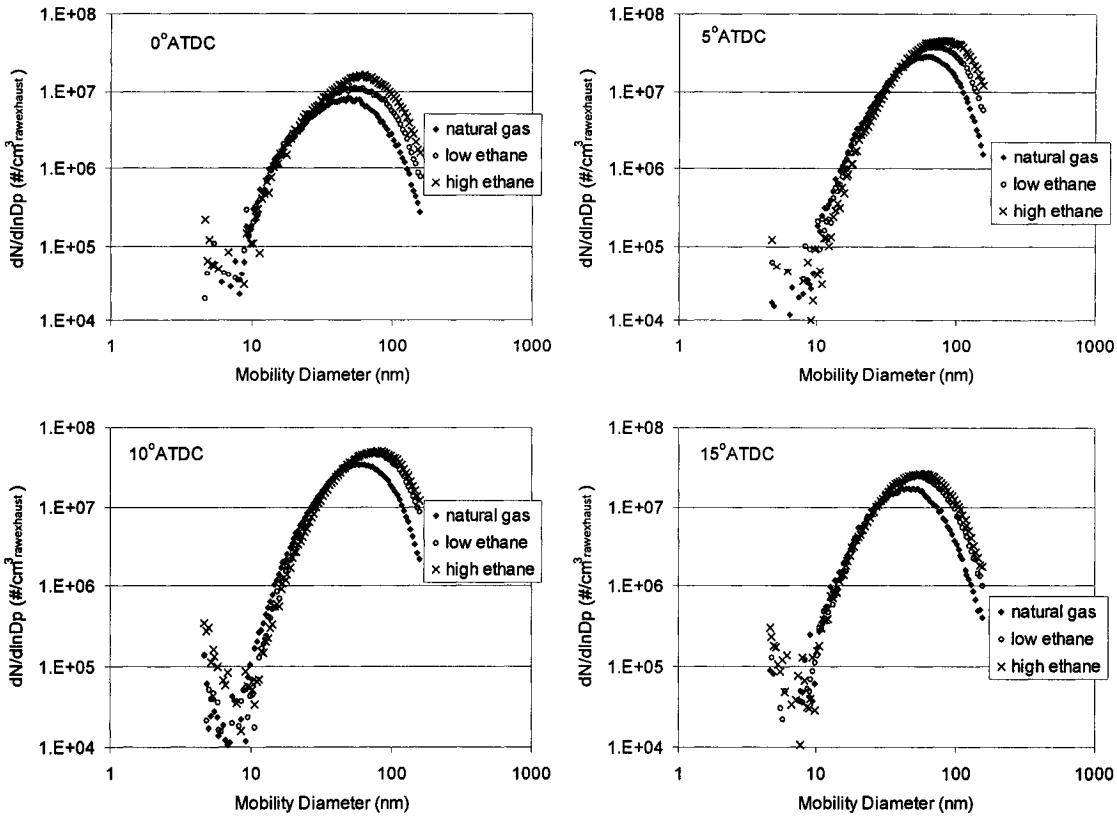

Figure 6.11: Particle size distributions for natural gas and two levels of ethane addition at four combustion timings (clockwise from top left: 0, 5, 10, 15°ATDC)

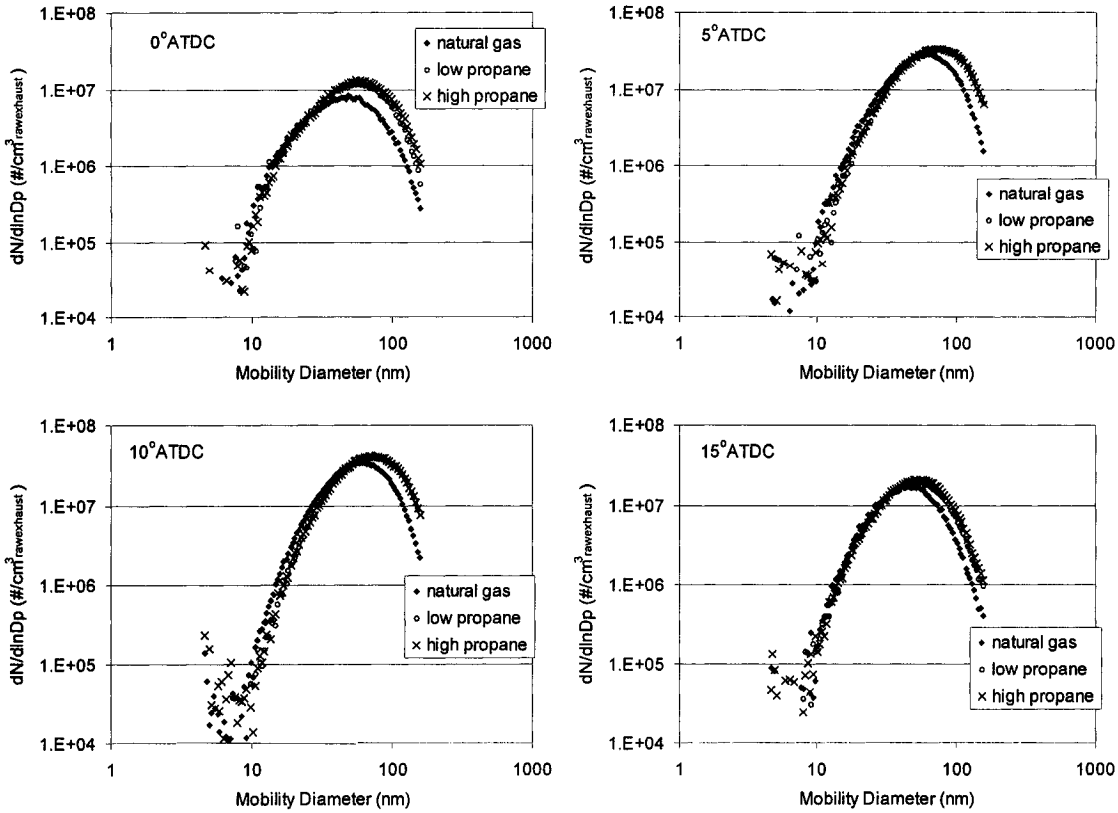

Figure 6.12: Particle size distributions for natural gas and two levels of propane addition at four combustion timings (clockwise from top left: 0, 5, 10, 15°ATDC)

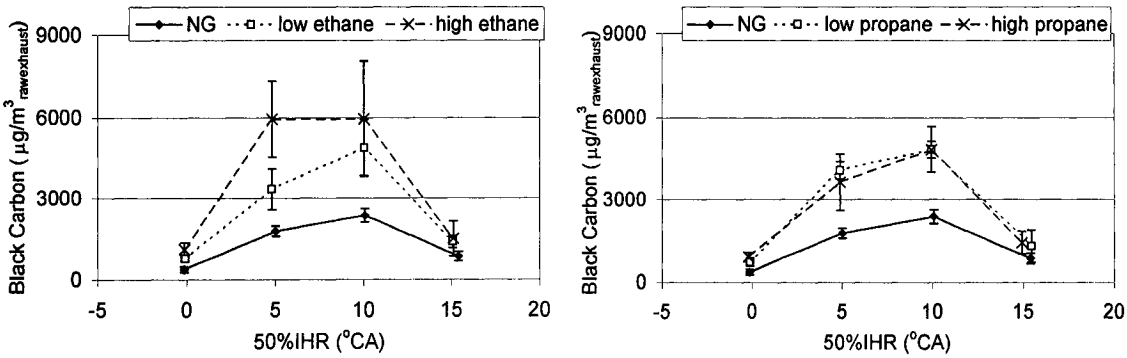

Figure 6.13: Aethalometer results, BC concentration as a function of timing for ethane (left) and propane (right) additives, compared to natural gas fuelling.

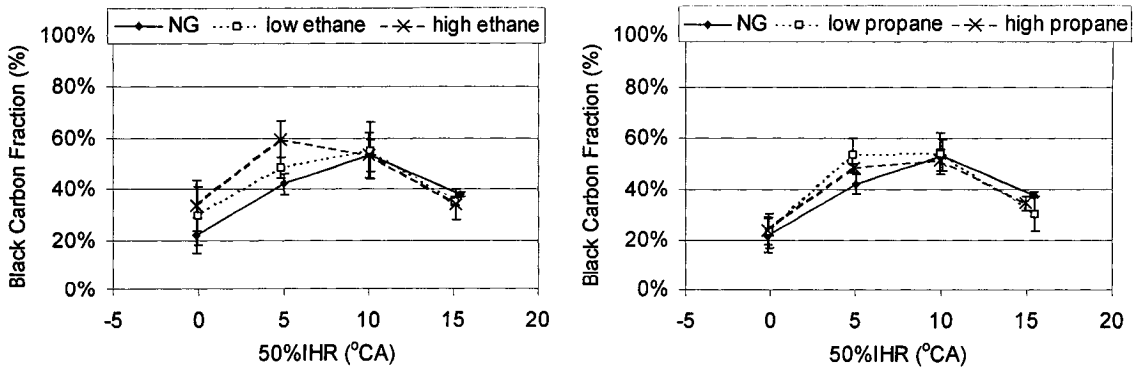

Figure 6.14: Black-carbon fraction (BC/PM total mass) as a function of timing for ethane (left) and propane (right) additives, compared to natural gas fuelling.

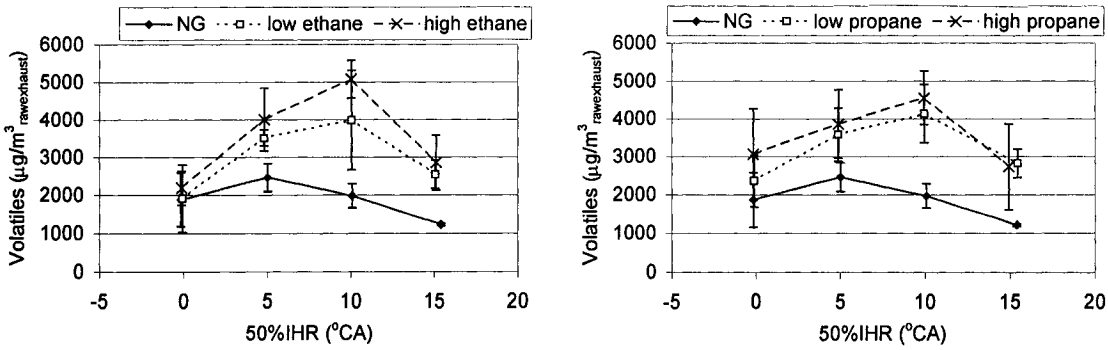

Figure 6.15: Volatile mass rate (PM total mass – BC mass) as a function of timing for ethane (left) and propane (right) additives, compared to natural gas fuelling.

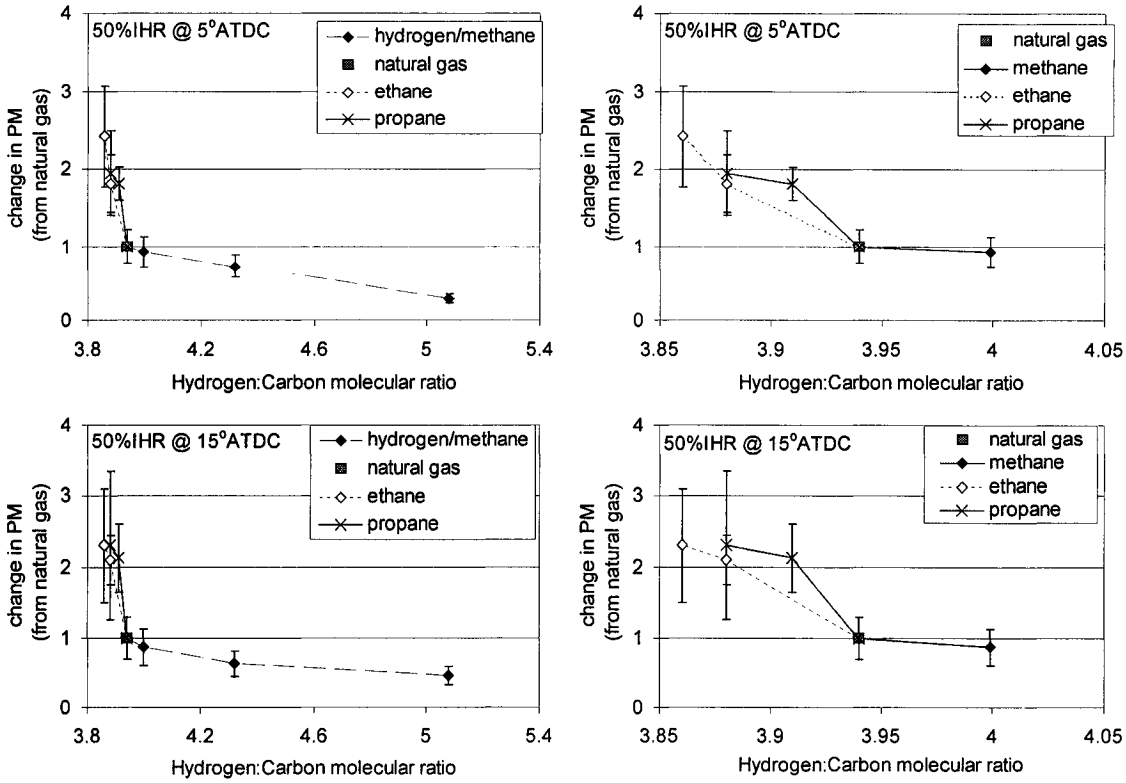

Figure 6.16: Effect of global hydrogen to carbon ratio on total change in PM emissions (PM measured / PM measured under natural gas fuelling) at 5 and 15°CA ATDC combustion timing. The right-hand plots exclude the hydrogen results.

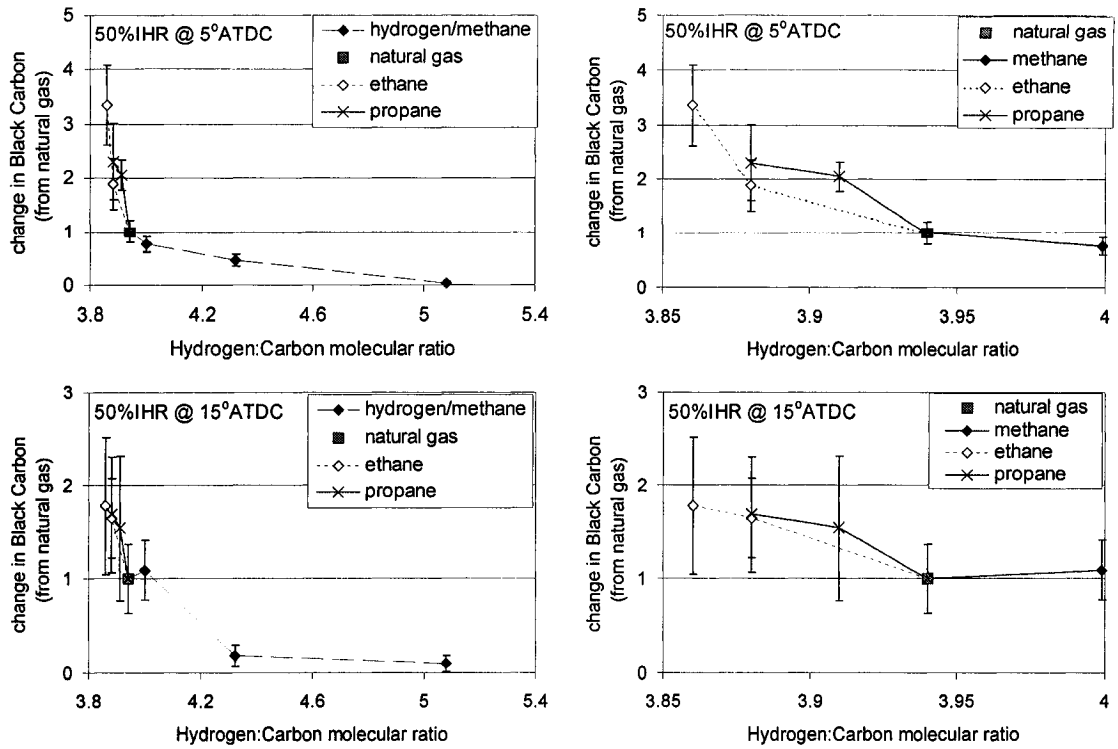

Figure 6.17: Effect of global hydrogen to carbon ratio on change in black carbon mass emissions (measured black carbon / black carbon with natural gas fuelling) at 5 and 15°CA ATDC combustion timing. The right-hand plots exclude the hydrogen results.

Chapter 7
Fuel Dilution with Nitrogen

7.1 Introduction

Variations in the composition of natural gas due to supplier, seasonal or geographical differences pose a significant challenge for engine developers. As discussed in Chapter 6, relatively low concentrations of heavy hydrocarbons can have a significant impact on the combustion process and emissions from a pilot-ignited, direct-injection of natural gas (PIDING) engine. Diluents in the fuel, such as N_2 and CO_2, may also have a significant impact on the combustion process, a result of both reduced energy density as well as direct effects on the pollutant formation kinetics. By studying the effects of varying the quantity of N_2 in the fuel, it should be possible to identify the sensitivity of the combustion system to fuel dilution. The principal influences of this dilution process are expected to be on the turbulent mixing of the gaseous jet, as well as on the turbulent kinetic energy of the post-injection combustion chamber gases.

7.2 Previous Work

The addition of diluents, in the form of EGR, to the oxidizer substantially reduces diesel and natural gas direct-injection engine NO_x emissions by lowering the combustion temperature [122,123]. In a non-premixed combustion event, the reaction rate and temperature depend on the concentration of the fuel, the oxidizer, and any inert species. Whether these inert species are originating from the fuel side or the oxidizer side is not an important factor. While the addition of exhaust gases to the fuel could raise certain safety and reliability issues, some diluents, in particular molecular nitrogen and carbon dioxide, are present in fossil natural gas at up to 4% by volume (see Appendix 5). Unconventional gases, including coal-based synthetic gas and landfill biogas, also contain substantial quantities of these species [224]. While their presence would pose numerous systems issues (larger quantity fuel storage devices, lower power density for the fuel, higher compression work requirements, etc.) they may also have a direct influence on the combustion process.

The effect of diluting a gaseous fuel with nitrogen has been investigated in various contexts. Crookes *et al.* [225] found that for a premixed charge engine, the results are

essentially identical to increasing the EGR fraction, which would be expected as the effect is essentially the same as displacing oxygen from the charge. By adding up to 14% N_2 in the fuel, Nellen and Boulouchos [60] found that while knock resistance is improved efficiency is impaired at constant fuel-air stoichiometry. These results are equivalent to those of tests with 'synthetic EGR' where nitrogen is added to the intake air [123]. The only case where nitrogen addition to the fuel in a premixed combustion system could significantly impact performance would be in cases with significant non-homogeneity in the fuel-air mixture.

The use of nitrogen as a diluent in fundamental non-premixed combustion studies is relatively common, primarily as a technique to reduce fuel concentrations. The effects of this nitrogen dilution have been quantified for a non-premixed opposed flow diffusion flame [226]. Typically, no significant effects are observed until the fuel stream contains >80% N_2 (by volume); above this level the temperature required for ignition to occur increases. These effects may be attributed to the increased heat capacity of the fuel, and are generally similar to the influences of increased energy dissipation through higher turbulent strain rates. N_2 concentrations below 80% have no significant effects. In a co-flow laminar flame, Gulder *et al.* report that the soot volume fraction in a flame is reduced proportionally with the reduction in methane concentration [227]. The authors attribute this directly to fuel dilution; no significant effect of the nitrogen on soot formation or oxidation kinetics is proposed. These results indicate that the principal influence of nitrogen addition manifests itself by reducing the energy density of the fuel. There is no evidence of direct effects on the reaction kinetics, even at very high N_2 concentrations. As a result, it is reasonable to expect that nitrogen addition to a turbulent non-premixed gaseous jet will not have a significant direct impact on the chemical kinetics.

One of the principal effects of nitrogen addition to the gaseous jet is reducing the energy density of the injected gas, resulting in a longer injection duration to provide the same amount of available chemical energy. Increasing the total mass injected also significantly increases the total kinetic energy transfer to the combustion chamber gases. However, the author was unable to identify any studies reported in the literature that attempt to evaluate the influence of nitrogen content in a turbulent non-premixed jet combustion system.

7.3 Experimental Information

The heavy-duty single cylinder research engine described in Chapter 3 was used to investigate the effects of nitrogen dilution on a gaseous-fuelled direct injection engine. For the work described here, the engine was operated using the more modern (17:1 compression ratio) piston. The diluted gaseous fuel was premixed and supplied through the standard fuel supply system. Gas blend preparation was carried out in large stationary storage vessels, with concentrations initially set using partial pressures. The fuel blend compositions tested were 20% and 40% by volume nitrogen with the remainder being commercial natural gas. The actual fuel compositions, as measured by gas chromatographic analysis of samples taken from just upstream of the engine, are shown in Table 7.1. These levels were selected to attempt to ensure that significant variations in combustion and emissions could be discerned. The 40% level was the upper limit to which the fuel tanks could be filled while still providing sufficient fuel to conduct the desired number of test conditions.

7.3.1 Operating Condition

This testing was carried out at a high-load, moderate speed operating condition, equivalent to the test point used in Chapter 6, and similar to the high-load point in Chapter 5 and the high-load mid-speed point in Chapter 4. The test condition is outlined in Table 7.2; the only variable was combustion timing, which was controlled (based on the midpoint of the heat release, 50%IHR, as discussed in Chapter 3) from 0° to 15° after top-dead-center (ATDC). All other parameters, including power (GIMEP), oxygen-based equivalence ratio (ϕ), speed, and intake oxygen mass fraction (Y_{intO2}) were fixed to minimize operating condition variability. As the power and injection pressure were held constant while the energy density of the fuel was reduced, the injection duration had to be increased to provide the same amount of chemical energy. As the timing was set to provide a constant mid-point of combustion, for the longer injection process with fuel dilution the start of injection had to be advanced, leading to an earlier start-of-combustion.

The addition of nitrogen to the fuel results in increases in the concentration of nitrogen in the exhaust and of the total mass of exhaust. This results in lower concentrations of the other species (including oxygen): for the high nitrogen concentration tests, this was reduced by ~3% (relative to pure natural gas). Therefore, to achieve the same Y_{intO2}, the EGR

mass flow-rate was slightly reduced (by ~2%), leading to reductions in the inducted mass of charge and EGR fraction (both <1% relative to the natural gas case). As these changes were substantially smaller than the variability in the experimental conditions, they did not have a significant impact on the operating condition set-point or on the measured results.

To improve the experimental accuracy, all the data points were replicated three times. Full randomization of the test plan was not possible, as only one gas blend could be prepared at a time. However, the sequence of the test points was fully randomized within each fuel composition. In view of the restrictions on randomization necessitated in the testing, the experimental design represents a blocked design, with the various fuel compositions representing the blocks and the other controlled variable being the combustion timing. As the only replications were within the blocks (rather than between blocks), it is not possible to identify any interaction term between the fuel composition variable and the combustion timing. Furthermore, as a result of this lack of randomization statistically valid tests between the different fuel blends are not possible, as the influence of fuel composition cannot be isolated from day-to-day random fluctuations in experimental conditions. Although these day-to-day fluctuations are small, they nonetheless restrict the statistical analyses.

7.4 Effects of Fuel Dilution

Previous studies relating to fuel dilution with nitrogen indicate that the principal influence is on physical mixing processes. In non-premixed gaseous jet combustion, these effects are expected to include increased in-cylinder turbulence (induced by the higher mass of gaseous mixture injected) as well as changes in the density gradient and mixing processes between the fuel jet and the charge. Changes in the fuel composition shift the stoichiometric combustion point towards a richer mixture (on a total mass of fuel including nitrogen / mass of charge basis). The lower rate of energy transfer into the combustion chamber also imposes greater restrictions on the combustion rate. These processes are expected to have a significant impact on the combustion process and pollutant emissions.

7.4.1 Combustion Effects

The addition of nitrogen to the fuel while holding the engine power constant results in a longer injection duration, lower energy-based injection rate, and a higher transfer of kinetic energy into the combustion chamber. To maintain the combustion timing (50%IHR)

constant, the injection timing must be advanced as nitrogen is added to the fuel (Figure 7.1). Contrary to oxidizer dilution, which tends to increase ignition delay [42,130], fuel dilution significantly reduces the gaseous ignition delay time (Figure 7.2). The pilot delay (also Figure 7.2) increases at the earliest combustion timings with 40% N_2; this is a result of the earlier injection, where the pilot enters a lower temperature and pressure environment. The fact that the 20% N_2 had a shorter gaseous fuel ignition delay than the 40% case is unexpected. These differences may be a result of competing influences between increased turbulent mixing of the early-injected fuel, higher shear rates between the fuel and the oxidizer, and lower energy content of the premixed fuel cloud. As well, the greater penetration of the gas jet (due to its higher density) may result in the ignitable mixture being in the vicinity of the pilot flame sooner, resulting in faster ignition. These results indicate that, at this condition, the injection process, and the subsequent mixing of the gaseous fuel, is exerting a substantial influence on the ignition of the gaseous fuel. This agrees with the observations from Chapters 5 and 6 that mixing is a key constraint on the ignition process.

The shorter ignition delay and reduced energy content of the diluted natural gas result in less chemical energy being contained in the premixed fuel cloud prior to ignition, resulting in a correspondingly lower peak heat-release rate (Figure 7.3). The energy release rate was also reduced, due to the lower (energy-basis) injection rate. Despite this, the overall combustion duration, as represented by the 10-90% IHR (also shown in Figure 7.3) is not increased by nitrogen addition, and at some conditions is actually slightly reduced. This is especially noticeable in the later combustion timing cases. This result may be attributed directly to the increased turbulent kinetic energy imparted from the gaseous jet, resulting in improved late-combustion phase mixing and more rapid completion of the combustion event in the post-injection period.

Further evidence of this more complete late-stage burnup is provided from the in-cylinder pressure and heat-release traces for early and late combustion timings (Figure 7.4). These plots clearly show the reduced peak heat-release rate, lower premixed-phase combustion, and longer mixing-controlled combustion with the 40% N_2 dilution. Pressure traces and heat-release rates for the other timings are provided in Appendix 6.

Diluting the fuel with nitrogen also improves the combustion stability, as shown in Figure 7.5. At the high nitrogen dilution level retarding the combustion enhances the

combustion stability; this is contrary to most previous results where retarding the combustion tended to degrade stability. This improvement in stability is observed for both the overall combustion stability (COV of the GIMEP) and the variations in the early combustion event (COV of the peak cylinder pressure). Improved late-cycle mixing due to the higher turbulence levels in the cylinder may explain these observed improvements in combustion stability. The higher turbulence results in more complete oxidation of the combustion by-products and more complete utilization of the hydrocarbon fuels. The improved combustion stability may also contribute to the reduced fuel consumption with nitrogen dilution, also shown in Figure 7.5. These results demonstrate the substantial combustion benefits of reducing the amount of premixed fuel prior to ignition and of increasing the late-cycle in-cylinder turbulence.

7.4.2 Gaseous Emissions

Dilution of the fuel with nitrogen significantly influences the emissions as well as the combustion event. As indicated in Figure 7.6, the emissions of all the measured gaseous emissions species (HC, CO, and NO_x) are significantly reduced. The hydrocarbons, which are more than 95% CH_4, are consistently reduced by approximately 0.35 g/GikWhr (~300 μg/cycle) at all timings for the high N_2 case. The reduction for the low nitrogen case is approximately half that of the high nitrogen case (~0.16 g/GikWhr). These emissions of unburned fuel are only approximately 0.2% of the total mass of CH_4 injected per cycle (~130 mg/cycle). However, the fact that the magnitude of the reduction is constant at all timings, and that the reduction is approximately 40% at the lowest emissions level (earliest timing), suggests that there is a constant volume of fuel that is not being consumed. Since the magnitude of the reduction is constant, it appears that there is more than one source of unburned fuel emissions; at the earlier timings, a volume-based effect is the principal source. One potential contributor to these emissions would be the injector, where gas in the nozzle holes and sac volume gradually vents into the combustion chamber as the cylinder pressure falls after the end of the injection process. Fuel that enters the combustion chamber in this manner is unlikely either to mix to a combustible mixture or to ignite, thereby providing a minimum volume of unburned fuel which will be emitted with the exhaust. At the later timings, the fact that the baseline emissions are substantially higher suggests that other mechanisms, such as increased bulk quenching or local turbulent strain extinction, may also

be contributing to unburned fuel emissions. Given that these mechanisms do not appear to be reduced by the addition of nitrogen to the fuel, it would appear that contributory mechanisms such as combustion variability (which was reduced) or late-cycle combustion rate (which was increased) are not the principal sources.

The lower intensity, longer duration combustion as well as the lower adiabatic flame temperature have significant impacts on the NO_x emissions (Figure 7.6). The NO_x emissions are no different between the natural gas and the low dilution level; a significant reduction is noticeable, however, between the low and high dilution cases. The change in adiabatic flame temperature (Table 7.1) is only 30K for the low nitrogen dilution case. Due to the thermal mechanism's high temperature dependence, this would be expected to reduce NO_x emissions by approximately 15% based on the flame temperature correlations developed in previous work [39,122]. For the high dilution case, the reduction in NO_x is expected to be on the order of 40%; only at the earliest timing is the observed reduction this significant. At later timings, reductions in NO_x emissions are only ~20%.

The fact that the reductions in NO_x emissions are not as significant as the changes in the adiabatic flame temperature would predict suggests that the nitrogen in the fuel may be influencing the principal NO formation mechanisms (section 2.2.2) through other effects. For the dominant thermal mechanism, the formation of N radicals is the limiting step in the reaction; hence, a higher N_2 concentration, especially on the fuel-rich side of the combustion zone, could increase NO formation. However, as the thermal mechanism typically occurs in the post-combustion gases, where N_2 from the oxidizer is abundant, the addition of N_2 to the fuel increases the N_2 concentration by less than 10%. As well, the residence time of the burned gases at high temperature is reduced by the more rapid turbulent mixing in the combustion chamber resulting from the higher jet kinetic energy. It is also possible that the contributions of other NO_x formation mechanisms are affected by nitrogen addition; for example, the prompt mechanism may be becoming more significant as the combustion temperature is reduced.

As for the other gaseous emissions, the CO emissions are substantially reduced with nitrogen addition (Figure 7.6). The fact that the CO emissions are independent of combustion timing with diluted fuel (as opposed to the increase at intermediate timings for the undiluted natural gas) suggests that the CO increase at mid-timings may not be due to jet interaction

with the piston. The higher density and longer injection duration of the diluted gaseous jet substantially increases the jet penetration distance, which would be expected to exacerbate any piston-jet interaction effects. It is likely the higher turbulent kinetic energy significantly increases the late-combustion burn-up of the CO, resulting in a significant reduction in emissions of CO as well as other combustion by-products.

7.4.3 Particulate Emissions

The enhanced oxidation of the combustion by-products by increased turbulence late in the combustion stroke may also have a substantial influence on the PM mass emissions (Figure 7.6). PM emissions are substantially reduced at the intermediate timings with fuel dilution. The higher turbulence intensity imparted by the higher density fuel may result in significant increases in the late-stage combustion event and burn-up, resulting in a substantial reduction in PM emissions at most timings. That the tail-end combustion is more complete is suggested in Figure 7.4; furthermore, Figure 7.7 shows that the heat released in the late combustion stages (post injection) is substantially higher for the nitrogen cases than for the pure natural gas. Interestingly, at the earliest timing PM emissions are increased with nitrogen dilution; the reasons for this effect are unclear. This suggests that the nitrogen addition is also influencing other PM formation and oxidation mechanisms. These mechanisms may include complicated chemical and physical effects relating to the increased concentration of nitrogen in the fuel. For example, the presence of a relatively inert species (N_2) in the fuel could enhance any third body reactions; changes in the local gradients in the reaction zone would strongly affect both energy and species distribution in the flame zone; or even direct participation of dissociated nitrogen molecules in the reactions may be important. Fundamental studies conducted under conditions directly equivalent to those in a direct-injection engine are required to further elucidate these effects. In general, however, these results indicate the PM mass emissions are formed from multiple complicated mechanisms which respond differently to changes in fuel composition.

The total mass emissions (Figure 7.6) indicate that the PM mass at the latest timing condition is essentially the same for all three fuel compositions. However, this value is similar to the minimum quantifiable PM mass identified in earlier work (Chapter 5). The ultrafine number distributions and integrated mobility volume, shown in Figures 7.8 and 7.9, suggest that both the number and the mobility volume of the particles have been reduced by

as much as 80% at the latest timing through fuel dilution. At the earlier timings, the integrated number distributions showed trends equivalent to those of the measured masses. This difference between the PM mass measurements and the mobility volume at the lowest mass concentrations is most likely due to volatile condensation, as discussed in Chapters 5 & 6. The size distributions also indicate that a nucleation-mode peak occurs at the later timings with both low and high N_2 levels. These nucleation mode peaks are typically attributed to volatile nucleation processes in the absence of sufficient solid PM surface area for condensation to occur (as discussed in section 5.3.2). Interestingly, at the latest timing, with high nitrogen dilution, the nucleation mode peak is not apparent. The lack of solid particles in the post-combustion gases may result in less volatile nucleation, resulting in higher vapour-phase concentrations. These concentrations may be sufficient to induce substantially earlier self-nucleation of the volatile species (for example upstream of the surge tank). With such earlier nucleation, more particle growth by accumulation and condensation may occur. As the total quantity of volatiles should not have been substantially affected by the nitrogen dilution of the fuel, the earlier nucleation and subsequent growth may result in the lower number of larger particles observed in the size distributions at the latest combustion timing.

The mass of black carbon in the exhaust stream is substantially reduced with nitrogen dilution, especially at the latest combustion timings, as shown in Figure 7.10. At the high nitrogen dilution case, the amount of black carbon in the sample is not detectable. This suggests that the observed ultrafine PM (Figure 7.8) is primarily nucleated volatile species. Hence, either the formation of carbonaceous PM is reduced, or oxidation is enhanced. It is likely that both effects are relevant; higher turbulence results in enhanced post-combustion mixing, possibly enhancing oxidation. Simultaneously, the lower temperatures and reduced carbon-to-oxygen ratio in the gas jet upstream of the combustion zone may result in reduced carbonaceous particulate formation.

7.5 Discussion

Diluting the fuel with an inert species, nitrogen, is the only technique investigated in this thesis which simultaneously reduces all measured emissions while retaining the PIDING engine's efficiency and performance. Although the use of high quantities of nitrogen diluent may pose technical and economic challenges, particularly for vehicular applications, these results do provide an indication that nitrogen dilution could be used to offset increases in

emissions resulting from higher concentrations of heavier hydrocarbons in different geographic locations.

7.5.1 Fuel Systems Issues

One of the main drawbacks of diluting the gaseous fuel with nitrogen is the need to compress an increased quantity of fuel. Assuming adiabatic compression with constant specific heats and ideal gas behaviour, the work required to compress an equal quantity of fuel on an energy basis can be roughly estimated. The results of this calculation, shown in Figure 7.11, indicate that more than twice the pumping work is required to compress the fuel with 40% nitrogen. The work required to compress 20% nitrogen is only 30% greater than the work for pure methane. This work is, however, still a relatively small fraction of the total energy content of the fuel. For comparison purposes, the work (per unit energy stored) required to compress 15% and 35% (by volume) blends of hydrogen are also shown; substantially less compression work is required for the hydrogen additive than for an equivalent amount (by volume) of nitrogen.

Another significant drawback to nitrogen (or hydrogen) blending in the fuel is the reduction in volumetric energy density. The effect of 40% nitrogen and 35% hydrogen blending on the gas volume required to store an equivalent amount of chemical energy (again assuming ideal gas behaviour) is also shown in Figure 7.11. At a pressure of 35 MPa (roughly 5000 psi), the volume required for the hydrogen is 50% greater than for pure methane and the volume required for nitrogen is almost twice the methane volume. Whether the improvements in engine performance and emissions warrant such substantial increases in parasitic load and fuel storage volume depends on the application. Cryogenic storage might be an option, since it provides improved energy density and reduced parasitic compressor work for conventional natural gas. Potential variations in fuel composition during extraction could pose a challenge for maintaining the desired fuel blend. Separate cryogenic storage of the additive might be required; this would impose a substantial increase in system complexity and cost. More research is required to further understand the cryogenic storage of blends of natural gas with high concentrations of nitrogen.

7.5.2 Fuel Composition Parameters

A number of different parameters have been previously suggested to provide a general overview of the effects of natural gas composition on engine performance. The most

widely used of these include the Wobbe Index (discussed in section 6.2) [221], the molar hydrogen-to-carbon (H:C) ratio and the higher heating value (HHV). The calculated values for these parameters for all the fuel compositions tested in this thesis are shown in Table 7.3. In particular, previous work suggests that for a constant Wobbe Index, combustion performance and emissions are not significantly affected by fuel composition [213]. The Wobbe Index, which has the same units as the mass-specific heating value (typically MJ/kg) is defined as:

$$WI = \frac{HHV}{\sqrt{specific\ gravity}}, \tag{7.1}$$

where the specific gravity is the density of the fuel blend relative to air at standard temperature and pressure. A comparison of the combustion duration and the peak heat-release rate as functions of the Wobbe Index are shown in Figure 7.12. The comparison includes the nitrogen blends tested in the current chapter, as well as the hydrogen blend results (Chapter 5) and the ethane and propane addition tests (Chapter 6). As the results indicate, the Wobbe Index does not provide a reasonable representation of the combustion parameters for the compositions tested. This is most likely due to the fact that it was established for premixed-charge combustion, where the specific gravity of the fuel has a more significant effect than in a non-premixed combustion event.

An investigation of the effect of fuel composition on the peak heat-release rate for PIDING combustion is informative, as this parameter is representative of the amount of energy released during the initial premixed combustion phase. Figure 7.13 demonstrates that the fuel composition has a significant influence on the peak heat-release rate (relative to the peak heat-release at the same timing condition using natural gas). Only the pure methane case indicates a higher peak heat-release rate than the natural gas, while the most significant reductions are observed for the high nitrogen dilution cases. All four of the fuel blends that include heavier hydrocarbons have virtually identical results. The sensitivity of peak HRR to fuel composition comes from two sources: the ignition delay time and the energy density of the fuel. Either shorter ignition delays or lower energy-density fuels result in less chemical energy being available to be released in the initial partially-premixed combustion event. The influence of gas ignition delay (GID) on the peak HRR for all the fuel blends is shown in Figure 7.14. The outlier points are for the high nitrogen case, where the chemical energy

available for the premixed combustion is reduced by dilution of the fuel. The effects of the shorter gas ignition delay time also contribute to the observed reduction in peak HRR at this condition. The fact that with a shorter GID, less fuel is available to burn after ignition occurs results in less of the fuel having mixed beyond a combustible stoichiometry, thereby reducing HC emissions. The significance of this influence on HC emissions is shown in Figure 7.14, although it is evident from the variability in the results that factors other than the GID are also contributing to HC emissions. Nor do these parameters provide any further insight into the changes in emissions of other species.

Another attribute which has a direct impact on emissions is the combustion variability, represented by the COV of the GIMEP. Figure 7.15 demonstrates that processes which reduce the combustion variability will also reduce emissions of both CO and HC. As with the GID, the variability in the data indicates that other mechanisms are also important.

From the results observed in the current chapter, as well as those from Chapters 5 and 6, fuel composition clearly has a significant impact on emissions of all combustion by-products. This result differs significantly from premixed charge combustion findings, which generally suggest that fuel composition has relatively small influences on emissions [217,228]. In the current work, the least substantial effects are, in general, found for the NO_x emissions. This may be attributed to relatively small changes in combustion temperature for most of the fuel blends. The only two fuel blends that show significant differences in NO_x emissions (high hydrogen and high nitrogen) are the two where the changes in flame temperature are most significant. The higher flame temperatures with hydrogen fuelling increase NO_x emissions (section 5.3.1) while the lower temperatures associated with nitrogen dilution reduce NO_x (section 7.4.2). Variations in other aspects of the NO formation mechanisms are also important; however, the results indicate that the principal effect is the combustion temperature, as suggested in previous work [39].

The effects of fuel composition on emissions of CO, HC, and PM are much more significant. It is expected that many physical and chemical effects are contributing to these variations. However, some of the principal influences may be encompassed in the volumetric energy content of the fuel (as represented by the HHV on a molar basis) and the carbon content of the fuel (represented by the H:C ratio). To provide further insight into the roles of

these parameters on the pollutant formation mechanisms, a new index (ξ) may be defined as:

$$\xi = \frac{HHV}{H:C}, \tag{7.2}$$

with units of MJ/kmol. The effects of this index on CO and HC emissions (relative to the baseline natural gas fuelling condition) over the full range of fuel compositions and timings tested are shown in Figure 7.16. A general increase in CO and HC emissions with increasing ξ (i.e. higher energy content and/or lower H:C ratio) is observed. The CO emissions are sensitive to combustion timing, indicating that other parameters are also having a significant impact. A potential cause for this is that variations in the in-cylinder pressure and temperature substantially influence CO emissions; a similar influence is apparent in the injection pressure studies discussed in Chapter 4. Hydrocarbon emissions (which in all cases were >95% CH_4) are less sensitive to the combustion timing. This also agrees with the results from the injection pressure study (Chapter 4), which indicate that HC emissions levels are less sensitive to variations in cylinder pressure and temperature than are CO emissions. In general, the HC emissions show substantial correlation with ξ for the hydrogen and nitrogen addition cases; however, for the heavier hydrocarbon cases, the effects are less clear.

The greatest influence of H:C ratio and the heating value (as represented by the parameter ξ) is observed on the particulate matter emissions, shown in Figure 7.17. In general, PM emissions are substantially greater for higher values of ξ. The total mass of PM, as measured by the TEOM, follows this general trend; however, the substantial contribution of volatile species to the PM emissions at the high nitrogen- and hydrogen-addition conditions results in significant PM mass variability at these fuelling conditions. This is not surprising, as the ξ term relates most directly to carbonaceous particulate formation, as represented by the black carbon measurements. The mobility volume values, calculated on the basis of the integration of the SMPS results (see section 3.2.2) reveal a similarly strong dependence on the ξ ratio. This provides further evidence that the black carbon and the ultrafine particles are closely related to each other and are primarily attributable to solid carbon (soot), possibly covered with condensed volatiles.

In general, the ξ ratio provides a useful indication of the changes in PM emissions, and especially of carbonaceous soot particles, which may be expected to occur with

variations in fuel composition. Due to the much wider variation of ξ with the hydrogen and nitrogen dilution studies, the relationship between the ξ term and PM emissions for the heavier hydrocarbon cases are less clear from Figure 7.17. To provide further insight, the same plots are reproduced in Figure 7.18 for only the heavier hydrocarbon and pure methane composition tests presented in Chapters 5 and 6. The results indicate that the combustion timing has a more significant effect on the PM emissions as a function of ξ for the heavier hydrocarbons than for the nitrogen and hydrogen test results. However, it is apparent that, yet again, ξ provides an indication of the relative potential increase in black carbon emissions with the addition of the heavier hydrocarbons, which simultaneously increase the HHV of the fuel and reduce the H:C ratio. This provides further confirmation that the H:C ratio and the HHV are two of the most important parameters relating to changes in PM emissions due to differences in fuel composition. By ensuring that the ξ parameter for a given fuel is relatively consistent, it should be possible to minimize the effects of fuel composition variations on emissions from a direct-injection of natural gas engine. A further complicating factor to the calculation of the ξ value pertains to the addition of carbon containing species such as CO or CO_2 to the fuel; for these species, it is likely that the carbon will need to be excluded from the H:C ratio. However, further research is required to validate this supposition.

7.6 Conclusions

1. The late-cycle combustion process is substantially enhanced by nitrogen addition. This may be attributed to higher in-cylinder turbulence, due to the larger mass of fuel injected and corresponding increase in gaseous jet kinetic energy. This more rapid, more complete combustion results in lower emissions of unburned fuel as well as contributing to reductions in the combustion variability.
2. Particulate matter total mass, black-carbon content, and ultrafine particle emissions are substantially reduced by nitrogen dilution. For the high-nitrogen dilution condition, black carbon emissions are not detectable at the later combustion timings. The measured mass of PM under high fuel dilution conditions may be attributed to volatiles condensing in the sample system.
3. Dilution of the fuel results in significant reductions in emissions of CO and HC (>95% CH_4). Reductions in HC are consistent at all operating conditions and are directly

proportional to the reductions in the concentration of methane in the fuel. The reduction in CO emissions is primarily attributed to the more rapid late-cycle combustion process; this factor may also contribute to the reduced HC emissions.

4. NO_x emissions are not affected with intermediate levels of nitrogen addition to the fuel but are significantly reduced at higher (40%) concentrations. This can be attributed to the substantial reduction in combustion temperature due to the high concentrations of diluent in the reaction zone.
5. The fuel conversion efficiency is slightly improved through the addition of nitrogen to the fuel. This may be a result of reduced unburned fuel and combustion by-product emissions.
6. Diluting the fuel with nitrogen reduces the peak heat-release rate, ignition delay, and cycle-to-cycle variability of the gaseous combustion event. Despite the lower heat-release rate and longer injection duration, the overall combustion duration is slightly reduced.
7. The parameter ξ provides a useful measure of the relative changes in emissions which may be expected from significant changes in fuel composition. However, it is somewhat sensitive to combustion timing; as a result, any specific parameters derived from this value will be applicable only for a given operating condition.

7.7 Tables and Figures

Table 7.1: Gaseous fuel compositions as measured by gas chromatograph analysis

Species	Natural Gas	Low Nitrogen	High Nitrogen
n-Butane	0.05	0.04	0.03
i-Butane	0.07	0.05	0.05
i-Pentane	0.02	0.02	0.01
n-Pentane	0.02	0.01	0.01
Hexane	0.01	0.00	0.00
Heptane	0.00	0.00	0.00
Octane	0.00	0.00	0.00
N_2	1.47	18.89	38.88
Methane	96.6	78.2	59.4
CO_2	0.44	0.28	0.24
C_2H_6	1.41	2.31	1.17
C_3H_8	0.32	0.25	0.22
MW (kg/kmol)	16.70	18.83	21.04
LHV (kJ/kg)	48080	35489	23792
HHV (kJ/kg)	53313	39338	26378
$T_{adiabatic}$ (K)	2485	2440	2400
H/C ratio	3.94	3.93	3.94

Table 7.2: Engine operating constants and variables

Parameter	Value
Speed (RPM)	1200
GIMEP (bars)	13.5
ϕ_{O2}	0.6
Y_{intO2}	0.19
Fuel Pressure (MPa)	21
50%IHR (°ATDC)	0, 5, 10, 15
Pilot (mg/inj)	5

Table 7.3: Representative parameters for all fuel composition results

Fuel	Higher Heating Value (HHV) *MJ/kmol*	Density (@STP) *kg/m^3*	H:C Ratio	Wobbe Index *MJ/kg*	ξ (HHV/H:C) *MJ/kmol*
Natural Gas	888.6	0.697	3.96	70.1	226.4
Pure Methane	888.0	0.677	4.00	74.6	222.0
Low Ethane	926.7	0.726	3.86	68.9	241.7
High Ethane	938.7	0.737	3.83	68.1	246.9
Low Propane	910.1	0.723	3.88	68.0	236.2
High Propane	922.8	0.745	3.83	66.0	242.7
Low Nitrogen	726.6	0.784	3.96	48.7	189.5
High Nitrogen	547.5	0.883	3.96	31.2	141.4
Low Hydrogen	803.7	0.598	4.32	79.6	187.8
High Hydrogen	676.0	0.469	5.08	96.4	133.0

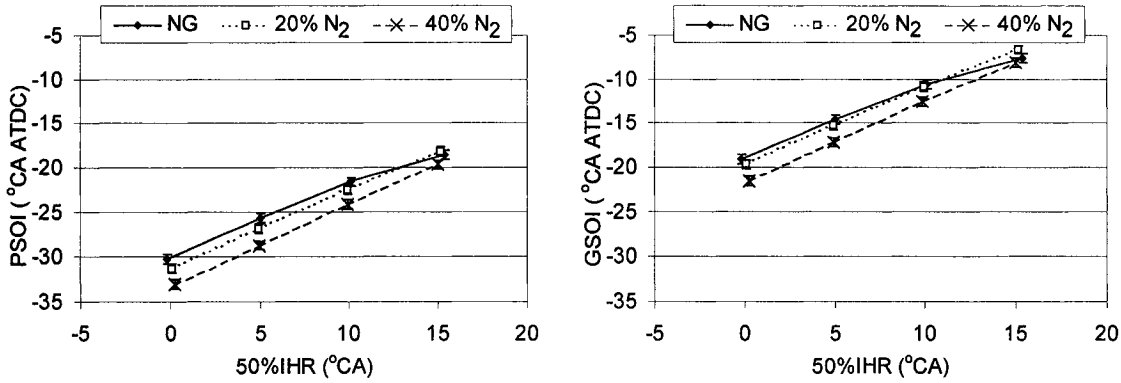

Figure 7.1: Commanded Injection Timings (pilot start-of-injection timing on left, gas start-of-injection on right).

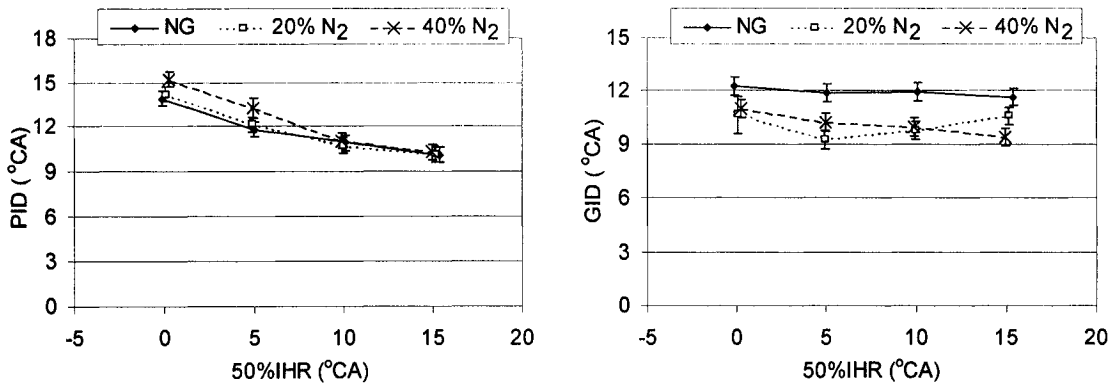

Figure 7.2: Ignition delay times (relative to commanded start-of-injection) for pilot (left) and gaseous fuel (right) with natural gas and nitrogen diluted fuels.

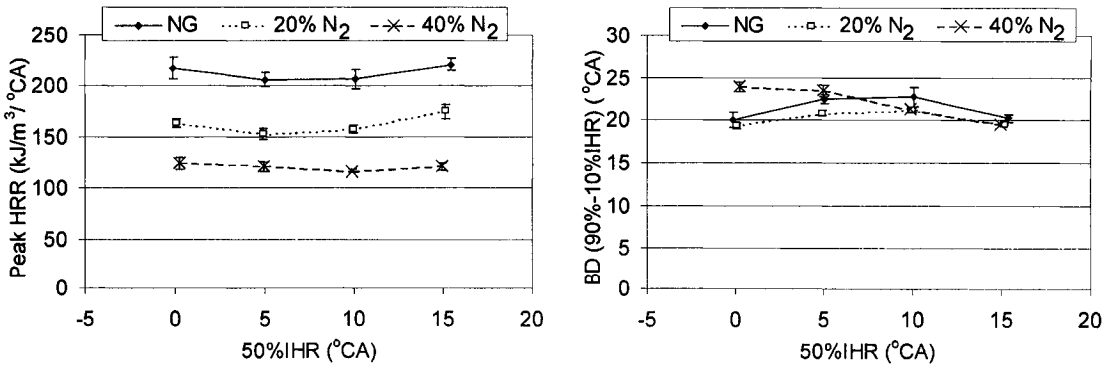

Figure 7.3: Peak heat-release rate and combustion duration (10-90% IHR) for natural gas and nitrogen diluted cases.

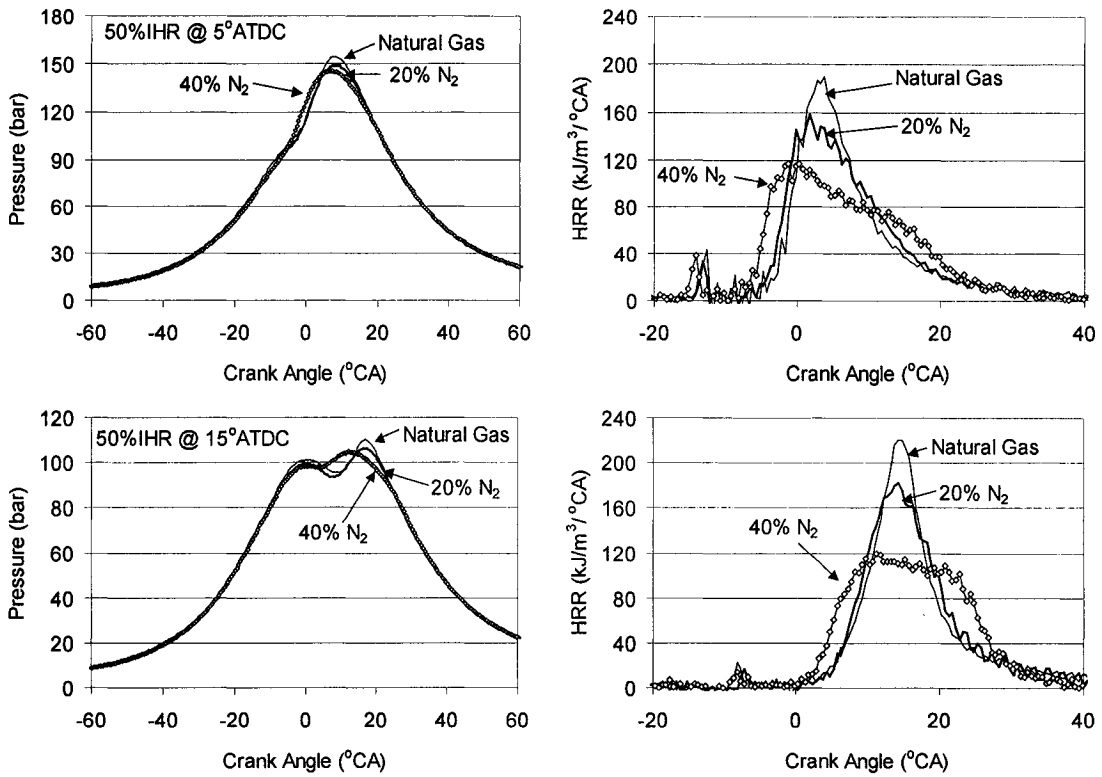

Figure 7.4: In-cylinder pressure and net heat-release rate for early (50%IHR at 5°ATDC, top) and late (50%IHR at 15°ATDC, bottom) combustion timings.

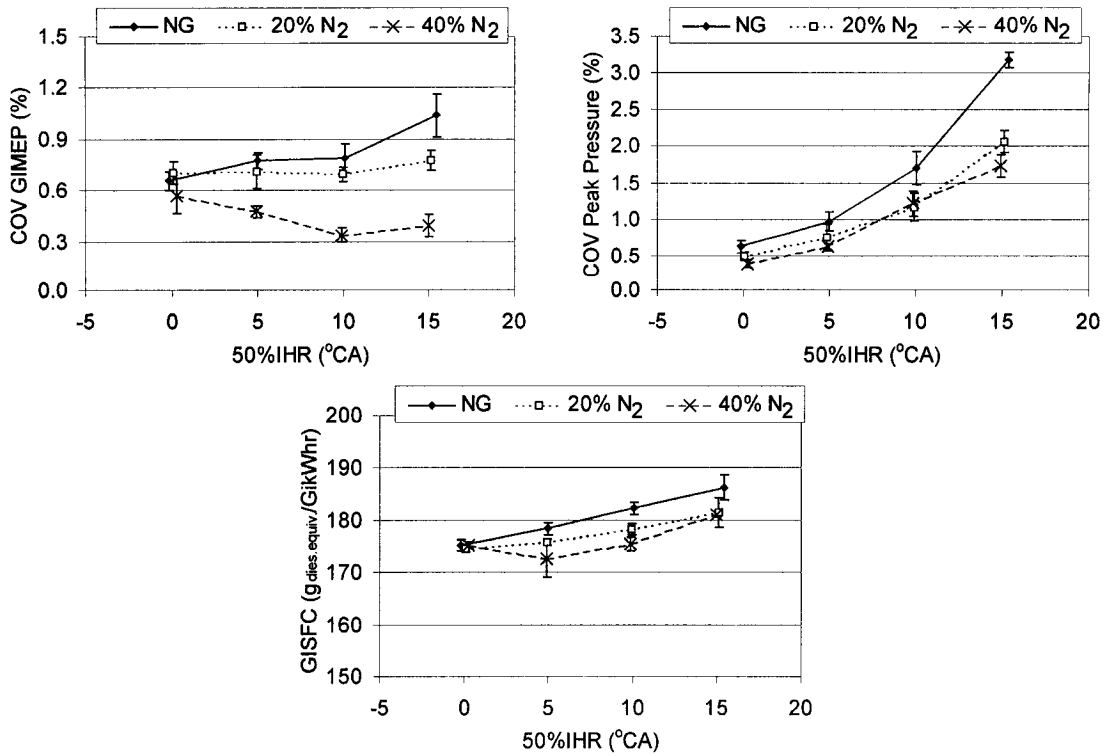

Figure 7.5: COV of GIMEP and peak cylinder pressure, as well as GISFC for natural gas and the nitrogen diluted cases.

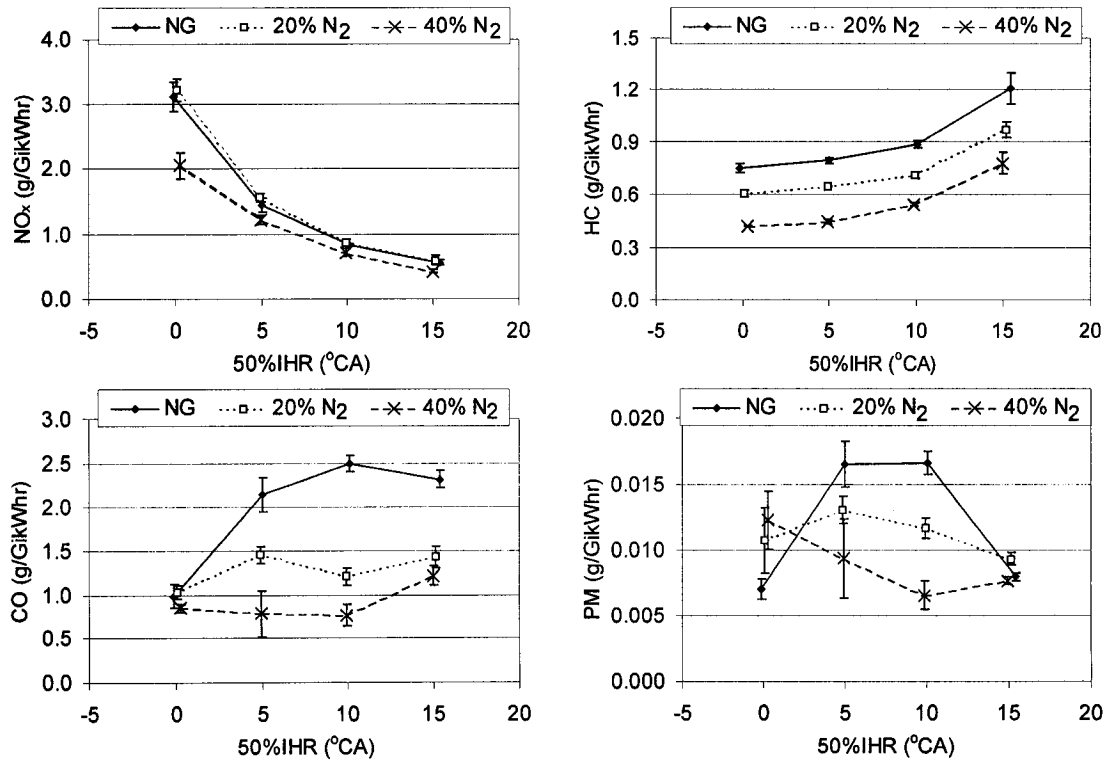

Figure 7.6: Emissions (CO, NO_x, HC, PM) for natural gas and nitrogen diluted cases.

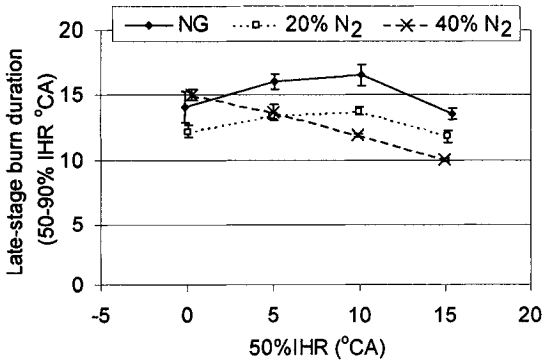

Figure 7.7: Percentage of total heat released after the end of injection, for natural gas and nitrogen diluted fuelling.

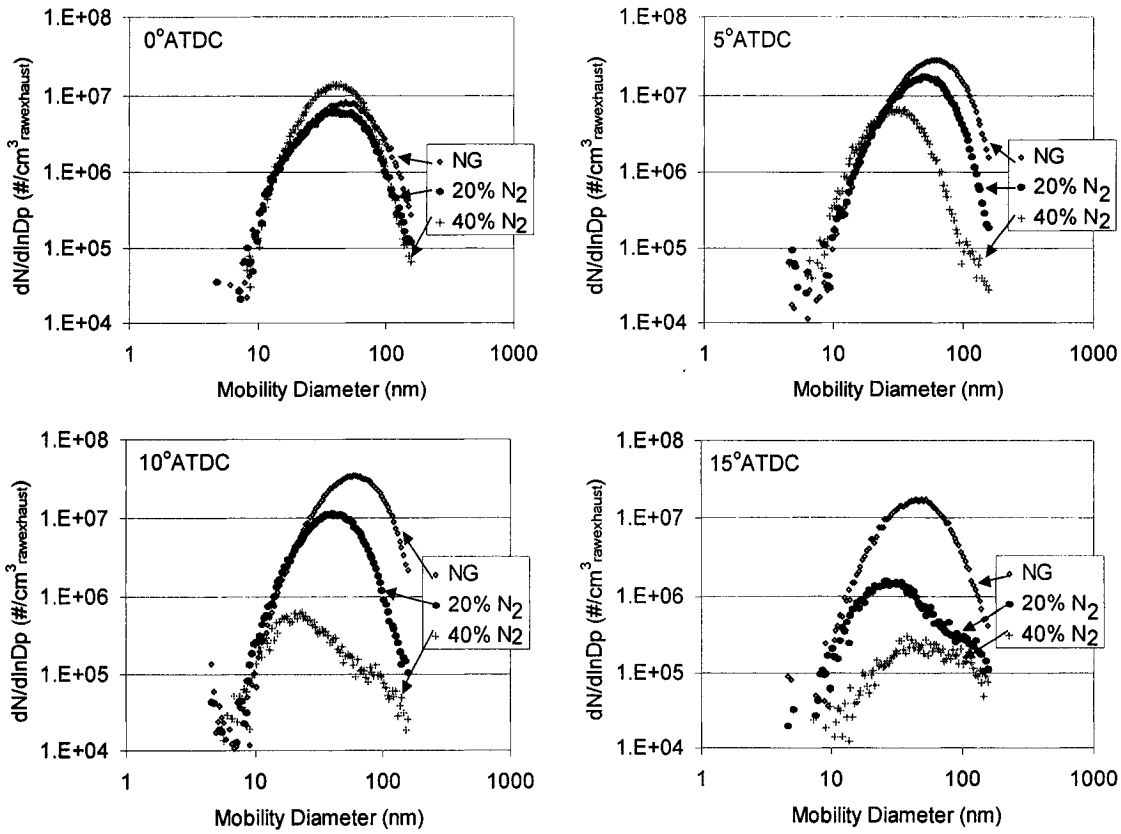

Figure 7.8: Particle number size distributions as measured by the SMPS for pure natural gas and nitrogen diluted fuelling.

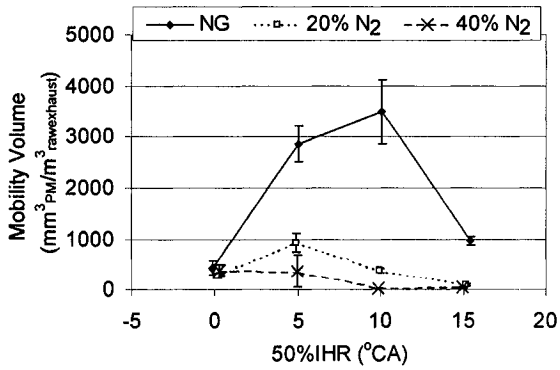

Figure 7.9: Particle mobility volume (integrated size distribution) as a function of combustion timing, for pure natural gas and nitrogen diluted fuelling.

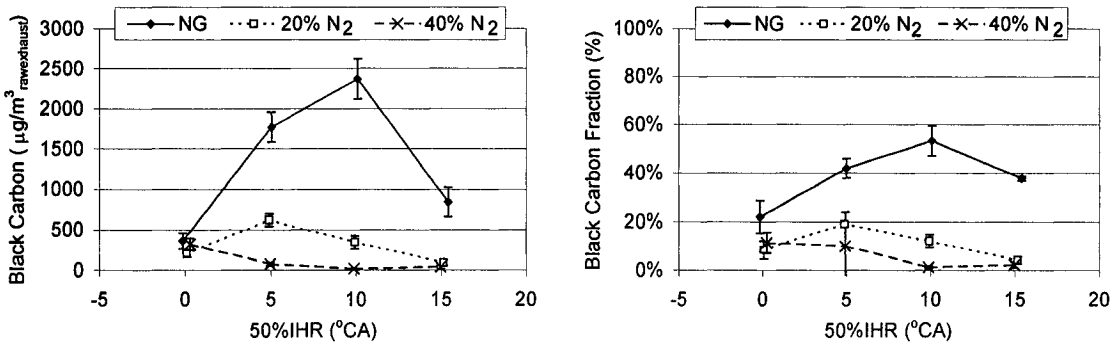

Figure 7.10: Black carbon mass measured by the Aethalometer (left) and black-carbon fraction (BC mass / total PM mass, right) as a function of combustion timing, for pure natural gas and nitrogen diluted fuelling.

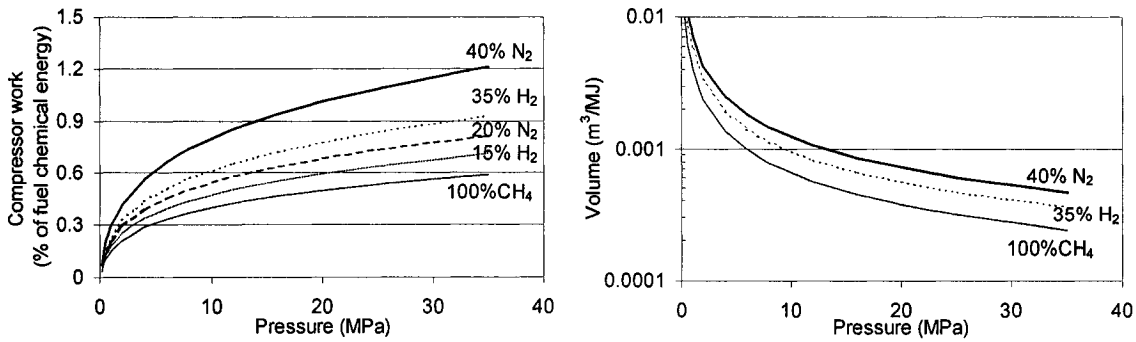

Figure 7.11: Estimated compression work (as a % of the chemical energy in the fuel) and the storage volume for various fuel blends. Calculated assuming an adiabatic ideal gas compression process with constant specific heat ratio.

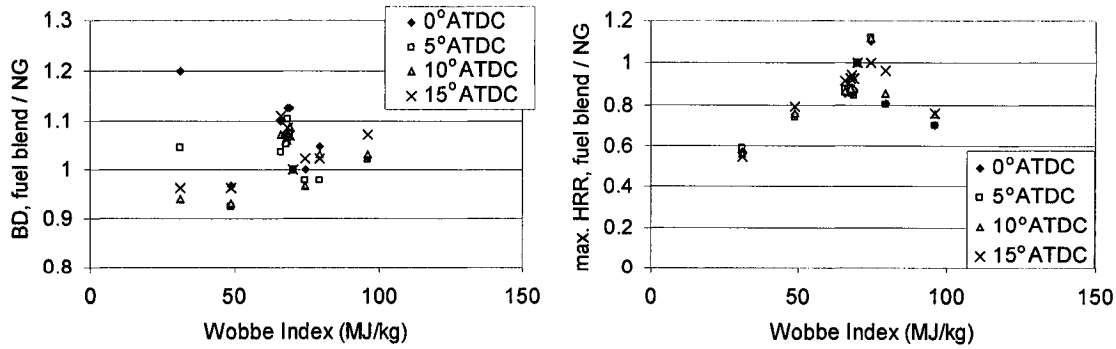

Figure 7.12: Combustion duration (10-90% IHR, left) and peak heat-release rate (right), for all gas blends (hydrogen, hydrocarbon, and nitrogen addition) relative to natural gas as functions of Wobbe Index.

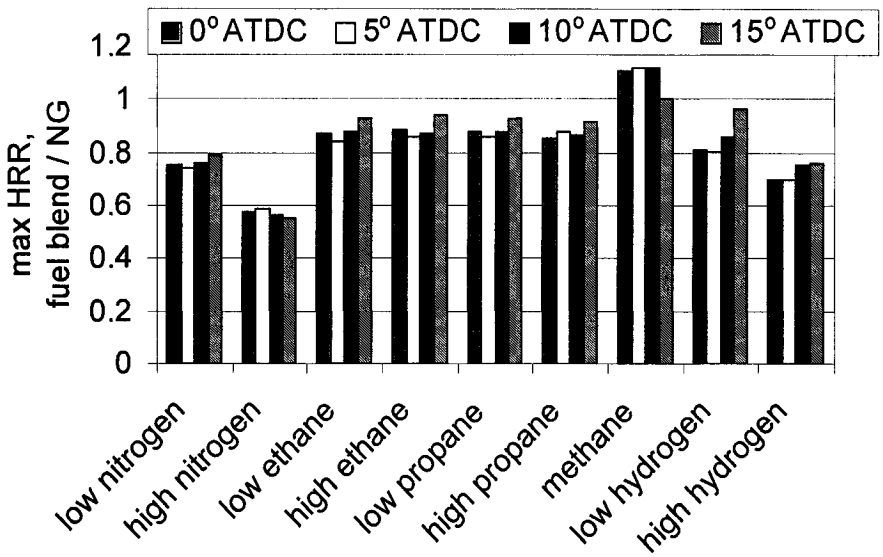

Figure 7.13: Peak heat-release rate relative to natural gas for all timings and all fuel blends.

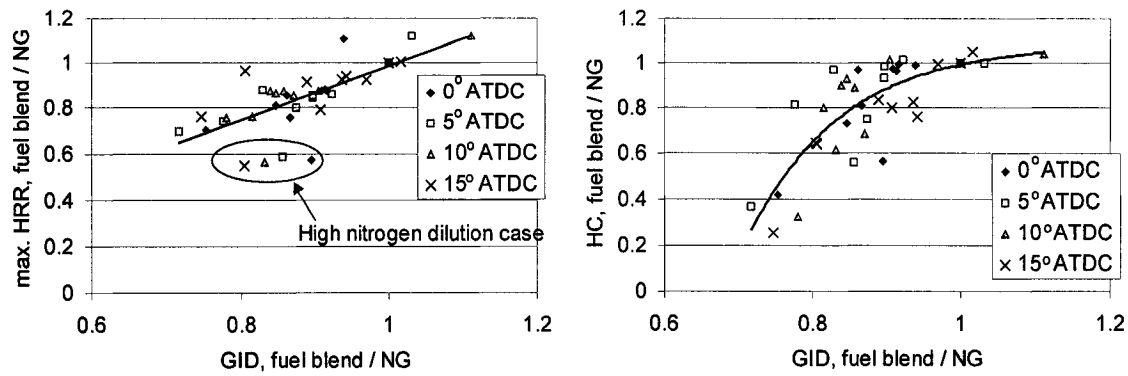

Figure 7.14: Influence of changes in gas ignition delay time (GID) on peak heat-release rate and hydrocarbon emissions from various fuel blends. Lines represent best fit through the data.

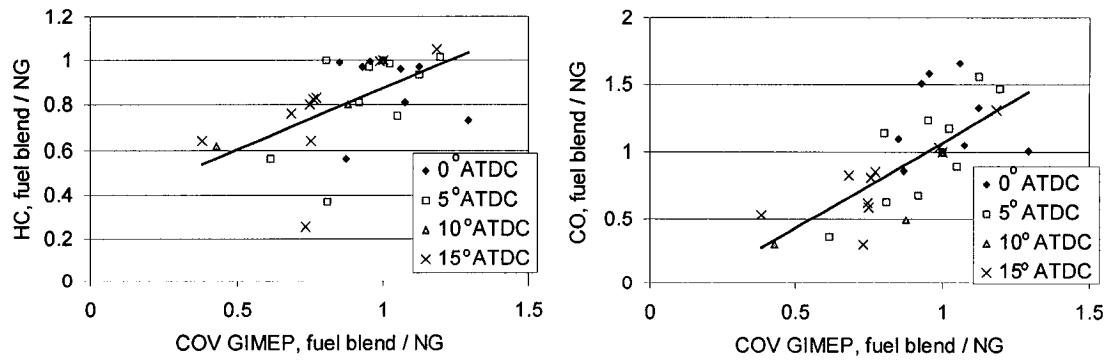

Figure 7.15: Influence of combustion variability (COV GIMEP) on HC and CO emissions for various fuel blends. Lines represent best fit through the data.

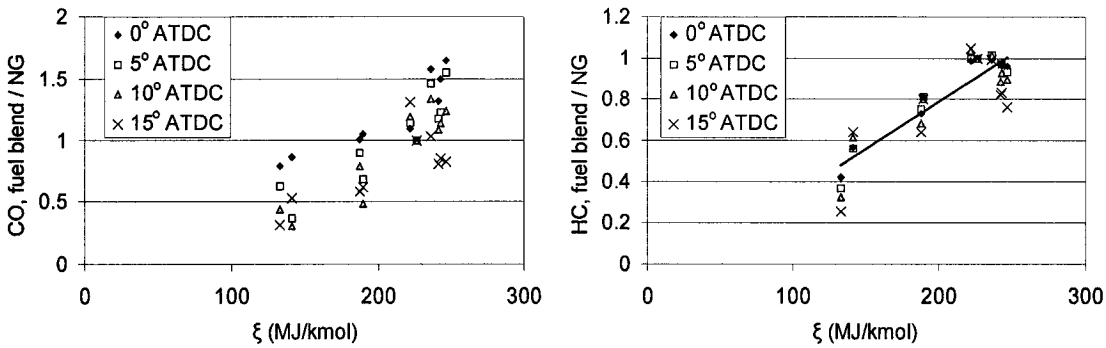

Figure 7.16: Comparison of HC and CO emissions for all fuel blends relative to natural gas as a function of ξ (HHV / H:C). Line represents best fit through the data.

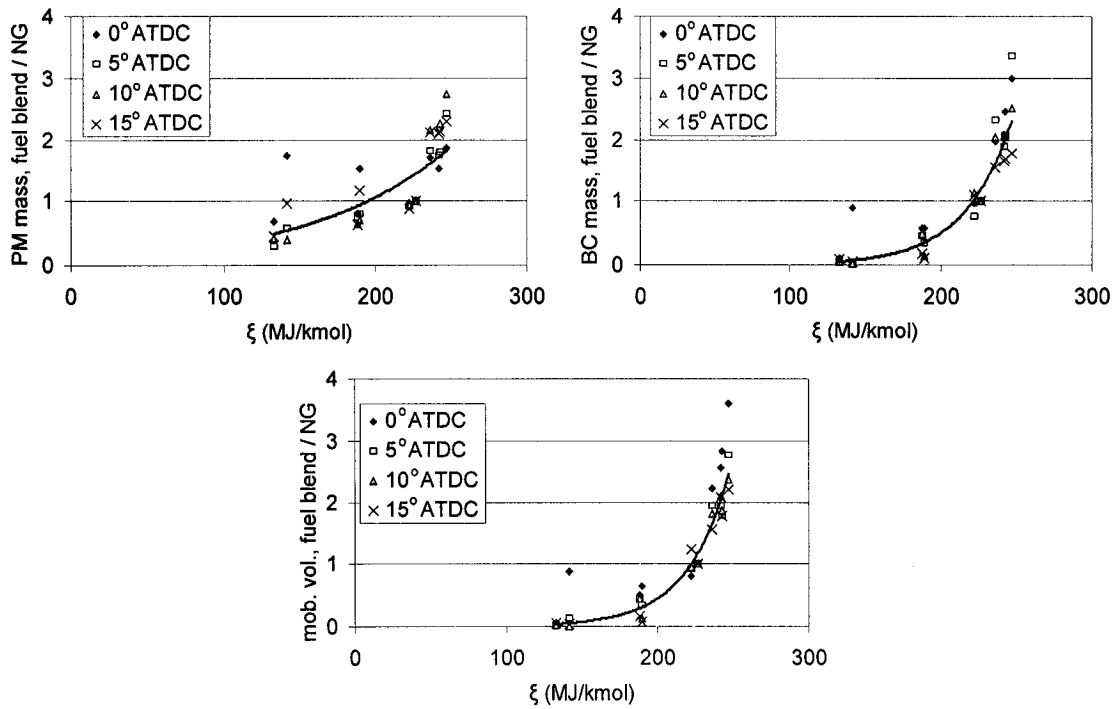

Figure 7.17: Comparison of PM emissions (total mass, black-carbon mass, ultrafine particle volume) for all fuel blends relative to natural gas emissions as a function of ξ (HHV / H:C). Lines are best fit (exponential) curves through the data.

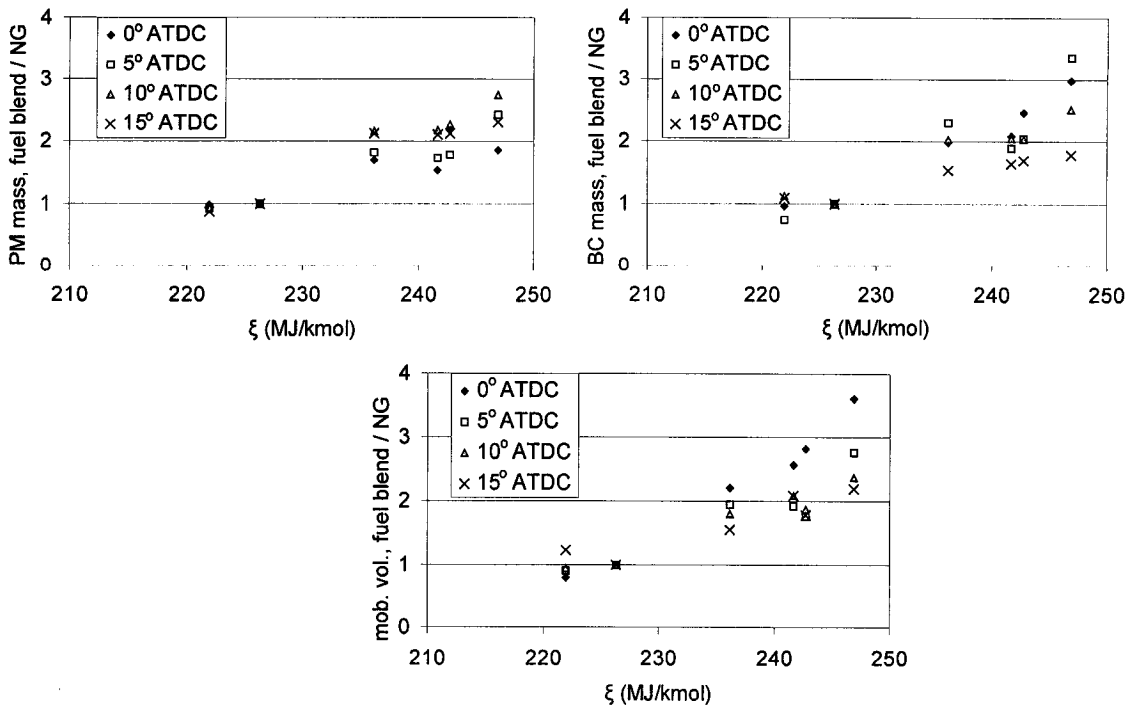

Figure 7.18: Comparison of PM emissions (total mass, black carbon mass, mobility volume) for methane and heavy hydrocarbon addition, relative to natural gas emissions as a function of ξ (HHV / H:C ratio)

Chapter 8
The Effects of Reingested Particles*

8.1 Introduction

In an effort to meet emissions standards for oxides of nitrogen (NO_x), exhaust gas recirculation (EGR) systems are widely used in new on-road heavy-duty diesel engines. EGR works by reducing the concentration of oxygen in the intake charge, thereby lowering the combustion temperature and hence impairing nitrogen oxide formation [123]. However, high levels of EGR increase emissions of particulate matter (PM) and impair fuel efficiency [229]. Although very high EGR fractions (>50%) reduce PM and NO_x emissions, this strategy is limited to low-load conditions and suffers from impaired fuel economy and high carbon monoxide (CO) and unburned hydrocarbon (HC) emissions [230]. As noted in previous chapters, the use of pilot-ignited, direct-injected natural gas (PIDING) is another technique to reduce NO_x and PM emissions from heavy-duty engines [40]. While very low NO_x levels can be achieved by combining high EGR fractions with direct-injected natural gas, emissions of CO, HC and PM are unacceptably high and efficiency is impaired [38].

For both diesel and natural gas direct-injection engines, the recirculated exhaust gases contain substantial quantities of PM. Subsequent particle nucleation, as well as growth by condensation and agglomeration, occurs when the EGR is mixed into the clean intake air at dilution ratios on the order of 3-7:1 (EGR fractions of 30%-15% by mass). Such low-ratio dilution processes strongly promote particulate nucleation and growth [99].

The effects of these recirculated particles on intake system fouling and engine wear have been studied extensively. The concentration of PM in unfiltered recirculated exhaust gas precludes introducing the EGR into the intake of the compressor system due to concerns over excessive fouling [229,231]. Deposition in the intake manifold and on the intake valves is also of concern. Increases in carbon contamination of the lubricating oil, and corresponding increases in engine wear, are also associated with EGR use [232,233]. This has been attributed mainly to higher overall in-cylinder soot concentrations in the post-

* A modified version of this chapter will be presentated at the SAE 2006 Fall Powertrain and Fluid Systems Conference. McTaggart-Cowan, G.P., S.N. Rogak, S.R. Munshi, P.G. Hill, and W.K. Bushe. The Effects of Reingested Particles on Emissions from a Heavy-Duty Direct Injection of Natural Gas Engine. SAE Technical Paper 2006-01-3433. 2006. Reprinted with permission from SAE.

combustion period [234]; however, increases in sulphuric and nitric acid concentrations in the ingested charge due to EGR may also be important sources of wear under some conditions [235,236]. These effects on engine wear and deposition are traditionally attributed to the PM recirculated with EGR.

From a combustion standpoint, studies using either filtered or synthetic EGR have generally shown increases in PM emissions with increasing charge dilution; however, no comparisons between filtered and unfiltered EGR conditions have been reported [123,237]. Inert particles in an atmospheric-pressure non-premixed flame influence the ignition process both by cooling the surrounding gases and (if the particle number density is high enough) by modifying the velocity field [238]. The author has been unable to identify any published work to date that specifically addresses the question of the effect of the recirculated carbonaceous particles on the combustion event. The current work, therefore, focuses specifically on identifying whether the recirculated particles contribute significantly to the observed increase in PM emissions with EGR.

8.2 Experimental Methodology

The testing was carried out on the heavy-duty single cylinder research engine described in Chapter 3, using the 17:1 compression ratio piston. The two major adaptations for the current set of tests were the installation of a filter in the EGR system (as shown in Figure 8.1) and the addition of an intake air sample line to the PM sampling system (Figure 8.2).

The filter selected for the EGR system was a Headline Filters grade 50C, constructed of PolyVinylidine DiFluoride (PVDF) fluorocarbon resin [239]. As the filter's rated temperature was only 150°C, the filter was installed downstream of the EGR cooler (Figure 8.1) to prevent thermal overloading. The filter was rated to remove in excess of 99.99% of solid and liquid particles larger than 100 nm. Performance for sizes smaller than 100 nm was not stated. As the engine exhaust contains many particles with mobility diameters less than 100 nm, the particle concentration in the intake was measured to determine whether the filter was adequately removing the small particles from the EGR.

As the PM loading in the intake stream with the filter was very low, the TEOM was not able to accurately measure the intake PM concentration. As a result, only the SMPS and the Aethalometer were used to measure intake concentrations. The intake air sample

bypassed the primary dilution system and was drawn directly into the secondary dilution system (Figure 8.2). The dilution ratio provided by the secondary dilution system was fixed at 6:1 by the constant flow rates through the two instruments and the maximum flow through the recirculation system. A full-flow ball valve was used to select between the intake and exhaust sample streams. For the intake system, a secondary vent line into the test cell ensured that the sample entering the dilution system was at ambient pressure. The effectiveness of the EGR filter at the various experimental conditions is presented in section 8.3.1.

8.2.1 Experimental Conditions

As discussed in section 3.3, the operation of the single-cylinder research engine can be fully defined from the equivalence ratio (ϕ), speed, indicated power, the intake oxygen mass fraction (Y_{intO2}), and the combustion timing (50%IHR). For the tests described here, the engine operating condition and the specific test modes used are shown in Table 8.1. Each test mode was repeated to establish a statistically valid sample for comparison between the filtered and unfiltered EGR conditions (the number of replications for each point are also shown in Table 8.1). The test modes were chosen to generate a range of exhaust particulate concentrations while minimizing the variability in engine operation. The non-EGR mode, A, provided a reference condition, as the presence of the filter should not influence the results with no EGR. An intermediate EGR case (B, $Y_{intO2} = 0.21$), and a pair of high EGR cases (C and D, $Y_{intO2} = 0.19$) provided a range of recirculated PM loadings and intake dilution levels. At the high EGR condition, the two timings (early timing, C, and late timing, D) provided low and high PM loadings in the recirculated exhaust at equivalent intake dilution levels. Complete randomization of the tests was impractical, so the tests were conducted in this order: 2 sets of non-filtered tests; 7 sets of filtered tests; 5 sets of non-filtered tests. The order of testing of the modes within the test sets was fully randomized. For each point, the engine operating condition was held stable for at least 5 minutes prior to collecting data. Data collection duration was a minimum of 10 minutes.

8.3 Results

To assess the influence of the EGR filter on engine operation, the in-cylinder pressure trace, gaseous emissions, and detailed particulate matter emissions are evaluated. The in-cylinder pressure and gaseous emissions would be affected only if the recirculated particulate

has a major effect on the overall combustion process. The particulate matter formation process, on the other hand, could be influenced by the recirculated particles without significantly influencing the overall combustion. However, before the impacts of the recirculated particles on the combustion and particulate formation processes are assessed, the effectiveness of the EGR filter needs to be discussed.

8.3.1 Filtration Effectiveness

To assess the effectiveness of the EGR filter at reducing particulate loading in the ingested charge, samples from the intake stream were analyzed with the SMPS and the Aethalometer. Figure 8.3 indicates the PM size distributions in the intake for modes A and D in a log-log format. The SMPS shows a 98% reduction in the peak particle number between the filtered and unfiltered conditions. Similarly, the Aethalometer indicates a reduction of over 96% in the intake black carbon concentration at all test modes (Figure 8.4) when the filter is added to the EGR line. Images of TEM grids sampled from the intake (at the same flow rate, dilution ratio, and sample time) show a very substantial reduction in particle concentration with the filter (see Appendix 7). The black carbon mass and size distributions in the intake for case A (Figure 8.3) are indistinguishable from background noise, as would be expected for this non-EGR case. These results indicate that the filter is effectively removing the PM from the intake stream. Furthermore, since no increase in nucleation mode particles is observed, it can be concluded that no direct nucleation of volatiles species is occurring in the intake downstream of the filter. Therefore, comparison of the filtered and unfiltered EGR cases should identify any substantial influences of the recirculated PM on the combustion and pollutant formation processes.

8.3.2 In-Cylinder Performance

If the recirculated particles do significantly influence the combustion event, differences in the in-cylinder pressure trace between the filtered and unfiltered cases would be expected. No significant differences in the pressure trace or heat release rate are observed at mode D, as shown in Figure 8.5. Similar results apply for the other operating modes (shown in Appendix 6). A comparison of combustion progress parameters, including the ignition delay times (for both the diesel pilot and the natural gas), the peak heat-release rate, and the burn duration, are shown in Figure 8.6. The pilot ignition delay time is not significantly different at any of the observed conditions. An increase in the natural gas

ignition delay time (commanded start of natural gas injection to observed start of gas combustion) is observed at only one mode, C. This can be attributed to the higher EGR fraction at that mode with the filter as shown in Figure 8.7. The longer ignition delay is consistent with previous results which suggest that increases in EGR can significantly increase gaseous ignition delay times [131]. The peak heat-release rate is also slightly higher at this mode, due to a higher intensity premixed burn phase resulting from the longer ignition delay period for the natural gas. The burn duration (as defined by the 10-90% integrated heat release rate), however, does not show any significant differences between the filtered and unfiltered cases. From these results, it is apparent that only at mode C are there significant differences, and that even at that condition, the recirculated particulate is not significantly influencing the overall combustion event. However, minor effects influencing the gaseous or particulate emissions are not necessarily discernable from the pressure trace.

8.3.3 Emissions and Performance

As indicated by the in-cylinder pressure results, the engine's operating condition remains relatively constant between the filtered and unfiltered cases; the most significant difference is the higher EGR level at mode C. This is a result of the greater variability in EGR level which results from the varying pressure drop through the filter. The higher EGR level has a significant influence on the combustion and emissions formation processes at mode C. All the other modes show good operating condition repeatability, including the EGR fraction and GIMEP (shown in Figure 8.7) as well as the overall equivalence ratio, combustion timing, and pilot fraction (not shown). No statistically significant variations are detectable at any mode in any of these parameters. As the engine operating conditions (aside from mode C) remain consistent between the filtered and non-filtered EGR tests, any differences in measured emissions are attributable to the recirculated PM. However, because the testing was not completely randomized, some error due to day-to-day variability may also have influenced the readings. A comparison of the results at mode A quantifies this effect, since the filter's presence or absence should have no influence when there is no flow through the EGR system.

Comparisons of the average emissions of NO_x, CO, HC, and PM between the filtered and non-filtered cases are shown in Figure 8.8. The error bars on the plot represent the 95% confidence intervals about the mean of the collected data. The data, including the

uncertainties, are shown in Table 8.2. For the gaseous emissions, the variations in the emissions are relatively small. The only statistically significant variation (at a 95% confidence level, determined through comparison of means using Student's T-test) is at mode C, where NO_x emissions are significantly lower with the filter than without, while PM levels are significantly higher (Figure 8.8); this is directly attributable to the differences in EGR level at this condition that were discussed earlier. At all other modes, the recirculated PM does not significantly influence emissions levels. However, the uncertainties on the PM total mass measurements are sufficiently large that subtle effects are not discernable.

8.3.4 Particulate Matter

The variability in the PM mass measurements is due primarily to the relatively low PM levels at most of the conditions. A day-to-day bias is also apparent, with the days where filtered testing was carried out having, on average, higher measured PM mass levels. This is observable even under conditions where the presence of the EGR filter should not influence the results (mode A, 0.23 Y_{intO2}). Further insight into the PM emissions may be developed from the average particle size distributions for the A and D cases. In Figure 8.9 under non-EGR conditions (case A), the number of particles for the unfiltered cases can be seen to be slightly increased. This is generally consistent with the observed increase in mass at this condition, and is indicative of the variability in both the mass and number measurements. At higher EGR levels (with late timing, case D), the total number of particles is reduced. The plots in Figure 8.9 also show the intake particle number concentrations; however, only the unfiltered case D sample shows a discernable number of particles.

The size distributions are the average values for all the data collected at the given operating condition. Further insight may be gained from integrating the size distributions to estimate a mobility volume of particles in the SMPS measurement range (ultra-fine particles, mobility diameter of 5-150nm). The mobility volume is not a measure of the true volume occupied by the particles, due to their non-spherical shape; however, it is representative of the total quantity of ultra-fine particulate. By multiplying the mobility volume by an effective density, an estimate of the mass can be generated [159,160,161]. However, from the current work there is insufficient information to determine the effective density for these particles, as discussed in section 3.2.2. Despite this, as the effective density depends primarily on size, changes in the mobility volume will be generally representative of changes in ultrafine

particle mass. The mobility volume results are shown in Figure 8.10. For mode D, a reduction in ultra-fine particle volume of approximately 15% is suggested with the EGR filter. Conversely, the other modes all show an increase in particle volume, generally consistent with the increase in total mass indicated in Figure 8.8. The effect of particles larger than 150 nm in diameter, as well as adsorption of volatiles and water vapour on the TEOM filter, may explain the substantially lower volumes at low EGR levels (relative to the high EGR modes) measured by the SMPS in comparison to the TEOM readings. Specifically, evaporated lubricating oil recondensing on the TEOM filter may be generating a baseline PM mass measurement that is not detectable by the SMPS. Day-to-day variability of the TEOM at low emissions levels may also be contributing to the discrepancies between the TEOM and SMPS measurements.

The black-carbon concentrations in the exhaust stream, as measured by the Aethalometer, are shown in Figure 8.10. The mass fraction of black-carbon (Aethalometer result / total mass as measured by TEOM) is also shown. These results indicate that the use of the filter substantially reduces the total mass of black carbon in the exhaust at the highest PM loading condition (mode D). At mode C, the increases in black carbon content and ultra-fine particle mass are only approximately one-half those of the increase in mass measured by the TEOM. This results in a reduction in the fraction of the total PM that is attributable either to the ultra-fine particles or to black carbon. The fact that these results are not observed in the TEOM data is most likely due to a corresponding increase in volatile fractions in the exhaust, possibly resulting from reduced particle surface area available for condensation.

8.4 Discussion

The general emissions and performance results are consistent in suggesting that the particles in the intake stream are not having a significant influence on the overall combustion event. However, there is indication of a reduction in black-carbon particle mass (soot) in the exhaust stream due to the filtering of the recirculated particles. If all the recirculated particles were passing unreacted through the combustion chamber, a reduction in exhaust PM mass of ~30% would be expected from the reduction of PM in the ingested charge. Since such a reduction is not observable in the collected data, it appears that much of the PM is being oxidized during the combustion process. As the engine was operating overall lean (ϕ_{O2} of 0.6), approximately 40% of the charge did not participate directly in the combustion event. If

the PM in this unreacted charge was not oxidized, a 10-15% reduction in exhaust PM mass would be expected; this figure is in fact roughly equivalent to the reductions suggested by the SMPS and the Aethalometer. These results indicate that the PM which is contained in the unreacted charge passes through the cylinder and is emitted, while the PM in the portion of the charge which participates in the combustion is consumed. This is not surprising, given that the environment in the vicinity of the combustion event would be at higher temperatures and would contain a significant pool of radicals to enhance the oxidation rate of the recirculated particles. This reasoning suggests that the bulk of the PM emitted during EGR operation is newly formed in the combustion event. At mode C, the increase in PM due to the higher EGR level for the filtered tests masks these effects. At mode B, the anticipated influence of the recirculated particles would be only half that at mode D, given the lower EGR flow. A 5% reduction would be expected at mode B; but this is not discernable in the data due, in all likelihood, to the variability in the PM levels.

These results have a number of significant implications for an operational system where EGR is used in conjunction with an exhaust particulate removal device. There is no apparent benefit, in terms of PM formation, to locating the EGR loop downstream of the exhaust PM trap. Nonetheless, there are other benefits of cleaning the exhaust gases before it is recirculated, including reducing particulate buildup in the EGR and intake systems as well as improving engine longevity and reducing oil degradation.

8.5 Conclusions

1. As long as the EGR rate is equivalent between the filtered and unfiltered cases, no statistically identifiable differences in gaseous emissions, total particle mass, or combustion performance occur.
2. In general, the formation of PM under EGR operation is independent of the quantity of the recirculated particulate. This suggests that the bulk of the PM emitted is freshly formed.
3. The black-carbon masses and ultrafine particle size distributions suggest that recirculated PM far from the reaction zone is emitted from the engine unreacted. The PM that is in the charge that participates in the combustion event is fully oxidized and does not influence the formation of new particles.

4. Without a filter in the EGR line, significant quantities of particulate are reingested into the engine when using EGR. Installing a filter can reduce the total PM loading in the intake stream by more than an order of magnitude.

8.6 Figures and Tables

Table 8.1: Base engine operating condition and test modes

Speed	1200 RPM
Load (GIMEP)	13.5 bar
O_2 EQR	0.6
Injection Pressure	21 MPa
Diesel Quantity	5 mg/inj

Mode	Y_{intO2}	EGR%	50%IHR (°ATDC)	Sample size Unfiltered	Filtered
A	0.23	0	10	6	6
B	0.21	15	10	8	6
C	0.19	30	0	7	6
D	0.19	30	10	7	7

(reprinted with permission from SAE 2006-01-3411. © SAE International 2006)

Table 8.2: Mean (Standard Deviation) of various parameters

Mode	Filter	GIMEP bar	ϕ_{O2}	EGR %	GISFC g/GikWhr	NOx g/GikWhr	CO g/GikWhr	HC g/GikWhr	PM g/GikWhr
A	unfiltered	13.42(0.07)	0.599(0.009)	0(0)	185.4(0.44)	5.30(0.10)	0.69(0.07)	0.30(0.01)	0.007(0.002)
	filtered	13.42(0.08)	0.607(0.010)	0(0)	186.1(0.93)	5.02(0.08)	0.81(0.08)	0.30(0.01)	0.010(0.003)
B	unfiltered	13.43(0.08)	0.601(0.007)	14.0(1.5)	184.6(0.74)	2.22(0.44)	1.43(0.39)	0.50(0.07)	0.014(0.006)
	filtered	13.43(0.07)	0.596(0.008)	13.8(3.2)	184.8(0.71)	2.29(0.43)	1.55(0.36)	0.47(0.06)	0.015(0.004)
C	unfiltered	13.90(0.07)	0.594(0.020)	24.3(0.8)	177.5(0.44)	3.45(0.30)	1.41(0.19)	0.69(0.05)	0.009(0.002)
	filtered	13.89(0.06)	0.593(0.013)	26.4(2.0)	177.3(0.50)	2.95(0.40)	1.67(0.24)	0.71(0.04)	0.014(0.003)
D	unfiltered	13.52(0.04)	0.588(0.008)	26.4(0.7)	183.1(0.88)	0.96(0.08)	2.92(0.22)	0.81(0.07)	0.027(0.003)
	filtered	13.43(0.08)	0.582(0.009)	26.4(2.4)	183.5(2.03)	1.00(0.18)	3.03(0.52)	0.81(0.09)	0.027(0.006)

(reprinted with permission from SAE 2006-01-3411. © SAE International 2006)

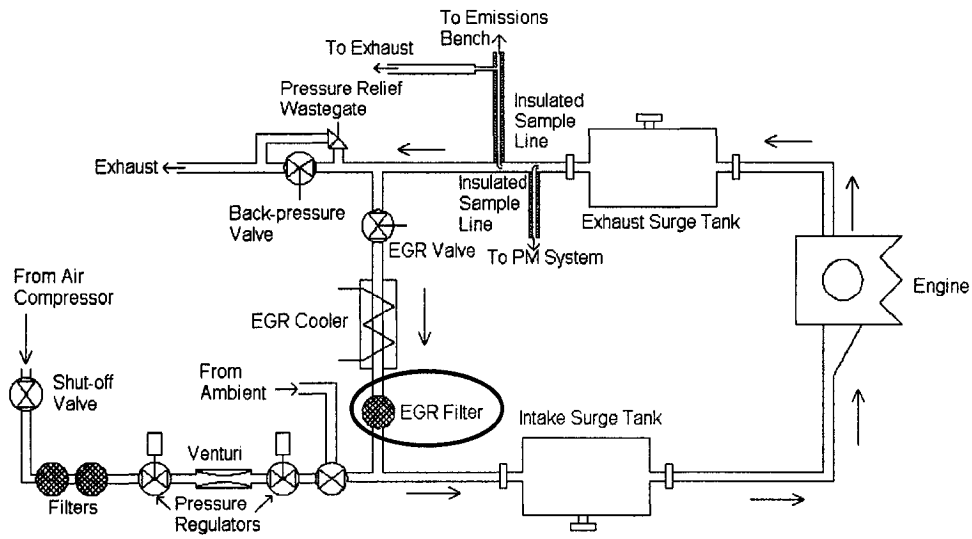

Figure 8.1: Engine air exchange system with EGR filter.

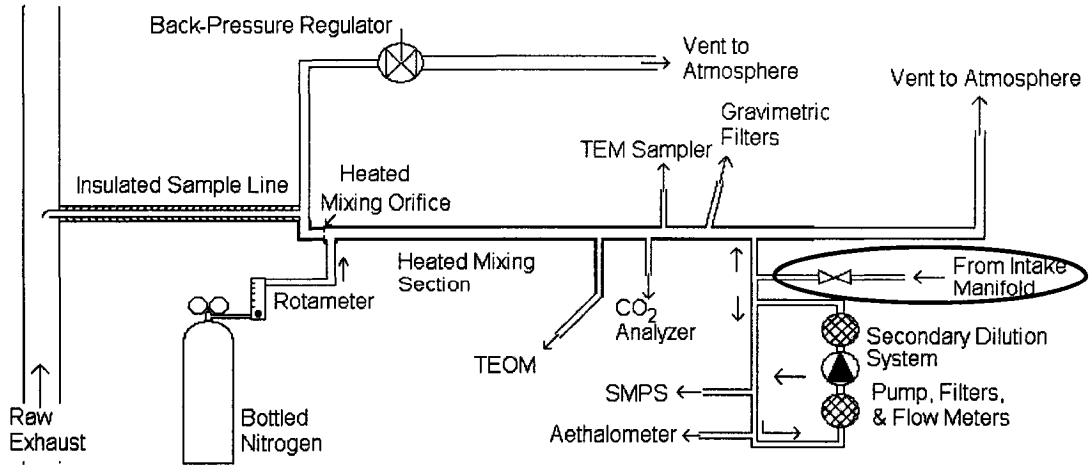

Figure 8.2: PM sampling system modified for intake sampling.

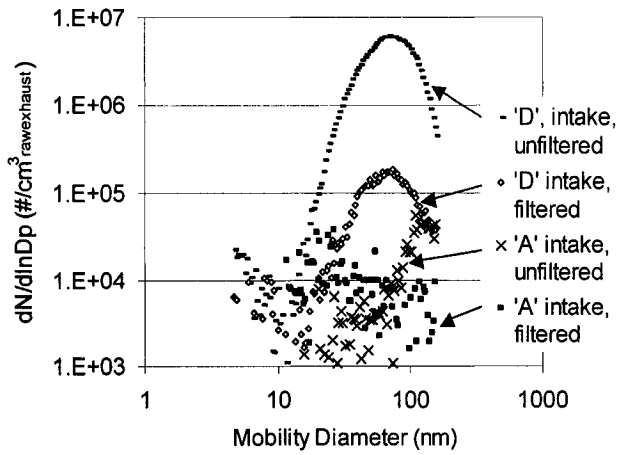

Figure 8.3: Intake PM size distributions, modes A and D. *(reprinted with permission from SAE 2006-01-3411. © SAE International 2006)*

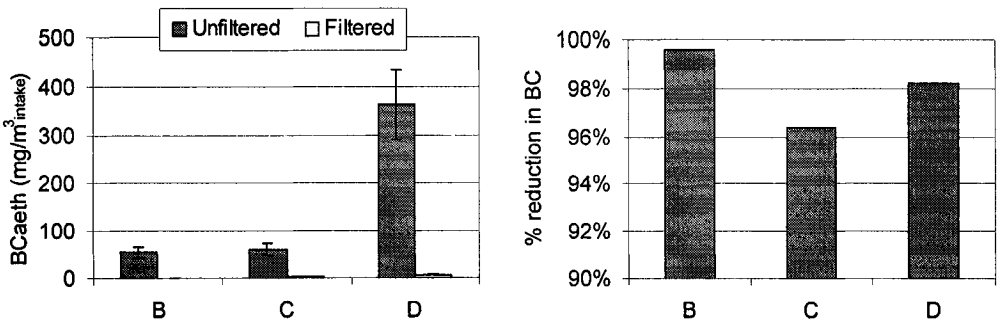

Figure 8.4: Aethalometer measurements of intake concentrations and % reduction in black carbon between filtered and unfiltered EGR at all EGR test modes. Error bars are based on the pooled uncertainty in the measured exhaust values (they are not shown for the right-hand plot as they are greater than the scale of the graph). *(reprinted with permission from SAE 2006-01-3411. © SAE International 2006)*

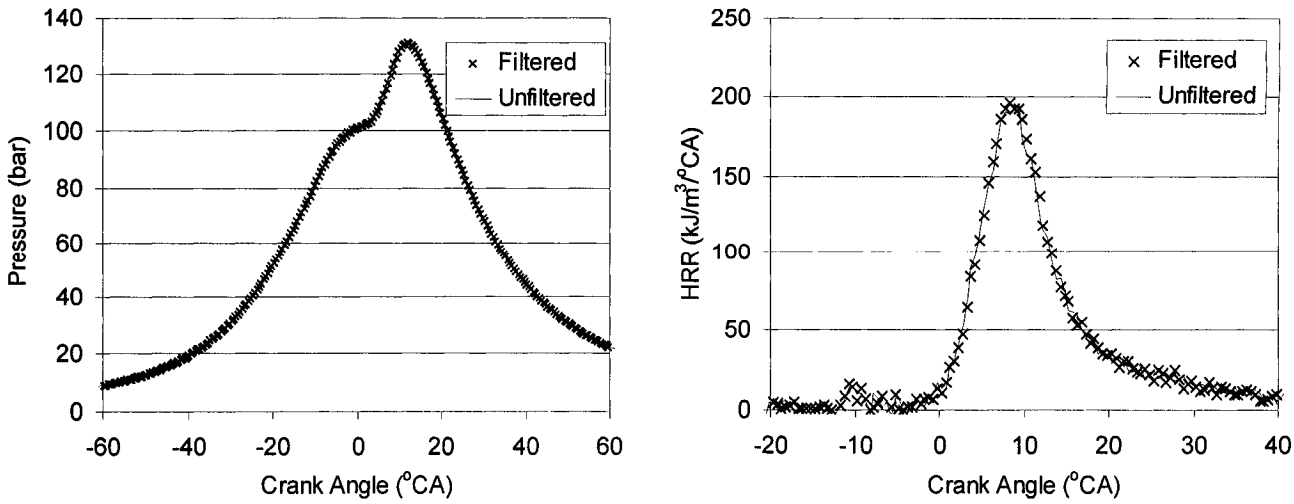

Figure 8.5: Pressure trace and heat-release rate at mode D (0.19 Y_{intO2}, 50%IHR at 10°ATDC) for individual filtered and non-filtered test points. *(reprinted with permission from SAE 2006-01-3411. © SAE International 2006)*

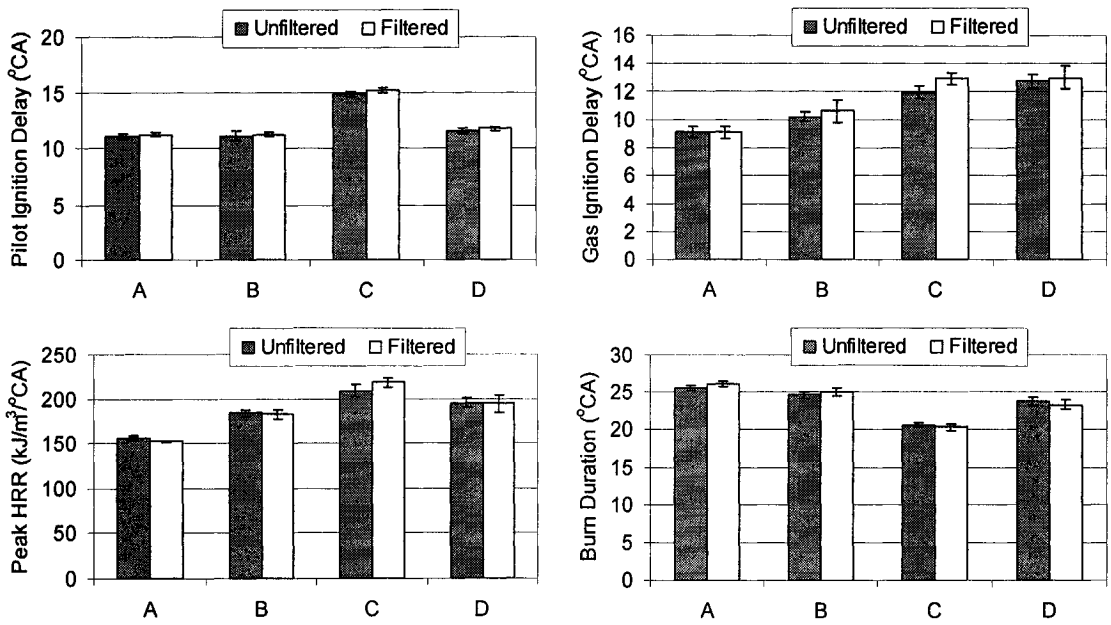

Figure 8.6: Ignition delay and combustion progression for filtered and unfiltered conditions. Error bars indicate 95% confidence intervals. *(reprinted with permission from SAE 2006-01-3411. © SAE International 2006)*

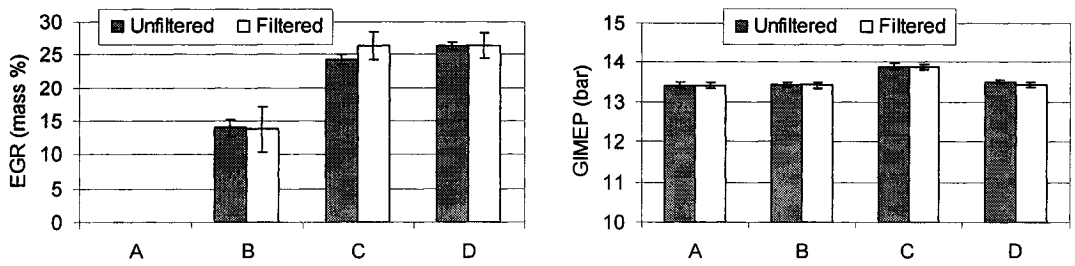

Figure 8.7: Operating condition variations as a function of test mode for filtered and unfiltered conditions. Error bars indicate 95% confidence intervals. *(reprinted with permission from SAE 2006-01-3411. © SAE International 2006)*

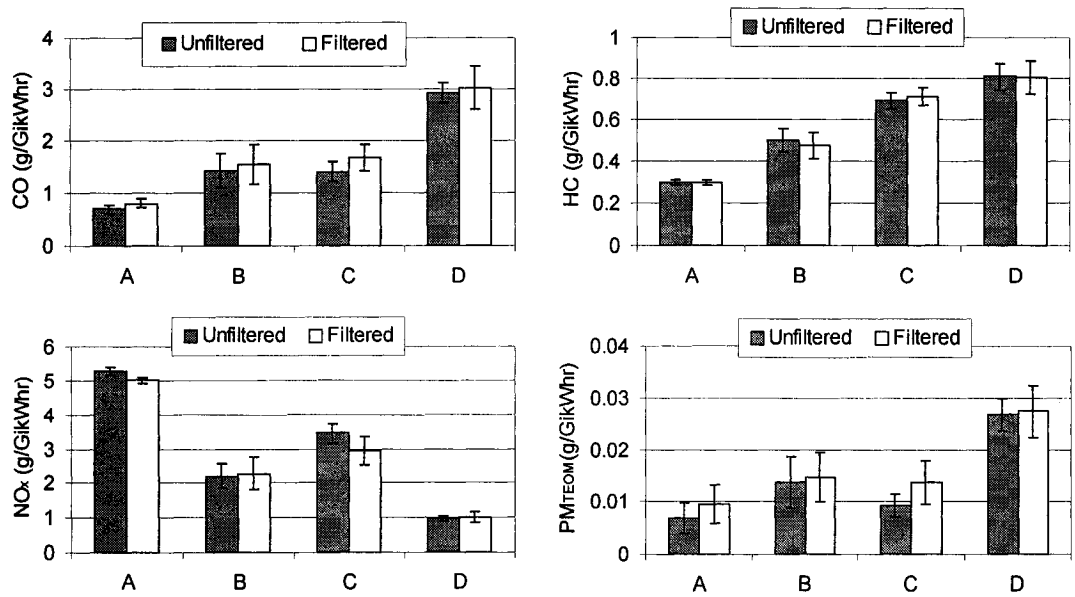

Figure 8.8: Power-specific emissions as a function of test mode for filtered and unfiltered conditions. Error bars indicate 95% confidence intervals. *(reprinted with permission from SAE 2006-01-3411. © SAE International 2006)*

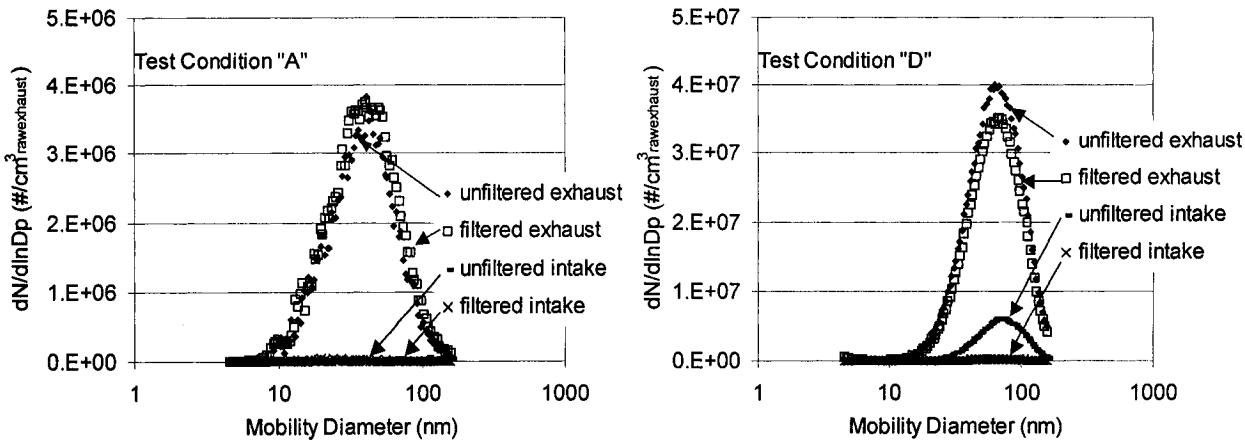

Figure 8.9: Particle size distributions in intake and exhaust streams at modes A and D. *(reprinted with permission from SAE 2006-01-3411. © SAE International 2006)*

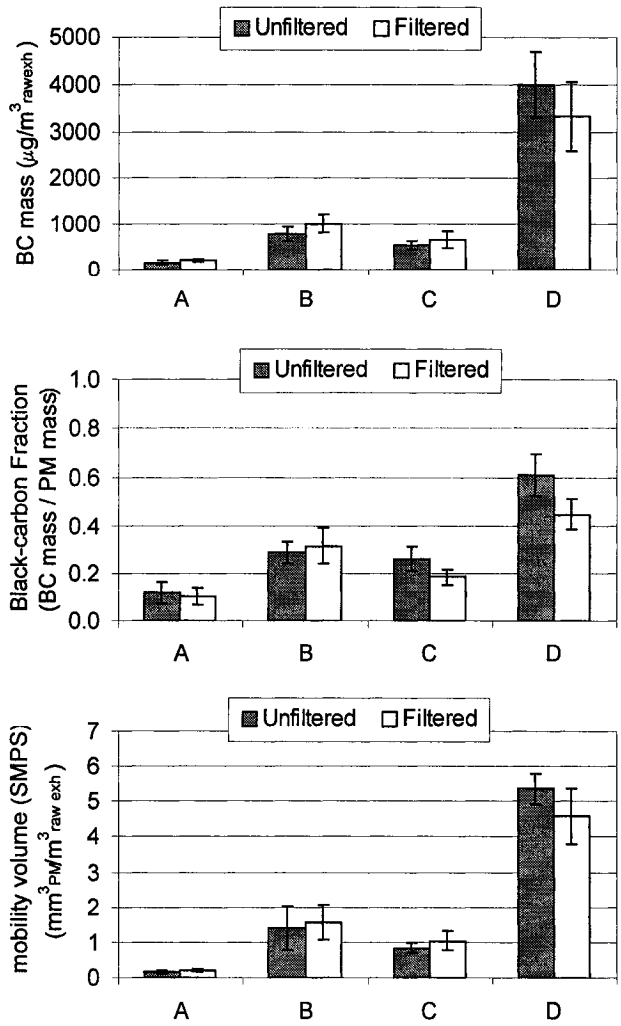

Figure 8.10: Black-carbon concentration, fraction of total particle mass and mobility volume (PM vol.) at all test modes. Error bars indicate 95% confidence intervals. *(reprinted with permission from SAE 2006-01-3411. © SAE International 2006)*

Chapter 9
Significant Findings and Recommendations

The objective of this research was to improve understanding of the gaseous fuel combustion process of a pilot-ignited, direct injection, gaseous-fuelled engine with intake-charge dilution. This objective has been addressed through studies where the gaseous jet energy, the fuel composition, and the charge composition were varied. This thesis has examined factors relating to the physical injection and mixing processes as well as fuel chemistry and charge composition. Because of interactions between these factors, it is difficult to isolate from any one of the studies the principal factors affecting the combustion process. However, by considering all the studies presented here in aggregate, it is possible to develop more robust conclusions.

The conclusions for the individual studies are set out in the corresponding chapters and will not be reproduced in detail here. The present chapter offers a general overview of the salient findings of the research and aims to provide an interpretation of these results in the context of improved understanding of the combustion process and the key factors leading to pollutant generation. Summary plots which combine results presented in previous chapters are presented where they augment the discussion. The implications of these findings to engine systems development are discussed. Finally, recommendations for future research to develop further understanding of the combustion and pollutant-formation processes, and to improve the combustion system, are presented.

9.1 Significant New Findings

Gaseous Fuel Composition

The composition of the gaseous fuel has a substantial impact on the combustion process and emissions. Higher ethane and propane concentrations increase PM and CO emissions even though they enhance the ignitability of the fuel. The addition of hydrogen reduces PM, HC and CO, most significantly at conditions where the combustion is most unstable and where the emission levels of these species are highest. Diluting the gaseous fuel with nitrogen substantially reduces emissions of PM, HC and CO, as well as NO_x. These effects, summarized in Figure 9.1 (note that the magnitude of the variations in PM are much larger than for the other species), are in general substantially greater than previously reported

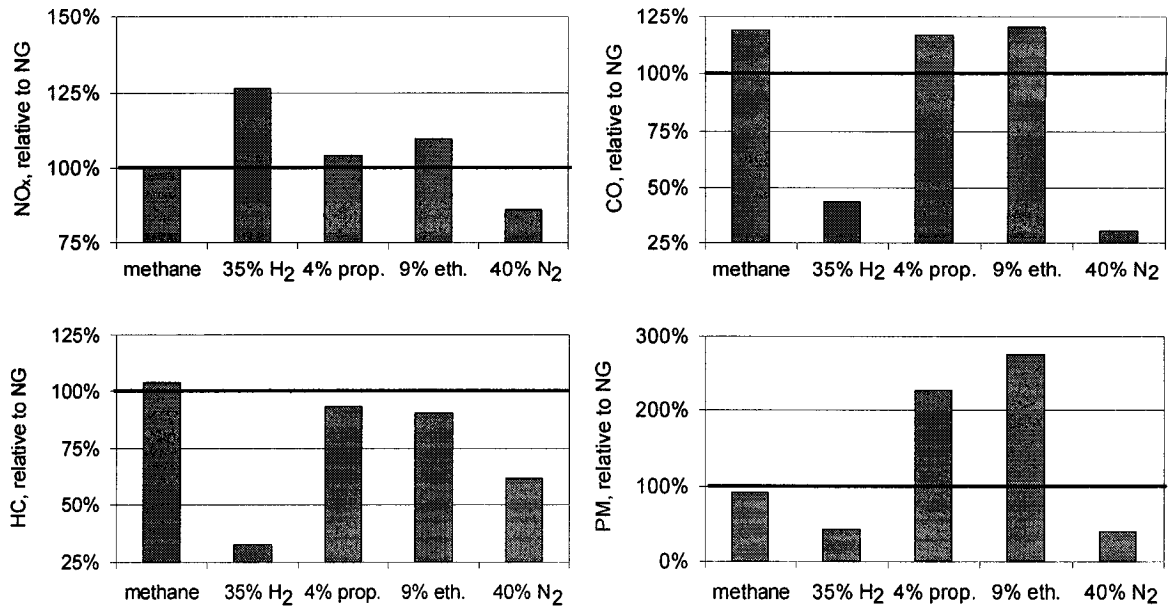

Figure 9.1: Summary of effects of fuel composition on emissions for the high levels of all fuel compositions at 1200 RPM, 13.5 bar GIMEP, 50%IHR = 10°ATDC (note scale change for PM plot).

for homogeneous-charge spark-ignition systems; this is due to fundamental differences in the PIDING engine's non-premixed combustion system.

Fuel composition has significant effects on emissions from a PIDING engine: as a result, variability in the composition of commercial-grade natural gas (not to mention the likelihood of even larger variations with the use of non-conventional fuel sources), will have a significant impact on the system's ability to meet emissions standards. It is evident that an easy way to evaluate the influences of different fuel blends on the combustion process is required. Previously proposed values, such as the Wobbe Index and the H:C ratio, are insufficient to describe the effects of fuel composition on a direct-injection of natural gas engine. A new index (ξ) is proposed, which includes both the volumetric energy density (molar heating value) of the fuel and the H:C ratio. This index is able to differentiate the effects of fuel composition on total PM and black-carbon emissions over a range of operating conditions (Figures 7.17 & 7.18). Therefore, it may be of use in determining what fuel blends will be able to meet future emissions standards, or to ensure that a given engine calibration is capable of meeting emissions standards over a range of gaseous fuel compositions.

Recirculated Particulate

Removing the recirculated particulate from the ingested charge has a negligible influence on the measured mass of PM in the exhaust, indicating that the bulk of the particulate emitted when operating with EGR is freshly formed in each cycle. Previous studies of the effects of the PM recirculated with EGR have focused on engine longevity and wear; the current study was the first to investigate the effects on the combustion process. Although the recirculated particulate had no measurable influence on the gaseous emissions or the total particulate matter emissions (Figure 8.8), both ultrafine particle volume and black-carbon mass are slightly reduced (Figure 8.10). The results indicate that the bulk of the recirculated PM is being oxidized in the high-temperature, oxygen-rich zone on the oxidizer side of the non-premixed combustion event, and the emitted particulate matter is freshly formed in the combustion chamber during each cycle. However, given that filtering the recirculated exhaust gases does reduce the ultrafine particle volume and black carbon mass, it appears that some particles – most likely those located in the extremities of the combustion chamber – are not being completely oxidized. The fact that this relatively small difference in emissions is not observed in the total PM mass results may be attributed to uncertainties in the mass measurements or the significant contribution of condensed volatile substances.

Injection Pressure and Operating Conditions

Increasing the injection pressure in a direct-injection of natural gas engine consistently reduces PM emissions at medium and high load conditions with and without charge dilution (EGR). The effects of injection pressure on all other emissions interacted strongly with engine speed, load, and EGR level.

Previous diesel-engine research has shown that increasing the injection pressure of direct-injection engines can reduce PM emissions; however, substantial differences between the combustion of a gaseous jet and a liquid spray mean that the results are not directly comparable to a PIDING engine. Preliminary studies at a single operating condition also demonstrated that higher injection pressures may reduce PM from a PIDING engine. The current research, on the other hand, revealed that while higher injection pressures reduce PM at high load conditions, at lower loads, where the differential pressure between the fuel rail and the combustion chamber is higher, increasing the injection pressure has less of an effect on PM (Figure 4.5). Similarly, the effects are less significant at high speed, as the relative

contribution of the gaseous jet to the overall turbulent motion in the combustion chamber is reduced. The other emissions (Figures 4.2 - 4.4) showed even stronger dependence on operating condition, with relatively less sensitivity to injection pressure. This demonstrates that interactions between the gaseous jet and the in-cylinder conditions (including temperature, pressure, and charge motion) have a substantial impact on the combustion event, and on the resulting emission levels.

Particulate Matter Emissions

The quantity and composition of PM emitted from a PIDING engine are significantly affected by combustion parameters including in-cylinder turbulence levels and fuel composition. Adding large amounts of nitrogen or hydrogen to the fuel reduces carbonaceous PM to undetectable levels; however, significant total mass emissions are still observed. These are attributed primarily to volatile species.

Increasing the in-cylinder turbulence (with higher injection pressures, Figure 4.5, or by diluting the fuel with nitrogen, Figure 7.6) substantially reduces PM emission levels. Increasing radical concentrations through the addition of hydrogen to the gaseous fuel can achieve similar results (Figures 5.1 & 5.2). Adding ethane or propane to the fuel increases PM emissions substantially (Figure 6.10), demonstrating the importance of the chemical structure of the fuel on PM formation. In general, black carbon and ultrafine particle emissions are reduced more than the total PM (as demonstrated for the hydrogen and nitrogen addition cases in Figure 9.2). At conditions where ultrafine and black carbon

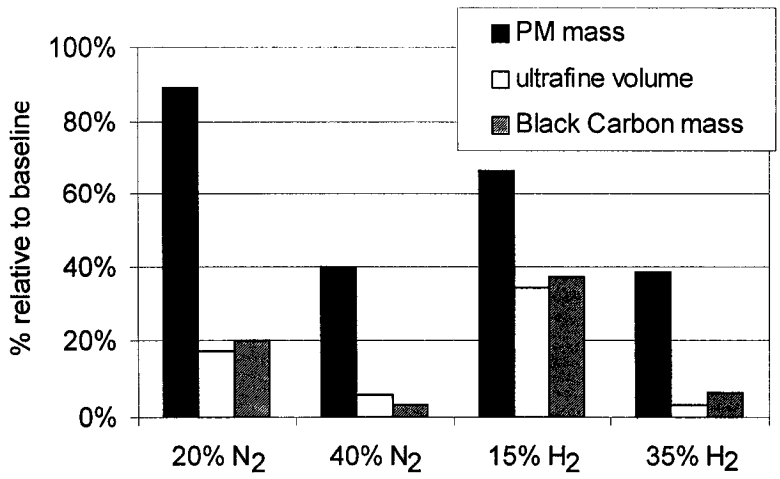

Figure 9.2: Summary of average PM total mass, ultrafine particle volume and black carbon mass emission reductions for nitrogen and hydrogen fuelling at 1200 RPM, 13.5 bar GIMEP, 50%IHR = 10°ATDC

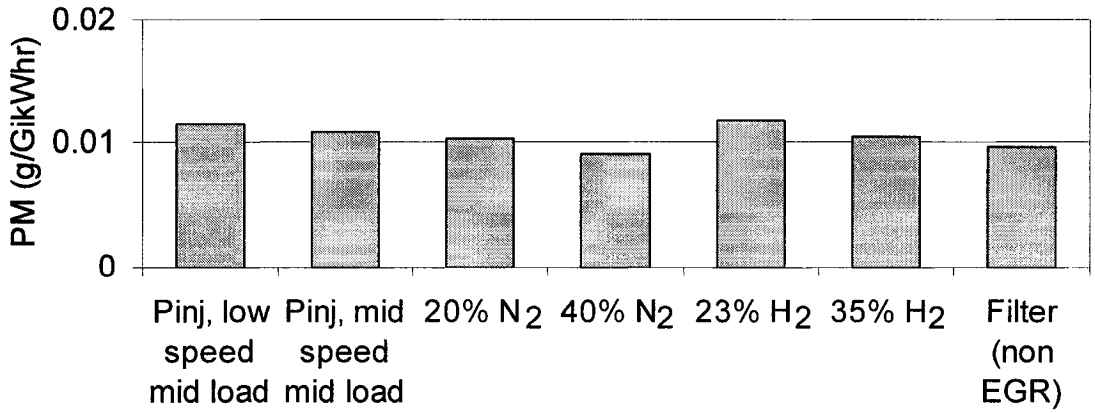

Figure 9.3: Minimum PM mass levels from all tests (including injection pressure, nitrogen, hydrogen at low and high loads, and filtered EGR tests for the non-EGR condition).

particulate emissions approach zero, a baseline level of PM mass emissions is still observed; the lowest PM total mass is relatively consistent for various test conditions, as shown in Figure 9.3. A large fraction of these total mass emissions is composed of non-black carbon (all the points shown had BC concentrations less than 15% of the total mass). These non-BC emissions are primarily condensed volatiles, most likely originating from the lubricating oil or pilot fuel. These emissions, whose levels are not substantially affected by mechanisms which reduce PM formation from the gaseous combustion event, are a serious concern in that they approach the upcoming regulatory limits for heavy-duty engine emissions (Table 1.1).

Gaseous Fuel Ignition Delay

Enhancing the reactivity of the gaseous fuel results in significant reductions in the ignition delay time. However, limitations to the reductions achievable through kinetic enhancements indicate that the fuel-air mixing process is also a critical component in this non-premixed pilot-flame-ignited combustion event.

The addition of hydrogen, ethane, or propane to natural gas fuel has been shown in the literature to increase the ignitability of natural gas. The current study investigated the influence of such kinetic effects on the ignition delay of the pilot-ignited gaseous fuel. Tests were conducted with moderate intake dilution (EGR~30%). Kinetic enhancement with hydrogen was tested at both mid-speed high-load and low-speed low-load; ethane or propane were only tested at the former condition. For the conditions tested, all three fuels indicated that kinetic enhancement significantly reduces the ignition delay of the gaseous jet (Figure

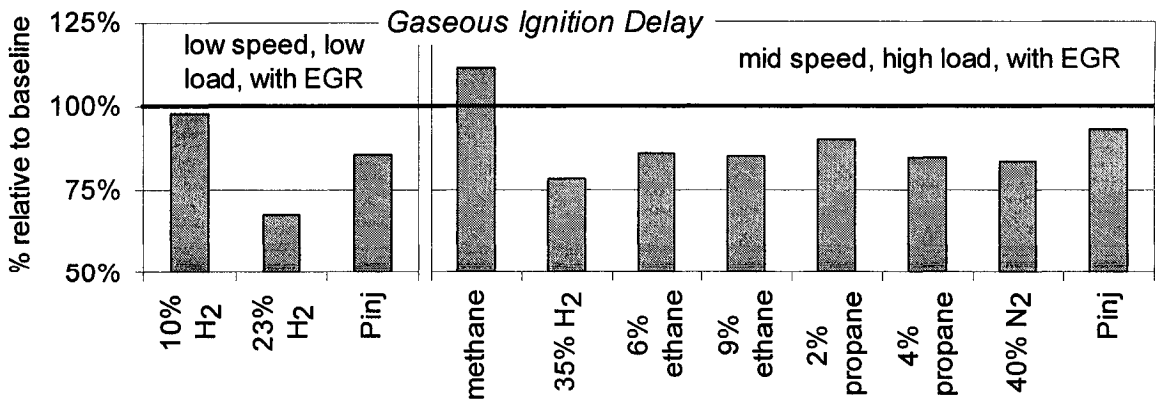

Figure 9.4: Changes (relative to natural gas) in gaseous fuel ignition delay (SOI to SOC), at low load and high load for fuel composition and injection pressure (Pinj) tests, all at 50%IHR = 10°ATDC, ~30%EGR

9.4). However, the ethane addition tests suggest a possible limitation on the potential for kinetic enhancement of the ignition process, with no further reduction in ignition delay between the intermediate and high ethane concentrations. This suggests that, as kinetics are improved, fuel-oxidizer mixing becomes the crucial factor limiting ignitability. Reductions in ignition delay are somewhat greater with high levels of hydrogen addition (35% by volume); at these high concentrations, the fluid mechanics of the gas injection and mixing are significantly affected by the jet composition. Both nitrogen dilution of the fuel and higher injection pressures demonstrate that enhanced fuel-air mixing can significantly reduce the ignition delay. While higher injection pressures increase the turbulent mixing in the early stages of the injection process, the nitrogen dilution may relate more to changing the spatial and temporal location of ignitable fuel-air mixture in the gaseous jet relative to the diesel pilot flame.

Gaseous Fuel Combustion Rate

Increasing the rate of fuel-air mixing reduces the gaseous fuel combustion duration at all operating conditions. Enhancing the reactivity of the fuel also increases the combustion rate at low load; however, it has no significant effect at high load. This indicates that the high load combustion is primarily limited by fuel-air mixing. At low loads, both mixing and chemical kinetics are important, because of the relatively greater importance of the ignition and premixed combustion event at these conditions.

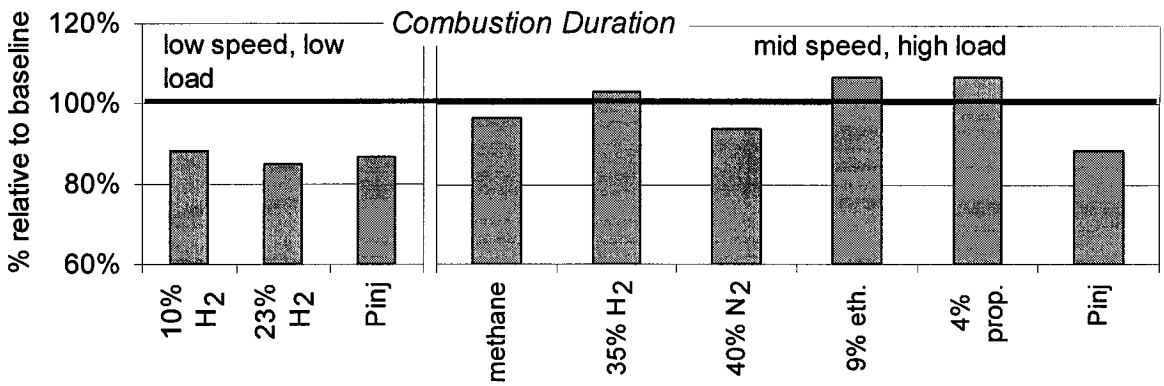

Figure 9.5: Changes (relative to natural gas) in combustion duration (10% to 90% IHR), at low load and high load for fuel composition and injection pressure (Pinj) tests, all at 50%IHR = 10°ATDC, ~30% EGR

Higher injection pressures increase the fuel injection rate, the turbulent shear stress, and the kinetic energy transfer to the charge. These factors all contribute to higher turbulent mixing intensities and significant reductions in the combustion duration (Figure 4.8). This has more of an impact at higher loads, where the in-cylinder pressures are higher, suggesting that mixing limitations become more significant as the differential pressure between the injected fuel and the cylinder charge is reduced (Table 4.4). By adding hydrogen, ethane, or propane to the fuel, the overall reactivity of the gaseous jet is enhanced; at low load, the hydrogen addition results in a significant reduction in combustion duration, but at high load, these additives do not significantly affect the overall combustion duration (Figure 9.5). Only higher injection pressures or the addition of nitrogen to the fuel reduces the combustion duration at high load; this is a result of increased kinetic energy transfer from the gaseous jet to the combustion chamber and hence enhanced late-cycle mixing. This finding is particularly interesting as the injection duration for the nitrogen dilution was twice that of conventional natural gas, because of the lower energy density of the fuel. These results show that at high load with moderate levels of intake dilution, mixing limitations dominate the combustion process, while at low loads both chemical kinetics and mixing can substantially enhance the combustion rate.

Processes which improve mixing, either for the gaseous jet or in the post-injection combustion chamber, reduce emissions of unburned hydrocarbons and particulate matter. On the other hand, carbon monoxide production depends on operating condition, suggesting that at some conditions, mechanisms other than mixing (possibly increased local extinction events due to high turbulent shear stresses) are contributing to the formation of this pollutant.

Improved mixing does not significantly affect the fuel conversion efficiency, but under certain conditions NO_x emissions are increased. More rapid mixing may also reduce the amount of time at which the fuel-rich zones are at high enough temperatures to form soot; the result is a reduction in PM emissions.

Combustion Stability

Increased combustion stability correlates directly with reduced emissions of CO and HC (Figure 7.15). The addition of hydrogen or nitrogen to the fuel improves the combustion stability and correspondingly reduces emissions. Ethane or propane addition has little impact on combustion stability at most conditions, and hence has little impact on HC emissions; however it does cause the CO emissions to increase. This increase indicates that other mechanisms besides combustion stability are contributing to these emissions. While processes which improve combustion stability also reduce emissions of CO and HC, it is unclear whether these are caused directly by improvements in combustion stability. Possible explanations include fewer local turbulent shear-related extinction events, more stable ignition processes, or more complete late-cycle oxidation of the combustion by-products.

Fuel Conversion Efficiency

Fuel conversion efficiency is relatively unaffected by modifications to the fuel composition or enhancement of the turbulent kinetic energy through gaseous jet modifications. When corrected for the energy density of the various fuel blends, nitrogen or propane addition slightly improved fuel conversion efficiency, while ethane slightly reduced it; neither hydrogen addition nor pure methane fuelling had any effect on efficiency (Figure 9.6). However, these effects were substantially smaller than the effects of operating condition, including injection timing (also shown in Figure 9.6), engine speed, and load (Figure 4.1). This reinforces the generally recognized dominance of operating condition on fuel conversion efficiency; it is interesting that intake dilution (EGR) has no significant effect on efficiency at the EGR levels investigated. It should be noted that very high dilution ratios (>40% EGR) were not tested; it is likely that, at conditions where combustion instability is very high, processes that reduce the combustion variability will enhance the combustion efficiency.

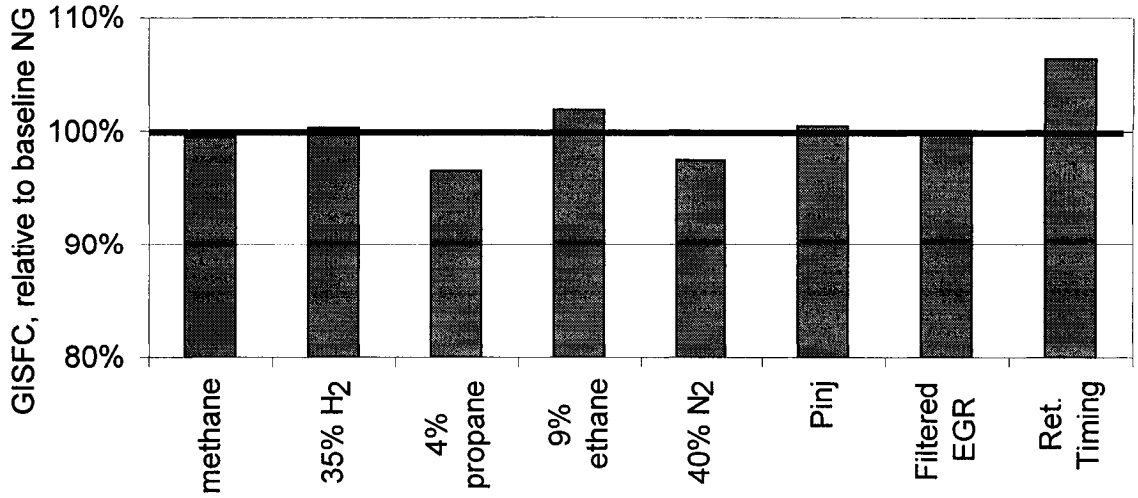

Figure 9.6: Changes (relative to natural gas) in fuel efficiency (GISFC), at 1200 RPM for fuel composition, injection pressure (Pinj), and filtered EGR tests, as well as for retarded timing conditions. All (except retarded) at 50%IHR = 10°ATDC, ~30% EGR

Engine Operating Conditions

The strong interactions between the engine's operating condition, the fuel composition, and the injection pressure indicate that multiple mechanisms are contributing to the formation of any given pollutant. These findings reinforce results from studies of other combustion systems which have shown that at different operating conditions, different pollutant formation mechanisms are dominant. For PIDING combustion, the combustion process responds differently to hydrogen addition under low-load and high-load conditions, with increases in combustion intensity at low load, but reduced combustion intensity at high load. Furthermore, the effects of injection pressure on CO emissions were contradictory between low and high engine speeds at the same intake dilution fraction and engine load. Even variations in combustion timing at constant operating condition have a significant effect; for example, while nitrogen dilution reduced PM emissions at most timings, at the earliest timing, the PM emissions increased significantly. These findings demonstrate the importance of conducting tests over the widest possible range of combustion conditions.

9.2 Engine System Implications

The conclusions outlined in the previous section have significant implications for optimizing engines using direct-injection gaseous-fuelled combustion systems. While not all the results are directly applicable to commercially competitive applications, they do provide considerable guidance for engine development.

The results indicate that increasing injection pressure tends to result in significant emissions reductions with no fuel conversion efficiency penalty (excluding compression work), especially at high load conditions. The impact of increased compression work can be minimized with a liquefied natural gas fuel storage system using a cryogenic pump to reach the desired pressures; however, this adds substantial system complexities. Increased injection pressures are most beneficial at conditions with higher in-cylinder pressures, which are typically the conditions where engine loads are highest. As a result, for a compressed natural gas system, increasing injection pressures with load would minimize the parasitic compressor work as a fraction of total engine power over the entire engine operating range. The injection pressure could be controlled using the engine's on-board computer.

The experimental results further indicate that techniques which enhance the late stage combustion process through enhanced in-cylinder turbulence also help to minimize emissions. While the addition of large quantities of nitrogen to the fuel as a diluent can satisfy this requirement, this increases both the compressor work and the storage volume, not to mention increased infrastructure system complexity. One potential technique for improving the late-cycle combustion would be to enhance the in-cylinder charge motion, either through modifications to the combustion chamber shape or through variations in the injection process, including multiple injections or variations in the injection rate.

The use of hydrogen as an additive to natural gas is a more likely alternative than nitrogen addition. Even in this case, however, there are significant potential barriers in this case, including reduced energy densities, higher compression work requirements, and more complex infrastructure requirements. However, this technique can achieve significant local air pollutant and GHG emission reductions. A potential opportunity would be to develop multiple calibrations of the engine system on a variety of hydrogen - natural gas blend compositions. Using this technique, engine efficiency could be optimized through the use of more advanced timings and higher levels of EGR (to control NO_x) when hydrogen levels are

high enough to ensure that PM emissions remain below legislated levels. Another possibility would be to offer a reduced aftertreatment system (potentially eliminating the PM trap, for example) if the engine is only to be run on hydrogen-blended natural gas. These are just two examples of techniques that could be used to maximize the effectiveness of hydrogen-blended gaseous-fuelled combustion systems

Varying natural gas compositions pose a significant challenge to engine developers, as the engine must be calibrated to meet emissions standards while still operating efficiently over the full range of fuel compositions. The results presented here indicate that while heavy hydrocarbon content does not significantly affect the combustion progression, it does substantially influence emissions. As a result, development of the engine system, including injection processes and aftertreatment, will need to ensure that emissions are not excessive with the worst fuel blends; this will result in higher system costs and reduced efficiency, even when normally high purity fuels are used. Adjusting the injection timing based on onboard sensing of fuel composition is one alternative to overcome this drawback; however, the substantial increases in PM observed with the levels of ethane and propane tested in this work suggest that substantially greater PM aftertreatment requirements are unavoidable if 'dirtier' fuel blends are to be accommodated. One option would be for regulators to provide a fuel quality standard for natural gas, similar to the standards in place for gasoline and diesel. Another solution would be to provide a fuel quality requirement for the engine, potentially in the form of a ξ value, which would allow increased levels of heavier hydrocarbons to be offset by H_2 or N_2 addition to the fuel.

The findings of this research indicate that there is no significant benefit for the combustion process in filtering the exhaust before it is recirculated in an EGR system. If a particulate filter is required to control PM emissions, the increased back-pressure generated by this system could be used to help generate the pressure differential needed to force some of the exhaust gases back into the intake stream. Furthermore, by reducing the flow rate of exhaust through the exhaust particulate filter, the size of the filter and its corresponding cost could be reduced. However, offsetting these benefits would be the potential for significant fouling of the intake system through the particulate carried with the recirculated exhaust gases. These are trade-offs which must be considered in the development of the engine

system; the results from this work may provide some further insight which can be applied when making design decisions.

9.3 Study Limitations

The work presented in this study provides insight into the combustion process of a direct-injection, natural gas fuelled engine. In general, fuel availability and system restrictions resulted in the testing being carried out over a limited range of operating conditions. The applicability of these results to extreme operating conditions, such as those encountered under very high charge dilution conditions or while undergoing transient engine operations is uncertain.

The experiments were conducted on a multi-cylinder engine modified for single cylinder operation. This maximized the similarity of the single cylinder engine, as the stock combustion chamber and intake and exhaust flow geometries were retained. The operating conditions were also selected to be as close as possible to those of an equivalent multi-cylinder engine. Despite these efforts, potential differences between the single-cylinder and an equivalent mutli-cylinder engine include differences in the magnitude and phasing of the pressure pulsations in the intake and exhaust system. These may cause differences in the charge motion and residual gas fraction between the single- and multi-cylinder engines. Pressure fluctuations in the fuel rails of the multi-cylinder engine due to the firing of neighbouring cylinders may also introduce significant influences which would not have been observed in the single-cylinder engine. These factors are of significant concern when considering absolute performance and emissions values; however, there is no reason to expect that the general effects identified in this work should be different between the single and multi-cylinder engines.

The results presented here, and the conclusions based on them, are drawn from an understanding of the composition of the intake and exhaust streams and a basic understanding of the combustion process as provided by the in-cylinder pressure. As no optical access into the combustion chamber was available, it was not possible to verify the conclusions based on visual observations of the combustion process. Potentially, further insight into the overall combustion process, as well as details regarding pollutant formation, could be achieved through a study of similar combustion processes in an optically-accessible engine.

9.4 Future Work

The results from the studies discussed here provide insight into some of the aspects of a direct injection natural gas combustion system. They also provide guidance for what aspects of future research might be pursued to achieve further reductions in emissions and improvements in efficiency.

The current work suggests that improving the late-cycle combustion process may achieve significant reductions in emissions of particulate matter, hydrocarbons and carbon monoxide. One of the drawbacks of the current combustion system is that the piston bowl shape is optimized for diesel combustion. Given the differences in the combustion processes between liquid diesel sprays and gaseous jets, it is very likely that the current geometry is suboptimal for the combustion of natural gas. As a result, substantial performance improvements may be achieved by modifying the combustion chamber geometry. However, addressing this issue will require careful planning, as the best technique would use an accurate combustion model validated against high quality experimental results. Currently, there is no combustion model that is adequately validated; nor do the experimental techniques provide sufficient information to reliably validate the details of combustion models. Almost certainly, quantified optical measurements of the charge motion within the combustion chamber will be required to provide model validation. In the meantime, some indication of possible combustion chamber improvements may be achieved through the experimental investigation of engine performance and emissions using various combustion chamber geometries. These results can be compared to simulation results to provide potential techniques to optimize the overall combustion process.

The use of multiple injections or injection rate-shaping may offer benefits which are complementary to combustion chamber optimization. By avoiding excessive gaseous-fuel premixing, emissions of unburned hydrocarbons can be reduced. Further, by providing a secondary injection of fuel, it may be possible to enhance fuel-air mixing and thereby augment the late-cycle combustion process. This could provide significant reductions in CO, HC, and PM emissions, although there could be a fuel efficiency penalty. The use of rate-shaping, where the injection rate is varied during the injection process by varying the injector needle lift, may also provide substantial benefits. As an initial step, starting with a relatively low injection rate prior to ignition would reduce early overmixing of the fuel and charge.

Increasing the injection rate late in the cycle could achieve substantial late-cycle combustion benefits. These techniques have the advantage that they could be optimized individually at every operating condition. Other parameters, such as the physical features of the injector (hole size, injection angle, or hole number, for example) are fixed and hence cannot be optimized for different operating conditions. However, optimization of the injector geometry, in conjunction with injection process and combustion chamber geometry improvements, is required to provide the best possible combustion system. The interrelatedness of a multitude of variables underlines the complexity of the optimization challenge. The fundamental requirement to assess all these variables concurrently reinforces the need to develop an efficient numerical model which can provide reasonable predictions of performance and pollutant formation to supplement experimental tests.

The influence of fuel composition on the combustion process and corresponding emissions are highlighted in the current work. The effects of some of the principal constituents in natural gas have been studied. However, further research over a wider range of operating conditions could provide information on the effect of small variations in natural gas composition. As well, there is a requirement for further research into the effects on engine operation of non-traditional gaseous additives. For example, coal synthesis gas (composed of large quantities of CO and H_2), landfill gas, or oxygenated biogases might be added to natural gas. The implications for global climate change and energy security concerns would be, in all likelihood, highly beneficial. However, negative impacts on combustion performance or overall emissions could put an unacceptably high price on any benefits. Substantially more research is required, at both fundamental and applied levels, to determine what role these fuel compositions could play as the engine evolves to meet the inseparable criteria of performance, efficiency, economic optimization, and environmental responsibility.

References

[1] Pischinger, S. The future of vehicle propulsion – combustion engines and alternatives. Topics in Catalysis. **30/31**. 2004. Pp. 5-16.

[2] Environment Canada. 2000 Criteria Air Contaminant Emissions Summary. Available from: www.ec.gc.ca/pdb/cac/ape_tables/canada2000_e.html. Accessed 28-11-2005.

[3] Seaton, A., W. MacNee, K. Donaldson, and D. Godden. Particulate air pollution and acute health effects. Lancet, 1995, **345** pp 176-178.

[4] Dockery, D.W., C.A. PopeIII, X. Xu *et al.* An association between air pollution and mortality in six US cities. New England Journal of Medicine, **329**, pp 1753-1759. 1993.

[5] Ontario Medical Association, The Illness Costs of Air Pollution. 2005-2026 Health & Economic Damage Estimates. 2005. Available from: www.oma.org/Health/smog/report/ICAP2005_Report.pdf. Accessed 27/11/2005.

[6] Seinfeld, J.H. and S.N. Pandis. Atmospheric Chemistry and Physics of Air Pollution: From Air Pollution to Global Climate Change. Wiley-interscience, New York, 1998.

[7] Pope, C.A. III, R.T. Burnett, M.J. Thun *et al.* Lung Cancer, Cardiopulmonary Mortality, and Long-Term Exposure to Fine Particulate Air Pollution. Journal of the American Medical Association, **287**. 2002. Pp. 1132-1143.

[8] Burnett, R.T., J.Brook, T. Dann, *et al.* Association between Particulate and Gas-Phase Components of Urban Air Pollution and Daily Mortality in Eight Canadian Cities. Inhalation Toxicology. **12**(supp. 4). 2000. Pp. 15-39

[9] Jerrett, M., R.T. Burnett, R. Ma, *et al.* Spatial Analysis of Air Pollution and Mortality in Los Angeles. Epidemiology. **16**(6). 2005. Pp. 727-736.

[10] Gauderman, W.J., E. Avol, F. Gilliland, *et al.* The Effect of Air Pollution on Lung Development from 10 to 18 Years of Age. New England Journal of Medicine. **351**(11). 2004. Pp. 1057-1067.

[11] Hahn, F.F., E. Barr, M.G. Menache and J.C. Seagrave. Particle Size and Composition Related to Adverse Health Effects in Aged, Sensitive Rats. Health Effects Institute Research Report 129. 2005. Available from: http://www.healtheffects.org/Pubs/Hahn.pdf. Accessed 7/12/2005.

[12] Oberdorster, G. Toxicology of ultrafine particles: *in vivo* studies. Philosophical Transactions of the Royal Society of London, A. **358**. 2000. Pp. 2719-2740.

[13] Biswas, P. and C.Y. Wu. Nanoparticles and the Environment. Journal of the Air and Waste Management Association. **55**. 2005. Pp. 708-746.

[14] Renwick. L.C., D. Brown, A. Clouter and K. Donaldson. Increased inflammation and altered macrophage chemotactic responses caused by two ultrafine particle types. Occupational and Environmental Medicine. **61**. 2002. Pp. 442-447.

[15] Donaldson, K., X.Y. Li and W. MacNee. Ultrafine (nanometer) particle-mediated lung injury. Journal of Aerosol Science, **29**. 1998. Pp. 553-560.

[16] Nemmar, A., P.H.M. Hoet, B. Vanquickenborne *et al.* Passage of inhaled paticles into the blood circulation in humans. Circulation **105**(4), 2002. Pp. 411-414.

[17] Delfino, R.J., C. Sioutas and S. Malik. Potential Role of Ultrafine Particles in Associations between Airborne Particle Mass and Cardiovascular Health. Environmental Health Perspectives, **113**(8). 2005. Pp. 934-946.

[18] Kittelson, D.B. Engines and Nanoparticles: A Review. Journal of Aerosol Science, **29**(5/6). pp. 575-588, 1998.

[19] Kagawa, J. Health effects of diesel exhaust emissions – a mixture of air pollutants of worldwide concern. Toxicology. 181-182. 2002. Pp. 349-353.

[20] California Air Resources Board. ARB Almanac 2003—Chapter 5: Toxic Air Contaminant Emissions, Air Quality, and Health Risk. Available from: www.arb.ca.gov/aqd/almanac/almanac03/pdf/chap503.pdf. Accessed 30/11/2005.

[21] Marr, L.C. and R.A. Harley. Spectral analysis of weekday-weekend differences in ambient ozone, nitrogen oxide, and non-methane hydrocarbon time series in California. Atmospheric Environment. **36**. 2002. Pp. 2327-2335.

[22] Fujita, E.M., W.R. Stockwell, D.E. Campbell, R.E. Keislar and D.R. Lawson. Evolution of the Magnitude and Spatial Extent of the Weekend Ozone Effect in California's South Coast Air Basin, 1981-2000. Journal of the Air and Waste Management Association. **53**(7). 2003. Pp. 802-815.

[23] Lawson, D.R. The Weekend Ozone Effect – The Weekly Ambient Emissions Control Experiment. EM(AWMA). July 2003. Pp. 17-26.

[24] Intergovernmental Panel on Climate Change (IPCC). Third Assessment Report, 2001. Available from: http://www.ipcc.ch/pub/online.htm. Accessed 07/04/06.

[25] Code of Federal Regulations (CFR) 40 Parts 69, 80, and 86: Control of Air Pollution from New Motor Vehicles: Heavy Duty Engine and Vehicle Standards and Highway Diesel Fuel Sulfur Control Requirements; Final Rule. US Federal Register. **66**(12). Pp. 5002-5050. 2001

[26] On Road Vehicle and Engine Emissions Regulations. Canada Gazette Part II. **137**(1). 2003. Pp. 21-27.

[27] Diesel Emissions Standards as published on www.dieselnet.org . Available from: www.dieselnet.org/standards. Accessed 23/01/2006.

[28] Heywood, J.B. Internal Combustion Engine Fundamental. McGraw-Hill, New York. 1988.

[29] Johnson, T.V. Diesel Emission Control Technology – 2003 in Review. SAE Technical Paper 2004-01-0070. 2004.

[30] Poulopoulos, S.G., D.P. Samara and C.J. Philippopoulos. Regulated and speciated hydrocarbon emissions from a catalyst equipped internal combustion engine. Atmospheric Environment (35). 2001. Pp. 4443-4450.

[31] Ayala, A., M.E. Gebel, R.A. Okamoto *et al.* Oxidation Catalyst Effect on CNG Transit Bus Emissions. SAE Technical Paper 2003-01-1900. 2003.

[32] Andersson, B., N. Cruise, M. Lunden et al. Methane and Nitric Oxide Conversion Over a Catalyst Dedicated for Natural Gas Vehicles. SAE Technical Paper 2000-01-2928. 2000.

[33] Hirasawa, Y., Y. Tanaka, Y. Banno and M. Nagata. Development of Methane Oxidation Catalyst and Its Mechanism. SAE Technical Paper 2005-01-1098. 2005.

[34] Chatterjee, S., C. McDonald, R. Conway, *et al.* Emission Reductions and Operational Experiences with Heavy Duty Diesel Fleet Vehicles Retrofitted with Continuously Regenerated Diesel Particulate Filters in Southern California. SAE Technical Paper 2001-01-0512

[35] Anon. Global Activity Blossoms as World Demand Climbs. World Oil. **226**(9). 2005.

[36] US Energy Information Agency (EIA). US Natural Gas Imports. Available from: http://tonto.eia.doe.gov/dnav/ng/ng_move_impc_s1_a.htm. Accessed 13/07/2006.

[37] Warnatz, J., U. Maas, and R.W. Dibble. Combustion. Physical and Chemical Fundamentals, Modeling and Simulation, Experiments, Pollutant Formation. 2nd Ed. Springer-Verlag, Berlin. 1999.

[38] McTaggart-Cowan, G.P., S.N. Rogak, P.G. Hill, W.K. Bushe and S.R. Munshi. Effects of Operating Condition on Particulate Matter and Nitrogen Oxides Emissions from a Heavy-Duty Direct Injection Natural Gas Engine using Cooled Exhaust Gas Recirculation. International Journal of Engine Research. **5**(6). 2004. Pp. 499-511.

[39] Hill, P.G. and G.P. McTaggart-Cowan. Nitrogen Oxide Production in a Diesel Engine Fueled by Natural Gas. SAE Technical Paper 2005-01-1727. SAE Transactions, Journal of Engines. **114**(3). 2005.

[40] Goudie, D., M.Dunn, S.R. Munshi, E. Lyford-Pike, J. Wright, V. Duggal and M. Frailey. Development of a Compression Ignition Heavy Duty Pilot-Ignited Natural Gas Fuelled Engine for Low NOx Emissions. SAE Technical Paper 2005-01-2954. 2005.

[41] Attar, A.A. and G. A. Karim. Knock Rating of Gaseous Fuels. ASME Journal of Engineering for Gas Turbines and Power. **125**, April 2003. Pp. 500-504.

[42] Kabori,S., T. Kamimoto and A.A. Aradi. A Study of Ignition Delay of Diesel Fuel Sprays. International Journal of Engine Research. **1**(1). 2000. Pp. 29-39.

[43] Huang, J., P.G. Hill, W.K. Bushe and S.R. Munshi. Shock-Tube Study of Methane Ignition Under Engine-Relevant Conditions: Experiments and Modelling. Combustion and Flame. **136**(1-2). 2004. Pp. 25-42.

[44] Dale, J.D., M.D. Checkel and P.R. Smy. Application of High Energy Ignition Systems to Engines. Progress in Energy and Combustion Science. **23**(5-6). 1997. Pp. 379-398.

[45] Reynolds, C.C.O.B. and R.L. Evans. Improving emissions and performance characteristics of lean burn natural gas engines through partial stratification. International Journal of Engine Research. **5**(1), 2004. Pp. 105-114.

[46] Chen, S.K. and N.J. Beck. Gas Engine Combustion Principles and Applications. SAE Technical Paper 2001-01-2489. 2001.

[47] John Deere Power Systems, Specification Sheet for 6081H Natural Gas Engine. Available from: http://jdpsesc.deere.com/ESComp/servlet/com.deere.enginedb.servlet.model2.EngineSearchResultsServlet. Accessed 19-01-2006.

[48] MAN Engines and Components. Available from: http://www.man-engines.com/en/Productsand Solutions/Vehicle_engines/Gas_engines.jsp. Accessed 20-01-2006.

[49] Cummins-Westport Inc. Specification sheets for B-gas, C-gas, and L-gas engines. Available from: http://www.cumminswestport.com/products/index.php. Accessed 19-01-2006.

[50] Chandler, K.L, P. Norton and N. Clark. Interim Results from Alternative Fuel Truck Evaluation Project. SAE Technical Paper 1999-01-1505. 1999.

[51] Ayala, A., N.Y Kado, R. A. Okamoto *et al.* Diesel and CNG Heavy-Duty Transit Bus Emissions Over Multiple Driving Schedules : Regulated Pollutants and Project Overview. SAE Technical Paper 2002-01-1722.

[52] Frailey, M., P. Norton, N.N. Clark and D. W. Lyons. An Evaluation of Natural Gas versus Diesel in Medium Duty Buses. SAE Technical Paper 2000-01-2822.

[53] McCormick, R.L., M.S. Graboski, T. Alleman *et al.*In-Use Emissions from Natural Gas Fueled Heavy-Duty Vehicles. SAE Technical paper 1999-01-1507.

[54] Kado, N.Y, R. A. Okamoto, P.A. Kuzmicky *et al.* Emissions of Toxic Pollutants from Compressed Natural Gas and Low Sulfur Diesel-Fueled Heavy-Duty Transit Buses Tested over Multiple Driving Cycles. Environmental Science and Technology. **39**. 2005. Pp. 7638-7649.

[55] Seagrave, J.C., A. Gigiliotti, J.D. McDonald, *et al.* Composition, Toxicity, and Mutagenicity of Particulate and Semivolatile Emissions from Heavy-Duty Compressed Natural Gas-Powered Vehicles. Toxicological Sciences. **87**(1). 2005. Pp. 232-241.

[56] Holmen, B.A. and A. Ayala. Ultrafine PM Emissions from Natural Gas, Oxidation-Catalyst Diesel and Particle-Trap Diesel Heavy-Duty Transit Buses. Environmental Science and Technology. **36**. 2002. Pp. 5041-5050.

[57] Kamel, M., E. Lyford-Pike, M. Frailey *et al.* An Emissions and Performance Comparison of the Natural Gas Cummins Westport Inc. C-Gas Plus Versus Diesel in Heavy-Duty Trucks. SAE Technical Paper 2002-01-2737.

[58] Melendez, M., J. Taylor, J. Zuboy, W.S. Wayne and D. Smith. Emission Testing of Washington Metropolitan Area Transit Authority (WMATA) Natural Gas and Diesel Transit Buses. NREL Report NREL/TP-540-36355. December 2005. Available from: http://www.nrel.gov/docs/fy06osti/36355.pdf . Accessed 26-04-2006

[59] Chiu, J.P., J. Wegrzyn and K.E. Murphy. Low Emissions Class 8 Heavy-Duty On-Highway Natural Gas and Gasoline Engine. SAE Technical Paper 2004-01-2982.

[60] Nellen, C. and K. Boulouchos. Natural Gas Engines for Cogeneration: Highest Efficiency and Near-Zero Emissions through Turbocharging, EGR and 3-Way Catalytic Converter. SAE Technical Paper 2000-01-2825.

[61] Park, T., R.J. Atkinson, N.N. Clark *et al.* Operation of a Compression Ignition Engine with a HEUI Injection System on Natural Gas with Diesel Pilot Injection. SAE Technical Paper 1999-01-3522. 1999.

[62] Wartsila. Wartsila 32DF Technology Review. Available at: http://www.wartsila.com/Wartsila/docs/en/ship_power/media_publications/brochures/product/engines/w32df_tr.pdf . Accessed 20-01-2006.

[63] Fairbanks-Morse. Available from: http://www.fairbanksmorse.com/engines/index.htm. Accessed 20-01-2006.

[64] MAN engines. Available from: http://www.manbw.com/products. Accessed 20-01-2006.

[65] Singh, S., S.R. Krishnan, K.K. Srinivasan, K.C. Midkiff and S.R. Bell. Effect of pilot injection timing, pilot quantity and intake charge conditions on performance and emissions for an advanced low-pilot-ignited natural gas engine. International Journal of Engine Research, **5**(4). 2004. Pp. 329-348.

[66] Zuo, C. and M. Yang. Operating Characteristics and Description of a Dual Fuel Engine for Diesel-Natural Gas Heavy-Duty Operation. SAE Technical Paper 1999-01-3523. 1999.

[67] Shenghua, L., W. Ziyan and R. Jiang. Development of compressed natural gas/diesel dual-fuel turbocharged compression ignition engine. Proceedings of the Institution of Mechanical Engineers, Part D – Journal of Automobile Engineering. **217**. 2003. Pp. 839-845.

[68] Pappagianakis, R.G., and D.T. Hountalas. Combustion and exhaust emissions characteristics of a dual fuel compression ignition engine operated with pilot Diesel fuel and natural gas. Energy Conversion and Management. **45**. 2004. Pp. 2971-2987.

[69] Wong, H.C. Next Generation Natural Gas Vehicle Program Phase I: Clean Air Power 0.5 g/hp-h NOx Engine Report – Final Report. NREL Report, NREL/SR-540-33957. July, 2003.

[70] Hiltner, J., S. Fivelan, R. Agama and M. Willi. System Efficiency Issues for Natural Gas Fueled HCCI Engines in Heavy-Duty Stationary Applications. SAE Technical Paper 2002-01-0417. 2002.

[71] Stanglmaier, R.H., T.W. Ryan and J.S. Souder. HCCI Operation of a Dual-Fuel Natural Gas Engine for Improved Fuel Efficiency and Ultra-Low NOx Emissions at Low to Moderate Engine Loads. SAE Technical Paper 2001-01-1897, 2001.

[72] Tominaga, R., S. Morimoto, Y. Kawabata *et al.* Effects of Heterogeneous EGR on the Natural Gas Fueled HCCI Engine Using Experiments, CFD and Detailed Kinetics. SAE Technical Paper 2004-01-0945. 2004.

[73] Huang, Z., S. Shiga, T. Ueda *et al.* Combustion Characteristics of Natural-Gas Direct Injection Combustion under Various Fuel Injection Timings. Proceedings of the Institution of Mechanical Engineers, Part D. Journal of Automobile Engineering. **217**. 2003. Pp. 393-401.

[74] F. Zhao, M.-C. Lai and D.L. Harrington, Automotive spark-ignited direct-injection gasoline engines. Progress in Energy and Combustion Sciences. **25**. 1999. Pp. 437–562.

[75] Aesoy, V. and H. Valland. Hot Surface Assisted Compression Ignition of Natural Gas in a Direct Injection Diesel Engine. SAE Technical Paper 960767, 1996.

[76] Caterpillar Inc. Development of a Direct-Injected Natural Gas Engine for Heavy Duty Vehicles. Phase 1 Report. NREL Report NREL/SR-540-27500. 2000.

[77] Rubas, P.J., M.A. Paul, G.C. Martin, R. Coverdill, R. Lucht, J. Peters, K. DelVecchio. Methane Jet Penetration in a Direct-Injection Natural Gas Engine. SAE Technical Paper 980143, 1998.

[78] Okada, M., H. Sugii, T. Wakao *et al.* Development of CNG Direct Injection Diesel-Cycle Engine. Proceeding of NGV 2004, 2004.

[79] Chandler, K. and K. Proc. Norcal Prototype LNG Truck Fleet: Final Results. U.S. Department of Energy Advanced Technology Vehicle Evaluation Report. July, 2004. Available from: http://www.eere.energy.gov/afdc/pdfs/36707.pdf Accessed 26-04-2006.

[80] Garner, G., K. Komuniecki, K. Wadley and B. Zehr. Clean Air Corridor Mid-Trial Report. Westport Innovations Inc. March 10, 2006. Available from: http://www.westport.com/programs/norcal.php. Accessed 26-04-2005.

[81] California Air Resources Board. Executive Order A-343-0003. Available from: http://www.arb.ca.gov/msprog/onroad/cert/mdehdehdv/2006 /westport_hhdd_a3430003_14d9_1d2-0d02_cngplusdiesel.pdf. Accessed 26-04-2006.

[82] Williams, G., K. Tanin, R. Ancimer *et al.* High Performance HCCI Natural Gas Technology for Distributed Generation. Proceedings of the 2005 Spring Technical Conference of the ASME Electric Power Conference. Paper # ICES05-55859. 2005.

[83] Turner, J.S. The 'Starting Plume' in Neutral Surroundings. Journal of Fluid Mechanics, 1962. **13**(3). Pp. 356-371.

[84] Hill, P.G. and P. Ouellette. Transient Turbulent Gaseous Fuel Jets for Diesel Engines. ASME Journal of Fluids Engineering. **121**. 1999. Pp. 93-101.

[85] Cossali, G.E., A. Coghe and L. Araneo. Near-Field Entrainment in an Impulsively Started Turbulent Gas Jet. Journal of the American Institute of Aeronautics and Astronautics. **39**(6). 2001. Pp. 113-1121.

[86] Petersen, B.R. and J.B. Ghandi. Transient High-Pressure Hydrogen Jet Measurements. SAE Technical Paper 2006-01-0652. 2006.

[87] Li, G., P. Ouellette, S. Dumitrescu, and P.G. Hill. Optimization Study of Pilot-Ignited Natural Gas Direct-Injection in Diesel Engines. SAE Technical Paper 1999-01-3556. SAE Transactions, Journal of Fuels and Lubricants. **108**(4). 1999.

[88] Dumitrescu, S., P.G. Hill, G. Li and P. Ouellette. Effects of Injection Changes on Efficiency and Emissions of a Diesel Engine Fueled by Direct Injection of Natural Gas. SAE Technical Paper 2000-01-1805. 2000.

[89] Sullivan, G.D., J. Huang, T.X. Wang, W. K. Bushe and S.N. Rogak. Emissions Variability in Gaseous Fuel Direct Injection Compression Ignition Combustion. SAE Technical Paper 2005-01-0917, 2005.

[90] Muniz, L. and M.G. Mungal. Instantaneous Flame-Stabilization Velocities in Lifted-Jet Diffusion Flames. Combustion and Flame. **111**(1-2). 1997. Pp. 16-30.

[91] Nishioka, M., Y. Kondoh and T. Takeno. Behaviour of Key Reactions on NO Formation in Methane-Air Flames. 26th International Symposium on Combustion. The Combustion Institute. 1996. Pp. 2139-2145.

[92] Easley, W.L. and A.M. Mellor. NO Decomposition in Diesel Engines. SAE Technical Paper 1999-01-3546. 1999.

[93] Ahmad, T. and S.L. Plee. Application of Flame Temperature Correlations to Emissions from a Direct-Injection Diesel Engine. SAE Technical Paper 831374. 1983.

[94] Tsurushima, T., L. Zhang and Y. Ishii. A Study of Unburnt Hydrocarbon Emission in small DI diesel engines. SAE Technical Paper 1999-01-0512. 1999.

[95] Shi, J.P. and R.M. Harrison. Investigation of Ultrafine Particle Formation during Diesel Exhaust Dilution. Environmental Science and Technology. **33**(21). 1999. Pp. 3730-3736.

[96] Baumgard, K. and J.H. Johnson. The effect of fuel and engine design on diesel exhaust particle size distributions. SAE Technical Paper 960131. 1996.

[97] Lev-On, M., C. LeTavec, J.Uihlein, T.L. Alleman, D.R. Lawson, K. Vertin, G.J. Thompson, M. Gautam, S. Wayne, B. Zielinska, J. Sagebiel. Chemical Speciation of Exhaust Emissions from Trucks and Buses Fueled on Ultra-Low Sulfur Diesel and CNG. SAE Technical Paper 2002-01-0432. 2002.

[98] Lloyd, A.C. and T.A. Cackette. Diesel Engines: Environmental Impact and Control. Journal of the Air and Waste Management Association **51**(6). 2001. Pp. 809-847.

[99] Khalek, I. A., D.B. Kittelson and F. Brear. Nanoparticle Growth During Dilution and Cooling of Diesel Exhaust: Experimental Investigation and Theoretical Assessment. SAE Technical Paper 2000-01-0515. 2000.

[100] Frenklach, M. Reaction Mechanism of Soot Formation in Flames. Physical Chemistry and Chemical Physics. **4**. 2002. Pp. 2028-2037.

[101] Tao, F., V.I. Golovitchev, J. Chomiak. A Phenomological Model for the Prediction of Soot Formation in Diesel Spray Combustion. Combustion and Flame. **136**. 2004. Pp. 270-282.

[102] Flynn, P.F., R.P. Durrett, G.L. Hunter, A.O.Z. Loye, O.C. Akinyemi, J.E. Dec and C.K. Westbrook. Diesel Combustion: An Integrated View Combining Laser Diagnostics, Chemical Kinetics, and Empirical Validation. SAE Technical Paper 1999-01-0509. 1999.

[103] Krestinin, A.V. Detailed Modeling of Soot Formation in Hydrocarbon Pyrolysis. Combustion and Flame. **121**. 2000. pp. 513-524.

[104] Higgins, K.J., H. Jung, D.B. Kittelson, J.T. Roberts and M.R. Zachariah. Kinetics of Diesel Nanoparticle Oxidation. Environmental Science and Technology. **37**. 2003. Pp. 1949-1954.

[105] Song, H., N. Ladommatos and H. Zhao. Diesel Soot Oxidation under Controlled Conditions. SAE Technical Paper 2001-01-3673. 2001.

[106] Roesler, J.F., S. Martinot, C.S. McEnally, L.D. Pfefferle, J.L. Delfau and C. Vovelle. Investigating the Role of Methane on the Growth of Aromatic Hydrocarbons and Soot in Fundamental Combustion Processes. Combustion and Flame. **134**. 2003. Pp. 249-260.

[107] McCrain, L.L. and W.L. Roberts. Measurements of the soot volume field in laminar diffusion flames at elevated pressure. Combustion and Flame. **140**. 2005. Pp. 60-69.

[108] Thomson, K.A., O.L. Gulder, E.J. Weckman, R.A. Fraser, G.J. Smallwood and D.R. Snelling. Soot Concentration and Temperature Measurements in Co-Annular, Non-Premixed CH_4/Air Laminar Flames at Pressures up to 4 MPa. Combustion and Flame. **140**. 2005. Pp. 222-232.

[109] Brookes, S.J. and J.B. Moss. Measurements of Soot Production and Thermal Radiation From Confined Turbulent Jet Diffusion Flames of Methane. Combustion and Flame. **116**. 1999. Pp. 49-61.

[110] Bohm, H., K. Kohse-Hoinghaus, F. Lacas, C. Rolon, N. Darabiha and S. Candel. On PAH Formation in Strained Counterflow Diffusion Flames. Combustion and Flame. **124**. 2001. Pp. 127-136.

[111] Skjoth-Rasmussen, M.S., P. Glarborg, M. Ostberg, J.T. Johannessen, H. Libbjerg, A.D. Jensen and T.S. Christense. Formation of Polycyclic Aromatic Hydrocarbons and Soot in Fuel-Rich Oxidation of Methane in a Laminar Flow Reactor. Combustion and Flame. **136**. 2004. Pp. 91-128.

[112] Gruenberger, T.M., M. Moghiman, P.J. Bowen and N. Syred. Dynamics of Soot Formation by Turbulent Combustion and Thermal Decomposition of Natural Gas. Combustion Science and Technology. **174**. 2002. Pp. 67-86.

[113] Smooke, M.D., C.S. McEnally, L.D. Pfefferle, R.J. hall and M.B. Colket. Computational and Experimental Study of Soot Formation in Coflow, Laminar Diffusion Flame. Combustion and Flame. **117**. 1999. Pp. 117-139.

[114] Zhu, X.L. and J.P. Gore. Radiation Effects on Combustion and Pollutant Emissions of High-Pressure Opposed Flow Methane/Air Diffusion Flames. Combustion and Flame. **141**. 2005. Pp. 118-130.

[115] Ning, Z., C.S. Cheung, S.X. Liu. Experimental Investigation of the Effect of Exhaust Gas Cooling on Diesel Particulate. Journal of Aerosol Science. **35**. 2004. Pp. 333-345.

[116] Luders, H., M. Kruger, P. Stommel, B. Luers. The Role of Sampling Conditions in Particle Size Distribution Measurements. SAE Technical Paper 981374. 1998.

[117] Mathis, U., J. Ristimaki, M. Mohr, J. Keskinen, L. Ntziachristos, Z. Samaras and P. Mikkanen. Sampling Conditions for the Measurement of Nucleation Mode Particles in the Exhaust of Diesel Engines. Aerosol Science and Technology. **38**. 2004. Pp. 1149-1160.

[118] Ingersoll, J.G. *Natural Gas Vehicles*. Fairmont Press, Upper Saddle River, New Jersey. 1996. p. 44.

[119] Yoon, S.S., S.M. Lee and S.H. Chung. Effect of Mixing Methane, Ethane, Propane, and Propene on PAH and Soot Formation in Ethylene Base Counterflow Diffusion Flames. Proceedings of the Combustion Institute. **30**. 2005. Pp. 1417-1424.

[120] Kuo, K. *Principles of Combustion. 2nd Ed.* Wiley, New York. 2005.

[121] Huang, J. and W.K. Bushe. Experimental and Kinetic Study of Autoignition in Methane/Ethane/Air and Methane/Propane/Air mixtures under Engine-Relevant Conditions. Combustion and Flame. **144**. 2006. Pp. 74-88

[122] McTaggart-Cowan, G.P., W.K. Bushe, P.G. Hill and S.R. Munshi. NOx Reduction from a Heavy-Duty Diesel Engine with Direct Injection of Natural gas and Cooled Exhaust Gas Recirculation. International Journal of Engine Research, **5**(2). 2004. Pp. 175-191.

[123] Ladommatos, N., S. Abdelhalim, H. Zhao. The Effects of Exhaust Gas Recirculation on Diesel Combustion and Emissions. International Journal of Engine Research. **1**(1). 2000. Pp. 107-126.

[124] Kreso, A.M., J.H Johnson, L.D. Gratz, S.T. Bagley and D.G. Leddy. A Study of the Effects of Exhaust Gas Recirculation on Heavy-Duty Diesel Engine Emissions. SAE Technical Paper 981422. 1998.

[125] Plee, S.L., T. Ahmad, J.P. Myers and G.M. Faeth. Diesel NO_x Emissions – A Simple Correlation Technique for Intake Air Effect. 19th International Sypmosium on Combustion. The Combustion Institute, Pittsburgh, Pa. 1982. Pp. 1495-1502.

[126] Flynn, P.F., G.L. Hunter, R.P. Durrett, L.A. Farrell and W.C. Akinyemi. Minimum engine flame temperature impacts on diesel and spark-ignition engine NOx production. SAE Technical Paper 2000-01-1177. 2000.

[127] Idicheria, C.A. and L.M Pickett. Soot Formation in Diesel Combustion under High-EGR Conditions. SAE Technical Paper 2005-01-3834. 2005.

[128] Alriksson, M., T. Rente and I. Denbratt. Low Soot, Low NOx in a Heavy Duty Diesel Engine Using High Levels of EGR. SAE Technical paper 2005-01-3836. 2005.

[129] Mastorakos, E., A.M. Taylor and J.H. Whitelaw. Extinction of Turbulent Counterflow Flames with Reactants Diluted by Hot Products. Combustion and Flame. **102**. 1995. Pp. 101-114.

[130] McTaggart-Cowan, G.P., W.K. Bushe, S.N. Rogak, P.G. Hill and S.R. Munshi. PM and NO_x Reduction by Injection Parameter Alterations in a Direct Injected, Pilot Ignited, Heavy Duty Natural Gas Engine with EGR at Various Operating Conditions. SAE Technical Paper 2005-01-1733. SAE Transactions, Journal of Engines. **114**(3). 2005.

[131] McTaggart-Cowan, G.P., W.K. Bushe, S.N. Rogak, P.G. Hill and S.R. Munshi. The Effects of Varying EGR Test Conditions on a Direct Injection of Natural Gas Heavy-Duty Engine with High EGR Levels. SAE Technical Paper 2004-01-2955. SAE Transactions, Journal of Engines. **113**(3). 2004. Pp. 1500-1509.

[132] Ouellette, P., P. Mtui and P.G. Hill. Numerical Simulations of Directly Injected Natural Gas and Pilot Diesel Fuel in a Two-Stroke Compression Ignition Engine. SAE Technical Paper 981400. 1998.

[133] Li, G., T. Lennox, D. Goudie and M. Dunn. Modeling HPDI Natural Gas Heavy Duty Engine Combustion. Proceedings of the ASME Internal Combustion Engine Division Fall Technical Conference. ASME Technical Paper ICEF2005-1307. 2005.

[134] Larson, C. Master's Thesis. University of British Columbia. 2002.

[135] McTaggart-Cowan, G.P., W.K. Bushe, S.N. Rogak, P.G. Hill and S.R. Munshi. Injection Parameter Effects on a Direct Injected, Pilot Ignited, Heavy Duty Natural Gas Engine with EGR. SAE Technical Paper 2003-01-3089. SAE Transactions, Journal of Fuels and Lubricants. **112**(4). 2003. Pp. 2103-2109.

[136] Yu, R.C. and S.M. Shahed. Effects of Injection Timing and Exhaust Gas Recirculation on Emissions from a D.I. Diesel Engine. SAE 811234. 1981.

[137] Harrington, J., S. Munshi, C. Nedelcu, P. Ouellette, J. Thomson and S. Whitfield. Direct Injection of Natural Gas in a Heavy-Duty Diesel Engine. SAE Technical Paper 2002-01-1630. 2002.

[138] Shen, J., J. Qin and M. Yao. Turbocharged CNG/Diesel Dual Fuel Engines with Intercooler: Combustion, Emissions, and Performance. SAE Technical Paper 2003-01-3082. 2003.

[139] Zhang, L. A Study of Pilot Injection in a DI Diesel Engine. SAE Technical Paper 1999-01-3493. 1999.

[140] Badami, M., F. Millo and D.D. D'Amato. Experimental Investigation on Soot and NO_x Formation in a DI Common-Rail Diesel Engine with Pilot Injection. SAE Technical Paper 2001-01-0657. 2001.

[141] Trueba, A., B. Barbeau, O. Pajot and K. Mokaddem. Pilot injection timing effect on the main injection development and combustion in a DI diesel engine. SAE Technical Paper 2002-01-0501. 2002.

[142] Jones, H.L., G.P. McTaggart-Cowan, S.N. Rogak, W.K. Bushe, S.R. Munshi and B.A. Buchholz. Source Apportionment of Particulate Matter from a Diesel Pilot-Ignited Natural Gas Fuelled Heavy Duty DI Engine. SAE Technical paper 2005-01-2149. SAE Transactions, Journal of Fuels and Lubricants. **114**(4). 2005.

[143] McTaggart-Cowan, G.P., W.K. Bushe, P.G. Hill and S.R. Munshi. A Supercharged Single-Cylinder Heavy-Duty Engine for High Pressure Direct Injection of Natural Gas. International Journal of Engine Research. **4**(4). 2004. Pp. 315-330.

[144] Harrington, J., S. Munshi, C. Nedelcu, P. Ouellette, J. Thompson and S. Whitfield. Direct Injection of Natural Gas in a Heavy-Duty Diesel Engine. SAE Technical Paper 2002-01-1630. 2002.

[145] Post, A.J., D. Mumford, B.D. Douville, S.M. Baker, T.M. Lennox, A.M. Touchette. Dual Fuel Injection Valve and Method of Operating a Dual Fuel Injection Valve. Canadian Patent Application #CA2465182. Filed Nov. 18 2002.

[146] United States Code of Federal Regulations (CFR)40 Part 1065. Engine Testing Procedures. Available From: http://ecfr.gpoaccess.gov/cgi/t/text/text-idx?c=ecfr&sid=0fcd6cf8e849852b2840c60b4ed53776 &rgn=div8&view=text&node=40:31.0.1.3.12.2.15.8&idno=40. Accessed 29-05-06.

[147] Holman, J.P. *Experimental Methods for Engineers, 7th ed.* McGraw-Hill, New York. 2001.

[148] Gilbert, M.S. and N.N. Clark. 2001. Measurement of Particulate Matter from Diesel Engine Exhaust Using a Tapered Element Oscillating Microbalance. International Journal of Engine Research, **2**(4). pp. 277-287.

[149] Okrent, D.A. Optimization of a third-generation TEOM^R monitor for measuring diesel particulate in real time. SAE Technical Paper 980409. 1998.

[150] United States Environmental Protection Agency. Particulate Filter Handling and Weighing. Reference #714D. Approved March 13 2006. Available from: www.epa.gov/otaq/emisslab/testproc/714d.pdf . Accessed 29-05-2006.

[151] Turpin, B.J., P. Saxena and E. Andrews. Measuring and Simulating Particulate Organics in the Atmosphere: Problems and Prospects. Atmospheric Environment. **34**(18). 2000. Pp. 2983-3013.

[152] Jarret, R.P. and N.N. Clark. Evaluation of Methods for Determining Continuous Particulate Matter from Transient Testing of Heavy-Duty Diesel Engines. SAE Technical Paper 2001-01-3573. 2001.

[153] Knutson, E.O. and K.T. Whitby. Aerosol Classification by Electric Mobility: Apparatus, Theory, and Applications. Journal of Aerosol Science, **6**. 1975. pp. 443-451.

[154] Wang, S.C. and R.C. Flagan. Scanning Electrical Mobility Spectrometer. Aerosol Science and Technology. **13**, 1990. Pp. 230-240.

[155] Burtscher, H. Physical Characterization of Particulate Emissions from Diesel Engines: A Review. Journal of Aerosol Science. **36**, 2005. Pp. 896-932.

[156] Kinsey, J.S., W.A. Mitchell, W.C. Squier, K. Linna, F.G. King, R. Logan, Y. Dong, G.J. Thompson and N.N. Clark. Evaluation of Methods for the Determination of Diesel-Generated Fine Particulate Matter: Physical Characterization Results. Journal of Aerosol Science. **37**(1). 2006. Pp. 63-87.

[157] Van Gulijk, C, JCM. Marijnissen, M. Makkee, JA. Moulijn and A. Schmidt-Ott Measuring Diesel Soot with a Scanning Mobility Particle Sizer and an Electrical Low Pressure Impactor: Performance Assessment with a Model for Fractal-Like Agglomerates. Journal of Aerosol Science. **35**. 2004. Pp. 633-655.

[158] Fuchs, N.A. On the Stationary Charge Distribution on Aerosol Particles in a Bipolar Ionic Atmosphere. Geophys. Pura Appl. 1963. pp. 56:185

[159] Virtanen, A., J. Ristimaki, M. Marjamaki, K. Vaaraslahti, J. Kesinen and M. Lappi. Effective Density of Diesel Exhaust Particles as a Function of Size. SAE Technical Paper 2002-01-0056. 2002.

[160] Park, K., F. Cao, D.B. Kittelson and P.H. McMurry Relationship Between Particle Mass and Mobility for Diesel Exhaust Particles. Environmental Science and Technology. **37**. 2003. Pp. 577-583.

[161] Rogak, S.N. and R.C. Flagan. Characterization of the Structure of Aerosol Particles. Particle and Particle Systems Characterization. **9**(1). 1992. Pp. 19-27.

[162] Virtanen, A., J. Ristimaki and J. Keskinen. Method for Measuring Effective Density and Fractal Dimension of Aerosol Agglomerates. Aerosol Science and Technology. **38**. 2004. pp. 437-446

[163] Koylu, U.O., G.M. Faeth, T.L. Farias and M.G. Carvalho. Fractal and Projected Structure Properties of Soot Aggregates. Combustion and Flame. **100**. 1995. Pp. 621-633.

[164] Skillas, G., S. Kunzel, H. Burtshcer, U. Baltensperger and K. Siegmann. High Fractal-Like Dimension of Diesel Soot Agglomerates. Journal of Aerosol Science. **29**(4). 1998. Pp. 411-419.

[165] Hansen, A.D.A., H. Rosen, T. Novakov. The Aethalometer – An Instrument for the Real-Time Measurement of Optical-Absorption by Aerosol Particles. Science of the Total Environment. **36**, 1984. Pp. 191-196.

[166] Wark, K. C.F. Warner and W. T. Davis. *Air Pollution: Its Origin and Control, 3rd ed.* Addison-Wesley. 1998.

[167] Weingartner, E., H. Saathoff, M. Schnaiter, N. Streit, B. Bitnar and U. Baltensperger. Absorption of Light by Soot Particles: Determination of the Absorption Coefficient by Means of Aethalometers. Journal of Aerosol Science. **34**, 2003. Pp. 1445-1463.

[168] McTaggart-Cowan, G.P. A Supercharged Single-Cylinder Research Engine for Direct Injection of Natural Gas. M.A.Sc. Thesis. University of British Columbia. 2001.

[169] Hicks, C.R. and K.V. Turner. *Fundamental Concepts in the Design of Experiments, 5th Ed.* Oxford University Press. 1999.

[170] Dodge, L., S. Simescu, G. Neely, M. Maymar, D. Dickey, and C. Savonen. Effect of Small Holes and High Injection Pressures on Diesel Engine Combustion. SAE Technical Paper 2002-01-0494. 2002.

[171] Benajes, J., S. Molina, J. Garci and R. Novella. Influence of Boost Pressure and Injection Pressure on Combustion Process and Exhaust Emissions in a HD Diesel Engine. SAE Technical Paper 2004-01-1842. 2004.

[172] Bertola, A., R. Schubiger, A. Kasper, U. Matter, A.M. Forss, M. Mohr, K. Boulouchos, and T. Lutz. Characterization of Diesel Particulate Emissions in Heavy-Duty DI Diesel Engines with Common Rail Fuel Injection - Influence of Injection Parameters and Fuel Composition. SAE Technical Paper 2001-01-3573. 2001.

[173] Morgan, R.E., M. Gold, O. Laguitton, C. Crua, and M. Heikal. Characterisation of the Soot Formation Processes in a High Pressure Combusting Diesel Fuel Spray. SAE Technical Paper 2003-01-3086. 2003.

[174] Rente, T., S. Gjirja, and I. Denbratt. Experimental Investigation of the Effect of Needle Opening (NOP) Pressure on Combustion and Emissions Formation in a Heavy Duty DI Diesel Engine. SAE Technical Paper 2004-01-2921. 2004.

[175] Shimazaki, N., H. Hatanaka, K. Yokota, and T. Nakahira. A Study of Diesel Combustion Process Under the Condition of EGR and High-Pressure Fuel Injection with Gas Sampling Method. SAE Technical Paper 960030. 1996.

[176] Singh, I., L. Zhong, M. Lai, N. Henein and W. Bryzik. Effect of Nozzle hole Geometry on a HSDI Diesel Engine-Out Emissions. SAE Technical Paper 2003-01-0704. 2003.

[177] Pagan, J. Study of Particle Size Distributions Emitted by a Diesel Engine. SAE Technical Paper 1999-01-1141. 1999.

[178] Collings, N. and B.R. Graskow. Particles from internal combustion engines – what we need to know. Philosophical Transactions of the Royal Society of London, Part A. **358**. 2000. pp. 2611-2623.

[179] Dec, J.E. A Conceptual Model of DI Diesel Combustion Based on Laser-Sheet Imaging. SAE Technical Paper 970873. 1997.

[180] Buick, B. Westport Innovations Inc. Personal Communications. July 2006.

[181] Abdul-Khalek, I., D.Kittelson, and F. Brear. The Influence of Dilution Conditions on Diesel Exhaust Particle Size Distribution Measurements. SAE Technical Paper 1999-01-1142. 1999.

[182] International Association of Natural Gas Vehicles. Available from: http://www.iangv.org/content/view/17/35/. Accessed 01-06-2006.

[183] Jorach, R., C. Enderle and R. Decker. Development of a Low-NOx Truck Hydrogen Engine with High Specific Power Output. Int. J. Hydrogen Energy, **22**(4), 1997. Pp. 423-427.

[184] Sorensen, H. The Boston Reformed Fuel Car – A Low Pollution Gasoline Fuel System for Internal Combustion Engines. SAE Technical Paper 729218, 1972.

[185] Houseman, J. and F.W. Hoehn. A Two-Charge Engine Concept: Hydrogen Enrichment. SAE Technical Paper 741169, 1974.

[186] Swain, M.R., M.J. Yusuf, Z. Dulger and M.N. Swain. The Effects of Hydrogen Addition on Natural Gas Engine Operation. SAE Technical Paper 932775, 1993.

[187] Sierens, R. and E. Rosseel. Variable Composition Hydrogen/Natural Gas Mixtures for Increased Engine Efficiency and Decreased Emissions. ASME Journal of Engineering for Gas Turbines and Power, **122**. 2000. Pp. 135-140.

[188] Munshi, S.R., C. Nedelcu, J. Harris, et al. Hydrogen Blended Natural Gas Operation of a Heavy Duty Turbocharged Lean Burn Spark Ignition Engine. SAE Technical Paper 2004-01-2956, 2004.

[189] Allenby, S., W-C. Chang, A. Megaritis and M.L. Wyszynski. Hydrogen Enrichment: A Way to Maintain Combustion Stability in a Natural Gas Fuelled Engine with Exhaust Gas Recirculation, the Potential of Fuel Reforming. Proceedings of the Institution of Mechanical Engineers, Part D. **215** 2001. Pp. 405-418.

[190] Collier, K., N. Mulligan, D. Shin and S. Brandon. Emission Results from the New Development of a Dedicated Hydrogen-Enriched Natural Gas Heavy Duty Engine. SAE Technical Paper 2005-01-0235, 2005.

[191] Larsen, J.F. and J.S. Wallace. Comparison of Emissions and Efficiency of a Turbocharged Lean-Burn Natural Gas and Hythane-Fueled Engine. ASME Journal of Engineering for Gas Turbines and Power, **119**. 1997. Pp. 218-226.

[192] Bauer, C.G. and T.W. Forest. Effect of hydrogen addition on the performance of methane-fueled vehicles. Part I: effect on S.I. engine performance. Int. J. of Hydrogen Energy, **26**. 2001. Pp. 55-70.

[193] Karim, G.A., I. Wierzba and Y. Al-Alousi. Methane-Hydrogen Mixtures as Fuels. Int. J. Hydrogen Energy, **21**(7), 1996. Pp. 625-631.

[194] Akansu, S.O., Z. Dulger, N. Kahraman and T. Veziroglu. Internal combustion engines fueled by natural gas-hydrogen mixtures. Int. J. of Hydrogen Energy, **29**. 2004. Pp. 1527-1539.

[195] Kido, H., M. Nakahara, J. Hashimot and D. Barat. Turbulent Burning Velocities of Two-Component Fuel Mixtures of Methane, Propane, and Hydrgoen. JSME International Journal, Series B., **45**(2), 2002. Pp. 355-362.

[196] Gauducheau, J.L., B. Denet and G. Searby. A Numerical Study of Lean CH4/H2/Air Premixed Flames at High Pressure. Combust. Sci. and Tech., **137**. 1998. Pp. 81-99.

[197] Schefer, R.W. Hydrogen enrichment for improved lean flame stability. Int. J. of Hydrogen Energy, **28**. 2003. Pp. 1131-1141.

[198] Karbasi, M. and I. Wierzba The Effects of Hydrogen Addition on the Stability Limits of Methane Jet Diffusion Flames. Int. J. Hydrogen Energy, **23**(2). 1998. Pp. 123-129.

[199] Law, C.K. and O.C. Kwon. Effects of hydrocarbon substation on atmospheric hydrogen-air flame propagation. Int. J. Hydrogen Energy, **29**. 2004. Pp. 867-879.

[200] Naha, S. and S.K. Aggarwal. Fuel effects on NOx emissions in partially premixed flames. Combustion and Flame, **139**. 2004. Pp. 90-105.

[201] Rortveit, G.J., K. Zepter, O. Skreiberg, M. Fossum and J.E. Hustad. A Comparison of Low-NOx burners for Combustion of Methane and hydrogen Mixtures. Proceedings of the Combustion Institute, **29**, 2002. Pp. 1123-1129.

[202] Naber, J.D. and D.L. Siebers. Hydrogen Combustion Under Diesel Engine Conditions. Int. J. Hydrogen Energy, **23**(5). 1998. Pp. 363-371.

[203] Huang, J., W.K. Bushe, P.G. Hill and S.R. Munshi Experimental and Kinetic Study of Shock Initiated Ignition in Homogeneous Methane-Hydrogen-Air Mixtures at Engine Relevant Conditions. Accepted for publication in Combustion and Flame, 2005.

[204] Fotache, C.G., T.G. Kreutz, and C.K. Law. Ignition of Hydrogen-Enriched Methane by Heated Air. Combustion and Flame, **110**. 1997. Pp. 429-440.

[205] Shudo, T., K. Shimamura and Y. Nakajima. Combustion and emissions in a methane DI stratified charge engine with hydrogen pre-mixing. JSAE Review. **21**. 2000. Pp. 3-7.

[206] Tsolakis, A., J.J Hernandez, A. Megaritis and M. Crampton. Dual Fuel Diesel Engine Operation Using H2. Effect on Particulate Emissions. Energy&Fuels, **19**. 2005. Pp. 418-425.

[207] Praxair Inc. Product Specification Sheet, Specialty Gases, Methane. Available from: http://www.praxair.com/praxair.nsf/0/3814994EBCA92CCE852565500400154/$file/Sec+C+-+PAGE+C-40.pdf. Accessed 19-05-2006.

[208] Khalil, E.B. and G.A. Karim. A Kinetic Investigation of the Role of Changes in the Composition of Natural Gas in Engine Applications. ASME Journal of Engineering for Gas Turbines and Power. **124**. 2002. Pp. 404-411.

[209] Hiltner, J., R. Agama, F. Mauss, B. Johansson and M. Christensen. Homogeneous Charge Compression Ignition Operation With Natural Gas: Fuel Composition Implications. ASME Journal of Engineering for Gas Turbines and Power. **125**. 2003. Pp. 837-844.

[210] Huang, J. and W.K. Bushe. Experimental and Kinetic Study of Autoignition in Methane/Ethane/Air and Methane/Propane/Air mixtures under Engine-Relevant Conditions. Combustion and Flame. **144**. 2006. Pp. 74-88.

[211] Soylu, S. and J.V. Gerpen. Development of an Autoignition Submodel for Natural Gas Engines. Fuel. **82**. 2003. Pp. 1699-1707.

[212] Fiveland, S.B., R. Agama, M. Christensen, B. Johansson, J. Hiltner, F. Maus and D.N. Assanis. Experimental and Simulated Results Detailing the Sensitivity of Natural Gas HCCI Engines to Fuel Compositon. SAE Technical Paper 2001-01-3609. 2001.

[213] King, S.R. The Impact of Natural Gas Composition on Fuel metering and Engine Operational Characteristics. SAE Technical paper 920593. 1992

[214] El-Sherif, A.S. Effects of Natural Gas Composition on the Nitrogen Oxide, Flame Structure, and Burning Velocity under Laminar Premixed Flame Conditions. Fuel. **77**(14). 1998. Pp. 1539-1547.

[215] Caillol, C. T. Delorme, P. Denis, G. Berardi and B. Porterie. A Combustion Model for Analyzing the Effects of Natural Gas Composition on the Operation of a Spark Ignition Engine. SAE Technical Paper 2002-01-2236. 2002.

[216] Kaiser, E.W., W.O. Siegl, Y.I. Henig, R.W. Anderson and F.H. Trinker. Effect of Fuel Structure on Emissions from a Spark-Ignited Engine. Environmental Science and Technology. **25**(12). 1991. Pp. 2005-2012.

[217] Graboski, M.S., R.L. McCormick, A.W. Newlin, D.L. Dunnick, M.M. Kamel and W.D. Ingle. Effect of fuel composition and altituted on regulated emissions from a Lean-Burn, Closed-Loop-Controlled Natural Gas Engine. SAE Technical paper 971707, 1997.

[218] Manivannan, A., P. Tamil Porai, S. Chandrasekara and S. Chandrasekaran. Lean Burn Natural Gas Spark Ignition Engine – An Overview. SAE Technical Paper 2003-01-0638. 2003.

[219] Clark, N.N., G.E. Mott, C.M. Atkinson, R.J. deJong, R.J. Atkinson, T. Latvakorsky and M.L. Traver. Effect of Fuel Composition on the Operation of a Lean Burn Natural Gas Engine. SAE Technical Paper 952560. 1995.

[220] Min, B.H., K.H. Bang, H.Y. Kim, J.T. Chung and S. Par k. Effects of Gas Compositon on the Performance and Hydrocarbon Emissions for CNG Engines. SAE Technical Paper 981918. 1998.

[221] Loubar, K., C. Rahmouni, O. Le Corre and M. Tazerout. Combustion Properties Determination of Natural Gas Using Thermal Conductivity and CO_2 Content. SAE Technical Paper 2005-01-3774. 2005.

[222] Naber, J.D., D.L. Siebers, C.K. Wetbrook, J.A. Caton and S. S. DiJulio. Natural Gas Autoginition Under Diesel Conditions: Experiments and Chemical Kinetic Modeling. SAE Technical paper 942034. 1994.

[223] Kuo, K. K. *Principles of Combustion. 2nd Ed.* Wiley, New York. 2005.

[224] Richards, G.A., M.M. McMillian, R.S. Gemmen, W.A. Rogers and S.R. Cully. Issues for Low-Emission, Fuel-Flexible Power Systems. Progress in Energy and Combustion Science. **27** 2001 Pp. 141-169

[225] Crookes, R.J. Comparitive Bio-Fuel Performance in Internal Combustion Engines. Biomass & Bioenergy. **30**. 2006. Pp. 461-468.

[226] Fotache, C.G., T.G. Kreutz and C.K. Law. Ignition of Counterflowing Methane versus Heater Air under Reduced and Elevated Pressures. Combustion and Flame. **108**. 1997. Pp. 442-470.

[227] Gulder, O.L. Effects of Oxygen on Soot Formation in Methane, Propane, and n-Butane Diffusion Flames. Combustion and Flame. **101**. 1995. Pp. 302-310.

[228] Manivannan, A., P. Tamil Porai, S. Chandrasekara and S. Chandrasekaran. Lean Burn Natural Gas Spark Ignition Engine – An Overview. SAE Technical Paper 2003-01-0638. 2003.

[229] Zelenka, P., H. Aufinger, W. Reczek, and W. Cartellieri. Cooled EGR – A Key Technology for Futer Efficient HD Diesels. SAE Technical Paper 980190. 1998.

[230] Johnson, T.V. Diesel Emission Control in Review. SAE Technical Paper 2006-01-0030. 2006.

[231] Leet, J.A., T. Friesen and A. Shadbourne. EGR's Effect on Oil Degratation and Intake System Performance. SAE Technical Paper 980179. 1998.

[232] Ryan, T.W. III, E. Owens, D. Naegeli, J. Doglio, G. Blyth, W.V. Dam, B. Damin, C. Olikara and F. Villforth. Effects of Exhaust Gas Recirculation on the Degradation Rates of Lubricating Oil in a Heavy-Duty Diesel Engine. SAE Technical Paper 1999-01-3574. 1999.

[233] Singh, S.K., A.K. Agarwal, and M. Sharma. Experiemental Investigations of Heavy Meatal Addition in Lubricating Oil and Soot Deposition in an EGR Operated Engine. Applied Thermal Engineering **26**. 2006. Pp. 259-266.

[234] Dennis, A.J., C.P. Garner and D.H.C. Taylor. The Effect of EGR on Diesel Engine Wear. SAE Technical Paper 1999-01-0839. 1999.

[235] Takakura, T., Y. Ishikawa and K. Ito. The Wear Mechanism of Piston Rings and Cylinder Liners Under Cooled-EGR Condition and the Development of Surface Treatment Technology for Effective Wear Reduction. SAE Technical Paper 2005-01-1655. 2005.

[236] Li, S., A.A. Csontos, B.M. Gable, C.A. Passut and T.C. Jao. Wear in Cummins M-11/EGR Test Engines. SAE Technical paper 2002-01-1672. 2002.

[237] Bae, M.W. A Study on the Effects of Recirculated Exhaust Gas Upon NOx and Soot Emissions in Diesel Engines with Scrubber EGR System. SAE Technical paper 1999-01-3266. 1999.

[238] Andac, M.G., F.N. Egolfopoulos and C.S. Campbell. Hot-Gas Ignition of Non-Premixed Methane Flames in the Presence of Inert Particles. Proceedings of the Combustion Institute. **30**. 2005. Pp. 431-437.

[239] United Filtration Systems. Filter Element Specifications. Available from: http://www.ufs-hf.com/prev/disposable.htm. Accessed 08-05-2006.

Appendix 1
Effect of Primary and Secondary Dilution Ratios

The use of dilution systems to measure particulate matter is standard practice in automotive and industrial stack emissions measuring environments [1]*. From a purely practical viewpoint, many particulate sampling instruments are not designed to operate at high concentrations, and hence the sample needs to be diluted to provide a reasonable measurement. More importantly, dilution of the exhaust stream simulates the dilution that would normally occur in the exhaust plume. Unlike most gaseous emissions, aerosol emissions change rapidly, in composition, state, size, and total quantity while undergoing dilution. As a result, understanding the effects of the dilution process is imperative for understanding the particulate matter masses measured in the exhaust stream.

A1.1 Environmental Exhaust Stream Dilution

For vehicular emissions, the 'real world' dilution process is a complex function of vehicle speed, vehicle size/shape, geographic profiles, relative wind direction and ambient atmospheric conditions (i.e. temperature, pressure, relative humidity). The momentum and buoyancy of the exhaust stream, highly dependant on engine operating condition, are also important [2]. Once emitted from the exhaust system, aerosol particles undergo a range of processes, including nucleation, condensation, and coagulation. These processes typically occur primarily during the first few seconds after emission, as the exhaust plume is diluted by ambient air.

A1.1.1 Nucleation

Nucleation involves the formation of new particles from gaseous precursors. For vehicle emissions, two mechanisms have been identified: binary sulphate-water nucleation and direct hydrocarbon nucleation. The binary sulphate-water mechanism, thought to be the most important for diesel engines [3,4], involves interactions between H_2SO_4 and H_2O molecules, resulting in the formation of small (~1nm diameter) sulphuric acid particles. The nucleation rate is highly dependent on relative humidity, temperature, and concentration of

* References for appendices are numbered independently in each appendix, with the references at the end of the corresponding appendix.

H_2SO_4 molecules. As was shown by Seinfeld [5], at 50% RH and 273 K, a change in sulphuric acid concentration of one order of magnitude resulted in a 10 order of magnitude change in nucleation rate. Abdul-Khalek *et al.* [3] also assessed the direct nucleation of hydrocarbon species in diesel engine exhaust. The exhaust hydrocarbon concentrations were found to be two orders of magnitude below what would have been required to induce hydrocarbon nucleation. The sulphate concentration, however, was 70 times greater than that required for nucleation, suggesting that sulphate nucleation was the primary source of nucleation-mode particles.

A1.1.2 Condensation

Nucleation of particles (in particular of sulphate droplets) generates very small particles – on the order of 1 nm diameter [3]. Once the particle has nucleated, it will grow by condensation of gas-phase species (either hydrocarbons or sulphates). While condensation increases the size of particles, the number of particles is unchanged. The particle growth rate will vary proportionally with the condensation 'driving force' – the difference between the free-gas and surface (equilibrium) partial pressures of the condensing species [5]. It will also vary inversely with the particle diameter; the smaller the particle, the more rapidly it will grow. The role of dilution is to reduce the gas-phase concentration of the condensing species, resulting in less incentive for nucleation. However, as the temperature also drops, the saturation pressure also drops, resulting in enhanced condensation. However, at constant temperatures, higher dilution ratios will reduce condensation rates.

A1.1.3 Coagulation

The other process which will substantially affect the aerosol size distribution during the exhaust and dilution process is coagulation. Coagulation occurs when two existing aerosols collide and stick together, forming a single larger particle. This results in a reduction in the total number of particles, but an increase in particle size. Coagulation depends primarily on the background aerosol concentration (the greater the concentration, the greater the probability of collisions, and hence the more rapid the change in volume) [5]. As the exhaust is diluted, coagulation rates drop; as a result, coagulation is most important in the pre-dilution exhaust stream, and results in the formation of carbon PM's characteristic agglomerate chains.

A1.1.4 Dilution Influences

More rapid dilution is expected to result in a greater total particle number with a smaller mean diameter, as coagulation is more rapidly quenched under these conditions. Higher dilution results in lower saturation ratios (for a given temperature). The relative humidity of the diluting air was also found to have a substantial influence [6], due to the relative rate of formation of sulphuric acid droplets (through binary nucleation of the H_2SO_4 - H_2O system). These results indicate the difficulty in attempting to simulate real-world dilution with a dilution system: while the dilution system provides a single finite dilution stage, in an exhaust plume turbulent mixing is continuously increasing the dilution ratio. This results in a relatively short period of time at which the dilution conditions are in the range where particulate nucleation and growth may be occurring: for a heavy-duty tractor moving at 55 mph, this has been estimated to be on the order of 200 ms [6].

A1.2 Effects of Dilution Conditions

A number of studies have investigated the effects of varying dilution parameters. Abdul-Khalek and Kittelson [3,7] investigated the effects of residence time, dilution ratio, diluent relative humidity and diluent temperature. They found that the dilution conditions affected nucleation mode particles (<50 nm) but did not significantly influence the accumulation mode particles (> 50 nm diameter). The concentration of volatiles which could nucleate was reduced by higher dilution, while higher temperatures increased the saturation concentration and hence reduced nucleation. Numerical analysis suggested that the concentration of volatile hydrocarbons was too low to generate substantial nucleation. Post-nucleation growth was attributed primarily to condensation of volatile hydrocabons, as the sulphate concentration was too low to explain the observed growth [3]. These results were supported by tandem-DMA analysis, where smaller particles were found to have a higher volatility than larger particles [8].

Other potential mechanisms have also been proposed to explain discrepancies between observed and predicted nucleation rates [9]. These have included involvement of ammonia in a tertiary sulphur-water-ammonia nucleation process (Napari *et al.* [10]) and ion-induced nanoparticle formation (Yu [11,12]). However, in general the effects of dilution ratio agreed with the findings of Abdul-Khalek *et al.* [3]. The results further indicated that at low RH's, nucleation was inhibited by a lack of water for the H_2SO_4 – H_2O binary nucleation

process. Luders *et al.* [13] demonstrated essentially equivalent results, with no nanoparticle nucleation occurring at dilution ratios in excess of approximately 15:1. Shi & Harrison [4] also investigated the effects of secondary dilution, and found that it did not influence the size distributions. However, these results all involved diesel engines with significant quantities of sulphur in the fuel; the effects of dilution for natural gas fuelled engines (where the sulphur content is typically below 7 ppm) requires further investigation.

A1.3 Experimental Methods

To evaluate the effects of varying the dilution conditions on the measured particulate emissions from a PIDING engine, a series of tests were conducted at various operating conditions. The influences of both the primary and the secondary dilution ratios on the measured particulate emissions, including total mass, size distributions, and black-carbon content were studied. For details of the measurement system and instruments, please refer to section 3.2.2. As is shown in Figure 3.4, the primary dilution ratio could potentially have influenced all the instruments. The secondary dilution ratio, however, could only have affected the size distribution and black-carbon measurements, as the total mass samples (for either the TEOM or the gravimetric filters) were sampled upstream of the secondary dilution.

The primary dilution system used in this work involved cold, dry nitrogen which was mixed with the hot exhaust gas. The tubing was heated to maintain a constant temperature in the dilution system of approximately 50°C. While residence time in the system varied somewhat, the use of constant diluent flow rates while varying the back-pressure minimized the changes in the residence time. The secondary dilution used a recirculating pump system.

Evaluations of the effects of dilution conditions were carried out at various points during the testing described in the main body of this thesis. The results from two specific test points will be included here. The points, identified in detail in Table A1.1, were selected as they provide a reasonably low level of PM, where small changes in dilution procedure are more likely to have a detectable influence on the PM measurements. For the first condition (tests conducted 15-03-05), the effects of primary dilution were investigated at low dilution ratios (between 3 and 10:1). For the second test condition (tests conducted 06-01-06), both the primary (8-22:1) and secondary (5.5 – 36:1) dilution ratios were evaluated. For the first tests, the black-carbon content was not measured. All PM data was collected for the second set of tests.

A1.4 Results

The primary objective for evaluating the influences of dilution ratio was to identify how sensitive the PM results were to these parameters. The effects of primary and secondary dilution ratio are presented independently. No attempt was made to identify the possibility of interaction between the two parameters: for the secondary dilution tests, the primary dilution was held constant at 15:1.

A1.4.1 Primary Dilution Ratio

The effects of low primary dilution ratios was investigated at a mid-load, low-speed condition (#1 in Table A1.1). The effects on the PM mass emissions and size distributions are shown in Figures A1.1 and A1.2. The measured mass emissions were significantly higher at low dilution ratios. Similarly, at low dilution ratios the particle size distributions were shifted towards more and larger particles. This suggests that condensation and/or coagulation was occurring more rapidly in the diluted sample stream at low primary dilution ratios. The principal effect was most likely that of increased nucleation through binary nucleation of sulphates and water in the diluted sample. As the dilution ratio increased, the volumetric concentration of these species was reduced, resulting in reduced nucleation and hence fewer particles. Furthermore, as the dilution ratio was increased, the concentration of existing particles would also have declined; this would have resulted in less particulate coagulation and hence a trend towards generally smaller particles.

A wider range of dilution ratios were studied at the mid-load mid-speed condition (#2 in Table A1.1). The total mass results (Figure A1.3) indicated that for dilution ratios from 9 to 18, there was no significant effect on measured mass emissions. However, a slight increase in mass appears to be present at the lowest dilution ratios (7), which agrees with the previous results that indicated that very low dilution ratios resulted in higher masses. These results were not observed in the black-carbon mass measurements (Figure A1.4), which indicated no significant effect of dilution ratio. This reinforces the supposition that low dilution ratios are primarily inducing nucleation of sulphates and water, as these species would not contribute to black carbon measurements. The particulate size distributions (Figure A1.5) also agree with the previous work, showing an increase in PM number at the lowest dilution ratio. In combination, these results indicate that over a range of primary dilution ratios between

approximately 10 and 18:1, this parameter has little or no influence on the particulate measurements.

A1.4.2 Secondary Dilution Ratio

The effects of the secondary dilution ratio were also investigated at the mid-load, mid-speed condition (#2 in Table A1.1). As mentioned previously, the total mass measurement was insensitive to this parameter, and hence is not reported here. The effects of the secondary dilution on the black-carbon concentration were only measured at three secondary dilution ratios (5.5, 7.2, and 9.4) as it was not possible to reach higher dilution ratios while using both the SMPS and the Aethalometer. However, the results (Figure A1.6) indicate that dilution ratio had no significant influence on the black carbon concentration over this range. The particle size distributions were measured at secondary dilution ratios up to 36:1, as shown in Figure A1.7. These results indicate that the secondary dilution had no effect on the particle size distributions at any of the measured conditions.

A1.5 Conclusions

1. The primary dilution ratio influenced particulate mass and size at ratios below 10 and above 18:1. However, between these values, the total mass, black-carbon concentration, and particle size distributions are insensitive to primary dilution ratio. To provide reliable comparisons, the dilution ratio should be kept in this range. For the work described in this thesis, primary dilution ratios were held between 13 and 16:1.
2. The secondary dilution ratio was found to have no significant impact on either the black-carbon concentration or the particle size distribution. To ensure similarity, secondary dilution ratios between 5 and 10:1 were used for all the tests reported in this thesis.

A1.6 Tables and Figures

Table A1.1: Experimental Conditions

Parameter	1	2
Engine Speed (RPM)	800	1200
Load (GIMEP)	8.5	8.5
Equivalence Ratio (ϕ)	0.45	0.45
EGR%	0	15
Y_{intO2}	*0.23*	*0.21*
Primary DR range	3-10	7-18
Secondary DR range		5-56
Equivalent point:	Chpt. 4, #2	Chpt. 8 #2

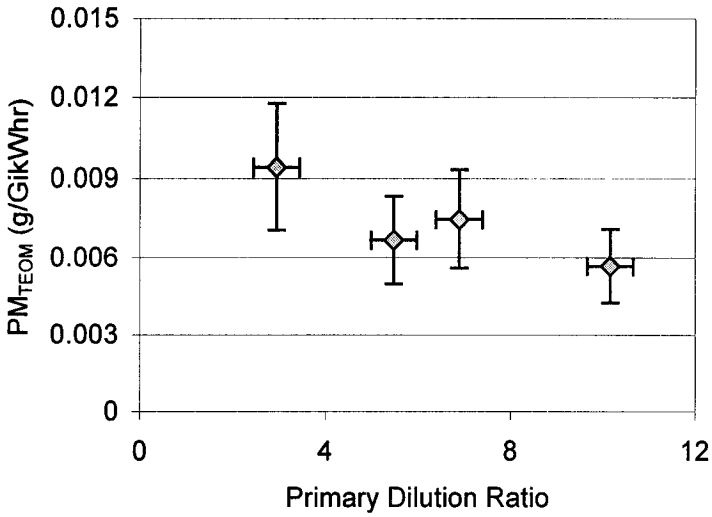

Figure A1.1: The effect of primary dilution ratio on particulate mass emissions, 800 RPM, 8.5 bar GIMEP, 0% EGR.

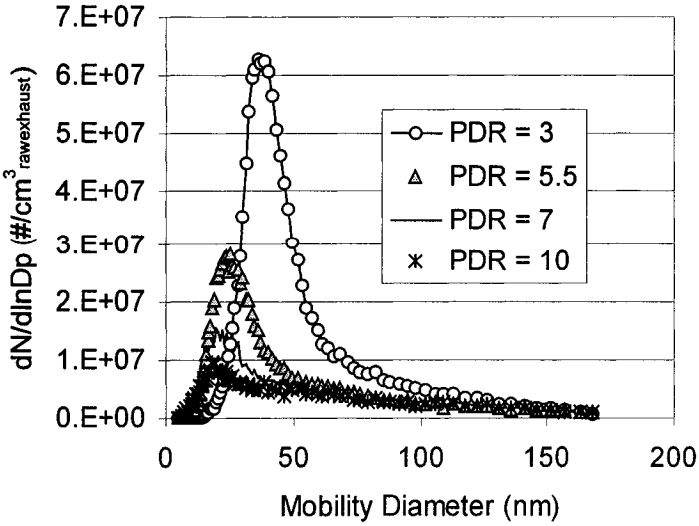

Figure A1.2: The effect of primary dilution ratio on particulate size distributions, 800 RPM, 8.5 bar GIMEP, 0% EGR.

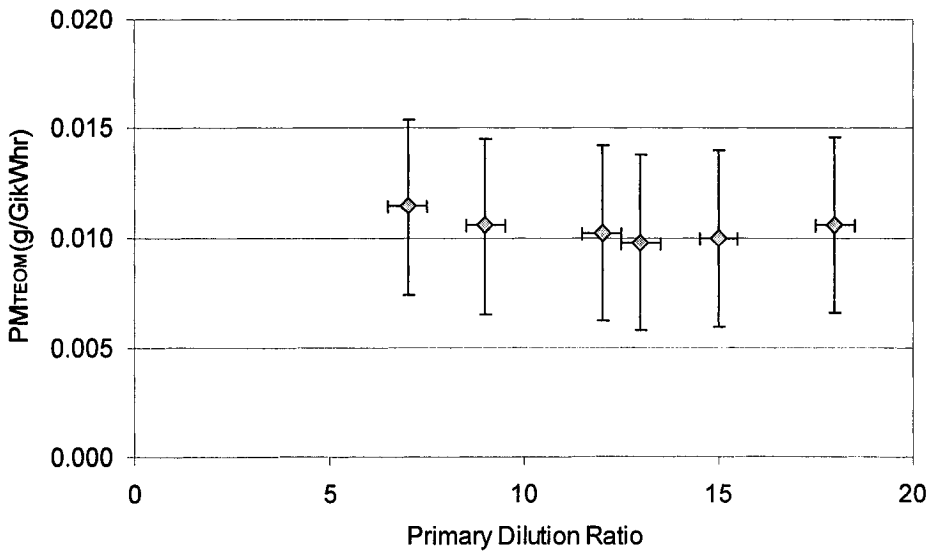

Figure A1.3: The effect of primary dilution ratio on particulate mass emissions, 1200 RPM, 8.5 bar GIMEP, 15% EGR.

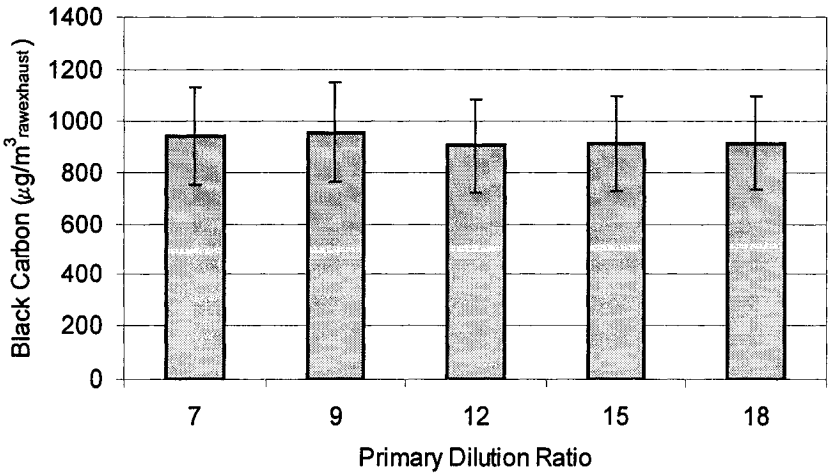

Figure A1.4: The effect of primary dilution ratio on black carbon concentration, 1200 RPM, 8.5 bar GIMEP, 15% EGR.

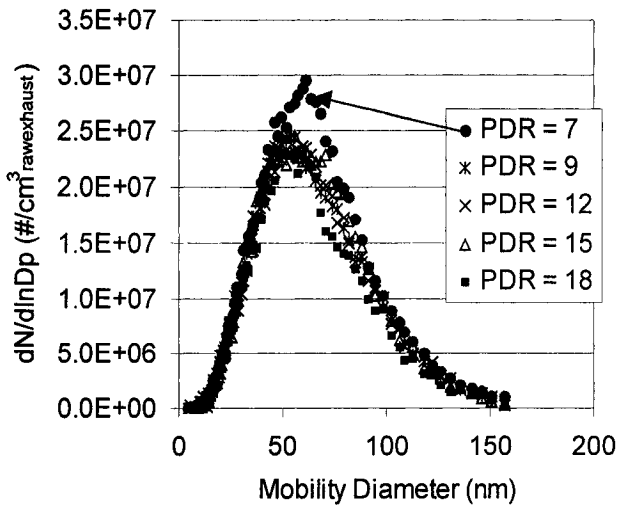

Figure A1.5: The effect of primary dilution ratio on particulate size distributions, 1200 RPM, 8.5 bar GIMEP, 15% EGR.

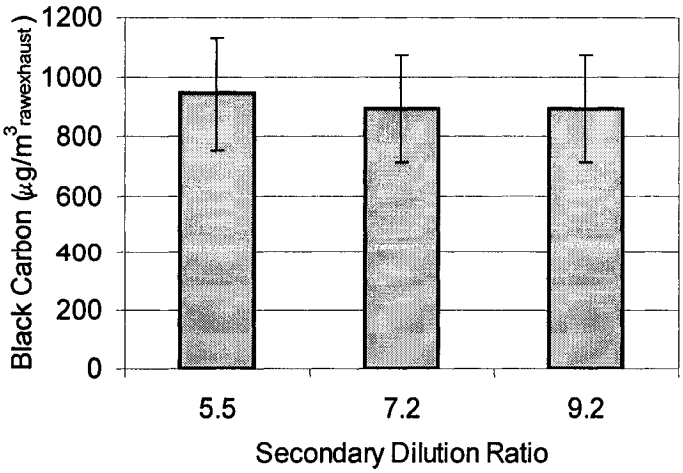

Figure A1.6: The effect of secondary dilution ratio on black carbon concentration, 1200 RPM, 8.5 bar GIMEP, 15% EGR, PDR = 15.

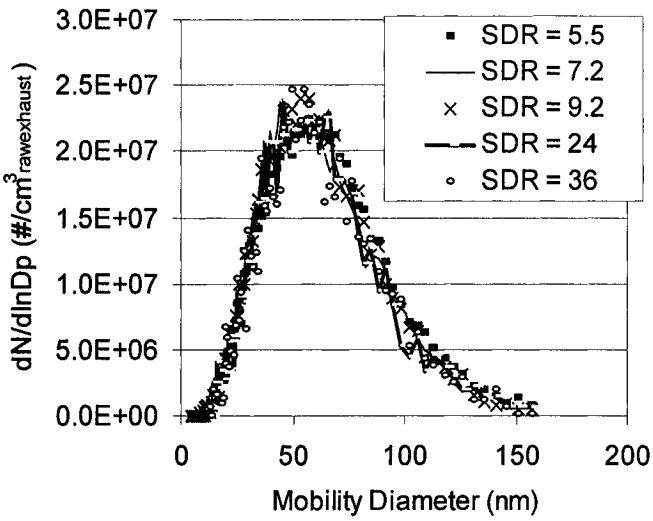

Figure A1.7: The effect of secondary dilution ratio on particulate size distributions, 1200 RPM, 8.5 bar GIMEP, 15% EGR, PDR = 15.

A1.7 References

[1] Wark, K., C.F. Warner and W.T. Davis. *Air Pollution, its Origin and Control. 3rd ed.* Addison Wesley, Berkely, California. 1998.

[2] Jiang, P., D.O. Lignell, K.E. Kelly, J.S. Lighty, A.F. Sarofim and C.J. Mongtomery. Simulation of the Evolution of Particle Size Distributions in a Vehicle Exhaust Plume with Unconfiend Dilution by Ambient Air. *Journal of the Air and Waste Management Association*, Vol. 55, pp. 437-445. 2005.

[3] Abdul-Khalek, I., D.B. Kittleson and F. Brear. Nanoparticle Growth During Dilution and Cooling of Diesel Exhaust: Experimental Investigation and Theoretical Assessment. *SAE Technical Paper 2000-01-0515*, 2000.

[4] Shi, J.P. and R.M. Harrison. Investigation of Ultrafine Particle Formation during Diesel Exhaust Dilution. *Envrionmental Science and Technology*, Vol. 33, pp. 3730-3736. 1999.

[5] Seinfeld, J.H., and S.N. Pandis. *Atmospheric Chemistry and Physics: From Air Pollution to Climate Change*. Wiley-Interscience, New York, 1998

[6] Kim, D., M. Gautam and D. Gera. Parametric Studies on the Formation of Diesel Particualte Matter via Nucleation and Coagulation Modes. *Journal of Aerosol Science*, vol. 33, pp. 1609-1621. 2002.

[7] Abdul-Khalek, I., D. Kittleson and F. Brear. The Influence of Dilution COnditions on Diesel Exhaust Particle Size Distribution Measurmentes *SAE Technical Paper 1999-01-1142*, 1999.

[8] Kwon, S.B, K.W. Lee, K. Saito, O. Shinozaki and T. Seto. Size-Dependent Volatility of Diesel Nanoparticles: Chassis Dynamometer Experiments. *Environmental Science and Technology*, Vol. 37 pp. 1794-1802. 2003.

[9] Mathis, U., J. Ristimaki, M. Mohr, J. Keskinen, L. Ntziachristos, Z. Samaras and P. Mikkanen. Sampling Conditions for the Measurement of Nucleation Mode Particles in the Exhaust of a Diesel Vehicle. *Aerosol Science and Technology*, Vol. 37, pp. 1149-1160. 2004.

[10] Napari, I., M. Kulmala and H. Vehkamaki. Ternary Nucleation of Inorganic Acids, Ammonia, and Water. *Journal of Chemical Physics*, Vol. 117, pp. 8418-8425. 2002.

[11] Yu, F. Chemiions and nanoparticle formation in diesel engine exhaust. *Geophysical Research letters*, Vol. 28 No. 22. pp. 4191-4194. 2001.

[12] Yu, F. Chemiions evolution in motor vehicle exhaust: Further evidence of its role in nanoparticle formation. *Geophysical Research letters*, Vol. 29 No. 15. pp. 1717-1720. 2002.

[13] Luders, H., M. Kruger, P. Stommel and B. Luers. The Role of Sampling Conditions in Particle Size Distribution Measurements. *SAE Technical Paper 981374*, 1998.

Appendix 2
Aethalometer Correction Procedure

The Aethalometer was developed [1] as a tool to measure the black-carbon concentration in an atmospheric sample. The Aethalometer measurement principle is based on the fact that the black carbon (BC) component of PM deposited on a filter reduces the intensity of visible light based on the Beer-Lambert law:

$$I = I_o e^{-b_{abs}x}$$

where I is the intensity of the attenuated light, I_o the intensity of the incident light, b_{abs} the absorption coefficient and x the distance that the light has passed through the sample [2]. By measuring the attenuation of the light intensity (normally given by $\ln[I/I_o]$), the quantity of 'black' carbon deposited on the filter can be determined [3].

The Aethalometer has been used for black-carbon measurement in both atmospheric and diluted exhaust system measurements [4,5,6]. Some results have indicated that the Aaethalometer's default calibration may not be accurate under all conditions [4]. Hitzenberger *et al.* [7] reported that while the absorption coefficient reported by the Aethalometer was equivalent to that of other measuring techniques, the calculated black carbon concentration (using the Aethalometer's internal calibration) varied substantially, suggesting that corrections to the data were required.

The Aethalometer reading is influenced by two parameters which may vary with the instrument set-up and operation. First, scattering of the light beam from the filter fibres results in an increase in the optical path length (x) and a corresponding increase in attenuation. Second, the build up of particulate on the filter over time results in a reduction in the amount of light scattered by the fibres and hence a reduction in the optical path length as the filter is loaded, referred to as the 'shadowing effect'. Both of these effects need to be accounted for when determining the exhaust black-carbon concentration from the light absorption measurements.

A2.1 Calculation Procedure

The attenuation coefficient of the captured particles (b_{atn}) can be calculated from:

$$b_{atn} = \frac{A}{Q}\frac{\Delta ATN}{\Delta t}$$

where A is the filter 'spot' area, Q is the volume flow rate, ΔATN is the %attenuation and Δt is the change in time. This equation can be used to determine the absorption coefficient (b_{abs}) with:

$$b_{abs} = {}^{b_{atn}}\!/_{C * R(ATN)}.$$

Where C and $R(ATN)$ are correction factors based on the nature of the sample and the instrument (discussed in following section). These values can then be used to calculate the measured ($M_{BC\text{-}measured}$) and corrected ($M_{BC\text{-}calculated}$) mass concentrations of black carbon in the sample from:

$$M_{BC-measured} = {}^{b_{atn}}\!/_{\sigma_{atn}}; \qquad M_{BC-calculated} = {}^{b_{abs}}\!/_{\sigma_{atn}},$$

where σ_{atn} represents the absorptivity of the collected particles, and is considered to be a constant (16.6 m^2/g) for the Aethalometer [8]. However, previous results have indicated that this value may vary from 9-19 m^2/g, which has a direct effect on the reported black-carbon mass concentration. The effects of varying σ_{atn} over this range are shown in Figure A2.1; as would be expected from the above equations, doubling the σ_{atn} halves the calculated BC concentration. Previous testing on this research apparatus has indicated that using a σ_{atn} value of 16.6 m^2/g resulted in a reasonable correlation between BC (corrected) and elemental carbon measurements, especially at high particulate loading (high BC concentration) [9]. Further research is required to assess possible variations in this parameter. However, as the effect is consistent at all conditions, comparisons between BC levels will not be affected. Measurements of BC fraction (where the absolute change in BC is compared to total PM mass) could be significantly affected.

As the preceding equations demonstrate, the BC concentration can be determined based on the measured attenuation, the sample time, the sample flow, and a pair of constants (A and σ_{atn}). The only unknown are the correction factors, C and $R(ATN)$.

A2.2 Correction Factors

The application of correction factors to the Aethalometer results has been studied extensively [3]. The correction factors have been applied to a wide range of sample situations, including both diesel exhaust and atmospheric sampling. The effects of the corrections are more significant in diesel exhaust measurements, as the sample concentrations are much higher than typical atmospheric samples, resulting in a more rapid accumulation of particulate on the filter tape. Although the equations described in section A2.1 can be used to calculate the corrected black carbon concentration, it is often easier to correct the measured values with:

$$M_{BC-calculated} = \frac{M_{BC-measured}}{C * R(ATN)},$$

where C and $R(ATN)$ are the correction factors which need to be determined.

A2.2.1 Attenuation Coefficient

The effect of light scattering from the filter fibres depends on the composition of the filter material. For the experiments reported here, a prebaked pure quartz filter was used. The effect of filter type should remain relatively constant for all tests conducted with the same type of filter. However, immediately after the filter is first exposed to the sample, the deposition of volatiles on the fibres may result in a small change in the value of the correction coefficient (C). Values for C for sampling from diesel exhaust with prebaked quartz filters have been on the order of 2.09±0.41 (450 nm wavelength) and 2.22±0.56 (660nm wavelength) [3]. However, the authors indicate that further research is required to provide a more solid theoretical foundation for these values. In the current work, a fixed value of C of 2.22 has been used, as this is valid for the wavelength closer to the wavelength used in the instrument (880nm).

A2.2.2 Shadowing Effect

The shadowing effect varies with the particle loading, so is more complicated to implement than the attenuation coefficient; however it has also seen more research, and hence is more thoroughly understood. The effect is accounted for by the empirically-determined term $R(ATN)$. The value is 1 for unloaded filters, with decreasing values as the filter is loaded, which represents the reduction in optical path length due to the shadowing effect. The shadowing parameter may be calculated from:

$$R(ATN) = \left(\frac{1}{f} - 1\right) * \frac{\ln(ATN) - \ln(10\%)}{\ln(50\%) - \ln(10\%)} + 1,$$

where ATN is the measured attenuation ($\ln[I/I_o]$) and f is a measure of the slope of the attenuation curve as a function of loading. This parameter is a function of the particulate composition, with higher values for more absorbative species, and values approaching unity for PM containing high quantities of volatiles. This is due to the scattering effect of the volatile species, which do not provide as strong a shadowing effect as do solid carbon. Values for f as high as 1.9 for fresh carbon particles have been proposed, while 1.41 has been identified for aged diesel exhaust [3].

For the results reported in this thesis, the f value was determined by calculating the slope of the attenuation curve for each data point (see example in Figure A2.2). For each operating condition, a least-squares minimization was used to calculate the optimal value for f. The results, provided in Table A2.1, indicate that the values were lower for those conditions where the PM loading was low, due to higher volatile concentrations in the PM. At high PM loadings, the f value increased to account for the greater shadowing effect of the more carbonaceous particles.

A2.2.3 Final Results

Using the correction values discussed in sections A2.2.1 and A2.2.2, the *R(ATN)* and *C* parameters were determined. From these parameters, and the measured BC mass concentration, the corrected black carbon concentration can be determined.

A2.3 Conclusions

1. The procedure by which the Aethalometer results were corrected was implemented based on the results from previous studies identified in the literature. These studies have shown generally acceptable correlations between the corrected BC concentrations measured by the Aethalometer and other representative techniques, both for exhaust-gas and atmospheric sampling.
2. The largest sources of uncertainty in the Aethalometer correction are the absorption coefficient (C) and the attenuation constant (σ_{atn}). Although both these parameters were considered as constant in the correction procedures identified above, previous results

have suggested that they depend on the nature of the particulate being sampled, and hence would be expected to be engine system dependent.

3. As the parameters identified above would be expected to be constant over a range of samples from the same test facility, comparisons between BC values are expected to be relatively accurate. However, the accuracy of comparisons with measurements from other systems, or with other absolute PM measurements, are somewhat less certain. As a result, parameters such as the BC fraction should be viewed as a qualitative, rather than a quantitative, assessment.

A2.4 Tables and Figures

Table A2.1: *f*-values for all data points

Chapter	Operating condition ID	Speed	Load	Y_{intO2}	50%IHR	*f*
5	NG-4	800	5	0.175	15	1.3
	NG-1,2,3 H_2-1,2,3,4	800	5	0.175	0,5,10 0,5,10,15	1.0
5,6,7	1	1200	13.5	0.19	0	1.155
	2	1200	13.5	0.19	5	1.373
	3	1200	13.5	0.19	10	1.285
	4	1200	13.5	0.19	15	1.09
8	A1	1200	8.5	0.23	10	1.05
	A2	1200	8.5	0.21	10	1.1
	A3-3	1200	8.5	0.19	10	1.62

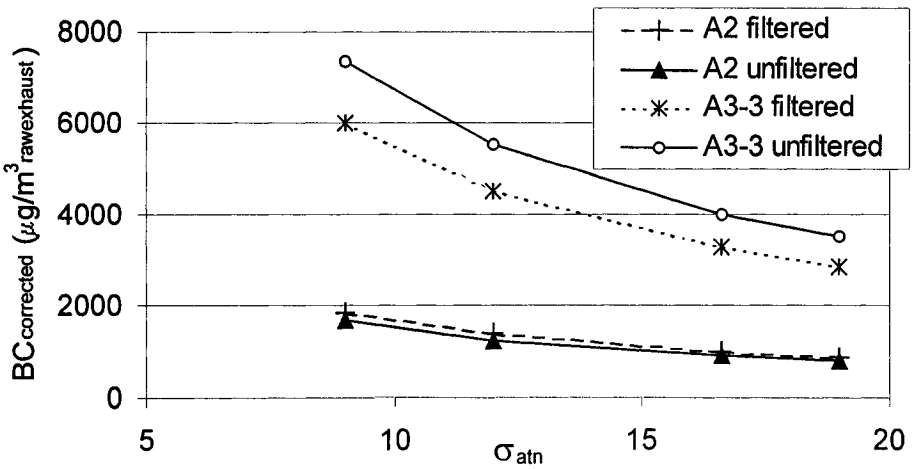

Figure A2.1: Effect of attenuation coefficient (σ_{atn}) on reported black carbon concentrations.

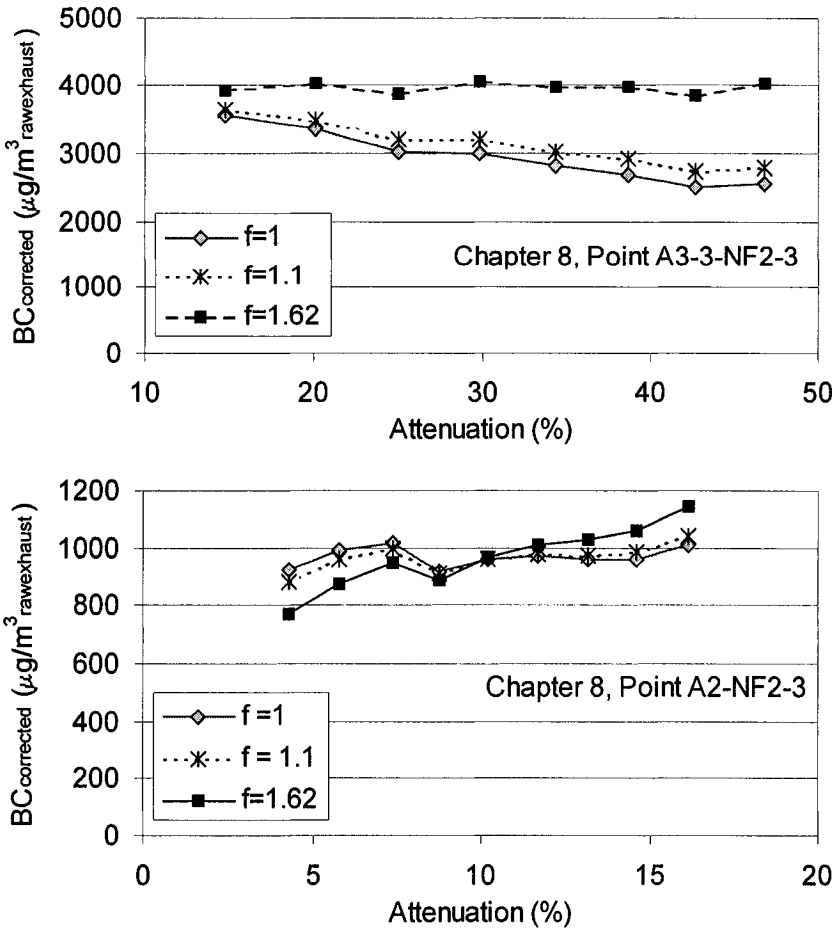

Figure A2.2: Absorption curve for various representative test conditions.

A2.5 References

[1] Hansen, A.D.A., H. Rosen, T. Novakov. The Aethalometer – An Instrument for the Real-Time Measurement of Optical-Absorption by Aerosol Particles. Science of the Total Environment. **36**, 1984. Pp. 191-196.

[2] Wark, K. C.F. Warner and W. T. Davis. *Air Pollution: Its Origin and Control, 3rd ed.* Addison-Wesley. 1998.

[3] Weingartner, E., H. Saathoff, M. Schnaiter, N. Streit, B. Bitnar and U. Baltensperger. Absorption of Light by Soot Particles: Determination of the Absorption Coefficient by Means of Aethalometers. Journal of Aerosol Science. **34**, 2003. Pp. 1445-1463.

[4] Lavanch, V.M.H., H.W. Gaggeler, S. Nyeki and U. Baltensperger. Elemental Carbon and Black Carbon Measurements with a Thermal Method and an Aethalometer at the High-Alpine Reesearch Station Jungfraujoch. Atmospheric Environment. **33**(17). 1999. Pp. 2759-2769.

[5] Moosmuller, H., W.P. Arnott, C.F. Rogers, J.L. Bowen, J.A. Gillies, W.R. Pierson, J.F. Collins, T.D. Durbin, and J.M. Norbeck. Time Resolved Characterization of Diesel Particulate

Emissions. 1. Instruments for Particle Mass Measurements. Environmental Science and Technology. **35**(4). 2001. Pp. 781-787.

[6] Fruin, S.A., A.M. Winer and C.E. Rodes. Black Carbon Concentrations in California Vehicles and Estimation of In-Vehicle Diesel Exhaust Particulate Matter Exposures. Atmospheric Environment. **38**. 2004. Pp. 4123-4133.

[7] Hitzenberger, R., S.G. Jennings, S.M. Larson, A. Dillner, H. Cachier, Z. Galambos, A. Rouc and T.G. Spain. Intercomparison of Measurement Methods for Black Carbon Aerosols. Atmospheric Environment. **33**(17). 1999. Pp. 2823-2833.

[8] Aethalometer AE21 operating manual. Magee Scientific. 1994. Available from: http://www.mageesci.com/book/Aethalometer_book_2005.07.03.doc. Accessed 06-07-06.

[9] Jones, H.L. Source and Characterization of Particulate Matter from a Pilot-Ignited Natural Gas Fuelled Engine. M.A.Sc. Thesis. University of British Columbia. 2004.

Appendix 3

Instrumentation List

Table A3.1: List of Instrumentation

Species	Manufacturer	Measuring Principal	Model/Serial Number	Range	Stated Accuracy
EMISSIONS MEASUREMENTS					
HC	Ratfisch	Flame Ionization (FID)	RS55/5-2-91	0-1000 ppm C_3H_8	
CH_4	Siemens	Non-Dispersive Infra-red (NDIR)	Ultramat 22P/ 7MB1123-C13-2BAI	0-5000 ppm	Noise < 1%FS* All others < 2%FS
CO	Siemens	NDIR	Ultramat 21P/ 7MB1122-1HA13-1BAI	0-1%	Noise < 1%FS All others < 2% FS
NO_x	Advanced Pollution Instrumentation	Chemi-luminescent	100/ 1L09003	0-3000 ppm (NO_2)	Lin. <1%FS Prec. 0.5%rdg† Drift < 1%FS / 24 hrs
O_2	Siemens	Paramagnetic	Oxymat 5E / C6-280	0-21%	Repr‡: 0.5%rdg Noise: 1%FS
CO_2 (exh)	Beckman Industrial	NDIR	880 / 2000449	0-20%	Noise < 1%FS Drift < 1%FS
CO_2 (int)	California Analytical	NDIR	100 / 1L09003	0-2% / 0-10%	Noise < 1%FS Drift < 1%FS
CO_2 (PM)	California Analytical	NDIR	100 / 1N12000	0-1%	Noise < 1%FS Drift < 1%FS
PM mass	Rupprecht & Pataschnik	Tapered Element Oscillating Microbalance (TEOM)	1105 / A201529909		
PM size	TSI	Condensation Particle Counter	3025A / 70419438	20-10^7 particles/cm^3	90% detection at 5 nm diameter; accuracy ±10%
		Electrostatic Classifier	3080 / 70422061		
		Nanoparticle Column (short)	3085 / 70418194	5-160 nm	
		Impactor		157 nm cut	

* FS: Full Scale
† rdg: Reading
‡ repr: Reproducibility

BC mass	Magee Scientific	Aethalometer (light absorption)	200		Limit of detection: 0.7 $mg/m^3_{diluted}$ ~700 $mg/m^3_{exhaust}$
DATA ACQUISITION SYSTEM					
DAQ Chassis	National Instruments	Modular Chassis	SCXI1001 / A6F0F0		
DAQ Cards	National Instruments	Thermocouple (2hz filter)	SCXI-1102		
		Voltage (200hz filter)	SCXI-1102B	±10V	
		Voltage (unfiltered)	SCXI-1100	±10V	
FLOWS					
Gaseous Fuel flow	Micromotion	Coriolis force	Sensor: CMF010P323 NC / 397665; Transmitter: RFT9739 / 7027956	0-15 kg/hr	±0.5%FS (for > 0.8 kg/hr)
Liquid Fuel	A-1 Scale	Gravimetric scale		0-6 kg	±0.1 g
Air Flow	UBC Design & constructed	Subsonic Venturi	N/A	0-500 kg/hr	*Estimated* ±2% FS
Diff. Pressure	*Omega*	*Diaphragm*	*PX2300-2DI / 1705557*	*0-2 psi*	*±1% FS*
Temp	*Omega*	*k-type thermocouple*	KMQSS-125U-6		*±0.75% rdg*
Abs. Pressure	*Setra*	*Strain Gage*	*209*	*0-150 psi*	*±0.25% FS*
PRESSURES AND TEMPERATURES					
All T	Omega	k-type thermocouple	(most): KMQSS-125U-6		±0.75% rdg
Air Pressures	Setra	Strain-gauge	209	From 0-2 to 0-5000 psi	±0.25% FS
Intake Manifold P	PCB	Piezoresistive	15-1C02EZ1V5 GBAR / 405	0-6 bar	

IN CYLINDER CONDITIONS					
Pressure	AVL	Piezoelectric	QC33C / M184	0-200 bar	Linearity ±0.2%; sensitivity 28.41 pC/bar
Charge Amplifier	Kistler		503 / 1033		
Crank Angle	BEI	Optical shaft encoder	XH25D-ss-720-ABCZ / AA042876		±0.5°
ENGINE CONDITIONS					
Torque	Artech Industries	Strain-gauge based load cell	20210	0-115kg	±0.05%FS
Speed		Magnetic Pick-up			
Dyna-mometer Controller	Digilog	PID Control on speed input			Observed: ±10RPM
Gas Composition Analysis (at Westport Innovations Inc.)					
Hydro-carbons	Agilent		G2890A/US0 3802378		
Hydrogen	SRI		8610C / N4591		

Appendix 4
Experimental Uncertainty Calculations

Various procedures for estimating the uncertainty in calculated values based on the uncertainty in the underlying measurements have been developed and are discussed in experimental methods textbooks [1,2]. The technique used in this work is based on that presented by Holman [1]. It is based on the calculated response, R, being a known function of a series of variables (x_i), each with a corresponding absolute uncertainty (w_i). Therefore, for an equation of the form $R=f(x_i)$, the total uncertainty W can be calculated based on:

$$W = \left[\sum_i \left(\left(\frac{\partial R}{\partial x_i} w_i\right)^2\right)\right]^{1/2}.$$

This formula can be used for any function where the underlying function and uncertainties are known. Simplifications of the formula for either purely additive or multiplicative functions can be derived.

A4.1 Sample Calculation

The equation above was used to calculate the uncertainties for the principal outcome variables presented in Table 3.3. The power-specific NO_x (NO_xps) emission calculations will be used to demonstrate the uncertainty analysis process:

1) The formula used is identified:	$NO_x ps\left(g/GikWhr\right) = \frac{NO_x\left(g/hr\right)}{P_{gross}};$
2) The partial derivatives of the formula are calculated:	$\frac{\partial(NO_x ps)}{\partial(NO_x)} = \frac{1}{P_{gross}}$; $\frac{\partial(NO_x ps)}{\partial(P_{gross})} = -\frac{NO_x\left(g/hr\right)}{(P_{gross})^2}$
3) Identify the uncertainties:	w_{NOx}, w_{Pgross}
4) The net uncertainty can then be calculated:	$W_{NOxps} = \sqrt{\left[\left(\frac{1}{P_{gross}} * w_{NOx}\right)^2 + \left(-\frac{NO_x\left(g/hr\right)}{(P_{gross})^2} * w_{Pgross}\right)^2\right]}$

Unfortunately, the uncertainty calculated above includes the uncertainty terms in the NO_x emissions rate (g/hr) and the uncertainty in the gross indicated power. To calculate the

overall uncertainty, these uncertainty terms must be calculated. For example, the uncertainty in the NO_x emissions rate can be determined from a similar procedure:

1) $$NO_x\left(\frac{g}{hr}\right) = \frac{0.046 * \dot{m}_{exhaust}\left(\frac{kg}{hr}\right) * NO_x msrd(ppm)}{MW_{exh}}$$

2) $$\frac{\partial(NO_x)}{\partial(\dot{m}_{exhaust})} = \frac{0.046 * NO_x msrd}{MW_{exh}};$$

$$\frac{\partial(NO_x)}{\partial(NO_x msrd)} = \frac{0.046 * \dot{m}_{exhaust}}{MW_{exh}};$$

$$\frac{\partial(NO_x)}{\partial(MW_{exh})} = -\frac{0.046 * \dot{m}_{exhaust} * NO_x msrd}{(MW_{exh})^2}$$

3) $w_{NOxmsrd}$ = 1%FS (from Appendix 4) = 30 ppm;
w_{MWexh} = calculate; $w_{mexhaust}$ = calculate

4) $$W_{NOxps} = \left[\left(\frac{0.046 * NO_x msrd}{MW_{exh}} * w_{mexhaust}\right)^2 + \left(\frac{0.046 * \dot{m}_{exhaust}}{MW_{exh}} * w_{NOxmsrd}\right) + \left(-\frac{0.046 * \dot{m}_{exhaust} * NO_x msrd}{(MW_{exh})^2} * w_{MWexh}\right)^2\right]^{\frac{1}{2}}$$

In this set of calculations, one of the primary measurements (NO_x) is included; however, further calculations are required to determine the uncertainty in the molecular weight and in the exhaust mass flow. By repeating these procedures, the underlying uncertainties in each of the measure values can be incorporated into the experimental uncertainty in the calculated response (R), which in this case is the power-specific NO_x emissions.

A4.2 References

[1] Holman, J.P. Experimental Methods for Engineers, 7th ed. McGraw-Hill, New York. 2001.

[2] Dally, J.W., W.F. Riley and K.G.McConnel. Instrumentation for Engineering Measurements, 2nd ed. Wiley, New York. 1993.

Appendix 5
Gaseous Fuel Composition

The composition of natural gas as reported in various parts of the world varies substantially. The principal component is methane (75-98%) with heavier hydrocarbons (ethane, propane, butane) and diluents (CO_2, N_2) typically making up the balance of the gas. Traces of other species, including sulphur and sulphur-related species, oxygen, and long-chain hydrocarbons may also be present. During periods of peak demand, local natural gas suppliers may supplement the natural gas with up to 50% (by volume) propane and air or inert species (to maintain a constant heating value) [1]. The use of 'unconventional' gaseous fuels, including landfill gas, biological-sourced gases, or coal synthesis gases, may add further species (including significant quantities of CO and H_2) into the gaseous mixture [2]. A review of the published literature of engine testing on natural gas over the past 10 years, shown in Table A5.1, indicates the range of natural gas compositions typically used in both engine test-bed and on-road research programs. Non-conventional gases were not included in this table.

Table A5.1: Fuel composition from reported engine research.

Authors	Pub. year	Ref.	Gas Source	Species (volume %)								sulfur (ppm)	LHV (MJ/kg)
				CH_4	C_2H_6	C_3H_8	C_4H_{10}	CO_2	N_2	$N_2 + CO_2$	O_2		
Stromman *et al.*	2006	[3]	Barents Sea (Norway)	82.0	9	2	1	6					42.4
Okamata *et al.*	2006	[4]	Los Angeles commercial supplier	94.9	1.4	0.3		0.9	2.4		0.05		
Crookes	2006	[5]	United Kingdom	93.3	3.3	0.6	0.3	0.3	2.2				
Kado *et al*	2005	[6]	Los Angeles commercial supplier	94.3	2.43	0.83				2.14	0.07	2.3	41.6
			Los Angeles commercial supplier	86.9	6.4	3.6				2.39	0.12	1.3	44.6
			California fuel specification	>88	<6	<3							
Ishiyama *et al.*	2005	[7]	Japanese 13A	88.0	6	4	2						
Bhave *et al.*	2005	[8]		91.3	5	1.8	1	0.6	0.3				
Jang & Lee	2005	[9]	Korea	89.1	8.62	1.71	0.4						
Kowalewicz & Wojtynkia	2005	[10]	Various	80-98	1-8	~2		0.2-1.5					
Singh *et al.*	2004	[11]		98.3	<1			<1	1.3				
Ogawa *et al.*	2003	[12]	Japanese 13A	84.9	7.5	5.1							
Caillol *et al.*	2002	[13]	France	92	6.3	0.7	0.1		0.9				49.0
Krishnan *et al.*	2002	[14]	USA	98.3	0.11	0.02	0.01	0.21	1.3			0.05	54
Yossefi *et al.*	2000	[15]	US Various	75-98	0.5-13								
Rousseau *et al.*	1999	[16]	Algeria	90.4	8.22	1.2	0.02		0.16				49.45
Das&Watson	1997	[17]	Australia	91.2	5.43	0.42	0.07	1.31	1.51				46.3

A5.1 References

[1] Soylu, S. and J.V. Gerpen. Development of an Autoignition Submodel for Natural Gas Engines. Fuel. **82.** 2003. Pp. 1699-1707.

[2] Richards, G.A., M.M. McMillian, R.S. Gemmen, W.A. Rogers and S.R. Cully. Issues for Low-Emission, Fuel Flexible Power Systems. Progress in Energy and Combustion Science. 27. 2001. Pp. 141-169.

[3] Stromman, A.H., C. Solli, E.G. Hertwich. Hybrid Life-Cycle Assessment of Natural Gas Based Fuel Chains for Transportation. Environmental Science and Technology. **40**. 2006. Pp. 2797-2804.

[4] Okamoto, R.A., N.Y. Kado, P.A. Kuzmicky, A. Ayala and R. Kobayashi. Unregulated Emissions from Compressed Natural Gas (CNG) Transit Buses Configures with and without Oxidation Catalyst. Environmental Science and Technology. **40**. 2006. Pp. 332-341.

[5] Crookes, R.J. Comparitive Bio-Fuel Performance in Internal Combustion Engines. Biomass & Bioenergy. **30**. 2006. Pp. 461-468.

[6] Kado, N.Y., R.A. Okamoto, P.A. Kuzmicky, R. Kobayashi, A. Ayala, M.E. Gebel, P.L. Rieger, C. Maddox and L. Zafonte. Emissions of Toxic Pollutants from Compressed Natural Gas and Low Sulfur Diesel-Fueled Heavy-Duty Transit Buses Tested over Multiple Driving Cycles. Environmental Science and Technology. **39**. 2005. Pp. 7638-7649.

[7] Ishiyama, T., H. Kawanabe, K. Ohashi, M. Shioji and S. Nakai. A Study on Premixed Charge Compression Ignition Combustion of Natural Gas with Direct Injection. International Journal of Engine Research. **6.** 2005. Pp. 443-453.

[8] Bhave, A., M. Balthasar, M. Kraft and F. Mauss. Analysis of a Natural Gas Fuelled Homogeneous Charge Compression Ignition Engine with Exhaust Gas Recirculation using a Stochastic Reactor Model. International Journal of Engine Research. **5**(1). 2004. Pp. 93-107.

[9] Jang, C., and J. Lee. Experimental Investigation of the Effects of Various Factors on the Emissions Characteristics of Low-Emission Natural Gas Vehicles. Proceedings of the Institute of Mechanical Engineers, Part D. **219.** 2005. Pp. 825-833.

[10] Kowalewicz, A. and M. Wojtyniak. Alternative Fuels and their Application to Combustion Engines. Proceedings of the Institute of Mechanical Engineers, Part D. **219** 2005. Pp. 103-127.

[11] Singh, S. S.R. Krishnan, K.K. Srinivasa, K.C. Midkiff and S.R. Bell. International Journal of Engine Research. **5**(4). 2004. Pp. 329-348.

[12] Ogawa, H., N. Miyamoto, C. Li, S. Nakazawa and K. Akao. Smokeless and low NO_x Combustion in a Dual-Fuel Diesel Engine with Induced Natural Gas as the Main Fuel. International Journal of Engine Research. **4**(1). 2003. Pp. 1-9.

[13] Caillol, C., T. Delorme, P. Denis, G. Berarid and B. Porterie. A Combustion Model for Analyzing the Effects of Natural Gas Composition on the Operation of a Spark Ignition Engine. SAE Technical paper 2002-01-2236. 2002.

[14] Krishnan, S.R., M. Biruduganti, Y. Mo, S.R. Bell and K.C. Midkiff. Performance and Heat Release Analysis of a Pilot-Ignited Natural Gas Engine. International Journal of Engine Research. **3**(3). 2002. Pp. 171-186.

[15] Yossefi, D. M.R. Belmont, S.J. Ashcroft, and S.J. Maskell. A Comparison of the Relative Effects of Fuel Composition and Ignition Energy on the Early Stages of Combustion in a Natural Gas Spark Ignition Engine using simulation. Proceedings of the Institute of Mechanical Engineers, Part D. **214.** 2000. Pp. 383-395.

[16] Rousseau, S., B. Lemoult and M. Tazerout. Combustion Characterization of Natural Gas in a Lean Burn Spark-Ignition Engine. Proceedings of the Institute of Mechanical Engineers, Part D. **213**. 1999. Pp. 481-491.

[17] Das, A. and H.C. Watson. Development of a Natural Gas Spark Ignition Engine for Optimum Performance. Proceedings of the Institute of Mechanical Engineers, Part D. **211** 1997. Pp. 361-380.

Appendix 6
In-Cylinder Pressure and Heat Release Rate Results

Due to the relatively large number of conditions tested, the in-cylinder conditions for many of the test points were not included in the body of the thesis. This appendix displays representative pressure traces and net heat-release rates for all the test points conducted. Where test points were replicated, the results from one of the samples is provided. For all the results, data from 45 consecutive cycles was collected and averaged. The heat-release rates were calculated based on these averaged results. No filtering of the heat-release rate was conducted. The results are subdivided by chapter.

A6.1 Effects of Injection Pressure

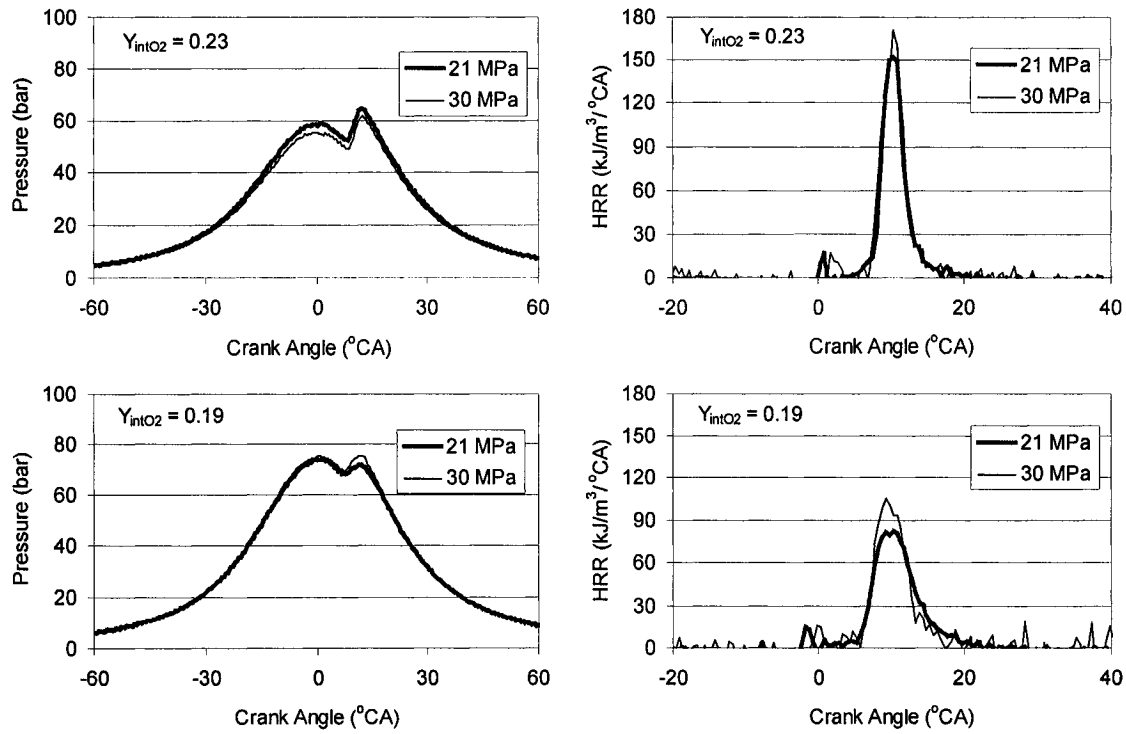

Figure A6.1: Pressure traces and heat-release rates from operating condition '1' (800 RPM, 3 bar GIMEP, 0.25 ϕ)

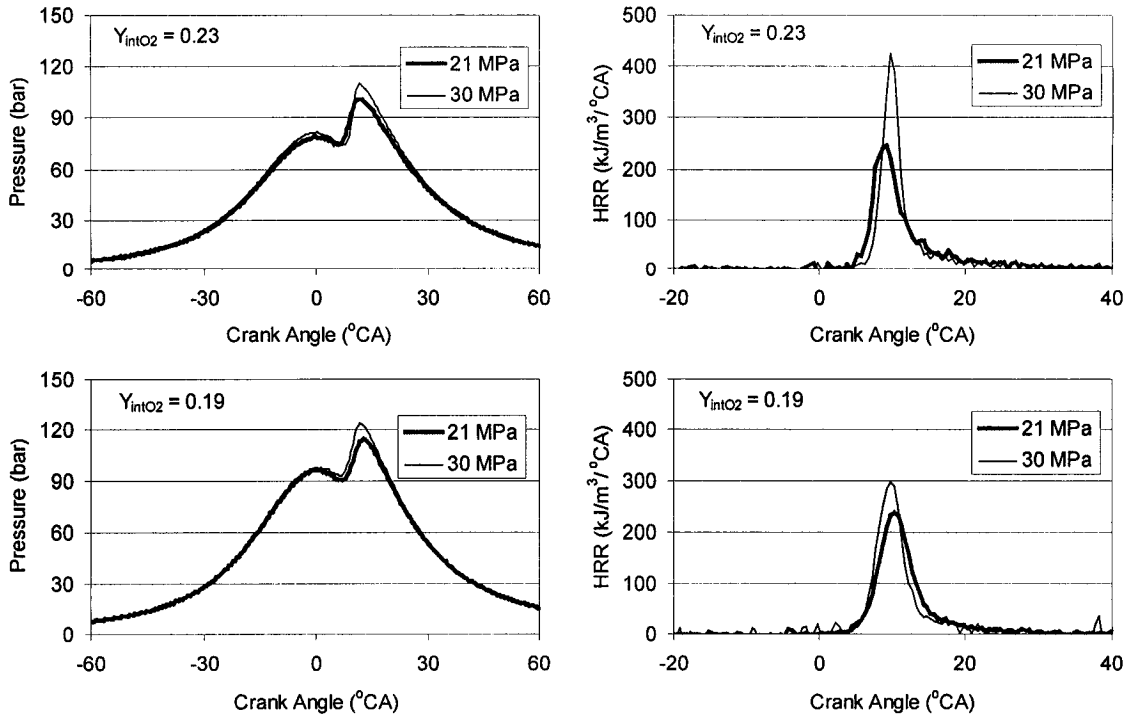

Figure A6.2: Pressure traces and heat-release rates from operating condition '2' (800 RPM, 8.5 bar GIMEP, 0.45 ϕ)

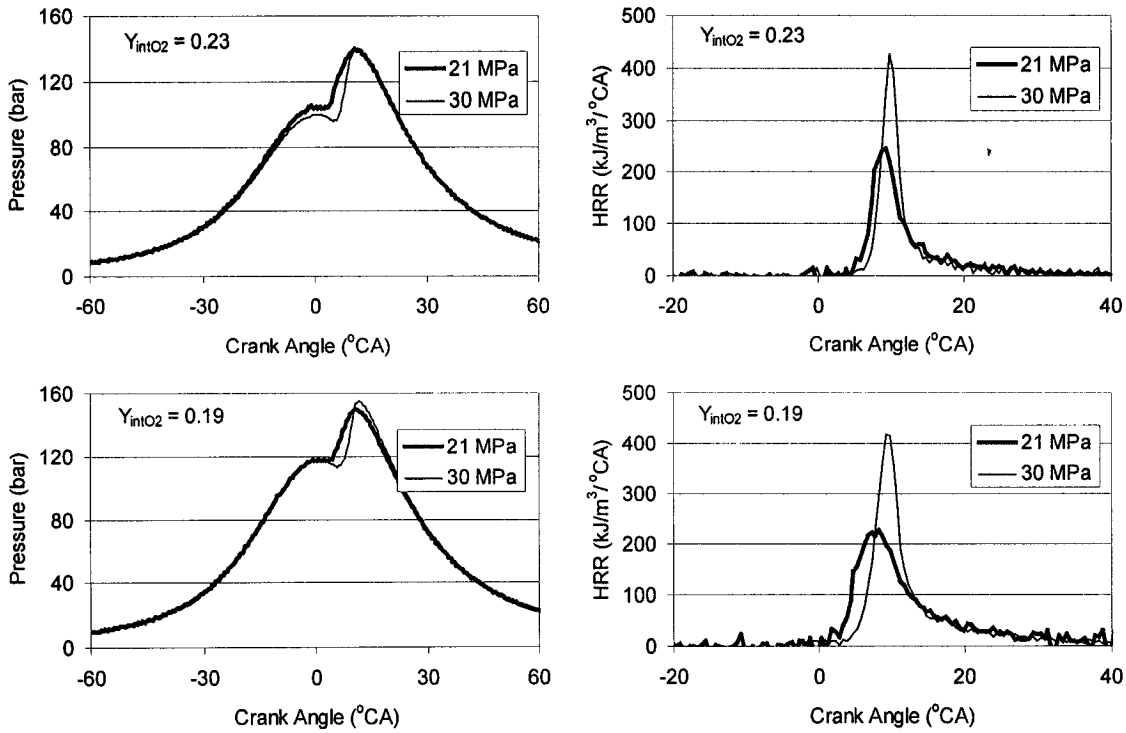

Figure A6.3: Pressure traces and heat-release rates from operating condition '3' (800 RPM, 13.5 bar GIMEP, 0.6 ϕ)

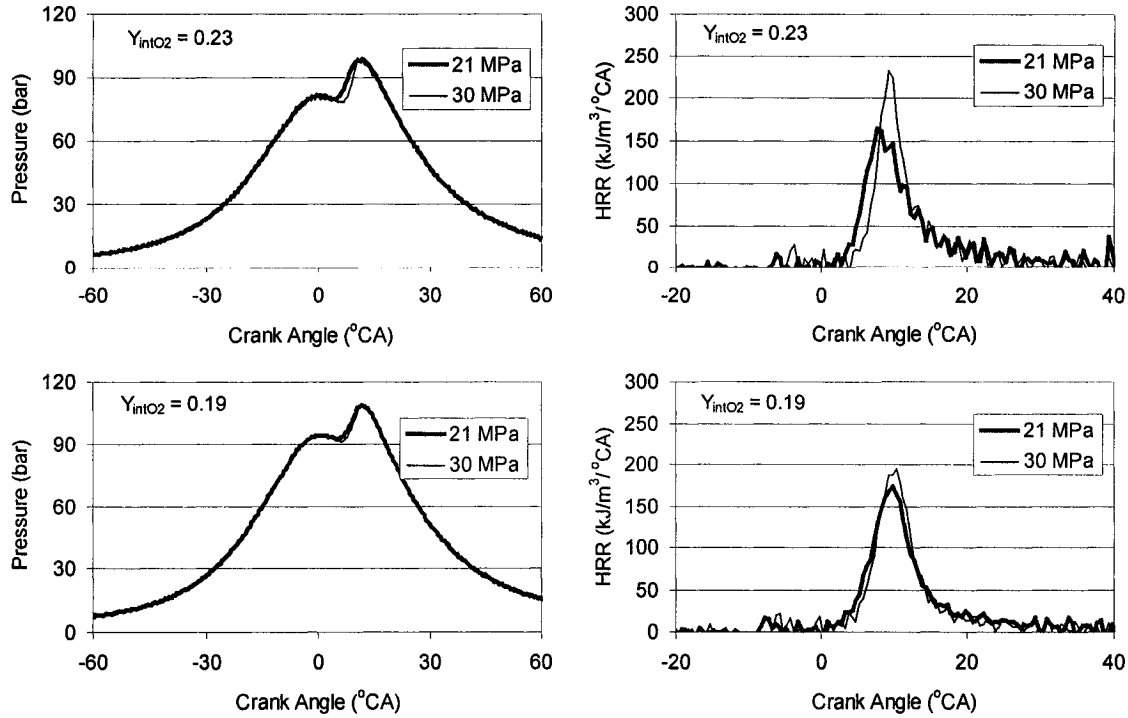

Figure A6.4: Pressure traces and heat-release rates from operating condition '4' (1200 RPM, 8.5 bar GIMEP, 0.45 ϕ)

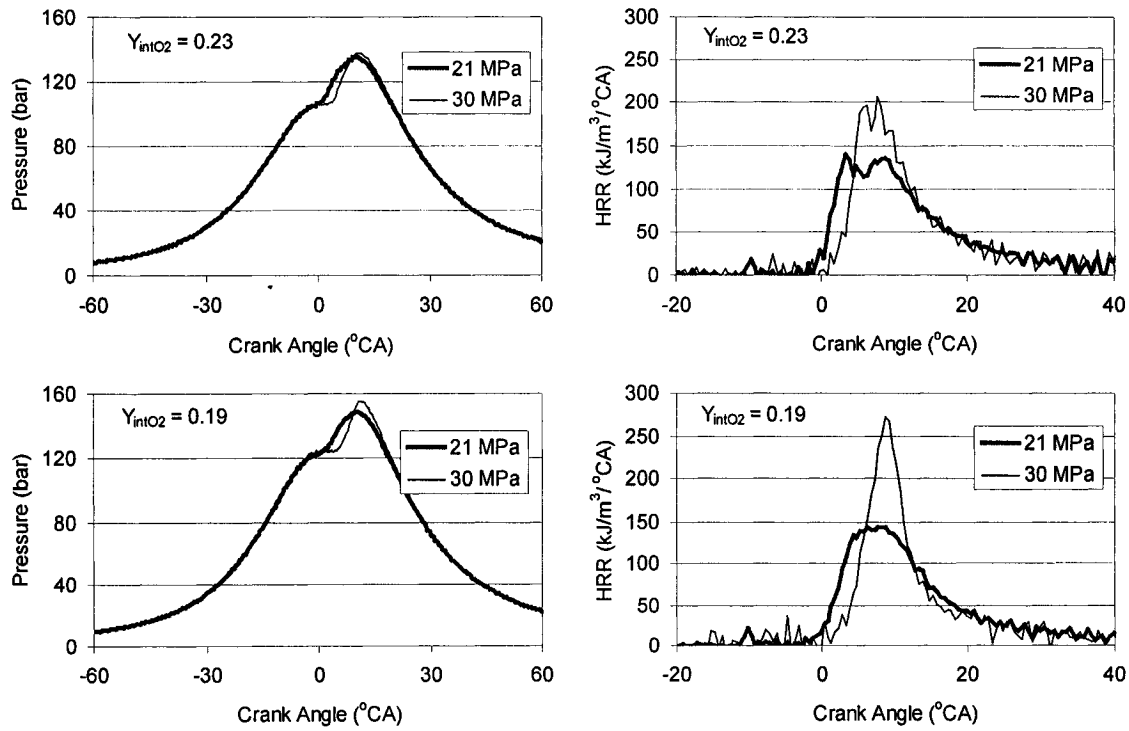

Figure A6.5: Pressure traces and heat-release rates from operating condition '5' (1200 RPM, 13.5 bar GIMEP, 0.6 ϕ)

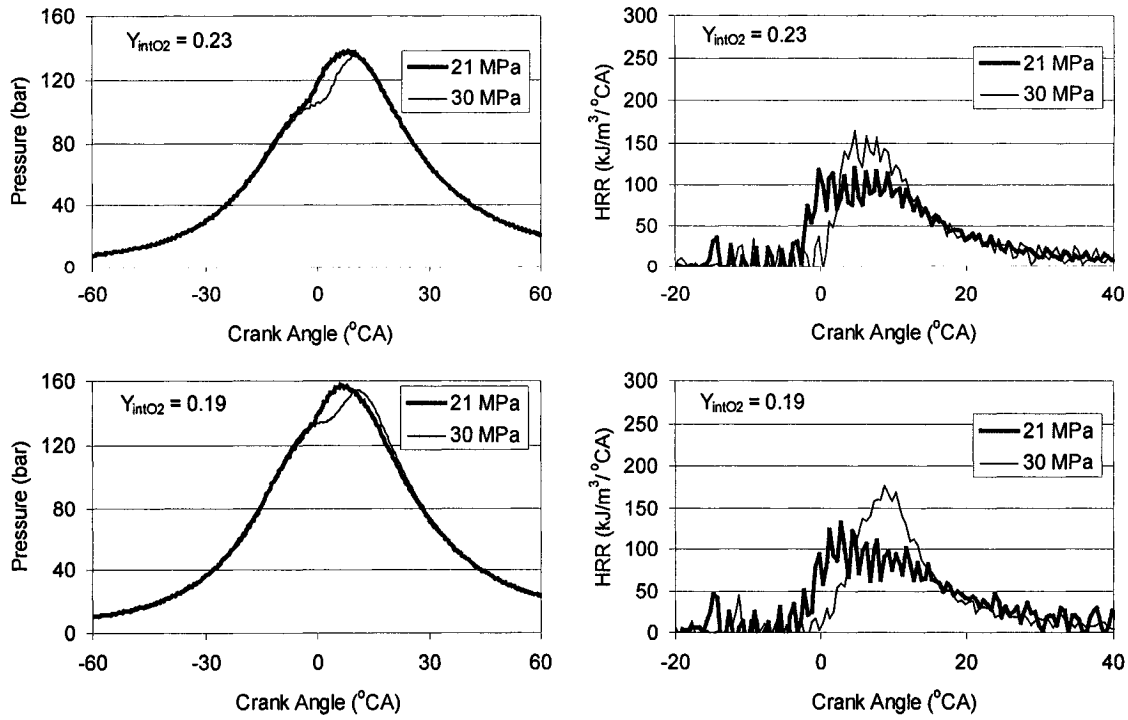

Figure A6.6: Pressure traces and heat-release rates from operating condition '6' (1600 RPM, 13.5 bar GIMEP, 0.6 ϕ)

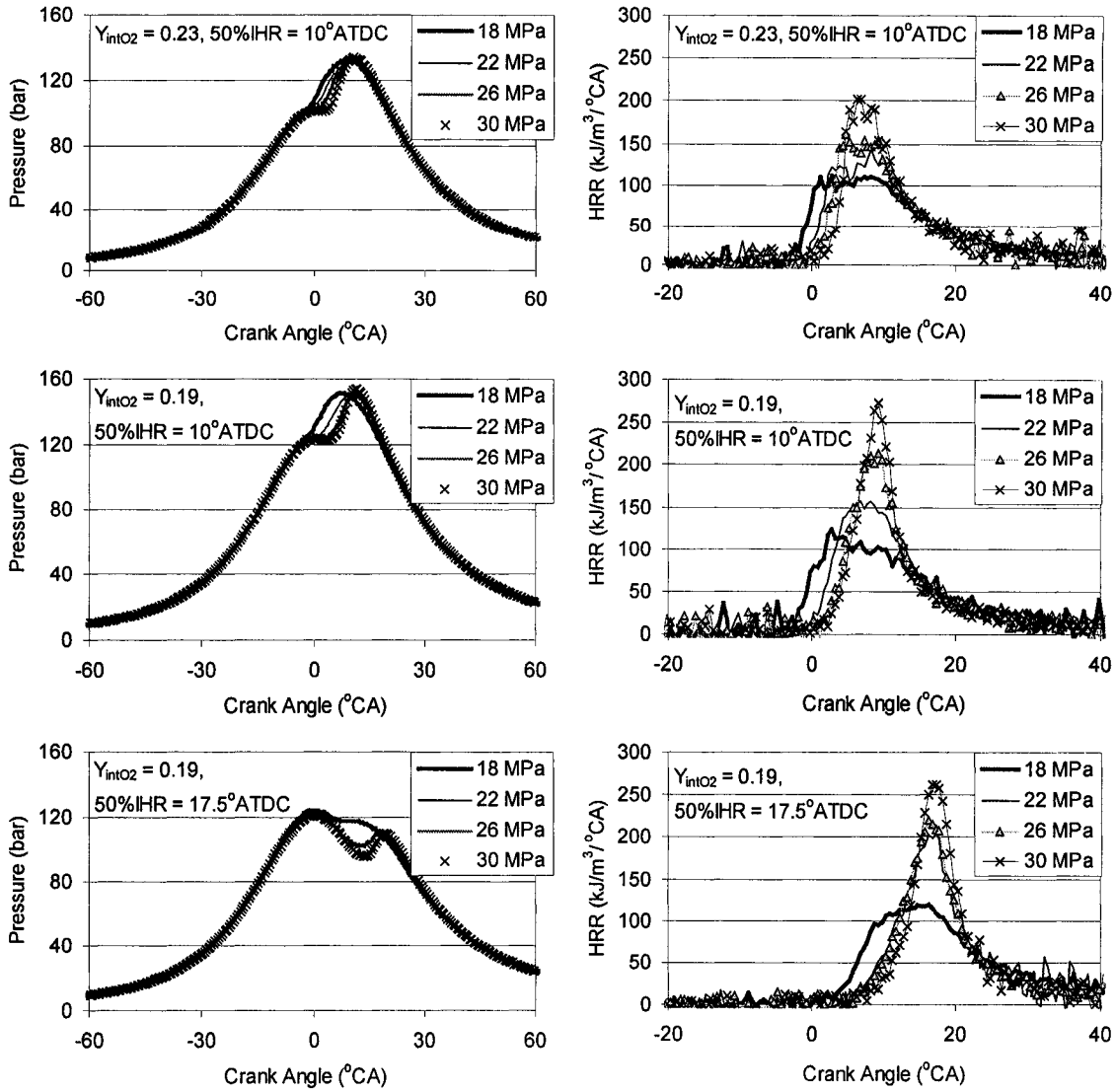

Figure A6.7: Pressure traces and heat-release rates from detail injection pressure study, 1200 RPM, 13.5 bar GIMEP, 0.6 ϕ

A6.2 Hydrogen Addition

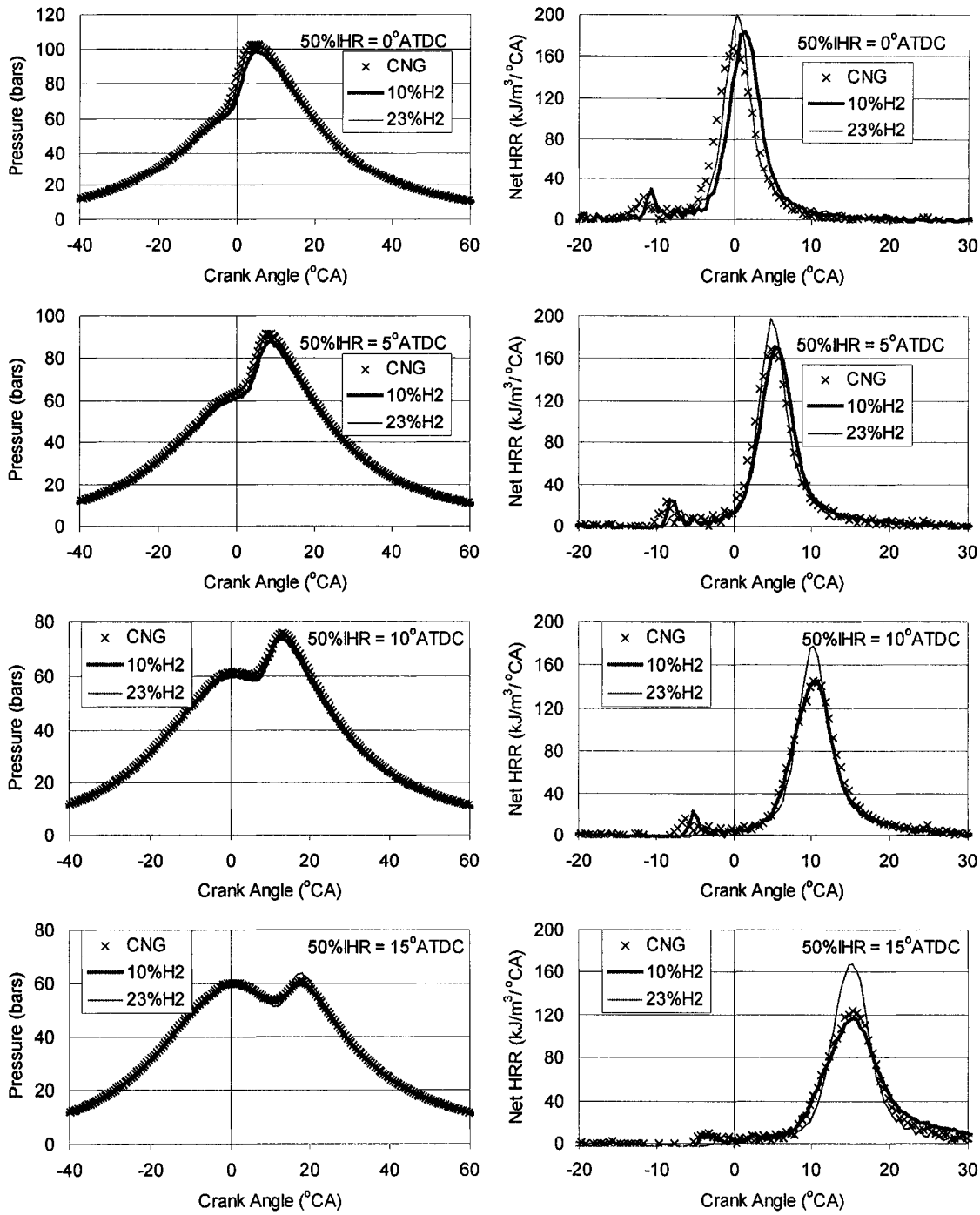

Figure A6.8: Pressure traces and heat-release rates for hydrogen addition testing. 800 RPM, 3.5 bar GIMEP, 0.5 ϕ, $Y_{intO2} = 0.175$

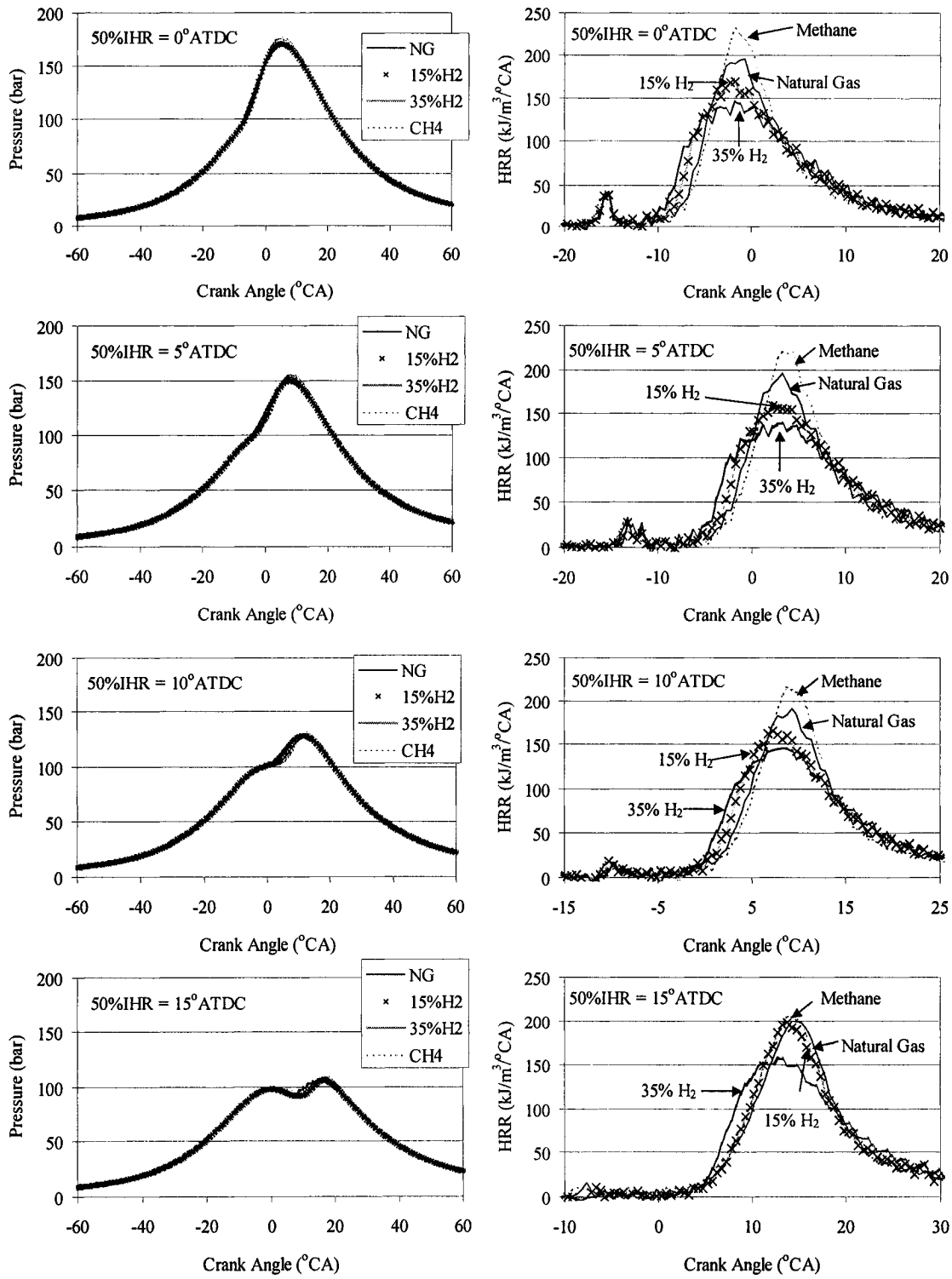

Figure A6.9: Pressure traces and heat-release rates for hydrogen addition testing. 1200 RPM, 13.5 bar GIMEP, 0.6 ϕ, $Y_{intO2} = 0.19$

A6.3 Heavy Hydrocarbon Addition

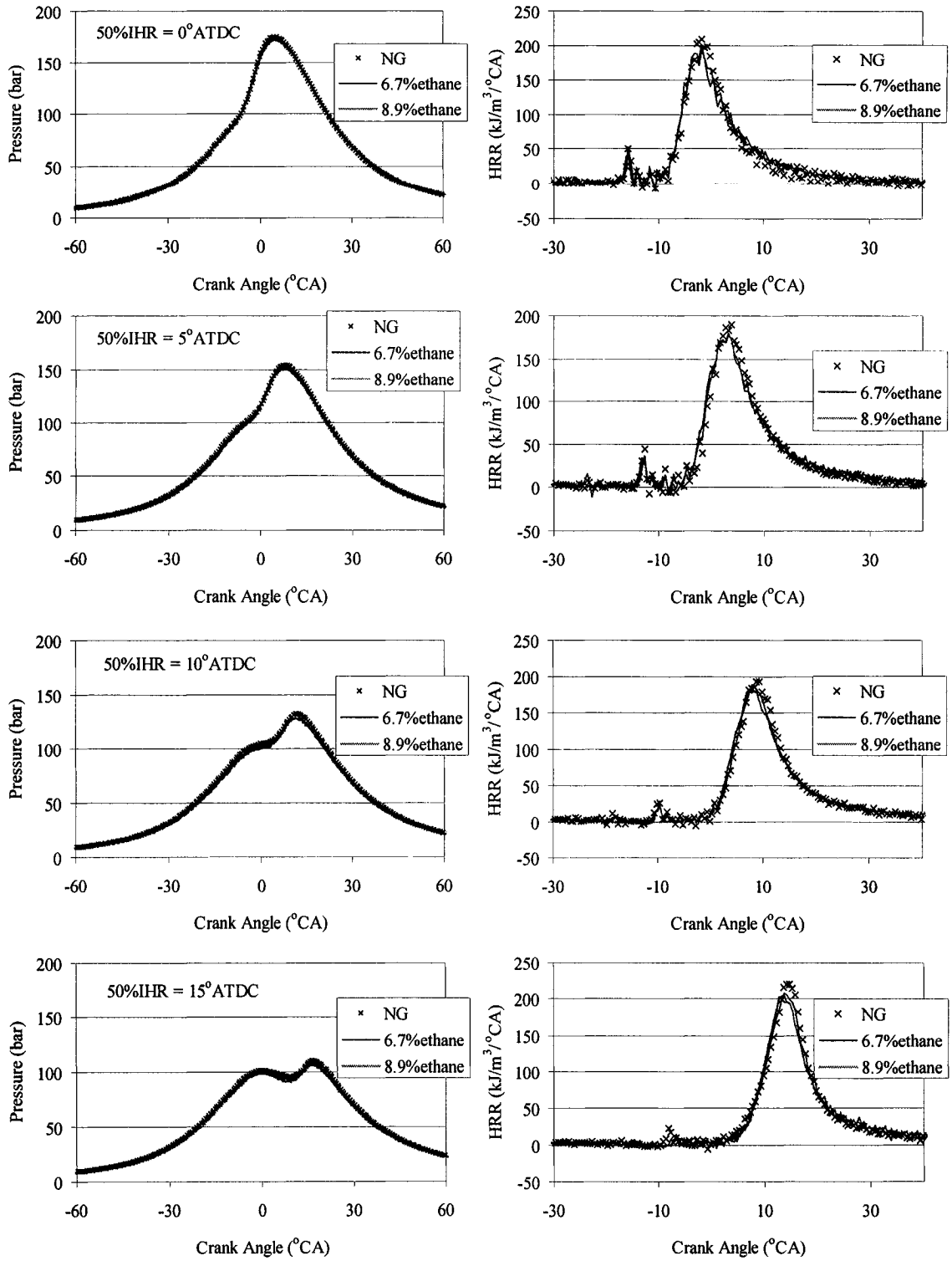

Figure A6.10: Pressure traces and heat-release rates for ethane addition testing. 1200 RPM, 13.5 bar GIMEP, 0.6 ϕ, $Y_{intO2} = 0.19$

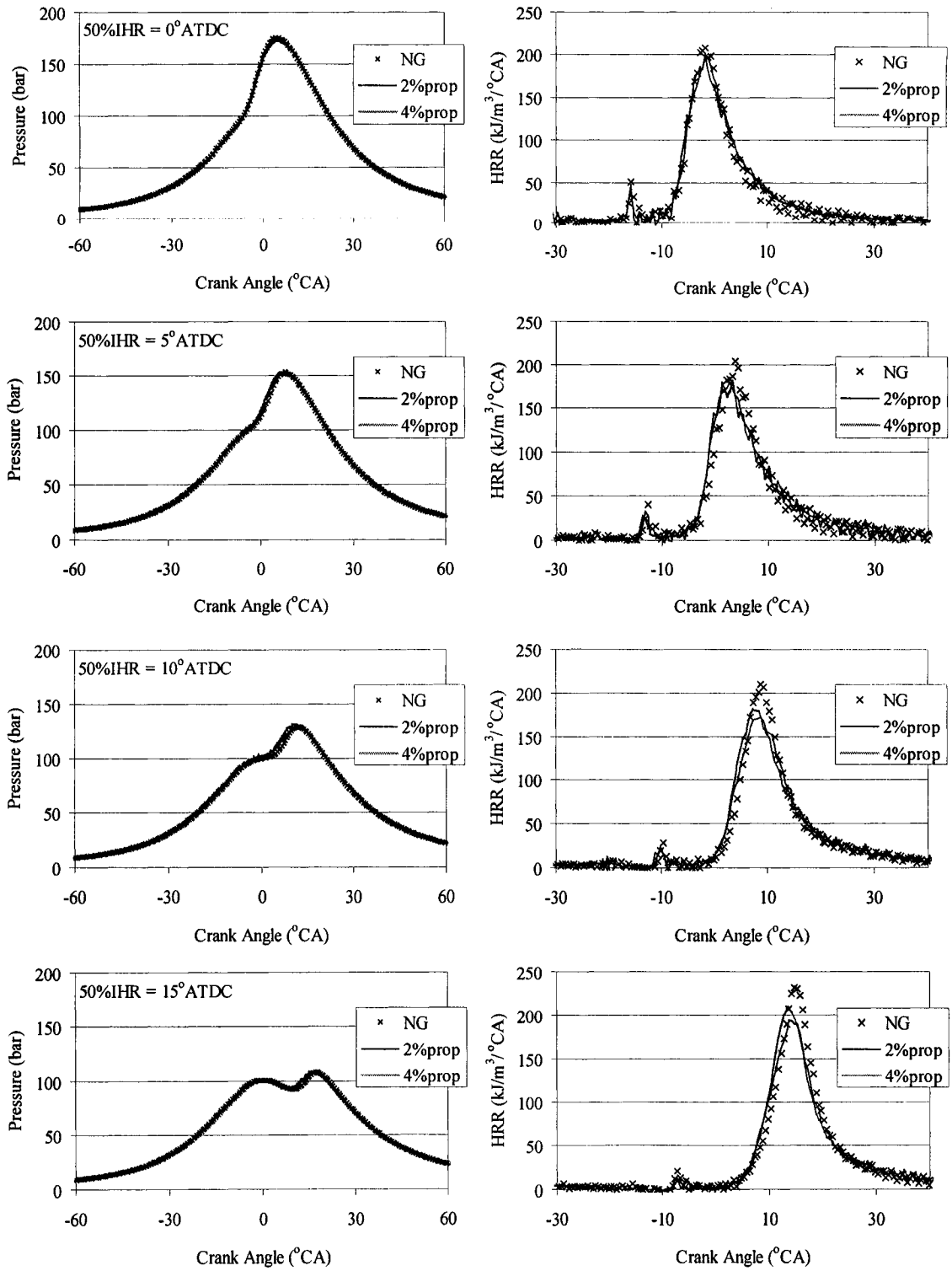

Figure A6.11: Pressure traces and heat-release rates for propane addition testing. 1200 RPM, 13.5 bar GIMEP, 0.6 ϕ, $Y_{intO2} = 0.19$

A6.4 Nitrogen Addition

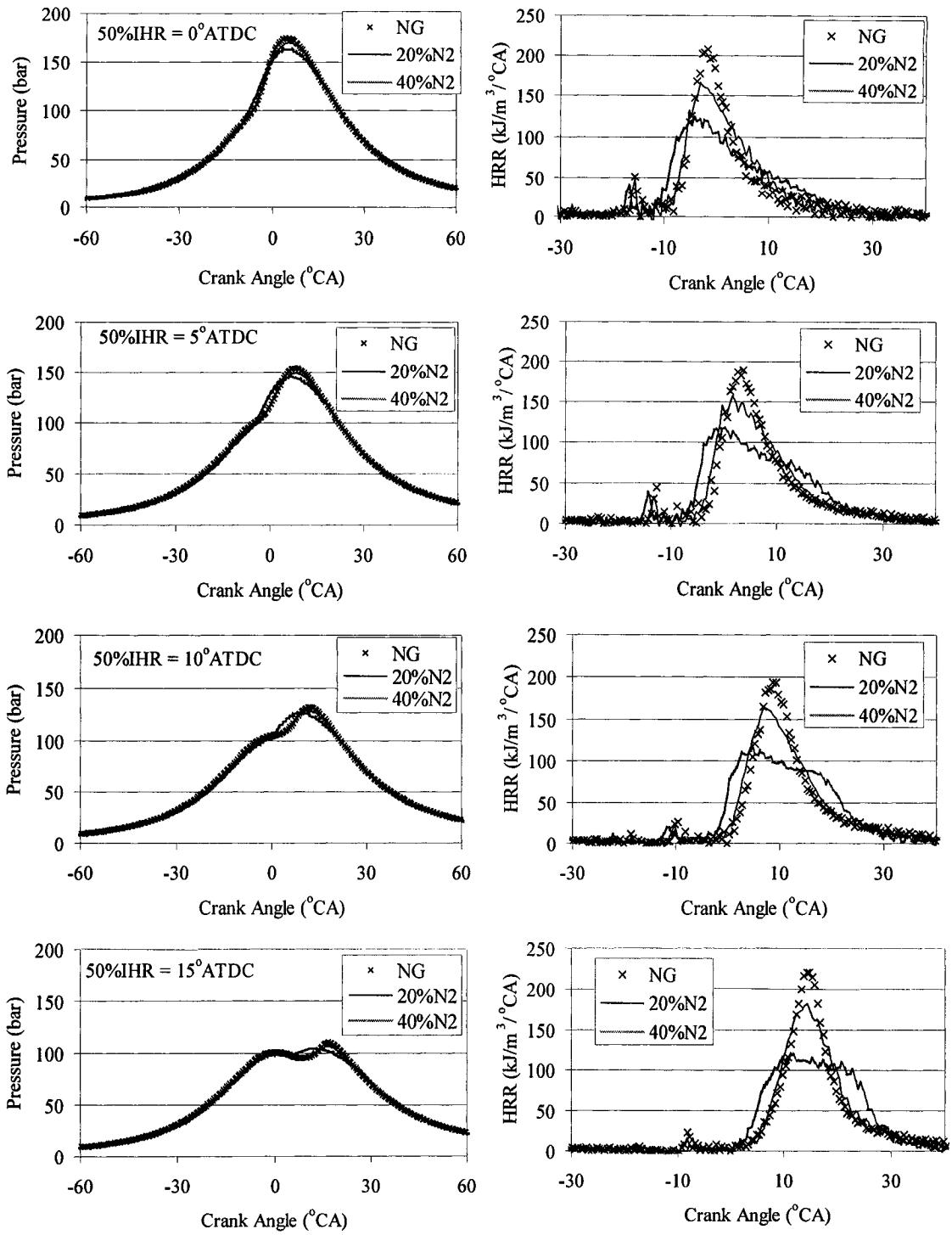

Figure A6.12: Pressure traces and heat-release rates for nitrogen addition testing. 1200 RPM, 13.5 bar GIMEP, 0.6 ϕ, $Y_{intO2} = 0.19$

A6.5 Filtered EGR

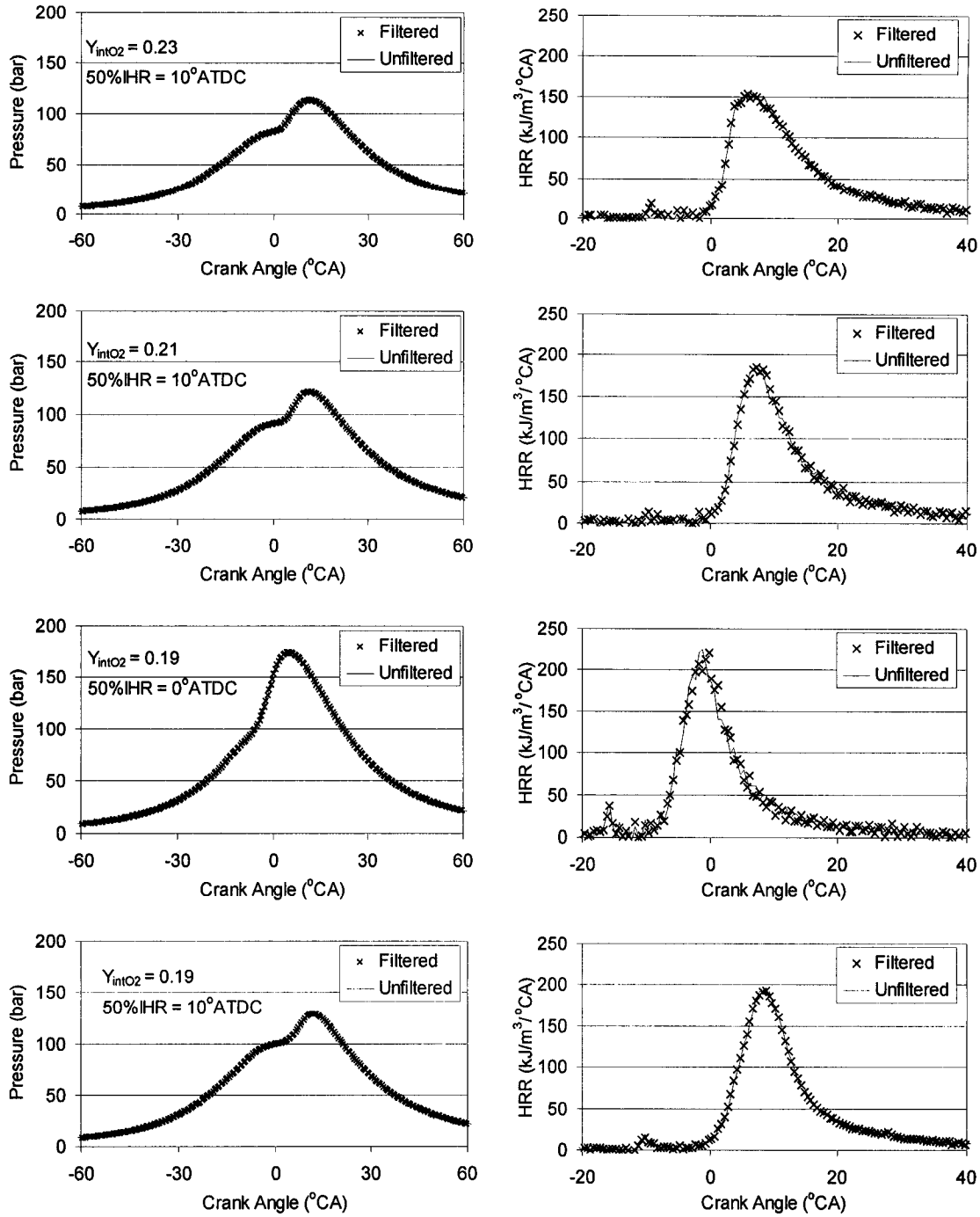

Figure A6.13: Pressure traces and heat-release rates with and without EGR filter. 1200 RPM, 8.5 bar GIMEP, 0.45 ϕ.

Appendix 7
Selected TEM Images

To provide further insight into the structure of the particulate from the PIDING engine, particles were captured on a lacey carbon grid. The particles were then imaged using the transmission electron microscope (TEM) located in the biological sciences imaging laboratory at the University of British Columbia. Images presented here include samples from the fuel composition testing (Chapter 7) and the filtered EGR work (Chapter 8). A scale is shown on each figure.

A7.1 Fuel Composition Particle Images

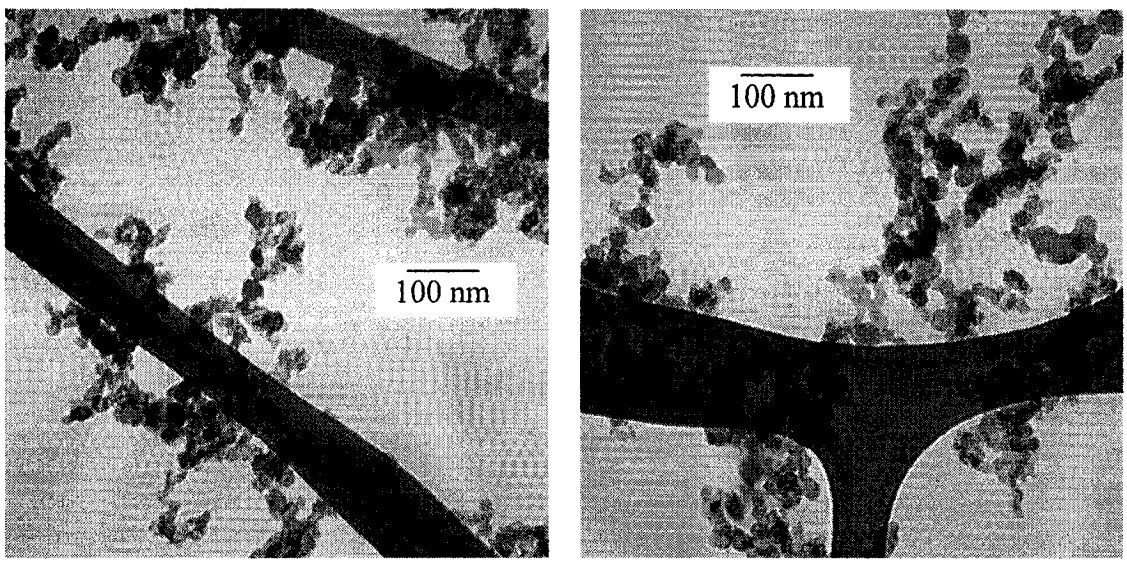

Figure A7.1: TEM images of particles sampled from exhaust stream on natural gas fuel (left) and high ethane additive (right). 1200 RPM, 13.5 bar GIMEP, 0.6 ϕ, Y_{intO2} = 0.19, 50%IHR = 10°ATDC (magnification 200k)

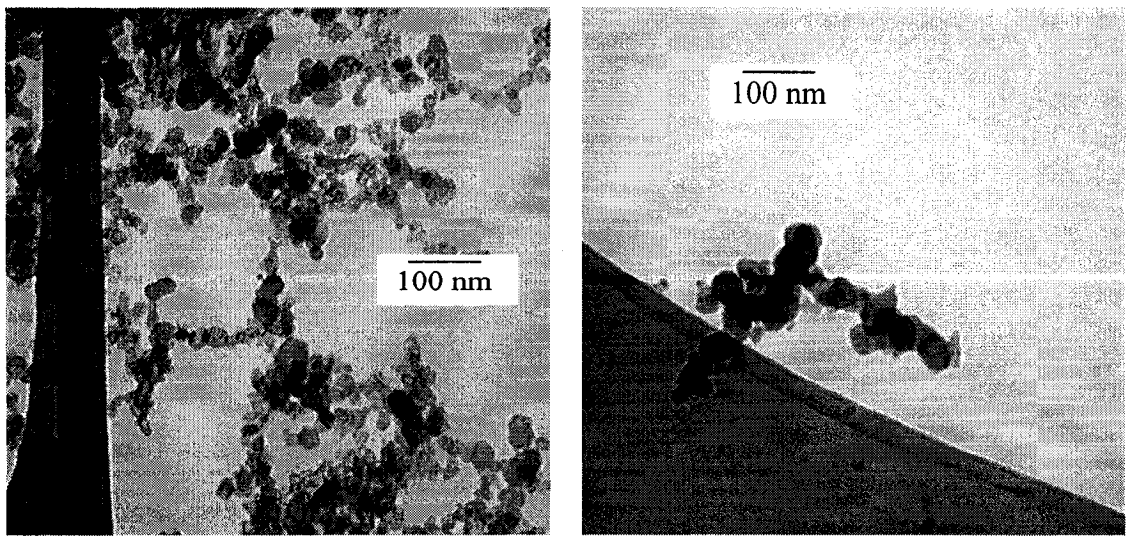

Figure A7.2: TEM images of particles sampled from exhaust stream with high propane additive (left) and high nitrogen additive (right). 1200 RPM, 13.5 bar GIMEP, 0.6 ϕ, Y_{intO2} = 0.19, 50%IHR = 10°ATDC (magnification 200k)

A7.2 Filtered EGR Particle Images

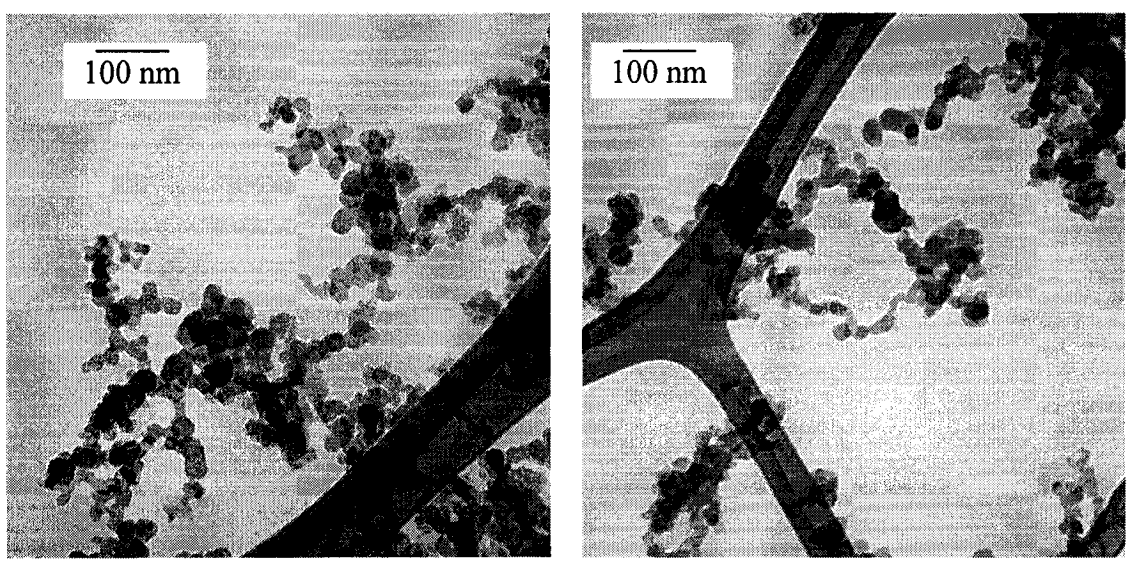

Figure A7.3: TEM images of particles sampled from exhaust stream with (left) and without (right) filter in EGR line. 1200 RPM, 8.5 bar GIMEP, 0.45 ϕ, Y_{intO2} = 0.19, 50%IHR = 10°ATDC (magnification 200k)

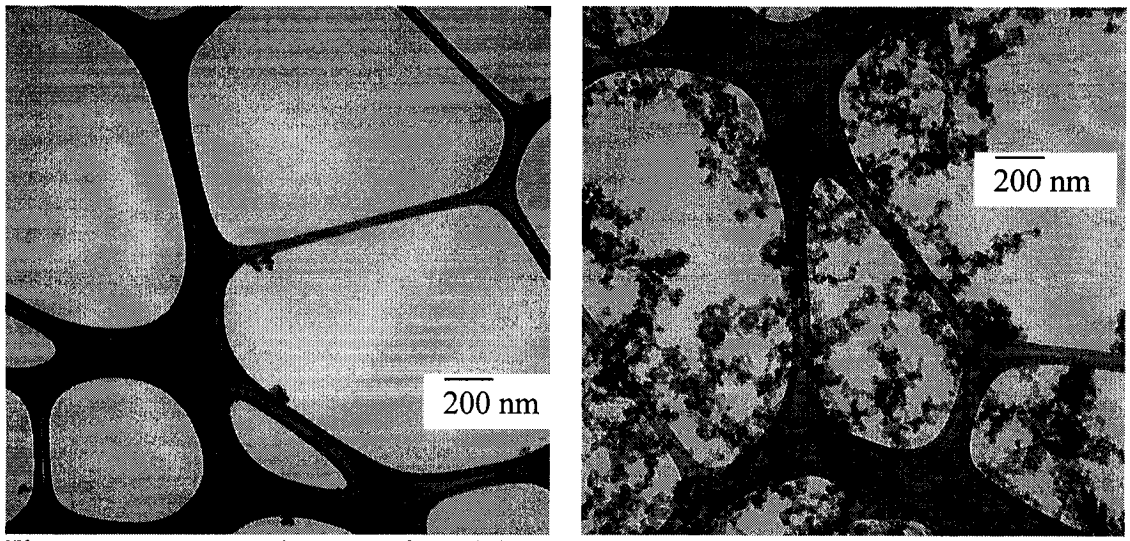

Figure A7.4: TEM images of particles sampled from intake stream with (left) and without (right) filter in EGR line. 1200 RPM, 8.5 bar GIMEP, 0.45 ϕ, $Y_{intO2} = 0.19$, 50%IHR = 10°ATDC (magnification 80k)